HEINRICH HEINE
UNIVERSITÄT DÜSSELDORF

Aberrant expression of microRNA in gliomas: Molecular mechanisms, functional consequences and clinical significance

Inaugural-Dissertation

zur Erlangung des Doktorgrades

der Mathematisch-Naturwissenschaftlichen Fakultät

der Heinrich-Heine-Universität Düsseldorf

vorgelegt von

Franziska Liesenberg

aus Sondershausen/Thüringen/Deutschland

Düsseldorf, Mai 2012

HEINRICH HEINE
UNIVERSITÄT DÜSSELDORF

Aberrant expression of microRNA in gliomas:

Molecular mechanisms, functional consequences and clinical significance

Inaugural-Dissertation

zur Erlangung des Doktorgrades

der Mathematisch-Naturwissenschaftlichen Fakultät

der Heinrich-Heine-Universität Düsseldorf

vorgelegt von

Franziska Liesenberg

aus Sondershausen/Thüringen/Deutschland

Düsseldorf, Mai 2012

Aus dem Institut für Neuropathologie
der Heinrich-Heine-Universität Düsseldorf

(Direktor: Prof. Dr. Guido Reifenberger)

Gedruckt mit der Genehmigung der
Mathematisch-Naturwissenschaftlichen Fakultät der
Heinrich-Heine-Universität Düsseldorf

Referent: Prof. Dr. G. Reifenberger

Korreferent: Prof. Dr. D. Willbold

Tag der mündlichen Prüfung: 19.06.2012

Geschrieben steht: "Im Anfang war das Wort!"

Hier stock ich schon! Wer hilft mir weiter fort?

Ich kann das Wort so hoch unmöglich schätzen,

Ich muss es anders übersetzen,....

...Mir hilft der Geist! Auf einmal seh ich Rat

Und schreibe getrost: Im Anfang war die Tat!

(Johann Wolfgang von Goethe: Faust, Studierzimmer)

Meinen Eltern in Liebe und Dankbarkeit gewidmet.

Contents

Abbreviations

AII	diffuse astrocytoma, WHO grade II
AAIII	anaplastic astrocytoma, WHO grade III
AO	anaplastic oligodendroglioma, WHO grade III
AOA	anaplastic oligoastrocytoma, WHO grade III
APS	ammonium persulfate
ATCC	American Type Culture Collection
5-Aza	5-aza-2`-deoxycytidine
BSA	bovine serum albumine
bp	basepairs
BTG2	*BTG family, member 2 /*
	NGF-inducible anti-proliferative protein PC3
°C	degree Celsius
cDNA	complementary DNA
ChIP	chromatin immunoprecipitation
COX10	*cytochrome c oxidase assembly protein 10*
CpG	Cytosine-phosphatidyl-Guanine
DEPC	diethylpyrocarbonate
DPBS	Dulbecco's Phosphate Buffered Saline
DMEM	Dulbecco's Modified Eagle Medium
DMSO	dimethylsulfoxid
DNA	desoxyribonucleic acid
dNTP	desoxyribonucleoside-5'-triphosphat

DTT	dithiothreitol
EDTA	ethylendiamintetraacetat
ELISA	enzyme linked immunosorbent assay
FCS	fetal calf serum
GFP	green fluorescent protein
GBM	glioblastoma (multiforme)
pGBIV	primary glioblastoma (WHO grade IV)
sGBIV	secondary glioblastoma (WHO grade IV)
GITC	guanidiniumisothiocyanate
GPD1L	*glycerol-3-phosphate dehydrogenase 1-like*
h	hour
HEPES	2-[4-(2-hydroxyethyl)piperazine-1-yl]ethanesulfonic acid
IgG	Immunoglobulin G
JARID1A	*Jumonji, AT-rich interactive domain 1A / RBP2 / KDM5A*
kb	kilobase
kDa	kilo-Dalton
LOH	loss of heterozygosity
M	molar
NB	non-neoplastic brain tissue
mA	milliampere
min	minute
ml	milliliter
mRNA	messenger ribonucleic acid
miRNA	microRNA
µl	microliter

O	oligodendroglioma, WHO grade II
OA	oligoastrocytoma, WHO grade II
PAGE	polyacrylamide gel electrophoresis
PAI	pilocytic astrocytoma, WHO grade I
PBS	phosphate buffered saline
PCR	polymerase chain reaction
PI	propidiumiodide
PLAGL2	*pleomorphic adenoma gene-like 2*
PMSF	phenylmethanesulfonyl fluoride
RNA	ribonucleic acid
rpm	revolutions per minute
RT	room temperature
RT-PCR	reverse transcription - polymerase chain reaction
SD	standard deviation
SDS	sodium dodecylsulfate
sec	second
sGBIV	secondary glioblastoma, WHO grade IV
shRNA	small hairpin RNA
SIRT1	*Sirtuin-1*
Taq	Thermus aquaticus
TBE	Tris-borate-EDTA
TBS-T	Tris-buffered saline with Tween 20
TE	Tris-EDTA

TEMED	N-N-N-N-Tetraethylmethyldiamine
Tris	Tris (hydroxymethyl)aminomethane
TSA	trichostatin A
U	unit
v/v	volume in volume
V	voltage
W	watt
w/v	weight in volume
WHO	World Health Organization

List of Figures page

List of Supplementary Figures page

List of Tables page

1 Introduction

Central Nervous System (CNS) cancers are a group of different tumor entities anatomically close to each other but diverse in terms of clinical behavior, molecular biology and morphology, site as well as presumably etiology (Crocetti et al 2012). The incidence of primary CNS cancers in Europe ranges from 4.5 to 11.2 cases per 100,000 men and from 1.6 to 8.5 per 100,000 women (Ferlay et al 2010). High-grade glioma and brain metastasis are the most common CNS cancers. They occur more frequently during adulthood and first of all among the elderly, with the peak of incidence by 18.5/100,000 in people aged ≥ 65 years (Crocetti et al 2012). The relative frequency of CNS tumors among all cancers is, however, highest during childhood (23 %), when CNS tumors represent the second most common tumor type after the leukaemias (Kaatsch 2010).

1.1 WHO classification of gliomas

Gliomas are the most common primary brain tumors (around 50 %). They comprise a heterogeneous group of neoplasms composed of neoplastically transformed glial cells (Louis et al 2007a). However, the cellular origin of gliomas is still unknown. Experimental data in mice proposed an origin from neoplastically transformed neural stem or progenitor cells (Riemenschneider et al 2010). According to the consensus criteria of the World Health Organisation (WHO) classification of CNS tumors, gliomas are classified by morphological features, growth pattern and molecular profile of the neoplastic cells (Louis et al 2007b, Silber et al 2009). The classification is mainly based on the separation of primary brain tumors into different histological subtypes and determines a specific WHO malignancy grade to each tumor, ranging from WHO grade I (benign) to WHO grade IV (highly malignant). Main types of glioma are astrocytic gliomas, oligodendroglial tumors, mixed oligoastrocytic gliomas and ependymal tumors (Figure 1). An accurate distinction between the different glioma entities is important because of its strong prognostic and therapeutic consequences.

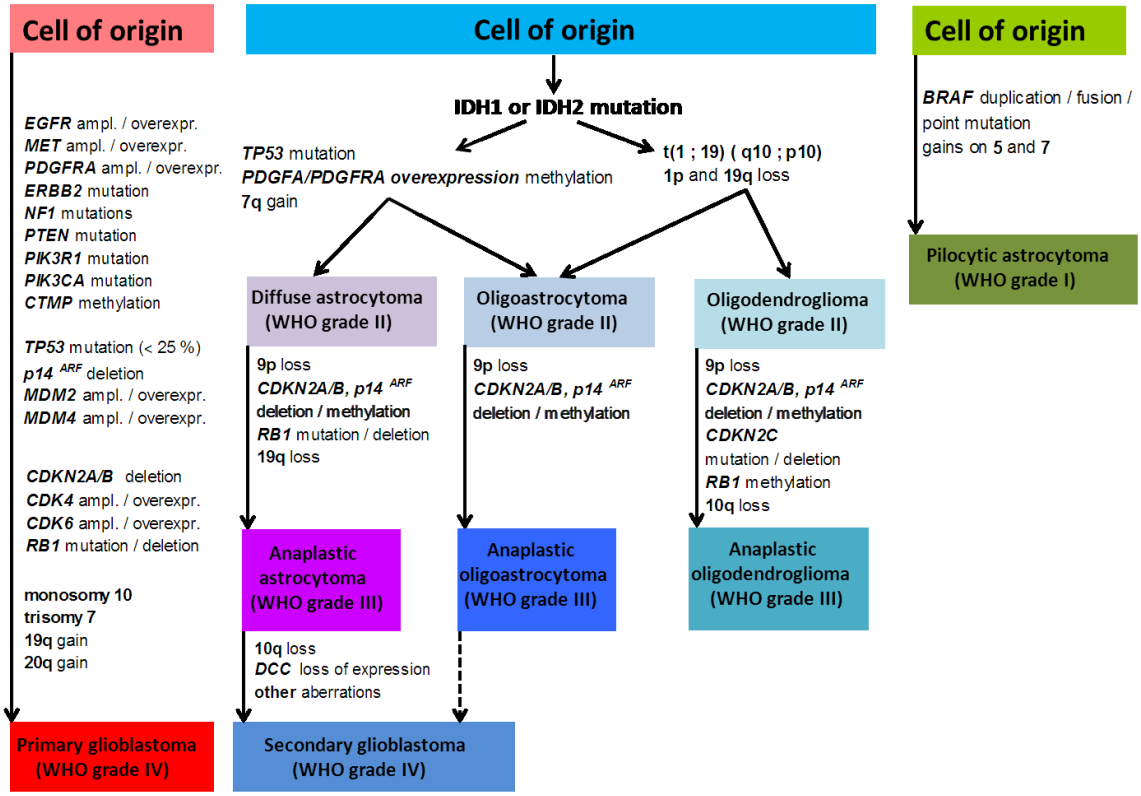

Figure 1: Summary of the most frequent molecular alterations in astrocytic, oligodendroglial and oligoastrocytic gliomas (Riemenschneider et al 2010).

WHO grade I tumors carry the best clinical outcome with demonstrate a low proliferative potential. WHO grade II tumors show low-level proliferative activity. These tumors are, however, often infiltrative in nature and have the potential to progress to higher grade tumors. The designation WHO grade III is assigned to tumors with a higher degree of anaplasia and proliferative activity as compared to the WHO grade II tumors. Patients with WHO grade III tumors receive adjuvant radiation and / or chemotherapy. Glioblastoma multiforme (GBM) - the most malignant form of primary brain neoplasm – is assigned to WHO grade IV. These tumors are associated with high-level proliferative activity, rapid pre- and postoperative disease evolution with fatal outcome. Histologically, they display microvascular proliferation and/or necrosis, and molecularly they demonstrate marked genomic instability (Louis et al 2007b, Silber et al 2009). Anaplastic astrocytoma, anaplastic oligodendroglioma, anaplastic oligoastrocytoma (WHO III) and glioblastoma multiforme (WHO IV) belong to the group of so-called high-grade gliomas representing the most common primary malignant tumors of the central nervous system (Louis et al 2007b, Wehming et al 2012).

Tremendous efforts have been made to improve the outcome of the patients by multi-modality treatment, including surgery, radiotherapy and chemotherapy, however, with still limited success concerning cure from the disease. Diffuse gliomas including glioblastomas are characterized by their diffusely infiltrative growth into the neighboring brain tissue, which renders them unsuitable for complete surgical resection. A further important point is the inherent resistance of these tumors to both radiation and chemotherapy. Due to this fact, the prognosis remains poor with median survival time for patients with WHO grade IV tumors being approximately 10 - 15 months after diagnosis, while patients with WHO grade III gliomas show median overall survival times of around 30 - 50 months (Hadziahmetovic et al 2011) (Nieder et al 2004). Important for the patients`prognosis in this context is that diffuse astrocytoma (WHO grade II) tends to spontaneous malignant progression to anaplastic astrocytoma (WHO grade III) and finally to secondary glioblastoma (WHO grade III) over time (Louis et al 2007a). Interestingly, it has been shown that primary glioblastoma and secondary glioblastoma are molecularly distinct entities characterized by different genetic pathways and molecular profiles (Pollo 2011). In fact, genetic alterations become increasingly important with respect to brain tumor classification into prognostically distinct subgroups (Louis et al 2007b, Riemenschneider et al 2010). These genetic alterations affect genes that control cell growth, apoptosis as well as angiogenesis and invasion (Nagarajan and Costello 2009).

1.2 Molecular pathology of gliomas

Relevant molecular characteristics were identified in gliomas over the last decades (Hu and Kesari 2012, Louis et al 2007b, Riemenschneider and Reifenberger 2009). These include various genetic and epigenetic mutations that change gene expression and protein function, which in turn lead to tumor initiation and progression by causing uncontrolled cell division, resistance to apoptosis and diffuse infiltration into the adjacent normal brain tissue (Nagarajan and Costello 2009). These genetic and epigenetic alterations are tumor grade and tumor subtype specific and become increasingly important with respect to both brain tumor classification into prognostically distinct subgroups as well as risk-adjusted therapeutic treatment (Louis et al 2007b, Riemenschneider et al 2010). Collectively, molecular biological studies over the past two decades revealed that more than half of the diffuse astrocytomas (WHO grade II) carry mutations of the tumor suppressor gene *TP53*, usually accompanied by loss of

heterozygosity (LOH) on 17p, thus resulting in complete abrogation of wild-type *p53* function in the tumor cells. Furthermore, gains on the long arm of chromosome 7 are often present (Riemenschneider and Reifenberger 2009, Riemenschneider et al 2010). In contrast, combined losses of the short arm of chromosome 1 and of the long arm of chromosome 19 were found in oligodendroglial tumors (Riemenschneider et al 2010). In addition, somatic mutations of codon 132 in the gene encoding *isocitrate dehydrogenase-1* (*IDH1*) were found in 50 - 80% of astrocytomas, oligodendrogliomas, oligoastrocytomas of WHO grades II and III, and secondary glioblastomas. They were, however, rarely detected in primary glioblastomas and never in other types of glioma (Balss et al 2008, Hartmann et al 2009, Ichimura 2012, Parsons et al 2008, Yan et al 2009). Anaplastic astrocytomas (WHO grade III) often carry additional chromosomal alterations, such as deletions on chromosomes 6, 11p, 22q and losses of the tumor suppressor genes *CDKN2A*, $p14^{ARF}$ and *CDKN2B* on chromosome 9p. Moreover, *CDK4* or *CDK6* amplification or inactivating alterations of *RB1* are present in a subset of anaplastic astrocytomas (Ichimura et al 2004). Another common alteration was demonstrated by (Hermanson et al 1992) who reported on overexpression of *PDGFRA* (platelet-derived growth factor receptor alpha) and its ligand *PDGFalpha* in gliomas, thus leading to an autocrine growth stimulation of the tumor cells (Hermanson et al 1992). Glioblastomas (WHO grade IV) show various chromosomal and genetic alterations affecting many tumor suppressor genes (*PTEN*, *CDKN2A, p14*^{ARF}, *EMP3*, *CTMP*) and proto-oncogenes (*EGFR*, *CDK4*, *MDM2*, *CDK6*, *CCND1/3*, *MDM4*, *PDGFRA*) (2008, Riemenschneider and Reifenberger 2009, Toedt et al 2011). Interestingly, primary glioblastomas (arising de novo, 95 %) and secondary glioblastomas (arising from lower-grade precursor lesions, 5 %) demonstrate different genetic aberrations (Ohgaki and Kleihues 2007). Primary glioblastomas bear frequent *EGFR* amplification and *PTEN* mutation but lack *IDH1* mutation. Secondary glioblastomas, similar to diffuse and anaplastic astrocytomas, show frequent mutation in the *TP53* and *IDH1* genes but typically lack *EGFR* amplification and *PTEN* mutation (Balss et al 2008, Ohgaki and Kleihues 2007, Riemenschneider et al 2010, Yan et al 2009). Despite these differences, most of the molecular alterations at the gene and transcript levels that have been detected in primary and secondary glioblastomas can be assigned to certain functional pathways, in particular the phosphoinositol 3 kinase/Akt, mitogen-activated kinase, p53 and pRb signalling cascades (2008, Riemenschneider and Reifenberger 2009).

1.3 MicroRNAs (miRNAs)

MicroRNAs are 19 to 24 nucleotide long, non-protein-coding RNAs. These small RNAs regulate the translation and degradation of target mRNAs through base pairing to perfect (in plants) or partially (in mammals) complementary sites mostly in the 3`- untranslated region (3`-UTR) of the target mRNAs (He and Hannon 2004, Lagos-Quintana et al 2001, Lee and Ambros 2001). MicroRNAs are involved in many fine-tuned biological processes, such as cell proliferation, differentiation, apoptosis, cell migration and metabolism, as well as in various human diseases, including cancer (Bartel 2004, Harfe 2005, Karius et al 2012). However, hotspots for pathological aberrations are miRNA genes and the mechanisms by which miRNAs are processed (Karius et al 2012). It has been shown that analyses of miRNA alteration patterns revealed promising cancer biomarkers as well as therapeutic targets, which might be specifically addressed by synthetic antisense oligonucleotides or miRNA mimetic molecules (Karius et al 2012).

1.3.1 Biogenesis of microRNAs

The microRNA biogenesis is tightly regulated through a multistep process. The first two steps are localized in the nucleus followed by maturation in the cytoplasm. Figure 2 summarized the principles of miRNA biogenesis and the cancer-associated alterations in microRNA pathways.

Genes, coding for miRNAs are located either in intergenic regions or in defined transcription units. It is well described that miRNA genes are frequently located in protein-coding genes, where they predominantly reside in introns (Rodriguez et al 2004) and long non-coding transcripts, and are consequently co-transcribed with their host gene (Karius et al 2012). MiRNAs genes are transcribed into polycistronic primary transcripts (pri-miRNA) usually by RNA polymerase (RNA Pol) II with lengths of 1-10 kb. MiRNAs located in Alu repeats are transcribed by RNA polymerase III (Karius et al 2012). Like other Pol II transcripts, pri-miRNAs posess a 5`-methyl cap structure and a 3`poly-A-tail as well as one hairpin structure of about 70 nucleotides (Cai et al 2004). The pri-miRNA transcript contains the mature miRNA within an imperfectly paired double stranded stem. In the canonical miRNA pathway, these structures are recognized by a multiprotein complex of double-stranded RNA specific endoribonuclease III Drosha, the *Di George Syndrome critical region gene 8* (*DGCR8*)

and the binding protein Pasha (Denli et al 2004, Gregory et al 2004, Karius et al 2012, Landthaler et al 2004, Lee et al 2003). Thereby, the double-stranded RNA-binding protein DGCR8 binds the base of the stem-loop structure and guides the positioning of the RNase III enzyme Drosha (Han et al 2006). Drosha cleaves the pri-miRNA into 70- to 100-nucleotide pre-miRNAs and generates a two nucleotide overhang at the 3`end (Gregory et al 2004, Han et al 2006). The mirtron pathway reveals an alternative mechanism of pri-miRNA processing. Here, pre-miRNA structures are generated from pri-miRNA-containing introns (mirtrons) through the nuclear splicing machinery (Karius et al 2012). The nuclear export receptor Exportin 5 recognizes the pre-miRNAs and following by transport from the nucleus to the cytoplasm in a Ran-GTP-dependent manner (Bohnsack et al 2004, Lund et al 2004, Yi et al 2003).

In the cytosol, the pre-miRNA is subsequently processed by the RNase III enzyme Dicer (Grishok et al 2001). This enzyme binds the 3`overhang of the pre-miRNA and positions the substrate correctly for cleavage by the two catalytic domains within the double-stranded stem (Macrae et al 2006, Zhang et al 2004). The Dicer cleavage results in a 19-24 nucleotide double-stranded miRNA/miRNA* duplex with 3`- dinucleotide overhangs of two nucleotide on both ends (Bartel 2009, Karius et al 2012). Dicer interacts with the trans-activator RNA binding protein (TRBP) and the protein kinase R (PKR) activating protein (PACT) in human cells (Kwak et al 2010). Interestingly, microRNAs are unable to silence their target genes alone (Karius et al 2012). Mature miRNAs require assembly into a multi-protein effector RNA-induced silencing complex called RISC. Thereby, the essential core components of the RISC are members of the Argonaute protein family (Ago) (Filipowicz 2005, Kwak et al 2010, Lee et al 1993, Liu et al 2004). RISC loading occurs by the ATP-dependent incorporation of the miRNA/miRNA* duplex into the Ago complex following by unwinding of the miRNA duplex. The miRNA* passenger strand is discarded from the RISC complex in an Ago 2 slicer-dependent or slicer-independent manner (Kwak et al 2010). The residual mature single-stranded microRNA determines the specifity of the RISC complex for its target mRNA through interacting with the 3`-untranslated region (UTR) of the target mRNA (Karius et al 2012). The target recognition is based on base-pairing of nucleotides in the “seed” region and is impaired by additional interactions in the middle of the 3`UTR (Parasramka et al 2012). In general, perfect base-pairing between miRNA and mRNA sequences and the presence of the Ago 2 endonuclease leads to mRNA degradation (Meister and Tuschl 2004). In contrast, imperfect miRNA/mRNA base pairing can either induce deadenylation and degradation or lead to

translational inhibition through the RNA-binding protein GW182 (Behm-Ansmant et al 2006). RISC-mediated mRNA-repression may also interfere with eIF4E for cap-binding or inhibit the late translation initiation steps, e.g. by recruitment of 60S ribosomal subunit which leads to translational inhibition (Kwak et al 2010, Standart and Jackson 2007). Moreover, the RISC complex has been postulated to act on post-initiation steps by inhibiting the elongation of the ribosomal machinery or by triggering the proteolysis of peptides, which are newly synthesized during translation (Kwak et al 2010). In addition, RISC complexes with captured target mRNAs can be transported to parking bodies (p-bodies). There, mRNA is degraded or stored for recycling (Eulalio et al 2007).

To conclude, these features allow fine-tuning of biological processes like development, cell metabolism, tissue differentiation, cell cycle regulation, senescence, apoptosis and cell migration (Ma et al 2007, Ryazansky and Gvozdev 2008, Valeri et al 2009).

1.3.2 MicroRNAs as dual cancer players

Genes encoding miRNAs are frequently located in cancer-associated genomic regions (Calin et al 2004). It is well described that about 50% of all annotated human miRNAs are located in amplification or chromosomal rearrangement hotspots, common breakpoints regions in or near oncogenes, tumor suppressor genes or fragile sites (Karius et al 2012). In addition, many of the known miRNAs appear in polycistronic transcripts. Deregulation of one member of the cluster is attended by deregulation of the other cluster members (Karius et al 2012, Tanzer and Stadler 2004). During the last decade, several cancer-relevant miRNAs have been found to act as onco-miRNAs or suppressor-miRNAs. Onco-miRNAs and suppressor-miRNAs negatively regulate tumor suppressor genes or proto-oncogenes, respectively. One explanation how the same miRNA could function as either tumor suppressor or tumor promoter would be that the same miRNA participates in distinct pathways in different cells resulting in different effects on cell growth, proliferation and cell survival depending on the cell type and its gene expression pattern (Fabbri et al 2007). This bivalent behavior of a given gene in malignant transformation is well-described feature of many protein-coding genes, like *ERB-A, FOSB, MAX* or *TP53* (Calin 1994). One example arises from expression studies showing that *miR-155* was overexpressed in several types of tumors including haematopoietic B cell malignancies and solid cancers of epithelial origin, thereby behaving as an oncogene (Calin and Croce 2006a, Calin and Croce 2006b, Esquela-

Kerscher and Slack 2006). In contrast, in endocrine pancreatic tumors, *miR-155* is significantly downregulated in malignant cells, supposedly acting as a tumor suppressor gene in this tumor type (Roldo et al 2006). A second example constitutes the involvement of the most highly conserved family of miRNAs in human cancer, the *let-7* family. Yanaiharan and colleagues showed that downregulation of the *let-7* family is frequent in lung cancers and associated with poor prognosis (Yanaihara et al 2006). On the other hand, Brueckner and co-workers demonstrated strong methylation by *DNMT3B* and *DNMT1* in the *let-7a-3*`s putative promoter region in normal human tissues as well as hypomethylation in lung adenocarcinoma. *Let-7a*-3`s promoter demethylation resulted in reactivation of *let-7a-3* and increased proliferation in lung cancer cells (Brueckner et al 2007). A third example is the polycistronic cluster *miR-17-92*. In B cell lymphomas, the *miR-17-92* cluster act as an oncogene by cooperating with c-Myc and results in tumor development (He et al 2005). In contrast, in B-cell lines which overexpress MYC, members of the *miR-17-5p/92* cluster showed tumor suppressor activity by decreasing *E2F1* expression, thereby leading to tightly regulated c-Myc-mediated cellular proliferation (O'Donnell et al 2005).

1.3.2.1 MicroRNAs as tumor suppressor genes

MiRNA expression patterns vary between healthy and pathological tissues as well as between different cancer types. Thereby, many regulatory mechanisms have been identified first for tumor suppressor miRNAs. Promoter methylation, histone modifications, mutations and DNA copy number abnormalities, such as genomic gains and amplifications, as well as copy number deletions and loss of heterozygosity (LOH) are among these mechanisms (Fabbri et al 2007, Hatziapostolou and Iliopoulos 2011, Iliou et al 2011, Weber et al 2007).

Chromosomal deletions and mutations

Remarkably, Calin and colleagues demonstrated for the first time the abnormal expression of the *miR-15a/miR-16-1* cluster in B-cell chromic lymphocytic leukemia (CLL). Both miRNAs, *miR-15a* and *miR-16-1*, are located at chromosomal position 13q14.3, which is frequently deleted in CLL, prostate cancer and lymphomas (Calin et al 2002, Dong et al 2001). Moreover, the authors observed that these miRNAs were deleted or downregulated in about 68 % of CLL cases (Calin et al 2005). The confirmation of the role of *miR-15a* and *miR-16-1* as tumor suppressor genes came

with the demonstration that their expression was inversely correlated with their target mRNA *anti-apoptotic B cell lymphoma 2 gene* (*BCL2*) resulting in induction of apoptosis in leukaemic cells (Cimmino et al 2005).
In addition, decreased expression of the mature form of the *miR-143* and *miR-145* cluster has been described in breast cancer, colorectal carcinoma and colon adenomas (Iorio et al 2005, Michael et al 2003). Interestingly, normal levels of the corresponding pre-miRNA were present in colon cancer. A possible block in Dicer processing could be a mechanism of reduced mature *miR-145* and *miR-143* expression (Michael et al 2003). Until now, a clear mechanism by which *miR-145* and *miR-143* practise tumor suppressor activity has not been demonstrated, but their chromosomal mapping to 5q32 (a region of LOH and deletion in myelodisplastic syndromes, Calin et al 2004) is in favor of their antineoplastic role (Fabbri et al 2007).

CpG methylation

Approximately half of all known human miRNA genes are associated with CpG islands (Karius et al 2012, Weber et al 2007). Consequently, aberrant DNA methylation-associated epigenetic silencing may also influence the miRNA network (Deng et al 2008). CpG islands were required to be located within 2000 bp upstream or downstream of the DNA sequence encoding the corresponding microRNA sequence. These regions were defined as areas equal to or exceeding 200 bp of DNA with a C+G content equal to or greater than 55 % and an observed CpG / expected CpG ratio in excess of 0.65 (Takai and Jones 2002). These findings indicate that several microRNA genes represent candidate targets of DNA methylation (Weber et al 2007).
Saito and colleagues have demonstrated that *miR-127* is located on human chromosome 14q32.31 and embedded in the largest miRNA cluster identified to date (with *miR-136*, *miR-431*, *miR-432* and *miR-433*) (Altuvia et al 2005, Saito et al 2006). *MiR-127* is located in a CpG island exhibiting imprinting in mice, and physiologically expressed in normal fibroblasts but strongly silenced and/or downregulated in cancer cells (Saito et al 2006). It was shown that this silencing was mediated by hypermethylation of the putative miRNA promoter region. Hypermethylation of the *miR-127* 5`putative promoter region could be reversed by combined treatment of human bladder cancer cells with the DNA methyltransferase inhibitor 5-aza-2`-deoxycytidine and the histone deacetylase (HDAC) inhibito 4- phenylbutyric acid (PBA) resulting in upregulation of *miR-127*. Interestingly, other miRNAs of the cluster were not affected by this mechanism pointing toward a fine-regulatory mechanism within the

clustered miRNAs (Saito et al 2006). The proto-oncogene *BCL6* was identified as one target of *miR-127* and was shown to be downregulated upon epigenetic reactivation of *miR-127*, suggesting that *miR-127* may function as a tumor suppressor gene (Saito et al 2006). DNA methylation and histone deacetylation affect miRNA expression in a tissue-specific manner because the re-expression of *miR-127* has not been observed in non-small cell lung cancer cells after treatment with demethylating agents and/or deacetylase inhibitors (Yanaihara et al 2006). Lujambio and co-workers reported on miRNA expression profiling in cancer cells genetically deficient for the DNA methyltransferase enzymes (DNMTs), responsible for *de novo* (*DNMT3B*) and maintenance (*DNMT1*) DNA methylation, and identified *miR-124a* as being silenced itself by promoter hypermethylation (Lujambio et al 2007). As a consequence of *miR-124a* silencing, *cyclin-dependent kinase 6* (*Cdk6*), a target of *miR-124a* with oncogenic function, was upregulated. *Cdk6* activation resulted in the phosphorylation and concomitant inactivation of the *retinoblastoma* (*RB*) tumor suppressor gene (Weber et al 2007). Another study showed that the human *let-7a-3* miRNA gene is also associated with a CpG island that was found to be methylated in all human tissue analyzed (Brueckner et al 2007). Similary, more microRNAs associated with CpG islands were found to be hypermethylated and silenced in several tumor samples, like *miR-9-1*, *miR-148a*, *miR-152* and *miR-663* in primary breast tumors (Lehmann et al 2008). *MiR-34b*, *miR-137*, *miR-193a* and *miR-203* were reported as being hypermethylated and silenced in oral squamous cell carcinoma (Kozaki et al 2008) whereas *miR-34b/c*, a crucial component of the p53-dependent tumor suppressor pathway, is silenced by hypermethylation in colorectal and gastric primary tumors and cell lines (Lujambio et al 2007, Suzuki et al 2010). In most of these cases, the treatment with 5-aza-deoxycytidine alone was able to restore miRNA expression in cancer cells (Lujambio et al 2007, Suzuki et al 2010, Toyota et al 2008). Moreover, several studies revealed increased *miR-132* expression after 5-Aza treatment in prostate cancer (Formosa et al 2012) and pancreatic cancer (Zhang et al 2011a).

Histone modifications

Chromatin is composed of nucleosome particles that consist of a protein octamer around the DNA is wrapped. The protein octamers contain two molecules of each histone protein H2A, H2B, H3 and H4 (Hatziapostolou and Iliopoulos 2011). Histone modifications (including acetylation, methylation, and phosphorylation) are important in chromatin packaging and cellular processes such as replication, transcription and repair, and are often associated with DNA methylation (Feinberg and Tycko 2004, Kouzarides 2007). Modifications occur in different histone proteins and different histone residues like lysine, arginine or serine. Unlike DNA methylation, histone modifications can lead to activation or repression depending on the type of modification and the modified residues (Hatziapostolou and Iliopoulos 2011). Several studies have shown that lysine acetylation correlated with transcriptional activation (Hebbes et al 1988). Lysine methylation resulted in transcriptional activation or repression depending on the locus of the residue that was modified and the degree of methylation (Hatziapostolou and Iliopoulos 2011). Trimethylation of lysine 4 on histone H3 (H3K4me3) is correlated with an activation of gene promoters (Liang et al 2004). Trimethylation of H3K9 (H3K9me3) and H3K27 (H3K27me3) is correlated with repression of gene promoters (Kouzarides 2007). These two modifications together constitute the main silencing mechanisms in mammalian cells. Thereby, H3K9me3 worked in concert with DNA methylation and H3K27me3 largely worked exclusive of DNA methylation (Hatziapostolou and Iliopoulos 2011). Modifications at lysines 16 and 20 on histone 4 had important role in determining chromatin structure and function. Thereby, deacethylation of K16 and trimethylation of K20 were hallmarks of heterochromatic domains in mammalian cells (Fraga et al 2005).

Earlier studies indicated that treatment of different cancer cells with DNA demethylation agents and/or HDAC inhibitors was able to alter the expression labels of miRNAs (Saito et al 2006, Scott et al 2006). As mentioned above, *miR-1*, *miR-124a* and *miR-127* were under the epigenetic control in human cancer due to the fact that they are embedded in CpG island regions and epigenetically silenced by promoter hypermethylation and histone modifications (Datta et al 2008, Lujambio et al 2007, Saito et al 2006). Furthermore, Saito and co-workers revealed increasing levels of acetylated histone H3 in the 5`genomic region of *miR-126* in HeLa (cervical cancer) and T24 (bladder cancer) cells after treatment with the histone deacetylase inhibitor 4-phenylbutyric acid (PBA) and DNA demethylating 5-Aza (Saito et al 2009). In addition, 13 microRNAs were identified in acute lymphoblastic leukemia, embedded in

CpG island with high heterochromatic markers like high levels of K9H3me2 and/or low levels of K4H3me3 (Agirre et al 2009, Roman-Gomez et al 2009). Furthermore, it has been demonstrated that transcription factors can recruit epigenetic effectors at miRNA promoter regions contributing to the regulation of their expression (Fazi et al 2007). Histone modifications associated with light exposure have been demonstrated to regulate *miR-132/miR-212* transcription at CREB transcription-binding sites within the 5`genomic region of *miR-132/miR-212* in the visual cortex of juvenile mice implicated in the plasticity of dendrites and spines (Tognini et al 2011, Wanet et al 2012).

1.3.2.2 MicroRNAs as oncogenes

The expression of oncogenic microRNAs may be abnormally increased in tumors due to chromosomal translocation, promoter hypomethylation or gene amplification (Fabbri et al 2007).

Chromosomal translocation

It has been found that *miR-142* is located 50 nucleotides from the t(8;17) translocation break point between chromosome 17 and *c-MYC*. Therefore, *miR-142* was presumably involved in the overexpression of *MYC* leading to aggressive acute prolymphocytic leukaemia (Calin et al 2004).

Genomic amplifications

The chromosome region 13q31-32 is known to undergo amplification in malignant B-cell lymphomas (Ota et al 2004). The c13orf25 gene is a pri-miRNA encoding a cluster of microRNAs with *miR-17-5p, miR-18a, miR-19a, miR-20a, miR-19b-1* and *miR-92*. The regarded amplification of c13orf25 explained the overexpression of the *miR-17-92* cluster in lymphomas (He et al 2005, Ota et al 2004). Moreover, members of the *miR-17-92* cluster were found to be overexpressed in colon, lung, breast, pancreas and prostate tumors (Hayashita et al 2005, He et al 2005, Volinia et al 2006), and constitute the only portion of the c13orf25 gene that are highly evolutionary conserved, suggesting that they are the only portion of this transcript with oncogenic activity (Fabbri et al 2007). Another miRNA whose overexpression has been identified as a result of amplification is *miR-21*, which maps in the 3`UTR of the vacuole membrane protein 1 gene at chromosome 17q23.2. This region was found frequently amplified in neuroblastomas, colon, breast and lung cancers. Similarly, *miR-21* was

also found to be upregulated in many solid cancers (breast, lung, colon, prostate, stomach and endocrine pancreas tumors) (Volinia et al 2006), including glioblastomas (Chan et al 2005, Ciafre et al 2005). Knockdown of *miR-21* induced caspase-mediated apoptosis in glioblastoma cells, further supporting the oncogenic role of this miRNA (Chan et al 2005).

Hypomethylation

Until now, the only known example of activating an oncogenic miRNA by hypomethylation is the hypomethylation of the *let-7a-3*`s putative promoter in human lung adenocarcinomas, as described above.

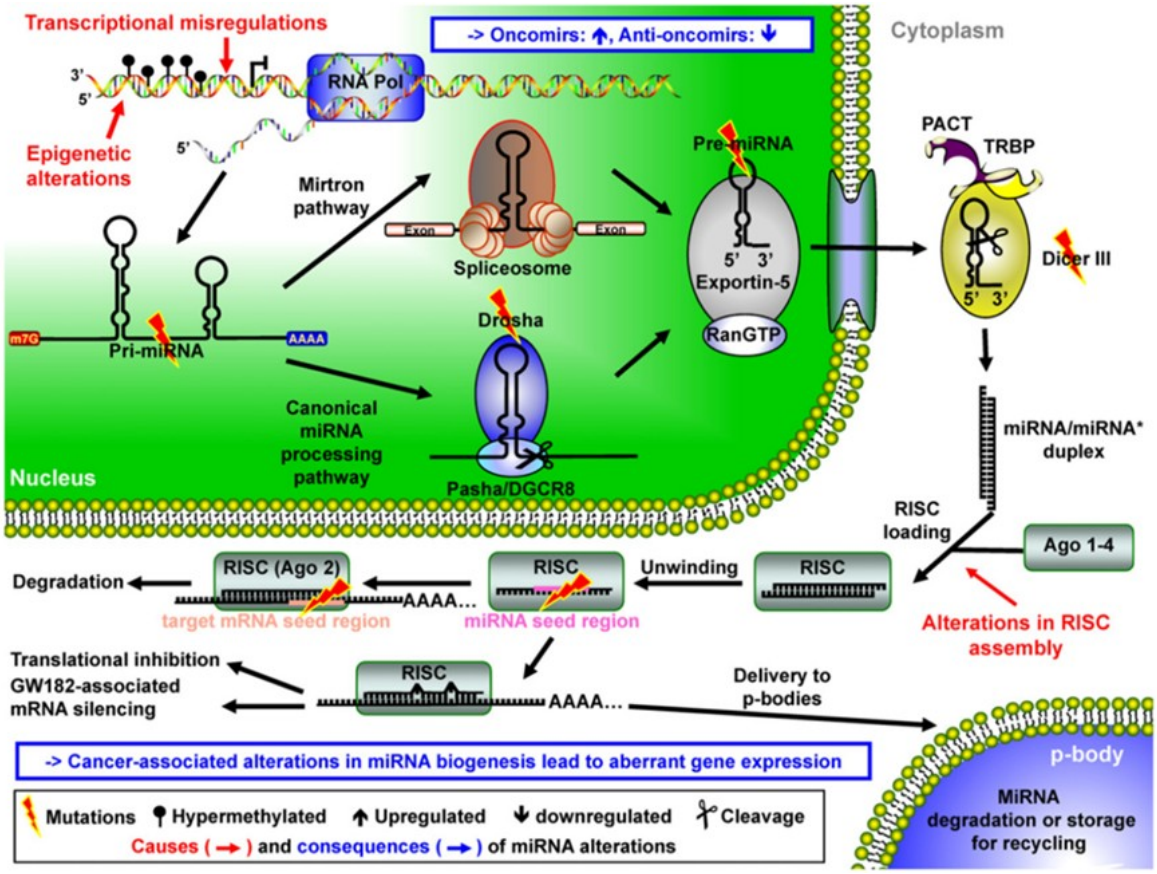

Figure 2: MicroRNA biogenesis and cancer-associated alterations in microRNA pathways (modified according to Karius et al 2012). Note, mutations can appear in intermediate stages of miRNAs (pri- and pre-miRNAs) as well as in the mature miRNA seed region, in the target mRNA sequence and in miRNA - processing proteins. Moreover, alterations in the expression pattern of miRNA - regulating transcription factors, prevention of the RISC assembly as well as aberrations in epigenetic mechanisms can increase expression of oncogenic miRNAs or suppress expression of tumor suppressive miRNAs. Finally, aberrant gene expression results as a consequence of alterations in the miRNAs biogenesis process.

1.3.3 Hypoxia as a regulator of miRNA expression in human cancers

Hypoxia is a common feature in malignant cancers that is associated with increased tumor invasiveness and resistance to therapy (Harris 2002). Kulshreshtha and co-workers demonstrated a specific microRNA signature of hypoxia (Kulshreshtha et al 2007). *MiR-23, miR-24, miR-26, miR-27, miR-103, miR-107, miR-181, miR-213* and *miR-210* were found to be induced in response to low oxygen, and for some of them direct regulation by hypoxia-inducible factor (HIF)-dependent mechanisms was demonstrated (Kulshreshtha et al 2007). *MiR-26, miR-107* and *miR-210* were also able to inhibit caspase activity in a hypoxic environment, which led to a decrease in the central components of apoptotic signaling (Kulshreshtha et al 2007). The majority of hypoxia-induced miRNAs are upregulated in several cancers (Kulshreshtha et al 2007). Moreover, *miR-98* has found to be upregulated in head and neck squamous cell carcinomas by hypoxic conditions (Hebert et al 2007). Interestingly, *HMGA2*, a target of *miR-98* had potential therapeutic implications, as *HMGA2* expression was associated with enhanced selective chemosensitivity towards doxorubicin in cancer cells. *MiR-98* overexpression could participate in a well-documented increase in chemoresistence of tumors characterized by low oxygenation (Kulshreshtha et al 2007).

1.3.4 MiRNAs in gliomas and potential therapeutic implications

The use of miRNAs as tumor biomarkers has gained growing interest in the last few years. MiRNAs influence the expression of numerous genes and thus finely tune critical points in disease pathways, restoration of native miRNA expression signatures is a promising therapeutic goal that could either be used as a direct anti-cancer treatment or as a part of a combination therapy, which than increase the sensitivity of tumor cells to traditional chemotherapeutics (Karius et al 2012).

More than one hundred studies have been published to date that address the role of miRNA in gliomas. Most of these reports examined the expression, targets and functional effects of selected miRNAs in glioma tissues *in situ* or glioma cells *in vitro*. Selected microRNAs that were investigated in more than a single publication are discussed in the following paragraphs.

miR-21

MiR-21 was the first miRNA that was linked to glioma pathogenesis. This particular miRNA was reported to be overexpressed in human glioma cells and most reports described *miR-21* as an oncogenic miRNA (Chan et al 2005, Conti et al 2009). Interestingly, *miR-21* levels correlated with tumor grade in gliomas and low *miR-21* levels in human tumors were associated with slightly better survival according to the cancer genome atlas (Gabriely et al 2008, Malzkorn et al 2010). Inhibition of *miR-21* induced glioma cell apoptosis, repressed growth, inhibited invasion, induced chemosensitization and inhibited *in vivo* xenograft growth (Chan et al 2005, Corsten et al 2007, Gabriely et al 2008, Zhang et al 2012). *MiR-21* induces glioma cell migration through inhibiting the matrix metalloproteinase regulators *RECK* and *TIMP3* (Gabriely et al 2008). Moreover, it may affect apoptosis and cell cycle regulation by inhibiting *heterogeneous nuclear ribonucleoprotein K* (*HNPRK*), the *tumor suppressor homologue of p53* (*Tap63*), *programmed cell death 4* (*PDCD4*), *EGFR* as well as *cyclin D* and *Bcl2* (Chen et al 2008, Papagiannakopoulos et al 2008, Zhou et al 2010). Interestingly, downregulation of *miR-21* contributed to the antitumor effects of IFN-beta (Zhang et al 2012). Ohno and colleagues pointed out that *miR-21* expression is negatively regulated by *STAT3* activation in human glioma cells and xenografts (Ohno et al 2009).

miR-221/miR-222

Several studies revealed *miR-221/miR-222* upregulation in gliomas (Gillies and Lorimer 2007). *MiR-221* was one of the most frequently upregulated miRNAs in human glioma tumors and cell lines (Ciafre et al 2005), and the *miR-221* levels were found to be higher in higher-grade tumors (Conrad and Barton 1978). In contrast, one report demonstrated significant downregulation of *miR-221/222* in glioblastomas associated with a better patient prognosis (Slaby et al 2010). The tumor suppressor and negative regulator of the cell cycle *p27* was identified as a direct target of *miR-221/miR-222* and downregulation of *p27* mediated the proliferative effects of *miR-221/miR-222* in glioma cells (Gillies and Lorimer 2007, Zhang et al 2009a). Knockdown of *miR-221/miR-222* indirectly led to *STAT1/2* upregulation (Zhang et al 2010).

miR-181a/miR-181b/miR-181c

In contrast to *miR-21* and *miR-221/miR-222*, which are upregulated in gliomas, *miR-181a*, *miR-181b* and *miR-181c* were identified as miRNAs that are downregulated in glioblastoma cells and tumors (Ciafre et al 2005). Both, *miR-181a* and *miR-181b* were reported as tumor suppressors that may inhibit growth and induce apoptosis of glioma cells (Shi et al 2008). *MiR-181a* overexpression sensitized glioma cells to radiation treatment concurrent with the downregulation of *Bcl2* (Chen et al 2010a). Moreover, expression of *miR-181b* and *miR-181c* was significantly decreased in patients who responded to radiation therapy and temozolomide related to patients with progressive disease. Therefore, expression levels of *miR-181b* and *miR-181c* may serve as a predictive marker of response to radiation therapy and temozolomide in glioblastoma patients (Slaby et al 2010).

miR-26a

MiR-26a was identified as a regulator of the *PTEN* tumor suppressor in gliomas (Huse et al 2009, Kim et al 2010). *PTEN* is frequently mutated and/or deleted in human glioblastomas (Abounader 2009, Li et al 2009). Huse and colleagues demonstrated that *miR-26a*-mediated *PTEN* repression in a mouse glioma model enhanced *de novo* tumor formation and precluded loss of heterozygosity at the *PTEN* locus (Huse et al 2009). Kim and co-workers found out that *miR-26a* was a cooperating component of a frequently occurring amplicon that also contained *CDK4* and *CENTG1*, two oncogenes which regulated the RB1 and PI3K/AKT pathways (Kim et al 2010). Furthermore, they found several targets of *miR-26a* in glioblastoma, including *PTEN*, *RB1* and *MAP3K2/MEKK2*. (Kim et al 2010). Interestingly, *miR-26a* alone could transform cells and promoted glioblastoma cell growth *in vitro* as well as in the mouse brain through decreased PTEN, RB1 and MAP3K2/MEKK2 protein expression, resulting in increased AKT activation, promoting proliferation and decreasing c-JUN N-terminal kinase-dependent apoptosis. Overexpression of *miR-26a* promoted tumor growth *in vivo* in *PTEN*-competent and *PTEN*-deficient glioblastoma cells and increased growth in *CDK4* or *CENTG1* overexpressing cells (Kim et al 2010). Glioblastoma patients whose tumors carry these amplifications displayed markedly decreased survival. Therefore, Kim and colleagues identified *miR-26a*, *CENTG1* and *CDK4* as a functionally integrated oncomir/oncogene DNA cluster that regulates aggressiveness in human malignant gliomas through targeting the pathways of RB1, PI3K/AKT and JNK (Kim et al 2010).

1.4 Goals and experimental approach of this study

The aim of this study was to identify miRNAs regulated by epigenetic changes and/or induced under hypoxic conditions in gliomas. The project was started by determining the expression of 365 distinct human miRNAs by stem-loop real-time reverse transcriptase PCR in four established glioblastoma cell lines (A172, U138MG, T98G, TP365MG), either untreated or treated with the demethylating agent 5-aza-2`-deoxycytidine (5-Aza) and the histone deacetylase inhibitor trichostatin A (TSA). A total of 50 miRNAs showed significantly higher expression levels in at least two of the four AZA/TSA-treated glioma cell lines when compared to the respective non-treated control cells. Among these candidate-miRNAs, *miR-132* and *miR-126* were selected for independent validation experiments and expression profiling of a larger series of 125 primary gliomas of different types and WHO grades. Moreover, promoter methylation analyses and ChIP (chromatin immunoprecipitation) studies were carried out to assess the role of epigenetic modifications, in particular DNA methylation and histone modifications, in the observed down-regulation of these miRNA in gliomas. Furthermore, these two miRNAs were functionally characterized by assessing the effect of overexpression of the respective pre-miRNAs in glioma cell lines on cell viability, proliferation and apoptosis. In addition, gene expression profiling was carried out to identify *miR-132* and *miR-126* regulated targets. Western-blot-analysis and 3'-UTR luciferase assays were used to validate *SIRT1* and *JARID1A* as direct targets of *miR-132*.

A second part of this doctoral thesis addressed the identification of miRNAs induced in glioma cells by hypoxia. Among those miRNAs demonstrating significantly up-regulated expression in all four investigated glioma cell lines exposed to hypoxia, *miR-210* was selected for further analyses. Independent validation experiments by targeted real-time stem-loop RT-PCR expression analyses revealed that hypoxia induced expression of *miR-210* in glioblastoma cell lines via HIF-1α. For the validation of putative target genes regulated by *miR-210* in glioma cells, dual-luciferase assays were carried out and identified *GPD1L* and *COX10* as direct targets of *miR-210* in glioblastoma cells.

Collectively, a variety of experimental approaches and different techniques based on the molecular analysis of primary glioma tissue specimens as well as cultured glioma cells were performed to improve our understanding of the role of aberrant miRNA expression in glioma pathogenesis, ranging from the characterization of tmechanisms leading to altered transcription of miRNA genes to the identification of novel target genes directly regulated in these tumors by aberrant miRNAs.

2 Materials

2.1 Tumor tissues samples and cell lines

All investigated tissue samples were selected from the tumor tissue collection of the Department of Neuropathology, Heinrich-Heine-University, Düsseldorf. These tissue samples were analyzed according to protocols approved by the institutional review board of Heinrich-Heine-University Düsseldorf. All tumors were classified according to the criteria of the World Health Organization (WHO) classification of tumors of the nervous system (Louis et al 2007b). Parts of each tumor were snap-frozen immediately after operation and stored at -80°C. Only tissue samples with an estimated tumor cell content of about 80% were used for molecular analyses.

The investigated tumor series comprised 125 human gliomas, including 54 primary glioblastomas, WHO grade IV (pGBIV), eight secondary glioblastoma (sGBIV), 11 anaplastic astrocytomas, WHO grade III (AAIII), seven diffuse astrocytomas, WHO grade II (AII), ten anaplastic oligoastrocytomas, WHO grade III (AOAIII), five oligoastrocytomas, WHO grade II (OAII), nine anaplastic oligodendrogliomas, WHO grade III (AOIII), and ten oligodendrogliomas, WHO grade II (OII) and eleven pilocytic astrocytomas (PAI).

In collaboration with Dr. Bernhard Radlwimmer (Molecular Genetics, DKFZ, Heidelberg) a mRNA expression profiling using oligonucleotide microarrays was performed in a large, partially overlapping series of 70 human astrocytic gliomas of different WHO grades (AAIII, anaplastic astrocytoma, WHO grade III; sGBIV, secondary glioblastoma, WHO grade IV; pGBIV, primary glioblastoma, WHO grade IV) and four normal brain tissue samples (NB) (Toedt et al 2011). These data were available for comparative analyses between selected miRNA genes and putative target mRNAs.

In collaboration with Prof. Dr. med. Markus Riemenschneider (Department of Neuropathology, University Hospital Regensburg) and Dr. Sabit Delic the expression of miRNAs was determined in the infiltration zone versus the solid tumor parts of five primary glioblastomas (WHO grade IV) and two anaplastic astrocytomas (WHO grade III).

The commercially available human non-neoplastic brain tissue RNA and DNA samples used for reference purposes are listed in the following Table 1.

Table 1: Commercially available RNA and DNA samples investigated in the study.

commercially available RNA	source	used for
total RNA-human normal tissue brain- ocipital lobe	BioChain Institute, Hayward, CA	1
total RNA-human normal tissue brain- temporal lobe	BioChain Institute, Hayward, CA	1
total RNA-human normal tissue brain- cerebral cortex	BioChain Institute, Hayward, CA	1
total RNA-human normal tissue brain-frontal lobe	BioChain Institute, Hayward, CA	1
total RNA-human normal tissue brain-corpus callosum	BioChain Institute, Hayward, CA	1
total RNA-human normal tissue brain	BioChain Institute, Hayward, CA	1/2
hu brain total RNA	Clontech, Mountain View, CA	1/2
hu fetal brain total RNA	Clontech, Mountain View, CA	1
MVP total RNA-human adult brain	Stratagene, Cedar Creek, TX	1/2
hu brain total RNA	Ambion, Huntington, UK	1/2
universal human reference RNA	Stratagene, Cedar Creek, TX	2
commercially available DNA	**source**	
CpGenome universal methylated DNA	Millipore AG, Billerica, US	3
genomic DNA human normal adult brain	BioChain Institute, Hayward, CA	3
genomic DNA human normal adult brain-occipital lobe	BioChain Institute, Hayward, CA	3
genomic DNA human fetal brain	BioChain Institute, Hayward, CA	3

1 = microRNA screening

2 = validation of the microRNA screening results

3 = sequencing of sodium bisulfite-modified DNA

2.1.1 Cell lines

Table 2 provides an overview of the different glioma cell lines used in this study. For the microRNA screening, total RNA samples from the following glioblastoma cell lines were available and used: A172 (untreated / 5-Aza+TSA treated), T98G (untreated / 5-Aza+TSA treated), U138MG (untreated / 5-Aza+TSA treated), TP365MG (untreated / 5-Aza+TSA treated), U251MG (untreated), U118MG (untreated), CRL1718 (untreated)

Table 2: Tumor cell lines used in this study.

glioma cell lines					
cell line	species	origin	source	cell line in culture	RNA available for screening or RNA extraction
A172	human	glioblastoma (WHO grade IV)	ATCC, Manassas, Virginia	yes	RNA available (UZ)
U138MG	human	glioblastoma (WHO grade IV)	ATCC, Manassas, Virginia	yes	RNA available (UZ)
T98G	human	glioblastoma (WHO grade IV)	ATCC, Manassas, Virginia	yes	RNA available (UZ)
TP365MG	human	glioblastoma (WHO grade IV)	V.P. Collins, Cambridge, UK	yes	RNA available (UZ)
U87MG	human	glioblastoma (WHO grade IV)	ATCC, Manassas, Virginia	yes	not investigated for screening
U118MG	human	glioblastoma (WHO grade IV)	ATCC, Manassas, Virginia	no	RNA available (UZ)
U251MG	human	glioblastoma (WHO grade IV)	ATCC, Manassas, Virginia	yes	RNA available (UZ)
G55TL	human	glioblastoma (WHO grade IV)	Sascha Seidel, Department of	no	RNA extraction by trizol
LN229	human	glioblastoma (WHO grade IV)	Neuropathology, Giessen, Germany	no	RNA extraction by trizol
CRL1718	human	astrocytoma (WHO grade IV)	ATCC, Manassas, Virginia	no	RNA available (UZ)
medulloblastoma cell line					
cell line	species	origin	source	cell line in culture	RNA available for screening or RNA extraction
DAOY	human	brain, cerebellum desmoplastic cerebellar medulloblastoma	ATCC, Manassas, Virginia	yes	not investigated for screening
glioblastoma stem cell lines					
cell line	species	origin	source	cell line in culture	RNA available for screening or RNA extraction
ED010	human	glioblastoma (WHO grade IV)	Sascha Seidel	no	RNA extraction by trizol
ED015	human	glioblastoma (WHO grade IV)	Department of Neuropathology	no	RNA extraction by trizol
ED022	human	glioblastoma (WHO grade IV)	Justus-Liebig-University	no	RNA extraction by trizol
ED026	human	glioblastoma (WHO grade IV)	Giessen	no	RNA extraction by trizol
ED031	human	glioblastoma (WHO grade IV)	Germany	no	RNA extraction by trizol
ED046x	human	glioblastoma (WHO grade IV)		no	RNA extraction by trizol
NCH644	human	glioblastoma (WHO grade IV)		no	RNA extraction by trizol
NCH421	human	glioblastoma (WHO grade IV)		no	RNA extraction by trizol
glioblastoma sphere cultures					
cell line	species	origin	source	cell line in culture	RNA available for screening or RNA extraction
GS1_p11	human	glioblastoma (WHO grade IV)	Prof. Dr. Katrin Lamszus	no	RNA extraction by trizol
GS2_p9	human	glioblastoma (WHO grade IV)	Department of Neurosurgery	no	RNA extraction by trizol
GS3_p27	human	glioblastoma (WHO grade IV)	University Hospital Hamburg	no	RNA extraction by trizol
GS4_p9	human	glioblastoma (WHO grade IV)		no	RNA extraction by trizol
GS5_p14	human	glioblastoma (WHO grade IV)		no	RNA extraction by trizol
GS7_p13	human	glioblastoma (WHO grade IV)		no	RNA extraction by trizol
GS8_p9	human	glioblastoma (WHO grade IV)		no	RNA extraction by trizol
GS9_p11	human	glioblastoma (WHO grade IV)		no	RNA extraction by trizol
GS11_p19	human	glioblastoma (WHO grade IV)		no	RNA extraction by trizol
GS12_p22	human	glioblastoma (WHO grade IV)		no	RNA extraction by trizol
GS13_p12	human	glioblastoma (WHO grade IV)		no	RNA extraction by trizol

2.1.2 Bacterial strains

For cloning experiments, chemically competent *Escherichia coli* DH5α (supE44, lac U169 (F 80lacZ M15), hsdR17, recA, endA1, gyrA96, thi-1, reA1) (Hanahan 1983) cells were used.

2.2 Laboratory equipment

Table 3 summarizes the most important laboratory equipment that was used in this study.

Table 3: Laboratory equipment used in this study.

equipment	version	manufacturer
bioanalyzer	2100	Agilent Technologies Inc., Santa Clara,CA
cell incubator	CB150	Binder GmbH, Tuttlingen
centrifuge	Rotina 46R	Hettich GmbH, Tuttlingen
centrifuge buckets and adapters		Heraeus, Hanau
centrifuge	BSB 6 und 4A	Gelaire, Sydney
centrifuge		Heraeus, Hanau
digital scale	ALC	Sartorius Ag, Göttingen
DNA sequencer	ABI PRISM ™ 377	Applied Biosystem, Foster City
ELISA reader, Paradigm ™ Detection Platform		Beckmann Coulter, Brea, CA
fast real-time PCR	7900 HT	Applied Biosystem, Foster City
fluorescence microscope	IX 50/ U-RFL-T	Olympus GmbH, Münster
freezer/fridge		Liebherr, Bulle, Swiss
freezer -80		Hettich GmbH, Tuttlingen
gel chamber (agarose gels)	Sub-Cell	PeqLab GmbH, Erlangen
gel chamber (protein)	Mini Protean	BioRad GmbH, München
gel documentation system		Bio-Budget GmbH, Krefeld
gel dryer	Model583	BioRad GmbH, München
imager	LAS-3000 mini	FUJIFILM, Düsseldorf
Laboratory Automation Workstation	Biomek FxP	Beckman Coulter, Brea, CA
Low Density Array Thermal Cycling Block		Applied Biosystem, Foster City
Low Density Array Sealer		Applied Biosystem, Foster City
Milli-Q-water		Millipore AG, Billerica, US
PCR thermocycler	T3	Biometra GmbH, Göttingen
pH meter	pH 525	WTW, Weilheim
pipettes		Gilson Inc., Middleton
pipettor		Labbay BV, Geldmeralsen, NL
photometer	nanodrop ND1000	PeqLap GmbH, Erlangen
power supply	PowerPAC 3000	BioRad GmbH, München
real time PCR	StepOnePlus™	Applied Biosystem, Foster City
7900HT System heated cover		Applied Biosystem, Foster City
refrigerated centrifuge	EBA 12R	Hettich GmbH, Tuttlingen
sequence detection system	ABI PRISM ®7900HT	Applied Biosystem, Foster City
shaker	3013	GFL GmbH, Burgwedel
swing out rotor	SW41 TI	Beckman Coulter, Brea, CA
table centrifuge	5417	Eppendorf AG, Hamburg
thermobloc	TD	Falc, Treviglio, Italy
ultracentrifuge	L8-M	Beckman Coulter, Brea, CA
ultrasonic processor	Vibracell 75022	Novodirect GmbH, Kehl/Rhein
ultra turrax	T25	IKA-Werke GmbH, Staufen
vacuum pump		KnF GmbH, Freiburg
vortexer	Zx3	VELP Scientifica, Usmate, Italy
water bath		GFL GmbH, Burgwedel
western blot chamber		BioRad GmbH, München

2.3 Consumables

Table 4 provides an overview of the different types of consumables used in this study.

Table 4: Consumables used in the study.

consumables	manufacturer
biotinylated protein ladder	Cell Signaling, Danvers, MA
cell dishes/flasks/well plates	Thermo Fisher Scientific, Waltham, MA
conical tubes (15 ml; 50 ml)	Greiner AG, Kremsmünster
cryo tubes	Thermo Scientific, Waltham, MA
DEPC treated water	Carl Roth GmbH, Karlsruhe
disposable pipet (1 ml, 5 ml, 10 ml, 25 ml)	Corning Inc., Corning, NY
DPBS (Dulbecco`s Phosphate buffered Saline)	LifeTechnologies, Carlsbad, CA
DMEM (Dulbecco`s Modified Eagle Medium)	LifeTechnologies, Carlsbad, CA
DNA ladder (100 bp)	Bio-Budget GmbH, Krefeld
DNA ladder (1 kbp)	Bio-Budget GmbH, Krefeld
dNTPs	Bio-Budget GmbH, Krefeld
DTT (dithiothreitol)	LifeTechnologies, Carlsbad, CA
fast AP ™ thermosensitive alkaline phosphatase	Fermentas GmbH, St. Leon-Rot
FCS (fetal calf serum)	LifeTechnologies, Carlsbad, CA
filter paper	Whatman GmbH, Dassel
first strand buffer (5x)	LifeTechnologies, Carlsbad, CA
gloves	Semperit GmbH, Wien
nitrocellulose membrane	Whatman GmbH, Dassel
PCR plates	Applied Biosystem, Foster City
PCR tubes	Bio-Budget GmbH, Krefeld
pd (N6), random hexamer phosphorylated	GeneLink, Hawthorne, NY
penicillin/ streptavidin	LifeTechnologies, Carlsbad, CA
pipets	VWR GmbH, Darmstadt
pipet tips (normal, plugged)	StarLab GmbH, Ahrensburg
prestained protein ladder	Fermentas GmbH, St. Leon-Rot
protease inhibitor tablets	Roche GmbH, Grenzach-Wyhlen
Q-solution	Qiagen, Hilden
reaction tubes (2 ml; 1.5 ml; 0.5 ml)	Sarstedt AG, Nümbrecht Eppendorf AG, Hamburg
trypsin EDTA	PAA GmbH, Pasching
ultracentrifuge polyallomer tubes	Herolab GmbH, Wiesloch
well plates (96, 24, 6)	Thermo Scietific, Waltham, MA

2.4 Chemicals, enzymes and antibodies

The various chemicals, enzymes and antibodies used in this study are listed in the following Tables 5 - 7.

Table 5: Chemicals used in this study.

5-aza-2'-deoxycytidine	Sigma-Aldrich GmbH, Steinheim
acetic acid	Merck KGaA, Darmstadt
acrylamide (40 %)	Merck KGaA, Darmstadt
acrylamide/bisacrylamide (40 %; 19:1)	Merck KGaA, Darmstadt
acrylamide/bisacrylamide (30 %; 37,5:1)	Carl Roth GmbH, Karlsruhe
acrylamide/bisacrylamide (30 %; 29:1)	Carl Roth GmbH, Karlsruhe
agarose	Bio-Budget GmbH, Krefeld
ammonium acetate	Fluka Chemie AG, Buchs, CH
ammonium persulphate	Sigma-Aldrich GmbH, Steinheim
bisacrylamide (2 %)	Merck KGaA, Darmstadt
bromophenole blue	Sigma-Aldrich GmbH, Steinheim
BSA (bovine serum albumin)	Carl Roth GmbH, Karlsruhe
calcium chloride	Merck KGaA, Darmstadt
chlorophorm	Merck KGaA, Darmstadt
deoxycholate	Sigma-Aldrich GmbH, Steinheim
DMSO (dimethyl sulfoxide)	Sigma-Aldrich GmbH, Steinheim
EDTA (ethylendiamintetraacetat)	Sigma-Aldrich GmbH, Steinheim
ethanol	Merck KGaA, Darmstadt
ethidiumbromid	Sigma-Aldrich GmbH, Steinheim
formamid	Merck KGaA, Darmstadt
formaldehyde	Merck KGaA, Darmstadt
glycerol	Merck KGaA, Darmstadt
glycine	Carl Roth GmbH, Karlsruhe
guanidinisothiocyanat	Carl Roth GmbH, Karlsruhe
hepes	Carl Roth GmbH, Karlsruhe
hydrochloric acid	Merck KGaA, Darmstadt
immobilon ™ western HRP substrate luminol reagent	Millipore AG, Billerica, US
immobilon ™ western HRP substrate peroxide solution	Millipore AG, Billerica, US
isoamylalcohol	Merck KGaA, Darmstadt
isopropanol	Merck KGaA, Darmstadt
mercaptoethanol	Fluka Chemie AG, Buchs, CH
methanol	Merck KGaA, Darmstadt
magnesium chloride	Carl Roth GmbH, Karlsruhe
milk powder	Carl Roth GmbH, Karlsruhe
nitric acid	Merck KGaA, Darmstadt
NP-40	Fluka Chemie AG, Buchs, CH
OPTI-MEM® reduced serum media	LifeTechnologies, Carlsbad, CA
phenol	Carl Roth GmbH, Karlsruhe
phenylmethanesulfonyl fluoride	Sigma-Aldrich GmbH, Steinheim
ponceau S	Sigma-Aldrich GmbH, Steinheim
potassium chloride	Merck KGaA, Darmstadt
SDS (sodium dodecyl sulfate) 20 % stock solution	Carl Roth GmbH, Karlsruhe
sodium acetate	Merck KGaA, Darmstadt
sodium carbonate	Merck KGaA, Darmstadt
sodium chloride	Carl Roth GmbH, Karlsruhe
supersignal west pico chemiluminescent substrate	Thermo Scientific, Waltham, MA
TEMED (N-N-N-N-tetraethylmethyldiamine)	Sigma-Aldrich GmbH, Steinheim
trichostatin A	Sigma-Aldrich GmbH, Steinheim
tricin	Sigma-Aldrich GmbH, Steinheim
tris	Merck KGaA, Darmstadt
tritonX-100	Carl Roth GmbH, Karlsruhe
trypton/pepton from casein	Carl Roth GmbH, Karlsruhe
tween-20	Carl Roth GmbH, Karlsruhe
urea	Merck KGaA, Darmstadt

Table 6: Enzymes used in this study.

enzymes	manufacturer
Taq DNA polymerase (#203205)	Qiagen, Hilden
Not I (10.000 U/ml)	New England BioLaps, Ipswich, USA
proteinase K (#70633)	Merck KGaA, Darmstadt
protease inhibitor tablets(#11836170001)	Roche GmbH, Grenzach-Wyhlen
RNAse A (#1010914200)	Roche GmbH, Grenzach-Wyhlen
RNAsin (#EO0381)	Fermentas GmbH, St. Leon-Rot
reverse transcriptase (#100004925)	LifeTechnologies, Carlsbad, CA
taq polymerase (#10342-020)	LifeTechnologies, Carlsbad, CA
T4 DNA ligase	LifeTechnologies, Carlsbad, CA
Xho I (20.000 U/ml)	New England BioLaps, Ipswich, USA

Table 7: Antibodies used in this study.

antibodies	dilution	manufacturer	catalog no.
goat-anti-biotin	1:1000 in TBS-T + 5 % milk	Cell Signaling, Danvers, MA	#7075
goat anti-rabbit	1:5000 in TBS-T + 5 % BSA	Thermo Fisher Scietific, Waltham, MA	#J6-126203)
goat-anti-mouse	1:5000 in TBS-T + 5 % BSA	Thermo Fisher Scietific, Waltham, MA	#31444
mouse anti-tubulin	1:10000 in TBS-T + 5% milk	Sigma-Aldrich GmbH, Steinheim	#T9026
rabbit anti-Histon H3ac (1 mg/ml)	10 µl per 2 ml	Upstate, Charlottesville, VA	#06-599
rabbit anti-Histon H4ac (1 mg/ml)	10 µl per 2 ml	Upstate, Charlottesville, VA	#17-630
mouse-SIRT1 (B-10)	1:100 in TBS-T + 5 % milk	Santa Cruz Inc., Santa Cruz, CA	sc-74504
rabbit-ß-actin antibody	1:1000 in TBS-T + 5 % BSA	Cell Signaling, Danvers, MA	#4967

2.5 Kits, reagents and assays

The following Table 8 provides a list of the different kits, reagents and assays that were employed in this study.

Table 8: Kits, reagents and assays used in this study.

Kits, reagents, assays	manufacturer
Apo-ONE® Homogeneous Caspase-3/7 Assay (#G7790)	Promega, Madison, WI
BigDye® terminator v1.1 cycle sequencing kit (#4336774)	Applied Biosystem, Foster City
Cell Proliferation ELISA BrdU chemiluminescence (#1669915)	Roche GmbH, Grenzach-Wyhlen
CellTiter-Glo® Luminescent Cell Viability Assay (#G7572)	Promega, Madison, WI
Chromatin Immunoprecipitate (ChIP) Assay Kit (#17-245)	Upstate, Charlottesville, VA
DNA clean up system (#A7280)	Promega, Madison, WI
Dual-Glo® Luciferase Assay System (#E2940)	Promega, Madison, WI
EZ DNA methylation-Gold ™ Kit (#D5006)	Zymo Research EZ, Irvine, CA
Invisorb® DNA clean up (#1020400300)	Stratec molecular GmbH, Birkenfeld
Jetquick Gel Extraction Kit (#420250)	GENOMED GmbH, Löhne
RNeasy® Plus Mini Kit (50) (#74134)	Qiagen, Hilden
NE-PER® Nuclear and Cytoplasmic Extraction Reagents (#78833)	Thermo Scietific, Waltham, MA
PeqGOLD Plasmid Mini Prep Kit (#12-6942-02)	PeqLab GmbH, Erlangen
PCR product purification spin kit (#410250)	GENOMED GmbH, Löhne
Platinum® SYBR® Green (#11733-046)	Invitrogen, Carlsbad, CA
RC DC protein assay (#500-0122)	BioRad GmbH, München
Rneasy Mini Eluate Cleanup Kit (#74204)	Qiagen, Hilden
TaqMan® Low Density Custom Arrays (Part No.: 4342265)	Applied Biosystem, Foster City
TaqMan® Universal PCR Master Mix (#4326614)	Applied Biosystem, Foster City
TaqMan® MicroRNA Reverse Transcription Kit (#4366596)	Applied Biosystem, Foster City
TRIzol®-reagent (#15596-018)	Invitrogen, Carlsbad, CA

2.6 Solutions and buffers

All solutions and buffers used in this study are listed in Table 9 a-c.

Table 9a: Solutions and buffers used in this study.

solutions	content
CHIP-analysis	
swelling buffer (1x)	25 mM HEPES, pH 7.8 1.5 mM MgCl2 10 mM KCl 0.1 % NP-40 1 mM DTT + 0.5 mM PMSF
elution buffer	0.1 M sodium bicarbonate 1 % SDS
separation of nuclei (CHiP analysis)	
nuclei extraction buffer	0.32 M sucrose 5 mM CaCl2 3 mM Mg(Ac)2 0.1 mM EDTA 10 mM Tris-HCl 1x protease inhibitor 0.1 mM PMSF 0.1 % Triton X-100 0.1 % NP-40
sucrose cushion	1.8 M sucrose 3 mM Mg(Ac)2 10 mM Tris-HCl (pH: 8)

Table 9b: Solutions and buffers used in this study.

solutions	content
DNA, RNA and protein extraction by ultracentrifugation	
GITC solution (4 M)	500 g guanidinisothiocyanate 26.6 ml sodium citrate (1 M, pH 7) 8.5 ml ß-mercaptoethanol 1058 ml distilled water pH 7 with NaOH
RNAsin mix	90 µl RNAsin (40 U/µl) 193.5 µl DTT (0.1 M) 6916.5 µl DEPC-treated water
CsCl solution	479.85 g caesium chloride 4.2 ml sodium acetate (3 M; pH 5) ad 500 ml DEPC-treated water
proteinase K buffer:	0.01 M Tris/HCl 0.005 M EDTA 0.5 % SDS
SDS-PAGE and western blot	
cell lysis buffer	50 mM Tris-HCl, pH: 8.0 150 mM NaCl 0.5 % TritonX-100 0.5 % deoxycholate
blocking buffer	5 % milk in TBS with 0.1 % Tween
running buffer for tris-gels (10x)	0.25 M Tris 2 M glycine 1 % SDS
running buffer for tricin-gel (1x)	0.1 M tricin 0.1 M tris 1 g SDS
transfer buffer (1x)	25 mM Tris 0.2 M glycine 20 % methanol
ponceau S (0,1% (w/v))	1 g ponceau S 50 ml acetic acid In 1 l distilled water
laemmli buffer (4x)	0.1 M Tris pH 6.8 6 % SDS 40 % glycerol 0.04 % bromphenol blue 4 % ß-mercaptoethanol

Table 9c: Solutions and buffers used in this study.

solutions	content
additional buffer and media used in this study	
loading buffer for sequencing	76.2 % formamid 19 % 25 mM EDTA-solution pH 8 4.8 % dextran blue
loading buffer for agarose gels	30 % glycerol 0.25 % xylene cyanol 0.25 % bromphenol blue
TAE buffer (50x)	2 M Tris 1 M acetic acid 50 mM EDTA pH 8.0
TBE buffer (1x)	0.89 M Tris base 0.89 M boracic acid 20 mM EDTA pH 8.0
TE buffer (1x)	10 mM Tris 1 mM EDTA pH 7.5
TBS buffer (10x)	1.37 M NaCl 0.2 M Tris pH 7.6
Binding buffer 100x	0.82 M $CaCl_2$ in steril water
LB media	1 % Bacto-Trypton 0.5 % Yeast-Extract 1 % NaCl (15 % Agar) 100 µg/ml Ampicillin
Lysis buffer	50 mM Tris-base, pH 8.0 150 mM NaCl 0.5 % TritonX-100 0.5 % Deoxychlorate (DOX) 1 mini PhosSTOP Tablet in 10 ml buffer
RIPA – buffer	1 x PBS 1 % TritonX-100 0.5 % Sodium Deoxycholate 0.1 % SDS 1 Complete Protease Inhibitor Cocktail Tablet, EDTA free per 10 ml 1 mini PhosSTOP tablet in 10 ml buffer
RNase A solution (10mg/ml)	25 mg RNase A in 10 mM Tris-base (pH: 7.5)

2.7 Gels

All gels used in this study are listed in Table 10.

Table 10: Gels used in this study.

gels	compounds
agarose gels (2 %)	2 g agarose 100 ml 1x TAE buffer
gels for sequencing (7 %; 29:1; 10 M urea)	21 g urea 8.4 ml acrylamid/bisacrylamide (30 %; 29:1) 6 ml 10x TBE 20 ml distilled water 350 µl APS (10 %) 30 µl TEMED
Tris-base separating gel (8 %)	1.4 ml acrylamid/bisacrylamide (30 %; 37.5:1) 1.3 ml tris (1.5 M; pH 8.8) 2.3 ml distilled water 0.025 ml SDS (20 %) 0.05 ml APS (10 %) 0.002 ml TEMED
tris stacking gel (5 %)	0.34 ml acrylamid/bisacrylamide (30 %; 37.5:1) 0.26 ml tris (1.5 M; pH 8.8) 1.36 ml distilled water 0.01 ml SDS (20 %) 0.02 ml APS (10 %) 0.002 ml TEMED
tricin separating gel (15 %)	7.5 ml acrylamid/bisacrylamide (30 %; 37.5:1) 5.18 tris (3 M, pH 8.5) 2.57 distilled water 0.05 ml APS 0.002 ml TEMED
tricin stacking gel (5 %)	0.7 ml acrylamid/bisacrylamide(30 %; 37.5:1) 1.27 tris (3 M, pH 8.5) 3.08 distilled water 0.02 ml APS 0.002 ml TEMED

2.8 Mature miRNAs and pre-miRNAs

All mature miRNAs, pre-miRNAs and scrambled oligonucleotides used in studiy are listed in Table 11.

Table 11: MiRNAs, pre-miRNAs and scrambled control oligonucleotides used in the study.

miRNAs/pre-miRNAs/scrambled oligonucleotides	manufacturer
mature miRNAs	Applied Biosystem, Foster City
TaqMan® MicroRNA Assays **hsa-miR-132** AB Assay ID:000457 Part Number: 4427975	
TaqMan® MicroRNA Assays **hsa-miR-126** AB Assay ID:000450 Part Number: 4427975	Applied Biosystem, Foster City
TaqMan® MicroRNA Assays **hsa-miR-210** AB Assay ID:000512 Part Number: 4427975	Applied Biosystem, Foster City
TaqMan® MicroRNA Assays **hsa-miR-30e-5p** AB Assay ID:000421 Part Number: 4427975	Applied Biosystem, Foster City
TaqMan® MicroRNA Assays **hsa-miR-218** AB Assay ID:000521 Part Number: 4427975	
pre- miRNAs	
Ambion Pre-miR miRNA Precursor **hsa-miR-132-3p** Pre-miR ID: PM10166	Applied Biosystem, Foster City
Ambion Pre-miR miRNA Precursor **hsa-miR-126-3p** Pre-miR ID: PM12841	Applied Biosystem, Foster City
Ambion Pre-miR miRNA Precursor **hsa-miR-210** Pre-miR ID: PM10516	Applied Biosystem, Foster City
Ambion Pre-miR miRNA Precursor **hsa-miR-212-3p** Pre-miR ID: PM10340	Applied Biosystem, Foster City
scrambled olinucleotides	
Pre-miR™ miRNA Precursor Molecules—Negative Control #1 Part Number: AM17110	Applied Biosystem, Foster City
Cy™3 dye-labeled Pre-miR™ Negative Control #1 (#AM17120)	Applied Biosystem, Foster City

2.9 Oligonucleotides

All oligonucleotides (Tables 12 - 14) were ordered from Eurofins MWG GmbH (Ebersberg, Germany).

Table 12: Primers used for mRNA expression.

application	gene	primer sequence	fragment size (bp)
Real-time-RT-PCR	*SIRT1*	5`- GCTCGCCTTGCTGTAGACTT - 3` (forward) 5`- TGTGACAGAGAGATGGCTGG - 3` (reverse)	142
	JARID1A	5`- TCCTGGATCTGTATGCTTTGA - 3`(forward) 5`- CAGTTCCTTTTCCTGGCAGA - 3` (reverse)	123
	BTG2	5`- AGCGAGCAGAGGCTTAAGGT - 3` (forward) 5`- GATGATGGGGTCCATCTTGT - 3` (reverse)	144
	PLAGL2	5`- AGGCGGAGAGTCAAGTGAAG - 3` (forward) 5`- GTCCTTGCGGTGAAACATCT - 3` (reverse)	236
	GPD1L	5`- CCCTGAAAGTGTGCATCGT - 3` (forward) 5`- CTGCCATTCACTGTTTCTTCA - 3` (reverse)	136
	COX10	5`- GTTGCGTAGGAGGCTCTGTC - 3` (forward) 5`- ACTTGCTGGTTGTGGCTTCT - 3` (reverse)	172
	p21/CDKN1A	5`- GCAGACCAGCATGACAGATTT - 3` (forward) 5`- AAGATGTAGAGCGGGCCTTT - 3` (reverse)	130
	ß-2-MG	**3`end:** 5`- GTTGCTCCACAGGTAGCTCTAG - 3` (forward) **3`end:** 5`- ACAAGCTTTGAGTGCAAGAGATTG - 3` (reverse) **5`end:** 5`- GTCTCGCTCCGTGGCCTTAG - 3` (forward) **5`end:** 5`- CATTCTCTGCTGGATGACGTGAG - 3` (reverse)	110 128
	ARF1	5´- GACCACGATCCTCTACAAGC - 3´ (forward) 5´- TCCCACACAGTGAAGCTGATG - 3` (reverse)	111
	GAPDH	5`- CATGACAACTTTGGTATCGTG - 3` (forward) 5`- GTCCACCACTGACACGTTG - 3` (reverse)	240
	U6 snRNA	5`- CTCGCTTCGGCAGCACA - 3` (forward) 5`- AACGCTTCACGAATTTGCGT - 3` (reverse)	94
Amplification of genomic sequences	*GAPDH*	5`- TACTAGCGGTTTTACGGGCG - 3` (forward) 5`- TCGAACAGGAGGAGCAGAGAGCGA - 3` (reverse)	166

Table 13: Primers used for sodium bisulfite sequencing and ChIP analyses.

application	miRNA	annotation	primer sequence	fragment size (bp)
Sodium bisulfite sequencing	***miR-132***	5´-CpG genomic region (1)	5`- TTTGGTTGGGATATTTTGGT – 3` (5`CpG 1-F) 5`- AAAATAACAATCTACAACCATA - 3` (5`CpG 1-R)	280
		5´-CpG genomic region (2)	5`- TTTGAGGGACGGGGATTG - 3` (5`CpG 2-F) 5`- ACCCCCTCTAAAACATCTTTA - 3` (5`CpG 2-R)	312
		5´-CpG genomic region (3)	5`- TTTGGGAGAATGGCGTAGG - 3` (5`CpG 3-F) 5`- CTTTTCCCATTTCCTAAATTC - 3` (5`CpG 3-R)	458
		5´-CpG genomic region (4)	5`- GAATTTAGGAAATGGGAAAAG - 3` (5`CpG 4-F) 5`- CCTCCCCGACCCCAAA - 3` (5`CpG 4-R)	175
		5´-CpG genomic region (5)	5`- TAGAGAGGTTTTGTATAGTT - 3` (5`CpG 5-F) 5`- CCCACTCCCTCTCCCATA - 3` (5`CpG 5-R)	343
		5´-CpG genomic region (6)	5`- TATGGGAGAGGGAGTGGG - 3` (5`CpG 6-F) 5`- CTATCCTCTAACCCCCATAA - 3` (5`CpG 6-R)	255
		5´-CpG genomic region (7)	5`- TTGGGGTTGTGTGTTTAG - 3` (5`CpG 7-F) 5`- AACTACGCTACCCTC - 3` (5`CpG 7-R)	383
		5´-CpG genomic region (8)	5`- TTGTGTAAGAAACGTTTTAAG - 3` (5`CpG 8-F) 5`- AACGAATAACAAACCTAAATAAC - 3` (5`CpG 8-R)	143
		5´-CpG genomic region (9)	5`- TAAGAGTTATAAGGATTCGGTT - 3` (5`CpG 9-F) 5`- ACATCTTCATATAACTAATAAAATTA -3` (5`CpG 9-R)	299
	miR-126	5´-CpG genomic region (1)	5`- TAATTTAATACGTTAAGGTTAG - 3` (5`CpG 1-F) 5`- AACAATAACTCTACTAAAACCC - 3` (5`CpG 1-R)	431
		5´-CpG genomic region (2)	5`- GGGTTTTGTTTGTATTTAG - 3` (5`CpG 2-F) 5`- CCCCAAACTCCCTCCTA - 3` (5`CpG 2-R)	343
	miR-210	5´-CpG genomic region	5`- GTGATTCGGGTGGGGTTTG - 3` (5`CpG-F) 5`- CCCCCTCCAAACTCCAAAA - 3` (5`CpG-R)	228
	miR-30e-5p	5´-CpG genomic region	5`- TTTGAGTAGAGGTGTGTGAGTGTG - 3` (5`CpG-F) 5`- CTCAAATTCCTTCATCACCCCCTAA - 3` (5`CpG-R)	362
ChIP	***miR-132***		5`- CGTGTCCGCACATCTGTCC - 3` (5`Histon-F) 5`- CGTCGGCAGCGCGTCAGTG - 3` (5`Histon-R)	181
	miR-126		5`- GGTGGTTTTCAGCCTGGG - 3` (5`Histon-F) 5`- GCAGTGACTCTGCTGGAAC - 3` (5`Histon-R)	239

Table 14: Primers used for 3`UTR luciferase reporter gene assays (miRNA target validation).

miRNA	luciferase constructs	primer sequence	fragment size (bp)
	psi-CHECK-2 (colony test PCR)	5´- GCGTGCTGAAGAACGAGC - 3´ (forward) 5´- CGAAGACTCATTTAGATCCTC - 3` (reverse)	insert dependent
miR-132	*wt-luc-SIRT1*	5` - gggtatctcgagGCTAGGACCATTACTGCCA - 3` (forward) 5`- ggctatgcggccgcAAAGTCAAATGACAATTTTAATAG - 3` (reverse)	388
	mut1-luc-SIRT1- OE - fragment 1	5` - gggtatctcgagGCTAGGACCATTACTGCCA - 3` (forward) 5`- GAGCTGAATTCACTGTAAAAATAATTTAAAAC - 3` (reverse)	212
	mut1-luc-SIRT1 - OE - fragment 2	5`- GTTTTAAATTATTTTTACAGTGAATTCAGCTC - 3` (forward) 5`- ggctatgcggccgcAAAGTCAAATGACAATTTTAATAG - 3` (reverse)	201
	mut1-luc-SIRT1 - OE	5` - gggtatctcgagGCTAGGACCATTACTGCCA - 3` (forward) 5`- ggctatgcggccgcAAAGTCAAATGACAATTTTAATAG - 3` (reverse)	381
	mut2-luc-SIRT1 - OE - fragment 1	5` - gggtatctcgagGCTAGGACCATTACTGCCA - 3` (forward) 5`- GTCATTATACAAAACATATGCCAGTAAATTAC - 3` (reverse)	277
	mut2-luc-SIRT1 - OE - fragment 2	5`- GTAATTTACTGGCATATGTTTTGTATAATGAC - 3` (forward) 5`- ggctatgcggccgcAAAGTCAAATGACAATTTTAATAG - 3` (reverse)	136
	mut2-luc-SIRT1 - OE	5` - gggtatctcgagGCTAGGACCATTACTGCCA - 3` (forward) 5`- ggctatgcggccgcAAAGTCAAATGACAATTTTAATAG - 3` (reverse)	381
	mut(1+2)-luc-SIRT1 - OE - fragment 1	5` - gggtatctcgagGCTAGGACCATTACTGCCA - 3` (forward) 5`- GAGCTGAATTCACTGTAAAAATAATTTAAAAC - 3` (reverse)	212
	mut(1+2)-luc-SIRT1 - OE - fragment 2	5`- GTTTTAAATTATTTTTACAGTGAATTCAGCTC - 3` (forward) 5`- ggctatgcggccgcAAAGTCAAATGACAATTTTAATAG - 3` (reverse)	194
	mut(1+2)-luc-SIRT1 - OE	5` - gggtatctcgagGCTAGGACCATTACTGCCA - 3` (forward) 5`- ggctatgcggccgcAAAGTCAAATGACAATTTTAATAG - 3` (reverse)	374
miR-132	*wt-luc-JARID1A*	5`- gggtatctcgagTGGCTTCATCAGAGGATGTG - 3` (forward) 5`- ggctatgcggccgcGATGGAGGAGGGAGTGCTAA - 3` (reverse)	349
miR-132	*wt-luc-BTG2*	5`- gggtatctcgagCTGGTTTGTGGGTTGAAACAA - 3` (forward) 5`-ggctatgcggccgcCTGTCAGAATAGCTTACAAAC - 3` (reverse)	272
miR-210	*wt-luc-GPD1L*	5`- gggtatctcgagCTTCACTCCCTGCGAGAAAT - 3` (forward) 5`-ggctatgcggccgcAAACTGGCATTGAGGGACAG - 3` (reverse)	369
	mut-luc-GPD1L - OE - fragment 1	5`- gggtatctcgagCTTCACTCCCTGCGAGAAAT - 3` (forward) 5`- CTTATTCCAGGTAATTCAGCAAAGCTGACATC -3` (reverse)	164
	mut-luc-GPD1L - OE - fragment 2	5`- GATGTCAGCTTTGCTGAATTACCTGGAATAAG - 3` (forward) 5`-ggctatgcggccgcAAACTGGCATTGAGGGACAG - 3` (reverse)	230
	mut-luc-GPD1L - OE	5`- gggtatctcgagCTTCACTCCCTGCGAGAAAT - 3` (forward) 5`-ggctatgcggccgcAAACTGGCATTGAGGGACAG - 3` (reverse)	362
miR-210	*wt-luc-COX10*	5`- gggtatctcgagTGTTTCTTCCTCCTCACATGG - 3` (forward) 5`- ggctatgcggccgcAGGGACCTGAGCTCACAGAA - 3` (reverse)	194
	mut-luc-COX10 - OE - fragment 1	5`- gggtatctcgagTGTTTCTTCCTCCTCACATGG - 3` (forward) 5`- GCTGGGCATGTGGAGGTGGTGTGGTGGTAAG - 3` (reverse)	100
	mut-luc-COX10 - OE - fragment 2	5`- CTTACCACCACACCACCTCCACATGCCCAGC - 3` (forward) 5`- ggctatgcggccgcAGGGACCTGAGCTCACAGAA - 3` (reverse)	118
	mut-luc-COX10 - OE	5`- gggtatctcgagTGTTTCTTCCTCCTCACATGG - 3` (forward) 5`- ggctatgcggccgcAGGGACCTGAGCTCACAGAA - 3` (reverse)	187
	OE = overlap extension polymerase chain reaction	ctcgag *Xho* I restriction site gcggccgc *Not* I restriction site	

2.10 Conditions used for glioma cell transfection

All investigated cell-based *in vitro* methods, glioma cell lines, cell counts, amounts of Lipofectamine 2000 and serum-reduced Opti-MEM, as well as the amounts of pre-miRNAs, 3`UTR-luciferase assay constructs, and time points after transfection are listed in Table 15.

Table 15: Overview of the investigated cell-based methods used in this study.

application	plates	Lipofectamine - Dilution			miRNA - Dilution		total RNA extraction protein extraction assay-system performance after transfection (h)
		cell seeding	Lipo-fectamine 2000 (µl)	serum reduced Opti-MEM (µl)	pre-miR molecules / pre-NC1 molecules (nM)	serum reduced Opti-MEM (µl)	
total RNA extraction	6-well	A172: 75,000 / well 2 ml	2	248	50 nM pre-miR-132 / 50 nM pre-NC1	in 250	72 h
			2	248	25 nM pre-miR-132 / 25 nM pre-NC1	in 250	72 h
			2	248	10 nM pre-miR-132 / 10 nM pre-NC1	in 250	72 h
			2	248	25 nM pre-miR-212 / 25 nM pre-NC1	in 250	72 h
			2	248	10 nM pre-miR-212 / 10 nM pre-NC1	in 250	72 h
			2	248	50 nM pre-miR-126 / 50 nM pre-NC1	in 250	72 h
			2	248	25 nM pre-miR-126 / 25 nM pre-NC1	in 250	72 h
			2	248	10 nM pre-miR-126 / 10 nM pre-NC1	in 250	72 h
		T98G: 50,000 / well 2 ml	2	248	50 nM pre-miR-132 / 50 nM pre-NC1	in 250	72 h
			2	248	25 nM pre-miR-132 / 25 nM pre-NC1	in 250	72 h
			2	248	10 nM pre-miR-132 / 10 nM pre-NC1	in 250	72 h
			2	248	25 nM pre-miR-212 / 25 nM pre-NC1	in 250	72 h
			2	248	10 nM pre-miR-212 / 10 nM pre-NC1	in 250	72 h
			2	248	50 nM pre-miR-126 / 50 nM pre-NC1	in 250	72 h
			2	248	25 nM pre-miR-126 / 25 nM pre-NC1	in 250	72 h
			2	248	10 nM pre-miR-126 / 10 nM pre-NC1	in 250	72 h
		U251: 60,000 / well 2 ml	2	248	50 nM pre-miR-132 / 50 nM pre-NC1	in 250	72 h
			2	248	25 nM pre-miR-132 / 25 nM pre-NC1	in 250	72 h
			2	248	10 nM pre-miR-132 / 10 nM pre-NC1	in 250	72 h
			2	248	50 nM pre-miR-126 / 50 nM pre-NC1	in 250	72 h
			2	248	25 nM pre-miR-126 / 25 nM pre-NC1	in 250	72 h
			2	248	10 nM pre-miR-126 / 10 nM pre-NC1	in 250	72 h
		DAOY: 60,000 / well 2 ml	2	248	50 nM pre-miR-132 / 50 nM pre-NC1	in 250	72 h
protein extraction	6-well	A172: 75,000 /well 2 ml	2	248	50 nM pre-miR-132 / 50 nM pre-NC1	in 250	72 h
			2	248	25 nM pre-miR-132 / 25 nM pre-NC1	in 250	72 h
			2	248	10 nM pre-miR-132 / 10 nM pre-NC1	in 250	72 h
		T98G: 50,000 / well 2 ml	2	248	50 nM pre-miR-132 / 50 nM pre-NC1	in 250	72 h
			2	248	25 nM pre-miR-132 / 25 nM pre-NC1	in 250	72 h
			2	248	10 nM pre-miR-132 / 10 nM pre-NC1	in 250	72 h
		U251: 60,000 / well 2 ml	2	248	50 nM pre-miR-132 / 50 nM pre-NC1	in 250	72 h
			2	248	25 nM pre-miR-132 / 25 nM pre-NC1	in 250	72 h
			2	248	10 nM pre-miR-132 / 10 nM pre-NC1	in 250	72 h
		DAOY: 75,000 / well 2 ml	2	248	50 nM pre-miR-132 / 50 nM pre-NC1	in 250	72 h
cell proliferation ELISA, BrdU (chemiluminescence) assay	96-well	A172: 2000 /100µl	0,2	24.8	25 nM pre-miR-132 / 25 nM pre-NC1	in 25	72 h
			0,2	24.8	10 nM pre-miR-132 / 10 nM pre-NC1	in 25	72 h
			0,2	24.8	25 nM pre-miR-126 / 25 nM pre-NC1	in 25	72 h
			0,2	24.8	10 nM pre-miR-126 / 10 nM pre-NC1	in 25	72 h
		T98G: 2000 /100 µl	0,2	24.8	25 nM pre-miR-132 / 25 nM pre-NC1	in 25	72 h
			0,2	24.8	10 nM pre-miR-132 / 10 nM pre-NC1	in 25	72 h
			0,2	24.8	25 nM pre-miR-126 / 25 nM pre-NC1	in 25	72 h
			0,2	24.8	10 nM pre-miR-126 / 10 nM pre-NC1	in 25	72 h
Apo-ONE® homogeneous caspase 3/7 assay	96-well	A172: 8000 /100µl	0,2	24.8	25 nM pre-miR-132 / 25 nM pre-NC1	in 25	72 h
			0,2	24.8	10 nM pre-miR-132 / 10 nM pre-NC1	in 25	72 h
			0,2	24.8	25 nM pre-miR-126 / 25 nM pre-NC1	in 25	72 h
			0,2	24.8	10 nM pre-miR-126 / 10 nM pre-NC1	in 25	72 h
		T98G: 8000 /100 µl	0,2	24.8	25 nM pre-miR-132 / 25 nM pre-NC1	in 25	72 h
			0,2	24.8	10 nM pre-miR-132 / 10 nM pre-NC1	in 25	72 h
			0,2	24.8	25 nM pre-miR-126 / 25 nM pre-NC1	in 25	72 h
			0,2	24.8	10 nM pre-miR-126 / 10 nM pre-NC1	in 25	72 h
CellTiter-Glo® luminescent cell viability assay	96-well	A172: 2000 /100µl	0,2	24.8	25 nM pre-miR-132 / 25 nM pre-NC1	in 25	72 h
			0,2	24.8	10 nM pre-miR-132 / 10 nM pre-NC1	in 25	72 h
			0,2	24.8	25 nM pre-miR-126 / 25 nM pre-NC1	in 25	72 h
			0,2	24.8	10 nM pre-miR-126 / 10 nM pre-NC1	in 25	72 h
		T98G: 2000 /100 µl	0,2	24.8	25 nM pre-miR-132 / 25 nM pre-NC1	in 25	72 h
			0,2	24.8	10 nM pre-miR-132 / 10 nM pre-NC1	in 25	72 h
			0,2	24.8	25 nM pre-miR-126 / 25 nM pre-NC1	in 25	72 h
			0,2	24.8	10 nM pre-miR-126 / 10 nM pre-NC1	in 25	72 h
Dual-Glo® Luciferase Assay	96-well	T98G: 8000 / 100 µl	0,5	24.5	50 nM pre-132 / 50 nM pre-NC1	in 25	24 h
			0,5	24.5	51 nM pre-132 / 50 nM pre-NC1	in 25	24 h
			0,5	24.5	52 nM pre-132 / 50 nM pre-NC1	in 25	24 h
			0,5	24.5	53 nM pre-132 / 50 nM pre-NC1	in 25	24 h
			0,5	24.5	54 nM pre-132 / 50 nM pre-NC1	in 25	24 h
			0,5	24.5	55 nM pre-132 / 50 nM pre-NC1	in 25	48 h
		U251: 8000 / 100 µl	0,5	24.5	50 nM pre-212 / 50 nM pre-NC1	in 25	24 h
			0,5	24.5	51 nM pre-212 / 50 nM pre-NC1	in 25	24 h
			0,5	24.5	52 nM pre-212 / 50 nM pre-NC1	in 25	24 h
			0,5	24.5	53 nM pre-212 / 50 nM pre-NC1	in 25	24 h
			0,5	24.5	54 nM pre-212 / 50 nM pre-NC1	in 25	72 h
			0,5	24.5	50 nM pre-210 / 50 nM pre-NC1	in 25	72 h
			0,5	24.5	51 nM pre-210 / 50 nM pre-NC1	in 25	72 h
			0,5	24.5	52 nM pre-210 / 50 nM pre-NC1	in 25	72 h
			0,5	24.5	53 nM pre-210 / 50 nM pre-NC1	in 25	72 h

2.11 Plasmids

The psi-CHECK™-2 vector from Promega (Madison, WI) was used for 3`UTR luciferase reporter gene assays (Figure 3).

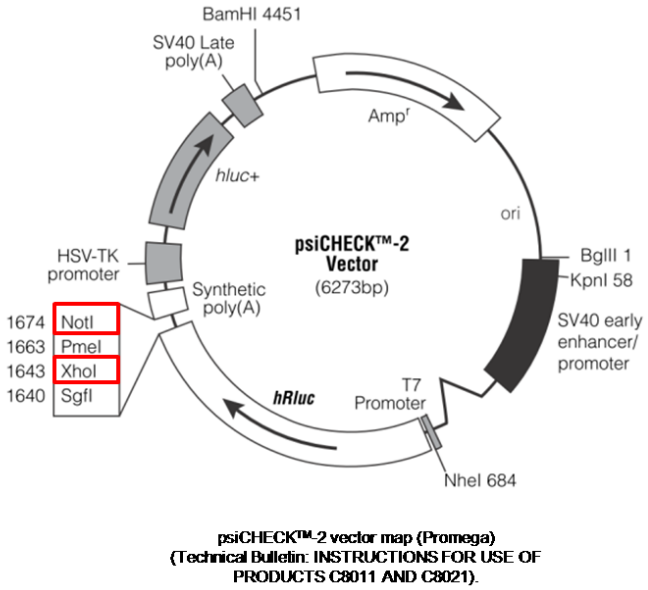

Figure 3: Vector map of the psi-CHECK™-2 vector.

3 Methods

3.1 Molecular biological methods

3.1.1 Extraction of nucleic acids from tumor tissue samples

RNA and DNA from frozen patient tumor tissue samples had been previously extracted by ultracentrifugation according to a published protocol (van den Boom et al 2003).

3.1.2 Real - time RT-PCR analyses

3.1.2.1 Expression profiling of miRNAs with TaqMan® Low Density Arrays

TaqMan® Array MicroRNA Cards (Applied Biosystems, Foster City, CA) were used for profiling of the expression of 365 miRNAs that were differentially expressed in glioma cells and tissues according to the manufacturer`s instructions. The cards consist of a set of multiplexed reverse transcription primer pools. Each pool comprised up to 48 reverse transcriptase (RT) stem-loop primers that are specific for mature miRNAs. Two endogenous controls provided for data normalization were included in this primer pool. The primers included in each pool are identical to those available for individual miRNA RT-PCR assays (TaqMan MicroRNA Assays). Therefore, miRNAs of interest were validated by individual assays as described in chapter 3.1.2.2. The TaqMan® Array MicroRNA Card is designed for two-step RT-PCR. In the first step, cDNA was reverse transcribed from total RNA samples using stem-loop primers specific for 365 microRNAs using the TaqMan MicroRNA Reverse Transcription Kit (Applied Biosystems, Foster City, CA). Thereby, up to 381 miRNAs and controls were reverse transcribed in a single reaction. Amplification of cDNA was the second step in the two-step RT-PCR experiment using TaqMan® Universal PCR Master Mix (Applied Biosystems, Foster City, CA). In this step, the sample-specific PCR mix was loaded into the loading ports of a 384-well TaqMan® Array MicroRNA Card that is pre-loaded with TaqMan® Gene Expression Assays (Applied Biosystems, Foster City, CA).

For quantitative real-time PCR analysis using the comparative CT (ΔΔCT) method, the TaqMan® Array MicroRNA cards were run on the 7900 HT system (Applied Biosystems). RealTime StatMiner® Software was used to evaluate differentially expressed miRNA candidates in 5-Aza/TSA-treated versus untreated glioblastoma cells in collaboration with a biostatistician (Edith Willscher, Interdisciplinary Centre for Bioinformatics, University of Leipzig, Germany). In addition, Dr. Marc Zapatka and Prof. Dr. Benedikt Brors (Division of Theoretical Bioinformatics, DKFZ Heidelberg, Germany) performed the bioinformatic analysis for the miRNA expression data of all other group-wise comparisons (Figure 15) according to published protocols (Tusher et al 2001, Vandesompele et al 2002). Figure 4 provides an overview of the stem-loop RT - PCR for detection of miRNAs and the TaqMan hydrolysis probe principles.

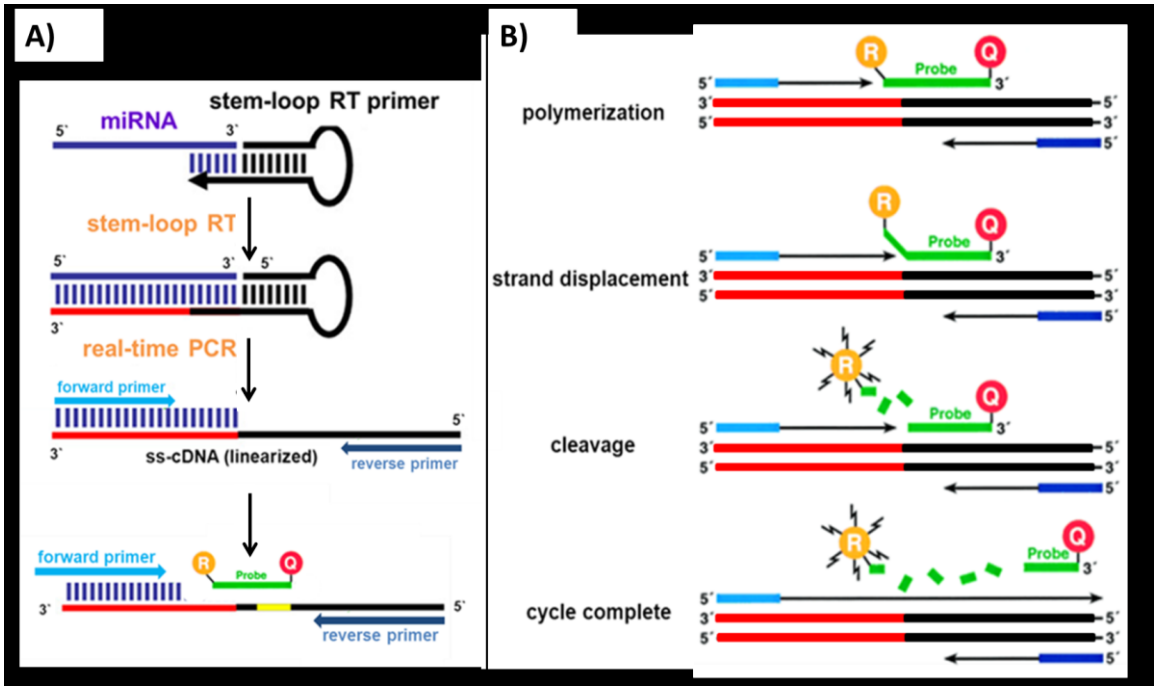

Figure 4: Principle of the stem-loop RT – PCR for detection of miRNAs (modified according to (Varkonyi-Gasic et al 2007, Varkonyi-Gasic and Hellens 2011). A) Stem-loop RT – PCR procedure consists of a two step microRNA detection method. First, stem-loop reverse transcriptase (RT) primers specific for each investigated miRNA are annealed to the 3` end of the mature miRNA. Afterwards, the first strand of cDNA is synthesized by reverse transcriptase (stem-loop RT). Next, the RT product is amplified using a microRNA-specific forward primer and a universal reverse primer (real-time PCR). Then, the quantification is achieved by the fluorescence generated upon cleavage of the TaqMan probe. **B)** TaqMan hydrolysis probe principle (modified according to Yuan et al 2000). The PCR reaction exploits the 5´ - exonuclease activity of thermostable DNA - polymerase to cleave a TaqMan probe during PCR. The TaqMan probe contains a reporter dye (R) at the 5´ end of the probe and a quencher dye (Q) at the 3´ end of the probe. During this reaction, cleavage of the probe separates the reporter dye and the quencher dye which results in increased fluorescence of the reporter. Accumulation of PCR products is detected directly by monitoring the increase in fluorescence of the reporter dye. If the target of interest is present, the probe specifically anneals to the target during PCR. The 5´ to 3´ nucleolytic activity of the polymerase cleaves the probe between the reporter and the quencher only if the probe hybridized to the target. As a result, the probe fragments are displaced from the target. Finally, the polymerization of the strand continues. The 3´ end of the probe is blocked to prevent extension of the probe during PCR. The process occurs in each cycle. It does not interfere with the exponential accumulation of the product. If the target sequence is complementary to the probe and is amplified during PCR, an increase of the fluorescence signal is detected.

3.1.2.2 Real-time PCR analysis using TaqMan® miRNA assays

Real-time PCR analysis of mature miRNAs was performed by TaqMan® miRNA assays specific for each investigated miRNA according to the manufacturer´s instruction (Applied biosystems). Real-time PCR was performed on the StepOnePlus™ qRT-PCR system (Applied Biosystems) (Table 16). Fluorescent data were converted into cycle threshold measurements by the SDS software and exported to Microsoft Excel. Fold expression changes relative to universal human RNA were calculated with the $2^{-\Delta\Delta CT}$ method (Livak and Schmittgen 2001). Human small nuclear U6 RNA was used for reference (Schmittgen et al 2004) since it showed robust expression in the investigated samples. U6snRNA amplification was measured by incorporation of SYBR® green fluorescent dye (LifeTechnologies, Carlsbad, CA) into the double-stranded DNA (Table 17), while the miRNAs were detected by TaqMan® technology (Applied Biosystems) according to Figure 4. After real-time PCR analysis, all PCR products were run on agarose gels to prove specific amplification of PCR products of correct size. All primer sequences used for miRNA amplification are listed at https://products.appliedbiosystems.com.

Table 16: Reaction mixture and PCR conditions for stem-loop RT reaction (A) and real-time PCR (B) using TaqMan® microRNA assays and SYBR® green fluorescent dye.

A)

reaction mix (1x)	volume (µ)	program
stem-loop RT		
dNTPs (100 mM)	0.15	16°C 30 min
MultiScribe reverse transcriptase (50 U/µl)	1	42°C 30 min
RT-buffer (10x)	1.5	85°C 5 min
RNAse inhibitor	0.19	4°C ∞
specific miRNA RT primer (5x)	2	
U6 - reverse primer (10 pmol)	2	
RNAse free water (Ambion)	3.16	
	10	
20 ng/µl total RNA	+ 5 µl	

B)

reaction mix (1x)	volume (µ)	program
real-time PCR		
U6		
SYBR green fluorescent dye (500 rxn)	10	95°C 10 min
U6 - forward primer (10 pmol)	1	95°C 15 sec
U6 - reverse primer (10 pmol)	1	60°C 1 min
DEPC-H_2O	7	4°C ∞
		40 cycles
RT-product	+ 1	

reaction mix (1x)	volume (µ)	program
real-time PCR		
microRNA		
TaqMan Gene Expression Mastermix	10	95°C 10 min
specific miRNA real-time primer (20x)	1	95°C 15 sec
RNAse free water (Ambion)	8	60°C 1 min
		4°C ∞
		40 cycles
RT-product	+ 1	

Table 17: SYBR® Green Dye assay chemistry, modified according to http://www.lifetechnologies.com.

1. **Reaction setup:** The SYBR® Green Dye fluoresces when bound to double-stranded DNA.

2. **Denaturation:** When the DNA is denatured, the SYBR® Green Dye is released and the fluorescence is drastically reduced.

3. **Polymerization:** During extension, primers anneal and PCR product is generated.

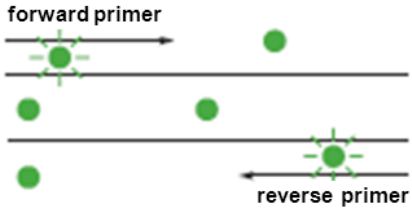

4. **Polymerization completed:** When polymerization is complete, SYBR® Green Dye binds to the double-stranded product, resulting in an increase of fluorescence which can be detected.

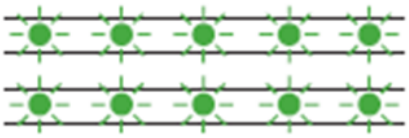

3.1.2.3 Expression analyses of mRNA targets

After reverse transcription, gene expression was determined by SYBR® green fluorescent dye-based real-time PCR (LifeTechnologies, Carlsbad, CA) using the StepOnePlus™ sequence detection system. Three micrograms of total RNA of each sample were reverse-transcribed into cDNA using SuperScript® reverse transcriptase (LifeTechnologies) and random primers. The total RNA was diluted in 30.4 µl DEPC-treated water and denatured for 5 min at 70 °C following incubation on ice for 5 min. Afterwards the reaction mix was added and reverse transcription was performed (Table 18).

Table 18: Reaction mix and PCR conditions for cDNA synthesis.

reaction mix (1x)	volume (µ)	program
BSA (1 mg/ml)	1.7	42°C 50 min
dNTPs (25 mM)	2.5	80°C 10 min
DTT (0.1 M)	0.4	4°C ∞
First strand buffer (5x)	10	
pd(N)6 (1.5 µg/µl)	3	
RNAsin (40 U/µl)	1	
Superscript II reverse transcriptase (200 U/µl)	1	
	19.6	

The cDNA quality and quantity was controlled by PCR with two different ß2-microglobulin primer pairs (Table 12) that cover amplicons in the 5' and 3' parts of this gene, respectively. The cDNA was diluted with water (1:25). Then 5 µl of diluted cDNA, SYBR® green mixture and specific primers for the gene of interest were mixed and analysed using qRT-PCR according to Table 19. Thereby, *adenosine-diphosphate-ribosylation factor 1* (*ARF1*) (NCBI GenBank accession no. M36340) was used as a reference gene. *ARF1* is expressed at similar levels in diverse subsets of glioma tumor samples of different grades (data not shown). All samples were run in duplicates.

Table 19: Reaction mix and qRT - PCR program for qRT - PCR reaction.

reaction mix (1x)	volume (µ)	program
SYBR green fluorescent dye (500 rxn)	12.5	90°C 10 min
forward primer (10 pmol)	X	95°C 15 sec
reverse primer (10 pmol)	X	60°C 1 min
DEPC-H_2O	X	4°C ∞
	20.0	40 cycles
cDNA (1:25)	+ 5	
	X = depending on primer relationship	

Expression levels were normalized to the expression levels of *ARF1* and compared to the normalized expression level of a reference sample (Universal human Reference RNA) using the $2^{-\Delta\Delta Ct}$ method described by (Livak and Schmittgen 2001). Thereby, the ΔC_t values were calculated by subtracting the C_t value of the reference gene (*ARF1*) from the C_t value of the gene of interest ($C_{t,\ target\ gene}$ - $C_{t,\ reference\ gene}$). Afterwards, the reversal of the logarithm of the ΔC_t value was calculated to get the $\Delta\Delta$ct value ($2^{-\Delta\Delta ct}$).

3.1.3 Sodium bisulfite treatment of genomic DNA

DNA methylation was investigated by direct sequencing of sodium bisulfite-modified DNA (Hayatsu and Shiragami 1979). As shown Figure 5, sodium bisulfite preferencially deaminates unmethylated cytosine to uracil, whereas methylated cytosines remain unconverted. Afterwards the recovered DNA is amplified by PCR. Changes can then be assessed by sequencing of the sodium bisulfite-treated DNA and can thus be used to investigate the methylation status of CpG dinucleotides in 5'-CpG islands.

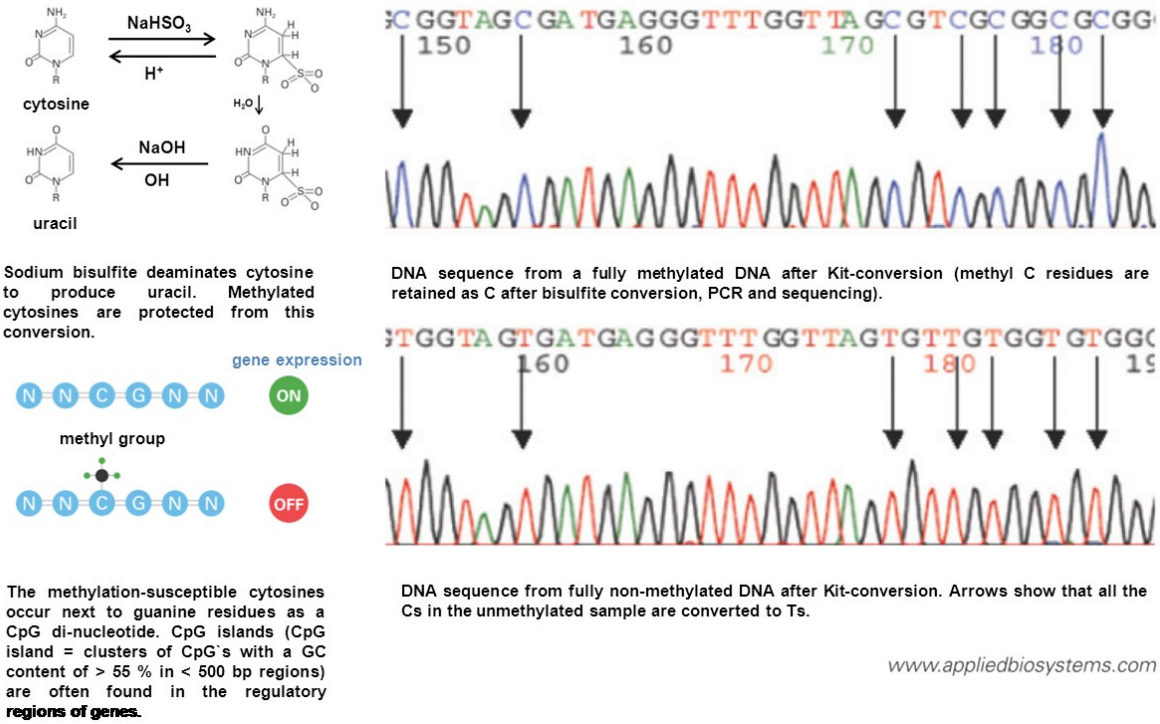

Figure 5: Conversion of unmethylated cytosine to uracil by sodium bisulfite treatment, modified according to PROTOCOL SUMMARY methylSEQr™ Kit DNA Conversion and Sequencing, Applied Biosystems, Foster City, CA. Left: A cytosine is changed into a sulphonated cytosine intermediate in the presence of bisulfite and afterwards converted into a sulphonated uracil through desamination. Finally, the sulpho-group is split off under alkaline conditions and uracil is generated. The generated sequence after bisulfite treatment is shown on the **right** side. Upper sequence: DNA sequence from a fully methylated DNA with methylated $C^{m}pG$; lower sequence: Cs in the unmethylated DNA sequence have been converted to Ts.

Bisulfite conversion was done following the manufacturer`s instructions (Zymo Research EZ, Irvine, CA). Genomic (sodium bisulfite-modified) DNA amplification was carried out using the HotStar Taq DNA polymerase kit (Qiagen, Hilden) with specific primers listed in Table 13 using the protocol listed in Table 20.

Table 20: PCR conditions for the amplification of the sodium bisulfite-modified DNA.

reaction mix	volume (µ)	program
10 x PCR-buffer	2	95°C 15 min
dNTPs (2 mM)	2	95°C 30 sec
primer forward (10 pmol)	2	56°C 60 sec
primer reverse (10 pmol)	2	72°C 120 sec
HotStar Taq (Qiagen) (5 U/µl)	0.1	72°C 10 min
Aqua dest.	10.9	4°C ∞
bisulfite-modified DNA	1	40 cycles

The PCR product purification spin kit (GENOMED GmbH, Löhne) was used for purification of the PCR products according to the company instructions. Afterwards the nucleotides of the PCR product were marked with the BigDye® terminator v1.1 cycle sequencing kit (Applied Biosystems, Foster City). This method uses dideoxynucleotide triphosphate (*ddNTPs*) as chain-terminating inhibitors for DNA sequencing (Sanger et al 1977). The reaction mix was prepared as listed in Table 21.

Table 21: Sequencing conditions.

reaction mix	volume (µ)	program
purified PCR-product	4 - 7.5	95°C 10 sec
reverse primer (10 pmol/µl)	0.5	50°C 5 sec
BigDye® Terminator Cycle Sequencing Mix	2	60°C 4 min
		4°C ∞
Aqua dest.	ad 10 µl	25 cycles

To separate non-inserted fluorescently labelled *ddNTPs*, 1 µl 3 M Natriumacetat pH 4,6 and 25 µl 95% ethanol were added to the sequencing reaction, mixed, and centrifuged for 20 minutes at 14,000 x g at 4 °C. The supernatant was removed. Then, the pellet was carefully washed twice with 200 µl 70 % ethanol, and dried for 5 to 10 min at 42 °C in a heating block. DNA pellet was resolved in 4 µl loading buffer. 2 µl of the diluted DNA pellet was applied to a denaturing PAA gel (composition of the PAA gel listed in Table 22) and analyzed using the ABI Prism™ 377 sequenzer (Applied Biosystems, Foster City).

Table 22: Composition of the denatured PAA gel.

composition PAA gel	
21 g	Urea
8.4 ml	30% acrylamide/bisacrylamide (29:1)
6 ml	10x TBE
20 ml	Aqua dest.
350 µl	10% APS
15 µl	TEMED

Direct bisulfite sequencing and semiquantitative calculation of a promoter methylation score were carried out as reported (Tepel et al 2008, Tews et al 2007). The methylation status at each of the analyzed CpG sites was semi-quantitatively rated using the following scale: 0, completely unmethylated; 1, a weakly methylated signal detectable in the sequence; 2, methylated signal approximately equal to unmethylated signal; 3, methylated signal markedly stronger than unmethylated signal. Based on this rating scale a cumulative promoter methylation score in percent was calculated for each tumor by adding the numbers determined at the individual CpG sites divided by the maximum possible methylation score at all analysed CpG sites (Tepel et al 2008). Tumors with methylation scores exceeding that of three non-neoplastic brain tissue-samples were regarded as being hypermethylated. As a positive control, a commercially available hypermethylated DNA (Upstate, Charlottesville, VA) was used.

3.1.4 Chromatin immunoprecipitation assay

Chromatin immunoprecipitation is a method to identify remodeled chromatin using reversible formaldehyde cross-linking of proteins and DNA as well as antibodies to immunoprecipitate DNA associated with acetylated or methylated histones. The method has provided new insights into the early events of transcriptional regulation (Christenson et al 2001). The ChIP method used in this study has been established in our group and optimized by Dr. Natalie Schmidt (Schmidt et al 2012). Figure 6 shows an overview of the experimental procedure.

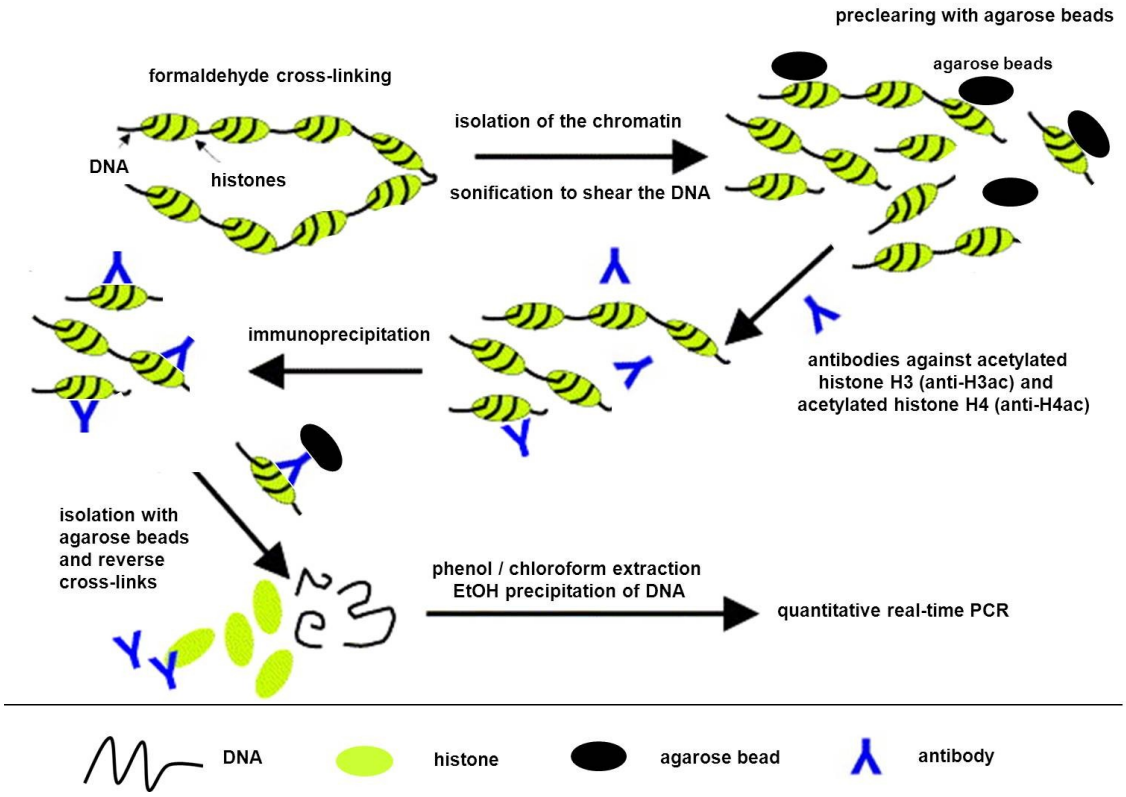

Figure 6: Overview of the ChIP assay protocol modified according to (Hiroi et al 2004). Proteins (green) and DNA (black lines) were cross-linked with formaldehyde. Then, the chromatin was isolated and DNA was sheared by sonification. Agarose beads (black ellipses) were used for preclearing to reduce unspecific binding. Afterwards immunoprecipitation with specific antibodies (blue) against acetylated histone H3 (anti-H3ac) and acetylated histone H4 (anti-H4ac) took place. Agarose beads were used to collect histone H3 and histone H4 antibodies bound to chromatin. After reversing the cross-link and the digestion of the proteins, the DNA was obtained by phenol / chloroform extraction and ethanol precipitation, and then analyzed by real-time PCR.

Chromatin immunoprecipitation was performed in cooperation with Dr. Natalie Schmidt from three TSA-treated and untreated glioblastoma cells (T98G, U87MG and U138MG). First, DNA and proteins from 1 x 10^6 glioblastoma cells were crosslinked with 1% formaldehyde for 10 minutes. Afterwards DNA and crosslinked proteins were resuspended in swelling buffer to isolate nuclei. Nuclei prepared from cells were further processed using a commercial ChIP assay kit (Upstate, Charlottesville, VA) according to the manufacturer's instructions. Cells were then resuspended in SDS-lysis buffer and sonication was performed. Genomic DNA was sheared to 200–800 bp fragments by sonification for 9 x 9 sec on ice with an ultrasonic processor. After sonification, the samples were precleared with protein A agarose/salmon sperm DNA for 30 min at 4°C to reduce non-specific binding of the beads to DNA. 5% of the sample volume was

saved as input control DNA and the remainder was used for immunoprecipitation with anti-H3ac (acetylated histone H3) or anti-H4ac (acetylated histone H4) antibodies at 4°C overnight. The rabbit anti-human IgG fraction served as a negative isotype control. The chromatin-antibody-protein complexes were collected by protein A agarose/salmon sperm DNA (1 h at 4°C). Briefly, histone/DNA complexes were eluted from the antibodies (2 x 15 min incubation at room temperature in freshly prepared elution buffer). NaCl was added to reverse the formaldehyde histone-DNA cross-links for 4-6 hours at 65°C. Finally, DNA was digested with proteinase K and DNA was purified by phenol/chloroform extraction and ethanol precipitation.

Immunoprecipitated DNA was assessed by using quantitative real-time PCR analysis with primers targeting the 5`genomic region of *miR-132* and *miR-126* normalized to the respective input fraction as a reference. Thereby, *GAPDH* was used as a negative control gene associated with euchromatin and not regulated by histone modifications whereas *p21/CDKN1A* served as a positive control gene previously shown to be regulated by histone modifications in human glioblastoma cells (Yin et al 2007) (Table 12 and Table 13). Results obtained from glioblastoma cells were based on the measurement of three biological replicates. To approve the efficiency of TSA treatment and the specificity of ChIP-antibody reactions, Tricin-SDS-PAGE was performed (Schagger 2006).

3.2 Protein biochemical methods

3.2.1 Extraction of nuclear and cytoplasmic protein fractions from cultured cells

Glioblastoma cells and medulloblastoma cells were plated in 6-well plates and transiently transfected with pre-miR-132 molecules or scrambled control molecules (NC1). Seventy-two hours after transfection, cells were harvested with trypsin-EDTA. The NE-PER® nuclear and cytoplasmic extraction kit (Thermo Scientific, Rockford, IL) was used to extract separately the nuclear and the cytoplasmic protein lysates according to the manufacturer`s instructions.

3.2.2 Protein quantification

The protein concentration of the cleared lysates was determined by using the Bradford protocol (Bradford 1976) and RC DC Bradford Protein Assay Reagent® (BioRad GmbH, Munich). Bovine serum albumin (BSA), 0 – 2 mg/ml) was used as protein standard.

3.2.3 Sodium Dodecyl Sulfate – Polyacrylamide Gel Electrophoresis (SDS-PAGE)

SDS-PAGE is a method to separate proteins according to their molecular weight based on the Laemmli protocol (Laemmli 1970). Figure 7 illustrates this method.

First, the separating gel (8 % acrylamide gel) was poured in an appropriate gel chamber and covered with isopropanol to avoid dehydration as well as the reaction with oxygen. Then, the isopropanol was removed thoroughly after polymerization. As a next step, the stacking gel was poured and the gel comb was inserted to generate the gel slots. The stacking gel above the separating gel was used to improve protein entry into the gel. Because of the lower pH and bigger pores, the proteins migrate very fast without separation. Therefore, proteins are collected and concentrated before separation. Proteins extracted from pre-miR-132 transfected and control (pre-NC1) transfected glioblastoma cells (T98G, A172, U251MG transfected with 10 nM, 25 nM or 50 nM pre-132 or pre-NC-1: SIRT1 protein: 20 µg nuclear or cytoplasmic proteins and medulloblastoma cells (DAOY, transfected with 50 nM pre-132 or pre-NC1, SIRT1 protein: nuclear: 50 µg) were mixed with loading buffer containing SDS + ß-mercaptoethanol. Afterwards, proteins were denatured at 95°C for 5 min. PageRuler™ Prestained Protein Ladder (Fermentas, Germany) was used as a molecular weight marker. The gels were run at 160 V for about 60 min and used for western blotting afterwards.

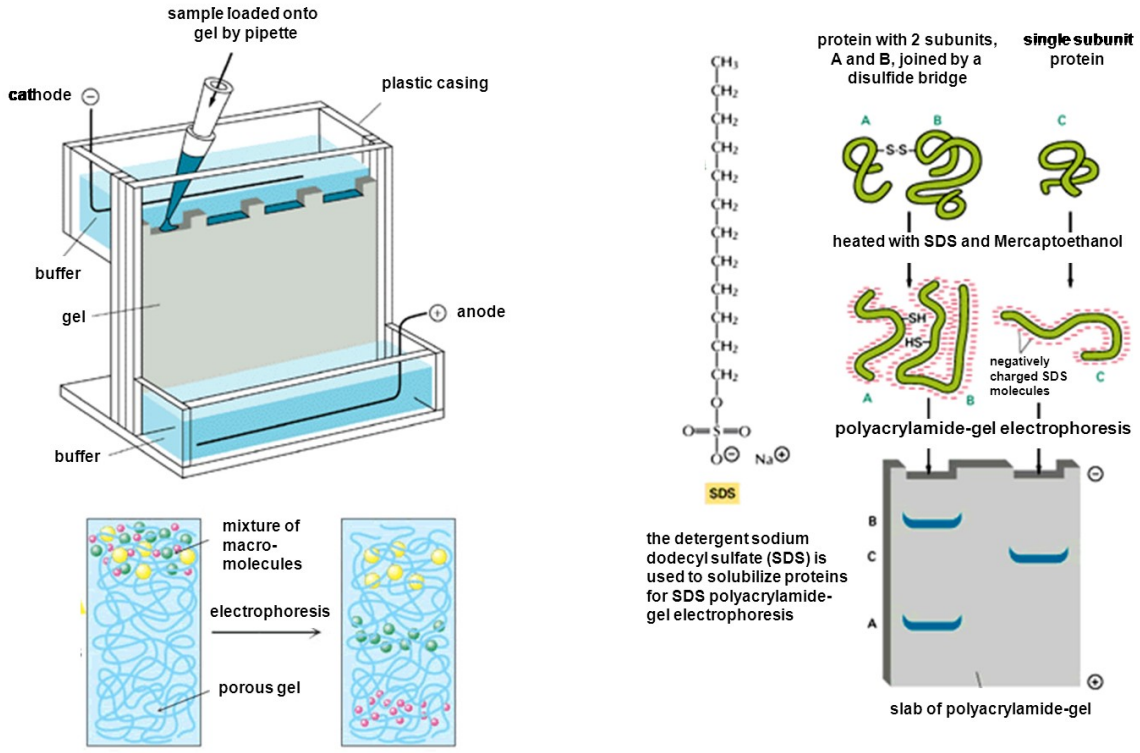

Figure 7: Schematic representation of the SDS-PAGE, modified according to http://www.imb-jena.de/~rake/Bioinformatics_WEB/proteins_purification.html. The polyacrylamide gels consist of a mixture of acrylamide and bisacrylamide and the polymers are cross-linked by APS and TEMED. According to the amount of polyacrylamide, the matrix is getting more or less dense with a different pore size. The detergent sodium dodecyl sulfate (SDS) is used to denature and solubilize proteins. These proteins also get a negative charge because of the sulfate groups of the SDS. Therefore, the separation only depends on the molecular weight of the proteins. Small proteins migrate faster through the matrix than large proteins.

3.2.4 Western blot analysis

Western blotting was used to transfer proteins from gels onto a nitrocellulose membrane using a Trans Blot Cell Blot module (BioRad) (Burnette 1981, Towbin et al 1979). The transferred proteins bind to the nitrocellulose membrane through hydrophobic interaction. After electrophoresis, nitrocellulose membranes, blotting pads and filters were wetted in 1 x transfer-buffer and the components were placed into the Trans Blot module according to the manufacturer`s instructions. The gel was laid on top of the nitrocellulose membrane followed by filter paper (Figure 8). The transfer was performed at a constant current of 300 mA and 4 °C for 120 min. After a short washing step the proteins can be visualized in a specific or unspecific manner.

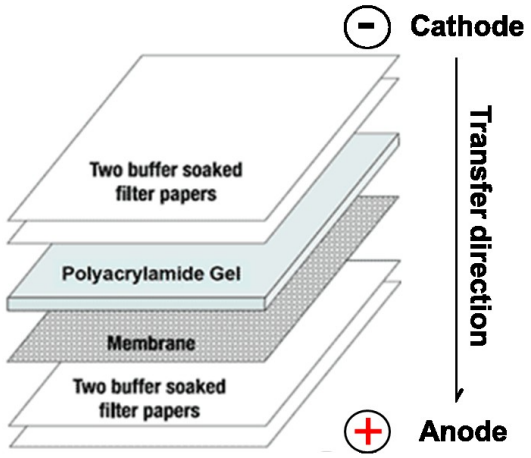

Figure 8: Schematic representation of a western blot transfer, modified according to http://technologyinscience.blogspot.de/2011/12/western-blot-protein-immunoblot.html. Filter papers on top, gel, western blot membrane, filter papers at the bottom. The transfer proceeds from the cathode to the anode, so that the proteins are transferred from the gel onto the membrane.

3.2.4.1 Non specific staining of proteins with Ponceau S

Ponceau S staining is a reversible and rapid method to detect proteins on a membrane. With this method the transfer of the proteins to the membrane was controlled. After blotting, the membrane was incubated with Ponceau S (0.1% (w/v) for three minutes at room temperature and was afterwards destained with water (Ponceau S: 20% methanol + 1g Ponceau S (Sigma-Aldrich GmbH, Steinheim) ad 50 ml acetic acid).

3.2.4.2 Specific antigen – antibody reaction

The principle for visualization of specific proteins on the nitrocellulose membrane is based on an antigen – antibody reaction. To reduce unspecific background binding, the membrane was blocked with 5 % dry milk powder in TBS-tween-20. Then, the membrane was incubated with the primary antibody (all antibody dilutions are listed in Table 7) overnight at 4°C. The primary antibody binds to its antigen (the target protein) while the secondary antibody is directed against the constant part of the primary antibody. All secondary antibodies were labeled with horseradish peroxidase (HRP).

This enzyme catalyzing the oxidation of luminol using peroxide as an oxidizing agent (Figure 9). This chemiluminescent reaction is detectable by a photometric methods using the chemiluminescent HRP substrate (Millipore, Charlottesville, VA).

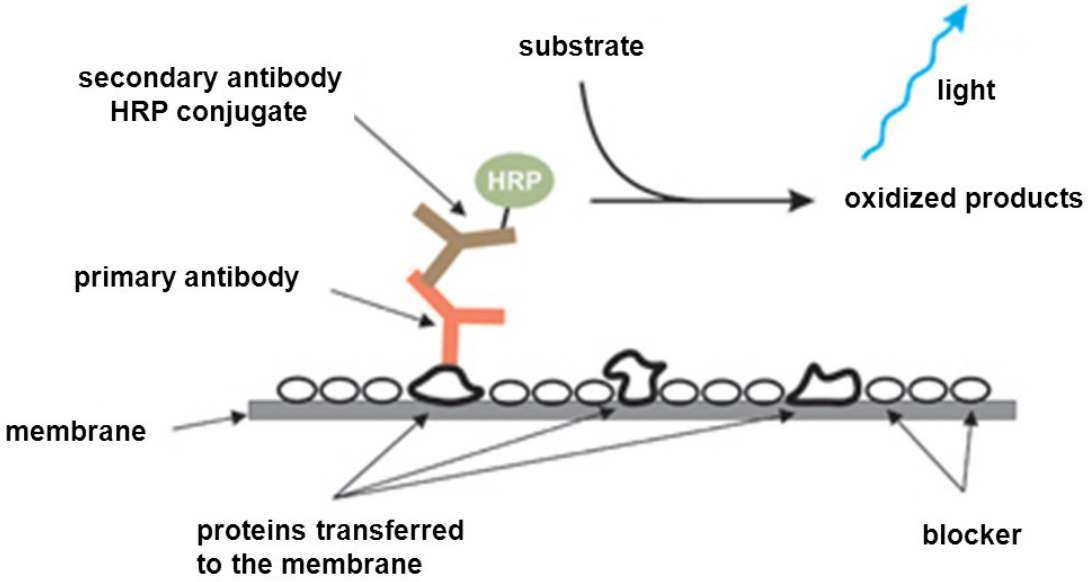

Figure 9: Chemiluminescent detection of Western blot, modified according to http://advansta.com/Chemiluminescent_Western_Detection.html. In chemiluminescent detection, the protein to be detected is immobilized on a basal support membrane. Afterwards, the protein binds to a primary antibody, which in turn attaches to a secondary antibody. The secondary antibody is detected using the conjugated HRP substrate, which generates light during the reaction. The light can then be visualized by CCD imaging (LAS – 3000 mini system, Fujifilm Life Science, Standford, CT).

3.2.4.3 Quantification of western blots

Band intensities were analyzed using the ImageJ software (freeware that can be downloaded from e.g. http://rsbweb.nih.gov/ij/). All detected proteins were measured by using the pixel calculator tool. After normalizing the data to control transfected cells, graphs were produced with Microsoft Excel.

3.3 Cell based methods

3.3.1 Cultivation of glioma cells

All investigated tumor cell lines (A172, T98G, TP365MG, U138MG, U87MG, U251MG, DAOY) were grown under standard condition. Dulbecco´s modified Eagle´s medium (DMEM) supplemented with 10% (v/v) heat-inactivated fetal bovine serum (FCS) and 1% (v/v) penicillin G/streptomycin (P+S) were added to the medium. Cells were incubated at 37 °C in a humidified atmosphere containing 5 % CO_2. Liquid nitrogen was used to store deep-frozen cells. Cells were stored in FCS containing 10 % DMSO to minimize the effect of freezing.

3.3.2 Treatment of glioblastoma cells with 5-Aza + TSA / 5-Aza or TSA

Five glioblastoma cell lines (A172, U138MG, T98G, TP365MG and U87MG) were either grown under standard conditions in DMEM/FCS/P+S or as follows:

1) AZA-TSA: Cell lines were grown in DMEM/FCS/P+S with 500 nM 5-Aza for 48 h, washed and grown for another 24 h in DMEM/FCS/P+S with 500 nM 5-Aza and 1 µM TSA.
2) TSA: Glioma cells were grown in DMEM/FCS/P+S with 1 µM TSA for 36 h.
3) AZA: Cells were grown in DMEM/FCS/P+S with 500 nM 5-Aza for 72 h.

After each treatment, cells were harvested and total RNA was extracted according to 3.3.3 and 3.3.4. Expression analyses of cells under the different treatment conditions compared to the untreated controls were performed by real-time reverse transcription PCR analysis as described above. Data were obtained in at least three independent biological experiments.

3.3.3 Extraction of RNA from cultured glioblastoma cells treated with either 5-Aza/TSA or 5-Aza

Total RNA from cultured glioblastoma cells treated with either 5-Aza and TSA or 5-Aza was extracted using the Rneasy Plus Mini Kit (Qiagen, Hilden) according to manufacturer's instructions. Afterwards, the RNA pellet was air dried and resuspended in 30 µl RNase free water. RNA concentration was measured with the Nano-Drop 1000 photometer at 260 nm and by running an aliquot of each RNA extract on a 1 % agarose gel for quality control.

3.3.4 Extraction of RNA from cultured glioblastoma cells treated with TSA

Total RNA from cultured glioblastoma cells treated with TSA was extracted using TRIzol®-reagent (Invitrogen, Carlsbad, CA) according to manufacturer's protocol. Then, the RNA pellet was air dried and resuspended in 15 µl RNase free water. RNA concentration was measured with the Nano-Drop 1000 at 260 nm and by running an aliquot of each RNA extract on a 1 % agarose gel for quality control.

3.3.5 Transient transfection of glioblastoma cells with pre-miRNA molecules

MiR-132, *miR-212*, *miR-126* and *miR-210* were over-expressed in glioblastoma cell lines by transient transfection of different amounts of precursor-miR molecules (Ambion/Applied Biosystems) using Lipofectamine™ 2000 reagent (LifeTechnologies, Carlsbad, CA). In parallel, cells were transiently transfected with commercially available negative control oligonucleotide molecules (pre-miR™ miRNA Precursor Molecules Negative Control ≠1) (Ambion / Applied Biosystems) to identify side-effects caused by transient transfection and / or reagent. Cells were plated in DMEM containing 10 % FCS and 1 % Pen/Strep, and incubated at 37 °C in a humidified atmosphere containing 5 % CO_2. After 24 h, the medium was replaced and fresh medium containing 10 % FCS was given to the cells (6-well plates: 1.5 ml; 96-well plates: 50 µl). Oligonucleotide solution and transfection reagent were diluted in serum-reduced Opti-MEM® medium (LifeTechnologies/GIBCO, Carlsbad, CA). The transfection reactions were incubated for 5 min at RT. Then, both dilutions were combined, mixed and incubated for additional 20 min at RT. The mixture of

oligonucleotide and transfection reagent was finally added to the cells. Cell-based methods with corresponding cell counts, amounts of Lipofectamine 2000, pre-miRNAs / pre-NC1 in serum-reduced OptiMEM and time points after transfection for RNA extraction / protein extraction or assay-system performance are listed in Table 15.

3.4 Functional assays

3.4.1 Apoptosis assay

Apoptosis is a programmed cell death that is involved in many biological processes (Wyllie et al 1980). An endogenous signal cascade leads to the characteristics of apoptosis like cell membrane blebbing, cell shrinkage, nuclear fragmentation, chromatin condensation, activation of caspases and chromosomal DNA fragmentation. The activity of caspases 3 and 7 is a hallmark for apoptosis. Both cleave proteins at the C-terminal side at the amino acid sequence DEVD (asp-glu-val-asp). In the assay the cells were permeabilized to maintain optimal caspase 3/7 activity. Thereby, rhodamine 110 is used as a profluorescent substrate that is linked to DEVD (Z-DEVD-R110). After sequential cleavage of the DEVD peptide from the substrate (Z-DEVD-R110) by caspase 3 and/or 7, rhodamine 110 becomes intensely fluorescent and can be measured with an excitation at 499 nm and an emission maximum of 521 nm (Figure 10).

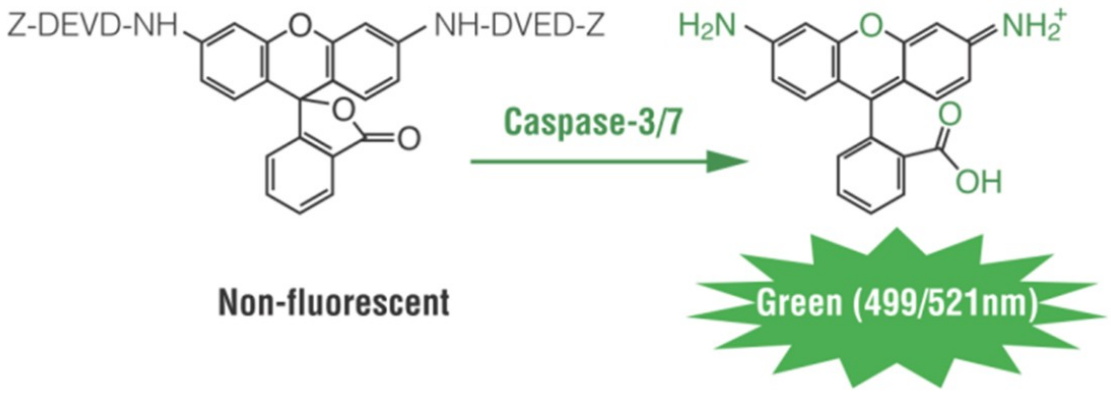

Figure 10: Cleavage of the non - fluorescent caspase substrate Z-DEVD-R110 (http://www.promega.com). Upon sequential cleavage and removal of the DEVD peptides by caspase 3/7 activity and excitation at 499 nm, the rhodamine 110 leaving group becomes intensely fluorescent with an emission maximum at 521 nm.

To determine the effect of *miR-132* and *miR-126* on apoptosis, A172 and T98G glioblastoma cell lines were transiently transfected with pre-miR-132 and pre-miR-126 molecules in relation to scrambled control (pre-NC1)-transfected cells (see 3.3.5). The transfected cell lines were investigated using a commercially available Apo-ONE homogeneous caspase-3/7 assay (Promega, Madison, WI). Cells were incubated in the dark with the Apo-ONE reagent by shacking at 300 - 500 rpm and measured after 30 min, followed by repeated measurements every hour for up to 6 h. Results were obtained in at least three independent biological experiments.

3.4.2 Proliferation assay

To determine the effect of *miR-132* and *miR-126* on cell proliferation, A172 and T98G glioblastoma cells were transiently transfected with pre-miR-132 and pre-miR-126 molecules in relation to scrambled control (pre-NC1)-transfected cells (see 3.3.5). A commercially available cell proliferation chemiluminescence ELISA assay (Roche, Mannheim, Germany) was used for the quantification of cell proliferation. This proliferation assay is based on the measurement of 5-bromo-2´-deoxyuridine (BrdU) (pyrimidine analogue) incorporation during DNA synthesis in proliferating cells instead of thymidine (Porstmann et al 1985). Incorporated BrdU is detected by immunoassay.
Glioblastoma cells were incubated with BrdU labeling reagent 48 h after transient transfection with subsequent incubation over night at 37 °C in a humidified atmosphere containing 5 % CO_2. Twenty-four hours after labeling, cells were fixed and incubated with the anti-BrdU antibody conjugated with peroxidase (POD) according to the manufacturer's instructions. BrdU-containing complexes were detected by the substrate reaction after a few washing steps. The chemiluminescent signals reflect the amount of incorporated BrdU during DNA synthesis and correlate with cell proliferation. Results were obtained in at least three independent biological experiments.

3.4.3 Viability assay

To determine the effect of *miR-132* and *miR-126* on cell viability, A172 and T98G glioblastoma cells were transiently transfected as described in chapter 3.3.5. The commercially available CellTiter-Glo® Luminescent Cell Viability Assay (Promega # G7572) was used determine the number of viable cells in culture according to the manufacturer's instructions. This assay is based on a luciferase reaction that detects adenosine triphosphate (ATP), which is released from living cells after breaking their membranes. The amount of released ATP correlates with cell viability (Figure 11). Seventy-two hours after transient transfection, cells were analyzed using the CellTiter-Glo® Reagent. Results were obtained in three independent biological experiments.

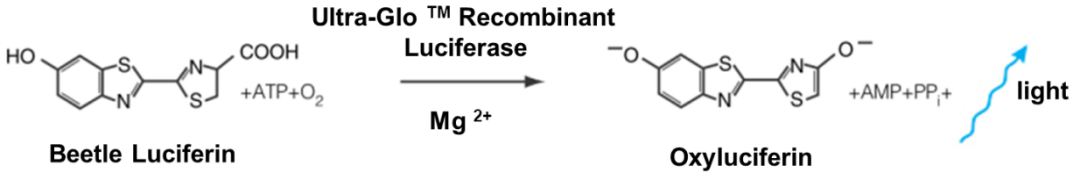

Figure 11: Reaction of Luciferin and ATP to Oxyluciferin, ADP and light (http://www.promega.com).

3.5 3`- Luciferase reporter gene assay system

3.5.1 Generation of wild-type 3-UTR fragments for cloning into the psiCHECK™-2 vector

PCR amplification with HotStar Taq DNA polymerase (#203205; Qiagen, Hilden) was used to generate wild-type 3-UTR fragments (see 3.1.2) from a pool of genomic DNAs that was used as template (Table 1). The PCR conditions are listed in Table 23. The PCR product purification spin kit (GENOMED GmbH, Löhne) was used for direct purification of the PCR products according to the company`s instructions. The purified PCR products contained the 3`UTR regions of the respective mRNAs that includes the respective miRNA binding sequences. All investigated wt-PCR-amplified DNA

fragments were flanked by *XhoI* and *NotI* restriction enzyme sequences. PCR products were digested and cloned into the psi-CHECK^{TM}-2 vector.

Table 23: PCR condition to generate wild-type (wt) 3'-UTR fragments of target mRNAs.

reaction mix for	volume (µ)	program
PCR-wt-amplified DNA fragment		
10x PCR-buffer	2.5	95°C 15 min
dNTPs (2 mM)	2.5	95°C 30 sec
wt-primer-F (10 pmol)	1	X°C 30 sec
wt-primer-R (10 pmol)	1	72°C 30 sec
HotStar Taq (5 U/µl)	0.125	72°C 5 min
Aqua dest.	12.86	4°C ∞
genomic DNA pool (20 ng/µl)	5	40 cycles
	25 µl	
		X = depending on wt-primer

3.5.2 Direct deletion of the miRNA binding site in the 3`-UTR of target genes by Overlap - Extension Polymerase Chain Reaction (OE-PCR)

The overlap-extension PCR combines two PCR products to generate a longer PCR fragment (Figure 12). The 3´- ends of the two PCR-products should have an overlap of approximately 15-25 bp including the sequence to be deleted or mutated. First, two PCR-fragments, which overlap in the region to be deleted, are generated as described in Table 24. The PCR-products were purified with the PCR product purification spin kit (GENOMED GmbH, Löhne) according to the company`s instructions. In the overlap-extension PCR step, both purified PCR-fragments were combined and denatured for 3 min at 95°C followed by two cycles of 94°C for 1 min, 52°C for 2 min and 72°C for 1 min in the presence of dNTPs and Taq DNA Polymerase but without the outer primers (Table 25 A). Then the primers were added and the PCR cycles were repeated for 12 times (Table 25 B). The amplified DNA fragment, containing the deleted miRNA binding site and flanking *XhoI* and *NotI* restriction enzyme sequences was gel purified and cloned into the respective sites of the psi-CHECK^{TM}-2 vector.

Table 24: 1. PCR conditions for the 1. PCR reaction to generate 3'- UTR fragment 1 (A) and for the 2. PCR reaction to generate 3'- UTR fragment 2 (B).

A)

reaction mix for	volume (µ)	program
3`- UTR fragment 1		
10 x PCR-buffer	2.5	95°C 5 min
dNTPs (2 mM)	2.5	95°C 30 sec
del-primer-F (10 pmol)	1	X°C 30 sec
wt-primer-R /10 pmol)	1	72°C 30 sec
Invitrogen Taq (5 U/µl)	0.2	72°C 5 min
$MgCl_2$ (25 mM)	1.5	4°C ∞
Aqua dest.	15.3	
wt-plasmid DNA (20 ng/µl)	1	40 cycles
	25 µl	
		X = depending on wt-primer-R

B)

reaction mix for	volume (µ)	program
3`- UTR fragment 2		
10 x PCR-buffer	2.5	95°C 5 min
dNTPs (2 mM)	2.5	95°C 30 sec
del-primer-R (10 pmol)	1	X°C 30 sec
wt-primer-F /10 pmol)	1	72°C 30 sec
Invitrogen Taq (5 U/µl)	0.2	72°C 5 min
$MgCl_2$ (25 mM)	1.5	4°C ∞
Aqua dest.	15.3	
wt-plasmid DNA (20 ng/µl)	1	40 cycles
	25 µl	
		X = depending on wt-primer-R

Table 25: Overlap-Extension PCR conditions to generate the 3'- UTR fragment with deleted miRNA binding site.

A)

reaction mix Overlap-extension PCR	volume (µ) or ng	program
3`UTR fragment 1	100 ng	94°C 3 min
3`UTR fragment 2	100 ng	94°C 1 min
10 x PCR-buffer	2.5	52 °C 2 min
dNTPs (2 mM)	2.5	72°C 1 min
Invitrogen Taq (5 U/µl)	0.5	72°C 5 min
$MgCl_2$ (25 mM)	1.5	4°C ∞
Aqua dest.	X	2 cycles
	23 µl	
	X = depending on PCR amplified DNA fragments	

B)

reaction mix addition of primers to the reaction mix	volume (µ)	program
wt-primer-F (10 pmol)	1	94°C 3 min
wt-primer-R (10 pmol)	1	94°C 1 min
		52 °C 2 min
		72°C 1 min
		72°C 5 min
		4°C ∞
		12 cycles

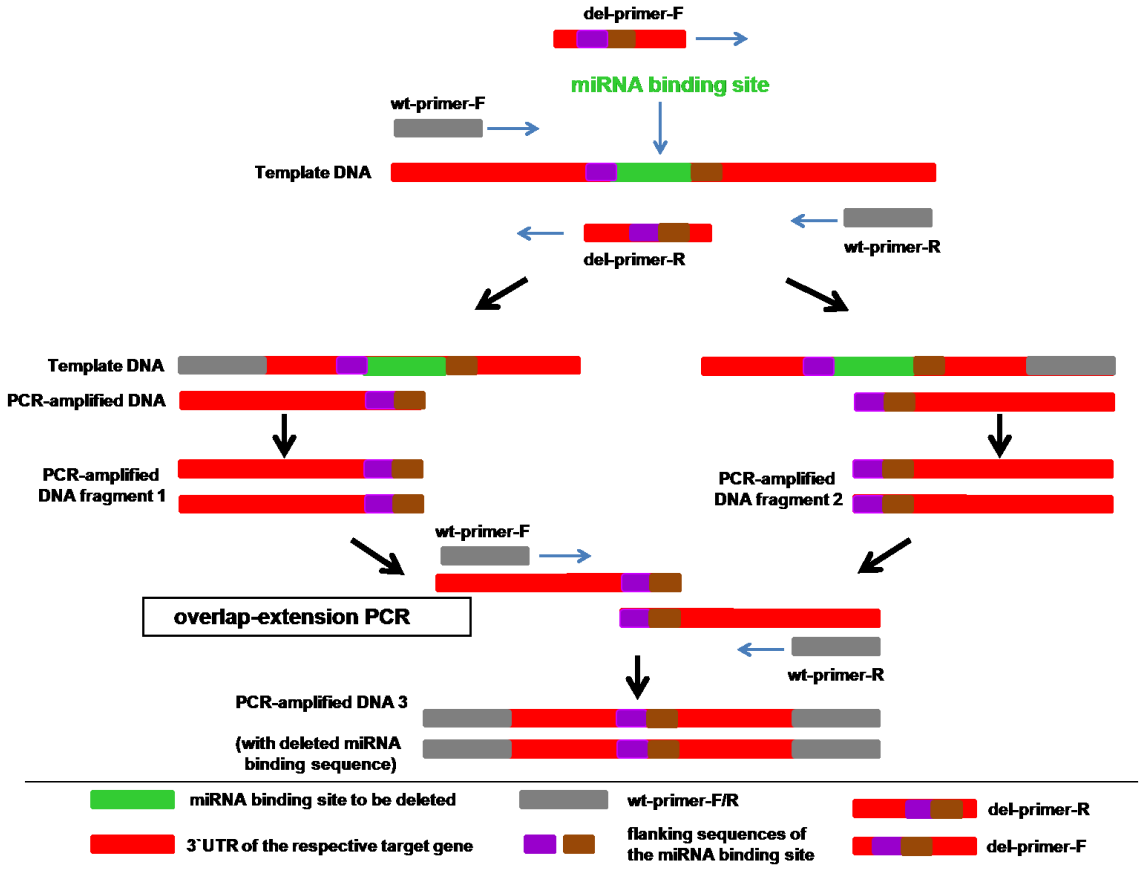

Figure 12: Schematic representation of the overlap extension polymerase chain reaction (OE-PCR).

3.5.3 Cloning of the 3`UTR of the putative miRNA targets into psiCHECK™-2 vector for the luciferase reporter gene assays

To validate the direct binding of the selected miRNAs to their putative mRNA targets, the 3`UTR regions of the respective mRNA genes were cloned into the commercially available luciferase reporter plasmid psiCHECK™-2 (Promega, Madison, WI), which is carrying two reporter genes called Firefly and Renilla. The Dual-Glo® Luciferase Assay System (Promega, Madison, WI) enables the quantification of luminescent signal from the two reporter genes Firefly and Renilla luciferase in a single sample. Thereby, the activity of the primary reporter Renilla luciferase is correlated with the effect of specific stimuli. Activity of the control reporter Firefly provides an internal control to normalize results (see also below 3.5.4).

PCR fragments containing parts of the *SIRT1* 3`UTR (Figure 52 B), *JARID1A* 3`UTR (Figure 55 B), *BTG2* 3`UTR (Figure 58), *GPD1L* 3`UTR or *COX10* 3`UTR (Figure 59 B) were cloned into the vector as followed. Restriction enzymes *XhoI* and *NotI* were used to digest the PCR products and the psiCHECK^{TM}-2 vector. The digested PCR products and the linearized psiCHECK^{TM}-2 vector were gel-purified using Invisorb® Spin DNA Extraction Kit (Invitek, Berlin). DNA was eluted in 20 µl distilled water according to the manufacturer`s instructions. The quantity and concentration of the DNA was determined photometrically with the Nano-Drop 1000 photometer.

100 ng of linearized vector DNA and about 300 ng of the respective target gene-PCR product were ligated by using 1 µl T4 DNA ligase (Fermentas, St. Leon-Rot) in a total volume of 50 µl overnight randomly for 1 minute 16 °C, then 22 °C, and 37 °C. 5 µl of the ligation were incubated with 100 µl DH5α competent cells on ice for 30 min. DNA was incorporated into the competent cells by using a heat shock at 42 °C for 30 sec followed by cooling down on ice for 2 min. Then, 250 µl of antibiotic free medium was added and cells were incubated for 1 hour at 37 °C to recover from the heat shock. Subsequently cells were shortly centrifuged, the supernatant was discarded and the pellet was resolved (in the final residual of antibiotic free medium) by mechanical movement. Finally the transformed cells were plated on LB plates containing 100 µg/ml ampicillin (Amp). The bacteria were incubated overnight at 37 °C. Single colonies were picked on the following day and were inoculated in 3 ml LB-Amp media over night. To test if the PCR fragment was inserted properly a colony PCR from each colony was performed in parallel. Colony PCR was performed using a forward primer located in the psi-CHECK^{TM}-2 vector backbone and a reverse primer located in the respective PCR fragment. Afterwards, PCR products were analyzed via agarose gel electrophoresis. DNA extraction was performed only from overnight cultures showing colonies with fragments of correct size. The peqGOLD Plasmid Miniprep Kit (PeqLab, Erlangen) was used to extract the respective plasmid DNA followed by DNA-plasmid-elution in 50 µl distilled water. A control digest was performed with 5 µl of the plasmid DNA, 0.5 µl *NotI*, 0.5 µl *XhoI* in a final volume of 20 µl. The reaction mixture was incubated for 1 hour at 37 °C and briefly analyzed via agarose gel electrophoresis. Finally, DNA of clones with insert was analyzed by sequencing (StarSEQ, Mainz) (http://www.starseq.com).

3.5.4 Determination of the luciferase activity

The first step of this assay consists of the measurement of the Firefly Luciferase by adding Luciferase Assay Reagent II to the cells. As a result, the cell membranes are broken and the beetle luciferin is oxidized. This reaction requires ATP, Mg^{2+} and O_2. Then, photon emission can be measured. Addition of Dual-Glo® Stop & Glo® Reagent quenches the luminescence from the Firefly reaction and provides the substrate for Renilla luciferase (Figure 14). For this assay, glioblastoma cells were seeded in 96-well plates and kept at 37 °C in a humidified atmosphere containing 5 % CO_2 for 24 h. The next day, cells were transiently transfected with 50 nM pre-miR / pre-NC1 molecules and 200 ng of the respective plasmid constructs using the transfection reagent Lipofectamine™ 2000 (Invitrogen, Carlsbad, CA). Oligonucleotide solution, plasmid constructs and transfection reagent were diluted in serum-reduced Opti-MEM® medium (LifeTechnologies/GIBCO, Carlsbad, CA) according to Table 15. The oligonucleotide-plasmid-construct-reaction as well as the lipofectamine reaction were incubated for 5 minutes at RT. Then, both dilutions were combined, mixed and incubated for an additional 20 min at RT. 50 µl of the mixed dilution was finally added to the cells. The measurements of Firefly and Renilla luciferases were done after respective time points (depending on the investigated plasmid construct) according to the manufacturer´s instructions. Results were collected from at least three independent biological experiments. Figure 13 provides an overview of the 3`UTR luciferase reporter gene assay procedure.

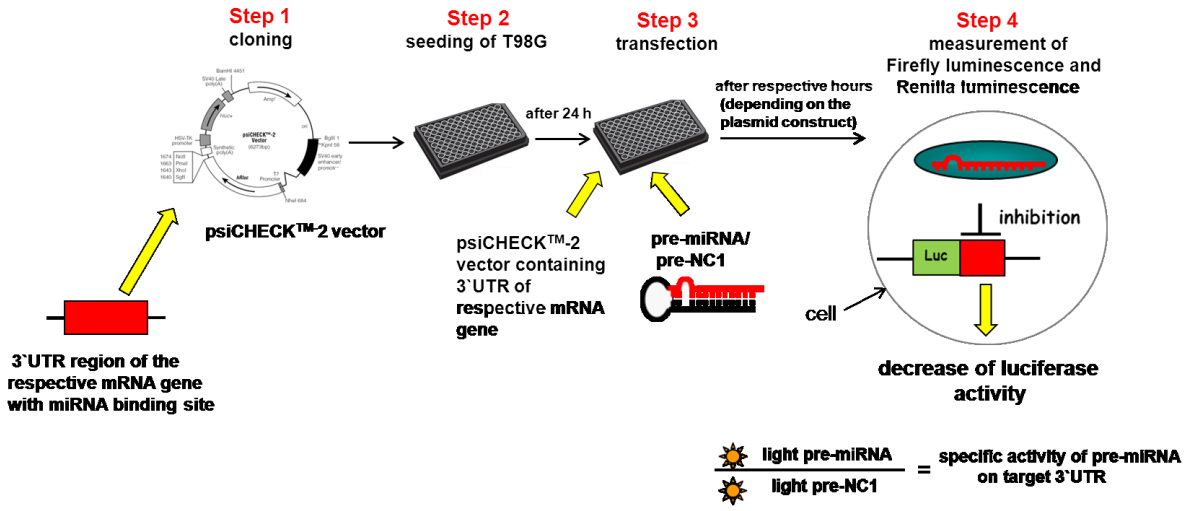

Figure 13: Schematic representation of the 3`UTR luciferase reporter gene assay procedure.

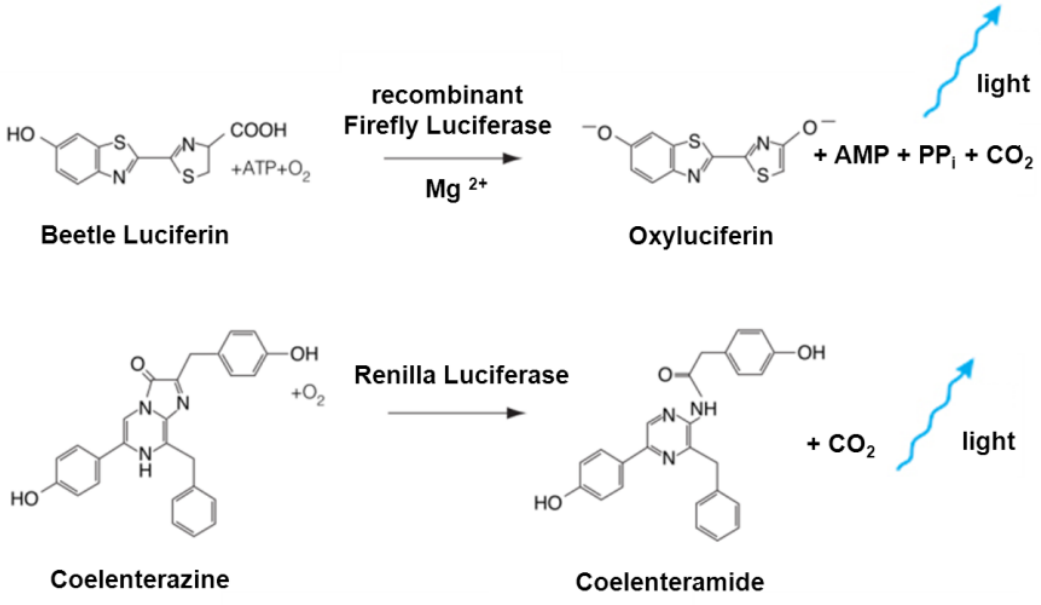

Figure 14: Schematic representation of the bioluminescent reaction catalyzed by Firefly and Renilla luciferases (modified according to http://www.promega.com).

3.6 Statistical methods

Table 26 provides an overview of the statistical methods used in this study. The bioinformatic analyses based on miRNA expression data were carried out by Dr. Marc Zapatka at the DKFZ Heidelberg (Tusher et al 2001, Vandesompele et al 2002).

Table 26: Overview of the statistical methods used in this study.

application	statistical method
miRNA profiling	determination of the most stable miRNAs according to Vandesompele et al. 2002 under exclusion of miRNAs with ct-values of 40 miRNA expression was determined relative to the expression of four miRNAs (miR-30a-5p, miR-30b, miR-30c, miR-30d) used as a reference differential miRNA expression analysis was based on Tusher et al. 2001
miRNA expression	
in astrocytic tumors in relation to non-neoplastic brain tissue samples	***miR-132***: Kruskal-Wallis test ***miR-126***: Kruskal-Wallis test ***miR-210***: Kruskal-Wallis test with Dunn`s Multiple Comparison test (* p < 0.05, ** p < 0.01 and *** p < 0.001)
in glioblastoma stem cells grown under hypoxic conditions in relation to cells grown under normoxic conditions	***miR-210***: Mann Whitney test (* p < 0.05, ** p < 0.01 and *** p < 0.001)
in 5-Aza/TSA treated glioma cells in relation to non-treated cells	***miR-132***: two-sided student´s t-test ***miR-126***: two-sided student´s t-test (* p < 0.05, ** p < 0.01 and *** p < 0.001)
sodium bisulfite sequencing	
miR-132 and miR-126 expression analysis in human gliomas in relation to the methylation status of the investigated genomic CpG sites	Mann Whitney test (* p < 0.05, ** p < 0.01 and *** p < 0.001)
mRNA expression analysis	
<u>in glioblastoma cell lines after TSA treatment</u> <u>in relation to non-treated cells</u> ***p21/CDKN1A***	two-sided student t-test (* p < 0.05, ** p < 0.01, *** p < 0.001)
<u>in astrocytic tumors in relation to non-neoplastic brain tissue samples</u> ***SIRT1***	Mann Whitney test (* p < 0.05, ** p < 0.01 and *** p < 0.001)
BTG2	Kruskal-Wallis test
JARID1A-probe 1-3	Kruskal-Wallis test
PLAGL2	Kruskal-Wallis test
GPD1L	Kruskal-Wallis test
COX10	Kruskal-Wallis test with Dunn`s Multiple Comparison test (* p < 0.05, ** p < 0.01 and *** p < 0.001)
<u>in pre-miRNA/pre-NC1 transfected glioblastoma cells</u>	***miR-132***
SIRT1	two-sided student t-test
BTG2	two-sided student t-test
JARID1A	two-sided student t-test (* p < 0.05, ** p < 0.01, *** p < 0.001)
miR-132 and miR-126 promotor DNA	
assessment of the increase of ***miR-132*** and ***miR-126*** immunoprecipitated promotor DNA bound to acetylated histone H3 and acetylated histone H4 after trichostatin A treatment in relation to non-treated cells	one-sided student t-test (* p < 0.05, ** p < 0.01, *** p < 0.001)
functional assays (pre-miRNA vs. pre-NC1)	***miR-132*** and ***miR-126***
cell proliferation ELISA, BrdU (chemiluminescence) assay	two-sided student t-test
Apo-ONE® homogeneous caspase 3/7 assay	two-sided student t-test
CellTiter-Glo® luminescent cell viability assay	two-sided student t-test (* p < 0.05, ** p < 0.01, *** p < 0.001)
3`UTR luciferase reporter gene assay (pre-miRNA vs. pre-NC1)	***miR-132, miR-212*** and ***miR-210***
Dual-Glo® Luciferase Assay	two-sided student t-test (* p < 0.05, ** p < 0.01, *** p < 0.001)

4 Results

4.1 MicroRNA profiling in primary gliomas and glioblastoma cells

The expression of 365 distinct microRNAs was determined in 125 astrocytic and oligodendroglial gliomas of different malignancy grades. Ten non-neoplastic brain tissue samples served as reference tissue for the expression profiling. In addition, four established glioblastoma cell lines treated with the demethylating agent 5-aza-2`-deoxycytidine (5-Aza) and/or the histone deacetylase inhibitor trichostatin A (TSA) were screened together with non-treated control cells for miRNA expression profiles. In collaboration with Prof. Dr. med. Markus Riemenschneider (Department of Neuropathology, University Hospital Regensburg), miRNA expression profiles of microdissected areas from the infiltration zone and solid tumor parts were determined in five primary glioblastomas (WHO grade IV) and two anaplastic astrocytomas (WHO grade III). To identify miRNAs regulated by hypoxia, miRNA expression profiles were analysed in four glioblastoma cell lines grown either under normoxia or under hypoxia for 48 h and 96 h (collaboration with Prof. Dr. med. Till Acker, Department of Neuropathology, University Hospital Giessen/Marburg). Furthermore, miRNA expression profiles in glioma stem cell cultures were compared with those in adherent glioma cell lines (collaboration with Prof. Dr. Katrin Lamszus, Department of Neurosurgery, University Hospital Hamburg-Eppendorf). Bioinformatician Edith Willscher (Interdisciplinary Centre for Bioinformatics, University of Leipzig, Germany) performed the bioinformatics analysis, based on the miRNA expression data of 5-Aza/TSA treated glioblastoma cells and Dr. Marc Zapatka as well as Prof. Dr. Benedikt Brors (Division of Theoretical Bioinformatics, DKFZ Heidelberg, Germany) performed the bioinformatic analysis, based on miRNA expression data of the other group-comparisons. Figure 15 provides a graphical overview of the experiments summarized in this thesis.

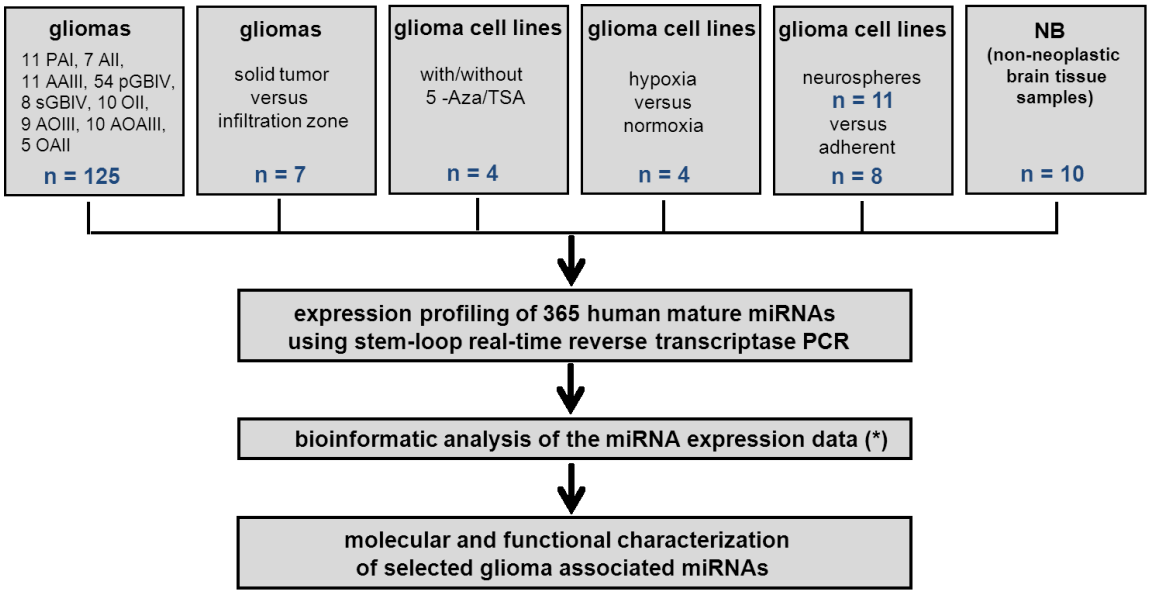

Figure 15: Schematic outline of the project and and overview of the experiments on gliomas and glioblastoma cells summarized in this doctoral thesis. (*) The bioinformatics analyses of the miRNA expression profiling data were carried out in collaboration with Dr. Marc Zapatka, DKFZ Heidelberg.

4.1.1 MiRNAs separating low-grade diffuse astrocytoma from glioblastoma

Microarray-based expression profiling of biological samples has proven to be a powerful tool for molecular classification and opens up the possibility of studying the biological relevance of expression differences (Vandesompele et al 2002). The miRNA profiling of 125 primary glioma tissues revealed a number of candidate miRNAs showing differential expression in different tumor types and grades, although it was not possible to correctly classify each tumor by unsupervised cluster analysis of the entire tumor cohort (data not shown). However, group-wise comparisons using cluster analysis or multidimensional scaling (MDS) revealed interesting results and promising candidate miRNAs as illustrated here by the comparison of diffuse astrocytomas WHO grade II with primary or secondary glioblastomas WHO grade IV. MDS is one powerful method that converts the structure in the similarity matrix to a simple geometrical picture (Chen and Meltzer 2005). Dr. Marc Zapatka and Prof. Dr. Benedikt Brors (Division of Theoretical Bioinformatics, DKFZ Heidelberg, Germany) performed the MDS-Plot of Proximity Matrix based expression data for 365 miRNAs of two group-comparisons to visualize the differences. The larger the dissimilarity between AII

versus pGBIV (A) or between AII versus sGBIV (B), the further apart are the data points representing the investigated tumor samples of each group in the picture. The MDS analysis summarized conspicuous separations between the data points of AII versus pGBIV and AII versus sGBIV, respectively (Figure 16).

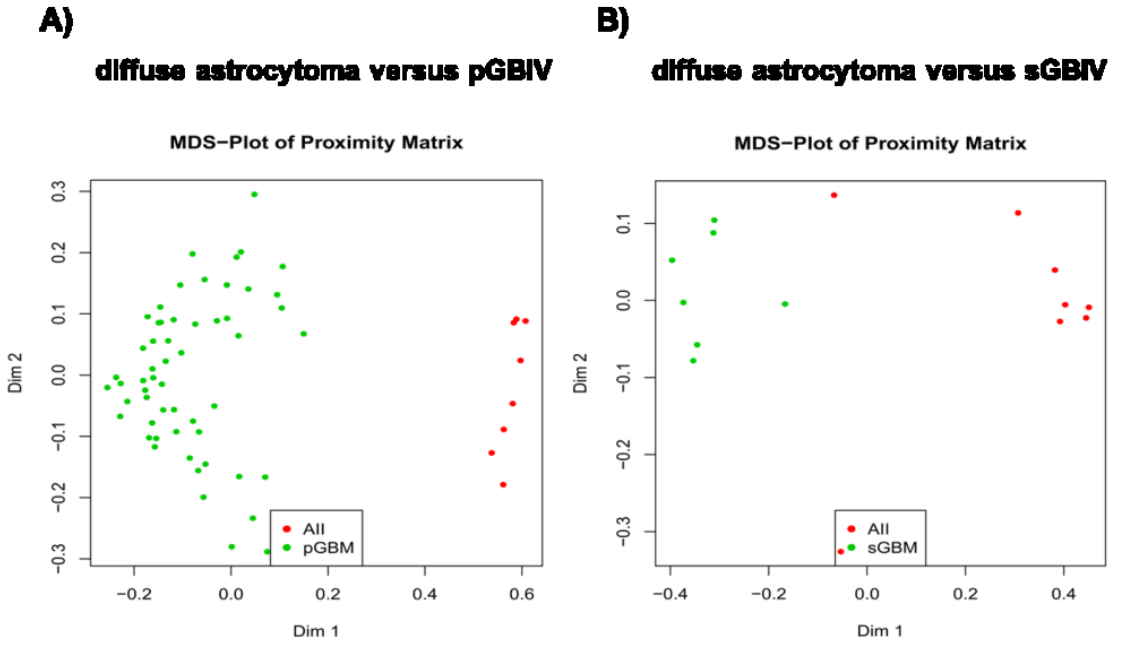

Figure 16: Multidimensional scaling analysis (MDS) of diffuse astrocytomas (AII) compared to either primary glioblastomas (pGBIV, A) or secondary glioblastomas (sGBIV, B). To visualize the difference between different groups a Random Forest classifier (Moorthy and Mohamad 2011) was trained on the expression of all expressed miRNAs (365 miRNAs) using strata for the groups and training 5000 trees. Based on the resulting trees, a proximity matrix was build considering the frequency that pairs of data points are in the same terminal nodes. Using Sammon mapping for multidimensional scaling this proximity matrix was visualized (DIM = dimension).

Furthermore, group-wise comparisons of diffuse astrocytomas with either primary glioblastomas or secondary glioblastomas using cluster analysis revealed several miRNAs (including *miR-126* and *miR-210*) that were differentially expressed between the individual tumor groups (Figure 17).

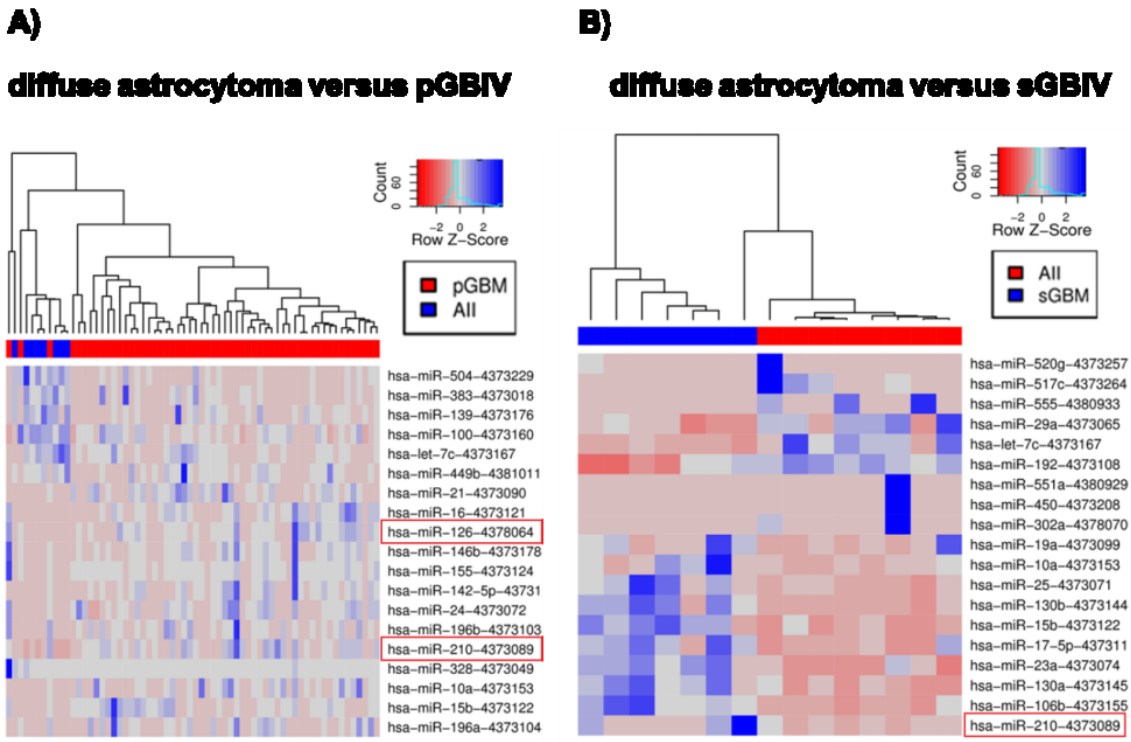

Figure 17: Group-wise comparisons using unsupervised cluster analysis of diffuse astrocytomas with either primary glioblastomas (pGBIV, A) or secondary glioblastomas (sGBIV, B). Candidate miRNAs, i.e. *miR-126* and *miR-210*, further investigated in this thesis are outlined in red.

4.1.2 Epigenetically regulated miRNAs in gliomas

To identify miRNAs regulated by epigenetic changes in gliomas, miRNA expression profiles were determined in four glioblastoma cell lines treated with a combination of DNA-demethylating and chromatin-modifying drugs, namely the demethylating agent 5'-aza-2'-deoxycytidine and the histone deacetylase inhibitor trichostatin A (5-Aza/TSA), in relation to the respective non-treated cell lines. Thereby, 50 miRNAs were identified that exhibited a more than 2-fold up-regulation of expression after treatment in at least two of four investigated cell lines (Figure 18) (Table 27).

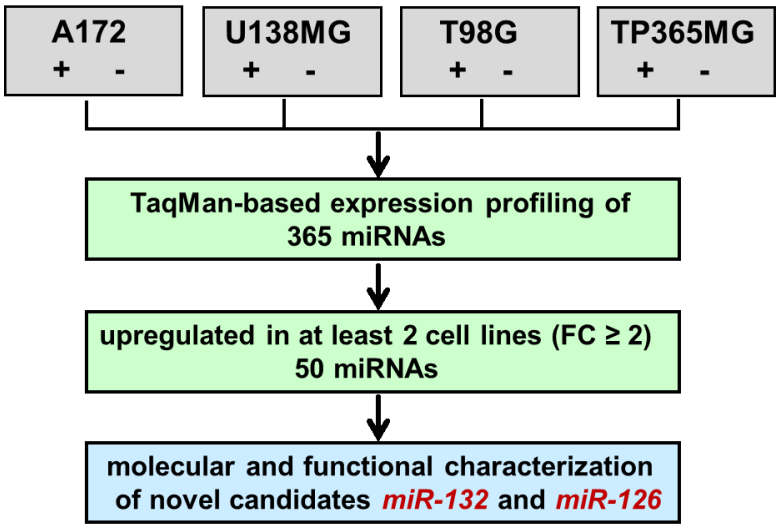

Figure 18: Flow Chart of the expression profiling of mature miRNAs in glioblastoma cell lines either treated with 5-Aza/TSA (+) or untreated (-). Note, small-nucleolar RNAs (RNU44 and RNU48) were used for miRNA expression normalisation.

Table 27: MiRNAs exhibiting a more than two-fold increased expression in at least 2 of the 4 glioblastoma cell lines treated with 5-Aza+TSA as compared to the respective untreated cell lines. The table also lists the respective chromosomal location of each miRNA, associated host genes and miRNA clusters, as well as the presence of 5'-CpG islands. Note that several candidate miRNAs belong to large miRNA clusters on 14q32.31 and 19q13.41, respectively (marked in orange and yellow).

increased expression in all 4 glioblastoma cell lines (FC ≥ 2) (2 miRNAs)				
miRNA	**location**	**gene**	**cluster**	**CpG-island**
miR-515-3p	19q13.41		19q13.41	
miR-30e-5p	1p34.2	NFYC	miR-30c-1	yes
increased expression in 3 out of 4 glioblastoma cell lines (FC ≥ 2) (11 miRNAs)				
miRNA	**location**	**gene**	**cluster**	**CpG-island**
miR-200c	12p13.31		miR-141	
miR-375	2q35			yes
miR-183	7q32.2		miR-182/miR-96	
miR-518b	19q13.41		19q13.41	
miR-518e	19q13.41		19q13.41	
miR-520g	19q13.41		19q13.41	
miR-133a-1	18q11.2	MIB1 opposite	miR-1-2	
miR-133a-2	20q13.33	C20orf166		
miR-330	19q13.32	EML2		yes
miR-518f	19q13.41		19q13.41	
miR-601	9q33.2	DENND1A		yes
increased expression in 2 out of 4 glioblastoma cell lines (FC ≥ 2) (37 miRNAs)				
miRNA	**location**	**gene**	**cluster**	**CpG-island**
miR-155	21q21.3			
miR-218-1	4p15.31	SLI2		yes
miR-218-2	5q35.1	SLIT3		yes
miR-449a	5q11.2	CDC20B	miR-449b/miR-449c	yes
miR-509-1	Xq27.3		miR-509-2/509-3	
miR-509-2	Xq27.3		miR-509-1/509-3	
miR-509-3	Xq27.3		miR-509-1/509-2	
miR-517c	19q13.41		19q13.41	
miR-518a-1	19q13.41		19q13.41	
miR-518a-2	19q13.41		19q13.41	
miR-127	14q32.31	RLT1 opposite	14q32.31	yes
miR-132	17p13.3		miR-212	yes
miR-135b	1q32.1			
miR-192	11q13.1		miR-194-2	
miR-299-5p	14q32.31		14q32.31	
miR-432	14q32.31	RLT1 opposite	14q32.31	yes
miR-433	14q32.31	RLT1 opposite	14q32.31	
miR-134	14q32.31		14q32.31	
miR-193a	17q11.2			yes
miR-182	7q32.2		miR-183/miR-96	
miR-422a	15q22.31			
miR-425	3p21.31	DALRD3	miR-191	yes
miR-126	9q34.3	EGFL7		yes
miR-139	11q13.4	PDE2A		yes
miR-195	17p13.1		miR-497	
miR-376a	14q32.31		14q32.31	
miR-146b	10q24.32			
miR-382	14q32.31		14q32.31	
miR-486	8p11.21	ANK1		yes
miR-519d	19q13.41		19q13.41	
miR-425-5p	3p21.31	DALRD3	miR-191	yes
miR-629	15q23	TLE3		yes
miR-642	19q13.32	GIPR		yes
miR-618	12q21.31	LIN7A		yes
miR-646	20q13.33			
miR-579	5p13.3	ZFR		yes
miR-512-3p	19q13.41		19q13.41	

Previous studies showed that the expression of a large subset of mammalian miRNAs is transcriptionally linked to the expression of protein-coding genes. Approximately one-third of human miRNAs are located within intronic regions of coding transcription units (Baskerville and Bartel 2005, Rodriguez et al 2004). Due to this fact, I focused as a matter of priority on miRNAs located within intronic regions of protein-coding genes. *MiR-30e-5p* is located within intron 5 of the *NFYC* gene (Homo sapiens nuclear transcription factor Y, gamma). Array-based expression profiling identified significantly increased expression levels of *miR-30e-5p* in all investigated human glioblastoma cell lines. Validation experiments based on targeted RT-PCR analysis, however, did not validate increased expression of *miR-30e-5p* and *NFYC* in the investigated glioblastoma cell lines after treatment with 5-Aza/TSA (data not shown). Furthermore, examination of the DNA methylation status in the 5`genomic region of *miR-30e-5p* revealed methylation in glioblastoma cells and non-neoplastic brain tissue samples. This finding indicates a tissue-, and not tumor-specific methylation of *miR-30e-5p* 5`genomic region in the central nervous system (data not shown). Consequently, this miRNA was not further investigated for epigenetic inactivation mechanisms in human gliomas. Another candidate, *miR-330*, is being studied by Dr. Marietta Wolter (Department of Neuropathology, Düsseldorf, Germany) in an independent project, and was therefore not further addressed here. In addition, *miR-601* was excluded from further analyses due to its weak expression in different non-neoplastic brain tissue samples and the fact that no functional annotation was known at the time of the miRNA screening. To limit the number of miRNAs increased in two out of four investigated cell lines after 5-Aza/TSA treatment, *miR-218* was excluded from further evaluations as Independent RT-PCR analysis failed to demonstrate increased levels of *miR-218* in glioblastoma cells after treatment (data not shown). In addition, a large number of miRNAs with increased expression in the 5-Aza+TSA treated glioblastoma cell lines are located in clusters on chromosome 19q13 (yellow) and 14q32 (orange) (Table 27). MicroRNA expression data revealed that several miRNAs, located in clusters on chromosome 19q13, are not expressed in non-neoplastic brain tissue samples. Thus, they were not further investigated. Previous studies reported that miRNAs mapping to chromosome 14q32.31 are transcribed as a long polycistronic transcript, spanning approximately 210 kb of the mouse genome (Kim et al 2009, Seitz et al 2004). In view of the large number of miRNAs 7 + 46 miRNAs in the bipartite cluster on chromosome 14q32.3 and the unknown complexity of their interaction and regulation, these candidates were further investigated for epigenetic inactivation mechanisms in human

gliomas. Finally, two candidate miRNAs, namely *miR-132* and *miR-126*, were selected for further epigenetic and functional analyses. These two miRNAs were significantly down-regulated in the investigated astrocytic tumor tissues when compared to non-neoplastic brain tissue samples (Figure 19). The miRNA *miR-126* is located within intron 7 of the *EGFL7* gene whereas *miR-132* is embedded within a large CpG island on chromosome arm 17p. Therefore, the expression of both miRNAs might be regulated by epigenetic changes.

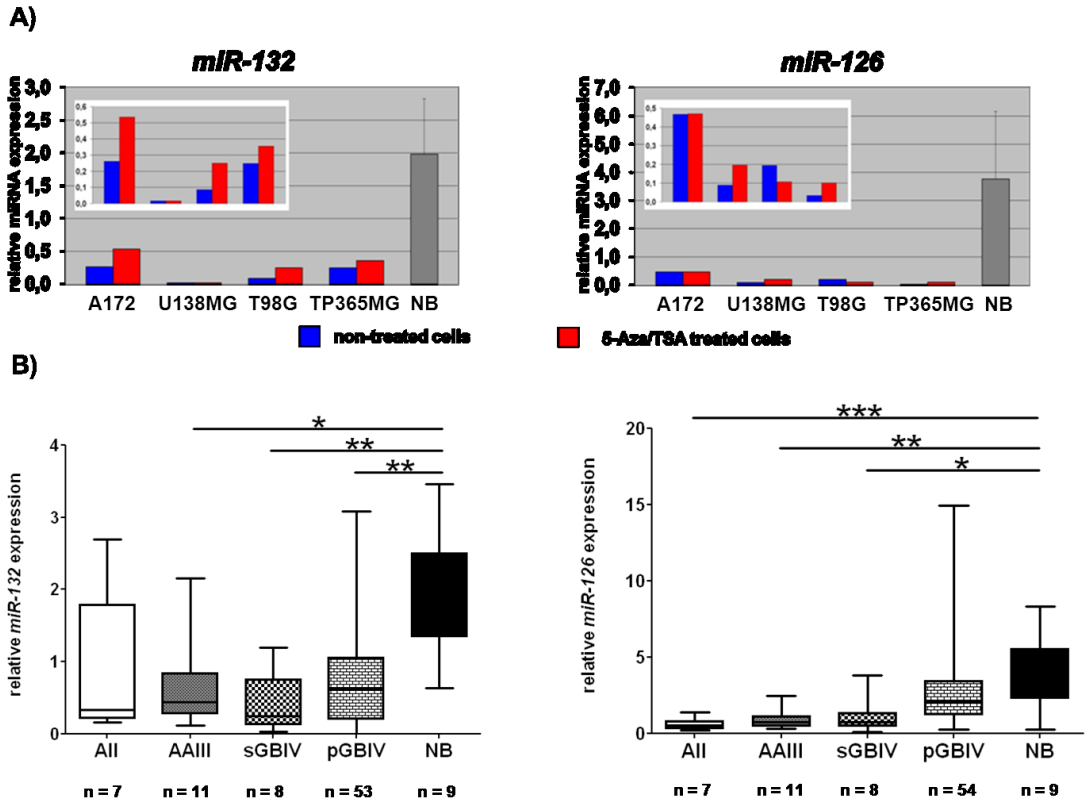

Figure 19: Increased expression of *miR-132* and *miR-126* in two of four human glioma cell lines treated with 5-Aza/TSA (A). Both miRNAs were found to be significantly down-regulated in several groups of astrocytic tumors when compared to non-neoplastic brain tissue samples (B). A) Glioblastoma cell lines were grown in 500 nM 5-Aza for 48 h, washed and grown for another 24 h in 500 nM 5-Aza and 1 µM TSA. Vertical bars represent the miRNA expression levels relative to the expression of four miRNAs (miR-30a-5p, miR-30b, miR-30c, miR-30d) used as reference. The represented data were obtained in the TaqMan® microfluidic card-based expression profiling experiments. For NB, the mean expression value of each miRNA in nine different brain tissue samples is shown with standard deviation. **B)** Box plots are depicted indicating median, lower and upper quartile as well as sample maximum and sample minimum of normalized expression values. Asterisks indicate significant expression differences (Kruskal-Wallis test with Dunn`s Multiple Comparison test: AII vs. NB, AAIII vs. NB, sGBIV vs. NB, pGBIV vs. NB) (* $p < 0.05$, ** $p < 0.01$ and *** $p < 0.001$). AII, diffuse astrocytoma, WHO grade II; AAIII, anaplastic astrocytoma, WHO grade III; sGBIV, secondary glioblastoma, WHO grade IV; pGBIV, primary glioblastoma, WHO grade IV; NB, normal brain tissue. n = number of investigated tissue samples

4.1.3 MiRNAs induced by hypoxia in glioblastoma stem cell lines

MiRNA profiling was performed for the identification of hypoxia-regulated miRNAs in four glioblastoma stem cell lines (ED010, ED015, ED022, ED026) grown under hypoxia (1 % O_2) for 48 h or 96 h in comparison to cells grown under normoxic conditions (21 % O_2) (Figure 20). The cell lines were cultured by Sascha Seidel (Seidel et al 2010, Department of Neuropathology, Justus-Liebig-University Giessen, Germany), who provided corresponding deep-frozen cell pellets for miRNA profiling. A total of 17 miRNAs were significantly differentially expressed under hypoxic growth conditions (Table 28).

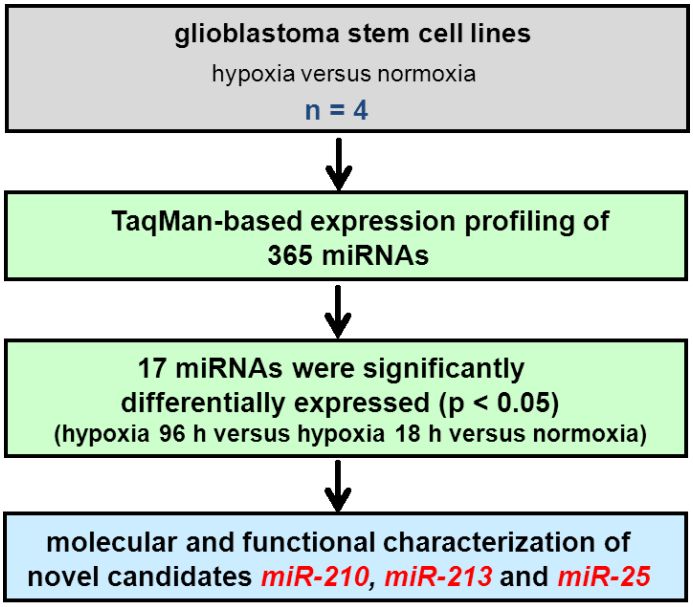

Figure 20: Flow chart of the expression profiling of mature miRNAs in glioblastoma cells grown under hypoxic versus normoxic condiditons.

Eight miRNAs were up-regulated while nine miRNAs were down-regulated after 18 h or 96 h of hypoxia in glioblastoma stem cells (Table 28). Follow-up experiments were focused on miRNAs induced by hypoxia (Figure 21). In this context, *miR-210* showed an elevated expression at 18 h and 96 h under hypoxia, which was significant at 96 h. Moreover, *miR-210* showed an increased expression in the primary glioblastoma group when compared to non-neoplastic brain tissue samples (Figure 22). Therefore, this miRNA was selected for further investigations. In addition, *miR-25 and miR-213*, which

both were upregulated following 18h of hypoxia were selected as candidates for further experiments, with *miR-25* also demonstrating elevated expression in astrocytic tumors as compared to non-neoplastic brain tissue.

Table 28: MicroRNAs exhibiting increased or decreased expression in glioblastoma stem cells grown for 18 h or 96 h under hypoxic (H) as compared to normoxic (N) conditions. The respective chromosomal locations as well as associated host genes and miRNA clusters/cluster partners are also listed in the table.

increased expression under hypoxia (N vs. H 18 h vs. H 96 h) ($p \leq 0.05$)			
miRNA	**location**	**gene**	**cluster**
miR-25	7q22.1	MCM7	miR-106b/miR-93
miR-23b	9q22.32	C9orf3	miR-27b/miR-3074/miR-24-1
miR-213	1q31.3		
miR-27b	9q22.32	C9orf3	miR-23b/miR-3074/miR-24-1
miR-378	5q33.1	PPARGC1B	
miR-34a	1p36.23		
hsa-let-7d	9q22.32		hsa-let-7a-1/hsa-let-7f-1
miR-210	11p15.5		
decreased expression under hypoxia (N vs. H 18 h vs. H 96 h) ($p \leq 0.05$)			
miR-200c	12p13.31		miR-141
miR-30a-3p	6q13		
miR-16	13q14.3/3q26.1		miR-15a/miR-15b
miR-324-3p	17p13.1	ACADVL	
miR-320	8p21.3		
miR-103	5q35.1	PANK3	miR-103b
miR-484	16p13.11	NDE1	
miR-93	7q22.1	MCM7	miR-106b/miR-25
miR-487b	14q32.31		14q32.31

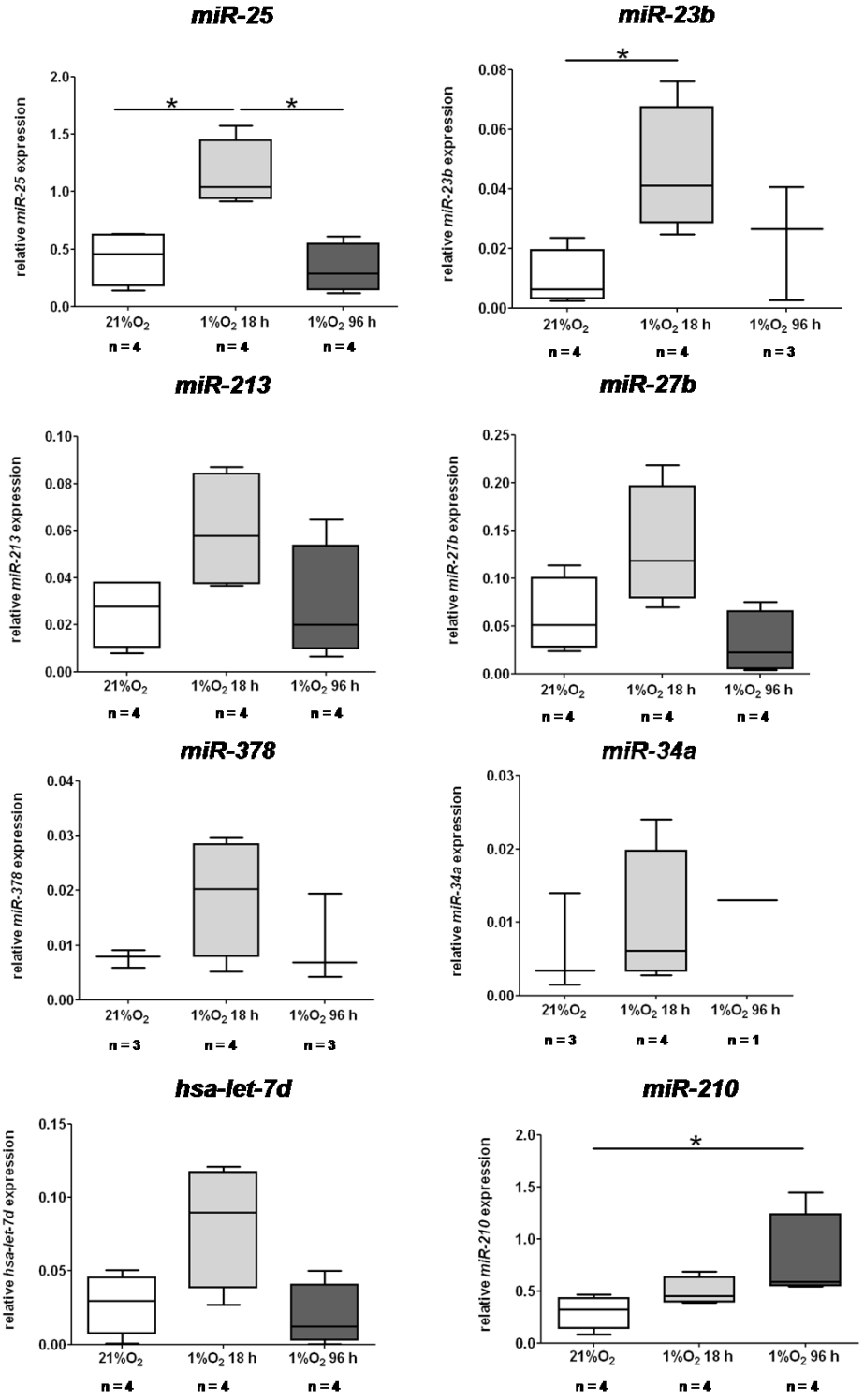

Figure 21: MicroRNAs exhibiting an increased expression in glioblastoma stem cells grown under hypoxic conditions (1% O_2) for either 18 h or 96 h in relation to cells grown under normoxia (21% O_2). Box plots are depicted indicating median, lower and upper quartile as well as sample maximum and sample minimum of normalized expression values. Asterisks indicate significant expression differences (Mann Whitney test: 21% O_2 vs. 1% O_2 18 h, 21% O_2 vs. 1% O_2 96 h, 1% O_2 18 h vs. 1% O_2 96 h) (* $p < 0.05$). n = number of investigated glioblastoma stem cell lines.

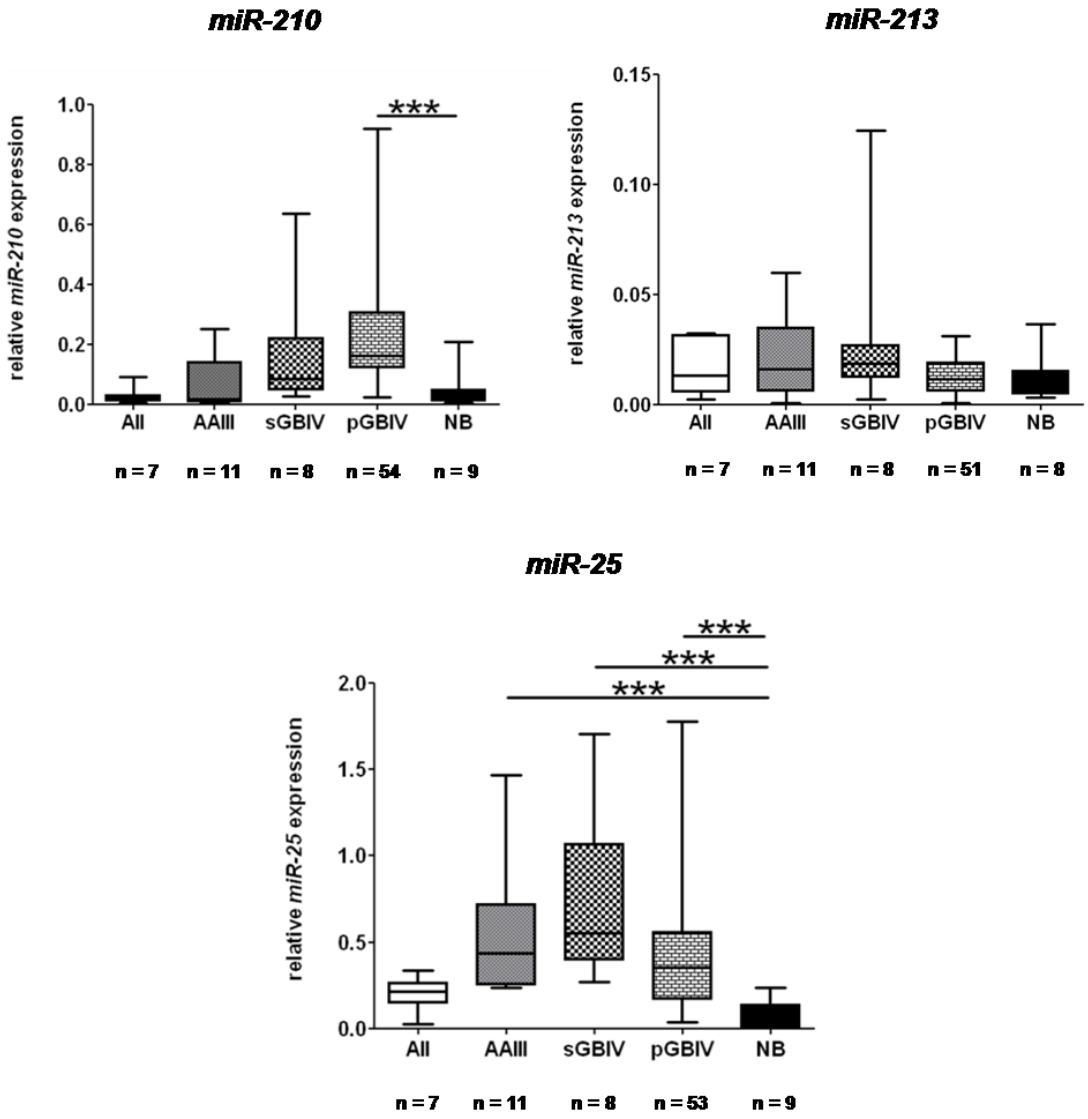

Figure 22: Expression of *miR-210*, *miR-213* and *miR-25* in astrocytic tumors. Asterisks indicate significant expression differences (Kruskal-Wallis test with Dunn`s Multiple Comparison test: AII vs. NB, AAIII vs. NB, sGBIV vs. NB, pGBIV vs. NB) (*** $p < 0.001$). AII, diffuse astrocytoma, WHO grade II; AAIII, anaplastic astrocytoma, WHO grade III; sGBIV, secondary glioblastoma, WHO grade IV; pGBIV, primary glioblastoma, WHO grade IV; NB, normal brain tissue. n = number of investigated tissue samples.

In summary, the miRNA expression profiling of primary glioma tissues, 5-Aza/TSA-treated glioma cell lines and hypoxic versus normoxic glioblastoma stem cell lines provide a number of interesting candidate miRNAs whose aberrant expression likely contributes to the development and progression of gliomas. Follow-up experiments were particularly focused on the molecular and functional analysis of *miR-132* and *miR-126*, which both were significantly up-regulated in glioblastoma cells after

5-Aza/TSA treatment and showed significant down-regulation in primary astrocytic tumors relative to non-neoplastic brain tissue samples. In addition, *miR-210*, *miR-213* and *miR-25*, which all showed evidence of regulation by hypoxia in glioblastoma stem cells were selected for further characterization of the mechanism underlying their regulation and possibly mediating their effects in terms of tumor growth promotion.

4.2 Expression analysis of *miR-132* and *miR-126* in glioblastoma cell lines treated with either 5-Aza/TSA, 5-Aza alone or TSA alone

To validate the increased expression levels of *miR-132* and *miR-126* detected in two of four human glioblastoma cell lines treated with 5-Aza/TSA in relation to untreated cells (Figure 19 A), targeted RT-PCR analyses were performed in five glioblastoma cell lines (A172, U138MG, T98G, TP365MG, U87MG) following treatment with either 5-Aza or TSA or both (Figure 23). *In vitro* treatment with 5-Aza/TSA increased the expression of *miR-132* and *miR-126* at least 2-fold in two of the five cell lines (*miR-132*: T98G: 2.8-fold, p = 0.23; TP365MG: 2.3-fold, p = 0.03; *miR-126*: U138MG: 3.2-fold, p = 0.07; TP365MG: 2.4-fold, p = 0.045) relative to the untreated control cells. After treatment with the DNA demethylating agent 5-Aza alone, *miR-132* was up-regulated in one cell line (TP365MG: 2.3-fold, p = 0.03) whereas *miR-126* expression appeared unaffected by 5-Aza treatment. *In vitro* treatment with TSA increased *miR-132* and *miR-126* expression levels at least 2-fold in three and two of five cell lines in comparison to untreated cells, respectively, which suggests a role of histone modifications in the transcriptional down-regulation of the investigated miRNAs. *MiR-132* was up-regulated by TSA treatment in A172, T98G and U87MG cells (A172: 2.9-fold, p = 0.04; T98G: 2.1-fold, p = 0.03; U87MG: 3.3-fold, p = 0.09). The expression of *miR-126* was increased by TSA treatment in A172 (2.7-fold, p = 0.06) and T98G (2.4-fold, p = 0.08) cells, although the differences here did not reach statistical significance. Taken together, *in vitro* treatment of glioblastoma cell lines with either 5-Aza/TSA, 5-Aza or TSA suggested that down-regulation of *miR-132* and *miR-126* in glioma may be due to either histone modifications and/or DNA methylation in the 5`genomic region of these miRNA loci.

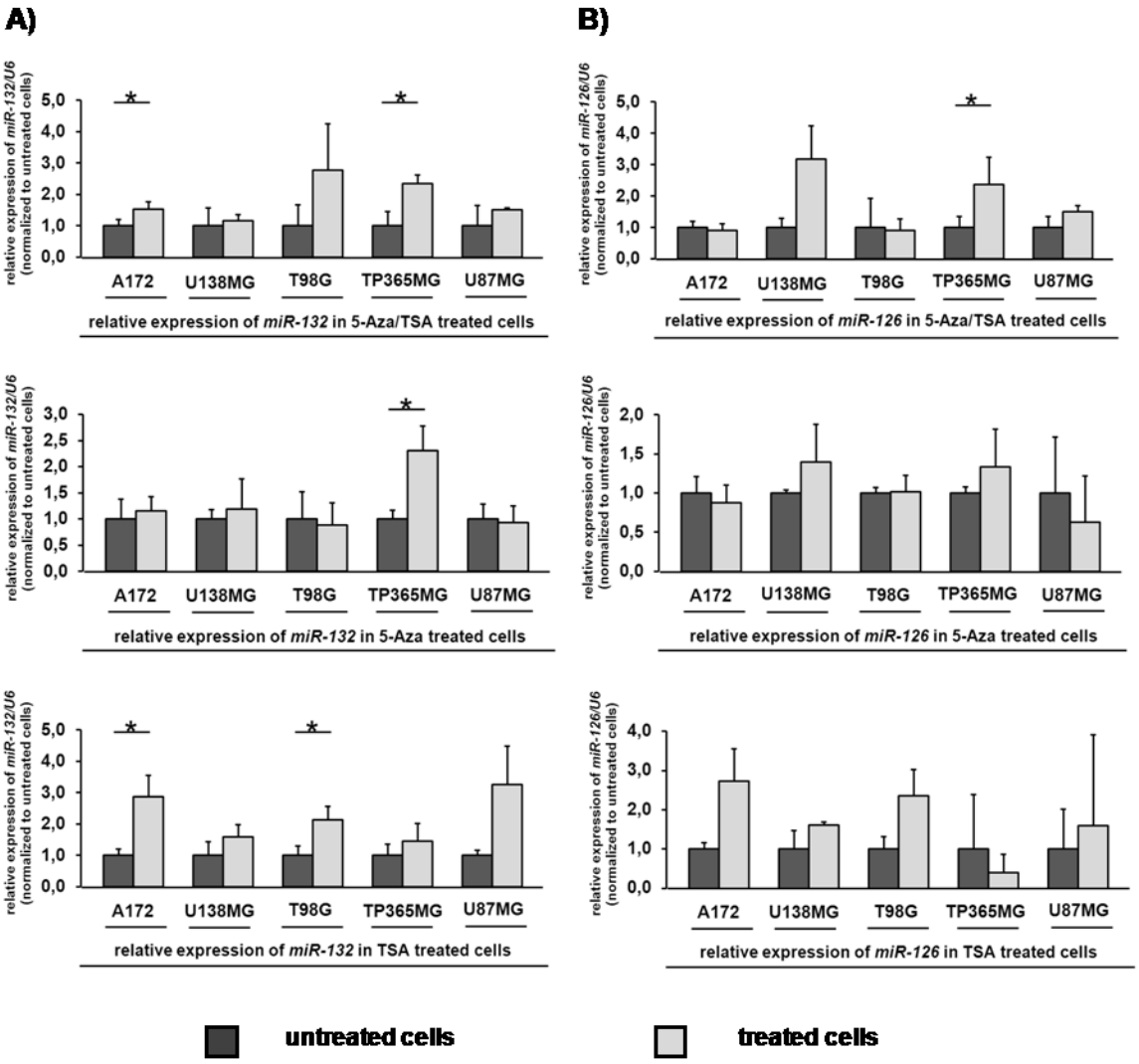

Figure 23: Increased expression of *miR-132* (A) and *miR-126* (B) in five human glioma cell lines treated with either 5-Aza/TSA, 5-Aza alone or TSA alone relative to untreated control cells. The glioblastoma cell lines were grown under three different treatment conditions with either 500 nM 5-Aza for 48 h, washed and grown for another 24 h in 500 nM 5-Aza and 1 µM TSA (5-Aza/TSA) or 500 nM 5-Aza for 72h (5-Aza).TSA treated cells were grown in 1 µM TSA for 36 h (TSA).The miRNA expression was determined using RT-PCR with U6 snRNA as an internal reference. The experiments were done three times. Statistics were made by student´s t-test, asterisks indicate significant expression differences (* $p < 0.05$).

4.3 Expression analysis of *miR-210*, *miR-213* and *miR-25* in a panel of glioblastoma cell lines grown under normoxic and hypoxic conditions

TaqMan Low Density Array-based expression profiling identified three miRNAs (*miR-210*, *miR-213* and *miR-25*) as being up-regulated in glioblastoma stem cells grown at 1% O_2 for either 18 h or 96 h in relation to control cells grown under normoxic conditions (21% O_2) (Figure 21). The respective cell treatments were carried out by Sascha Seidel (Department of Neuropathology, Justus-Liebig-University Giessen, Germany), who provided deep frozen cell pellets for miRNA extraction and analysis. The screening results were validated by RT-PCR on RNA from a panel of primary glioblastoma stem cell lines (ED010, ED015, ED022, ED026, ED031, ED046x, NCH 644, NCH 421) and established glioblastoma cell lines (G55TL, LN229) grown under normoxic and hypoxic conditions. Figure 24 A shows that expression of *miR-210* was up-regulated in all investigated glioma cell lines grown under hypoxia (1% O_2) in comparison to the control cells grown under normoxia (21% O_2). Eight out of ten cell lines showed an at least 2-fold increased *miR-210* expression levels at 1% O_2 for 18 h, while nine out of ten cell lines exhibited an at least 2-fold up-regulation of *miR-210* following incubation at 1% O_2 for 96 h. The increase in *miR-210* expression was more pronounced in cells incubated for 96 h under hypoxia than in cells grown for 18 h under hypoxia. By contrast, cell growth under hypoxic conditions led to an at least 1.5-fold increase of *miR-213* expression in three out of six primary glioblastoma stem cell lines (Figure 24 B). Hypoxia-induced increased expression of *miR-25*, as suggested by the screening experiments, could not be convincingly demonstrated in the validation experiments, which revealed only small or no effects of hypoxia on *miR-25* expression levels (Figure 24 C).

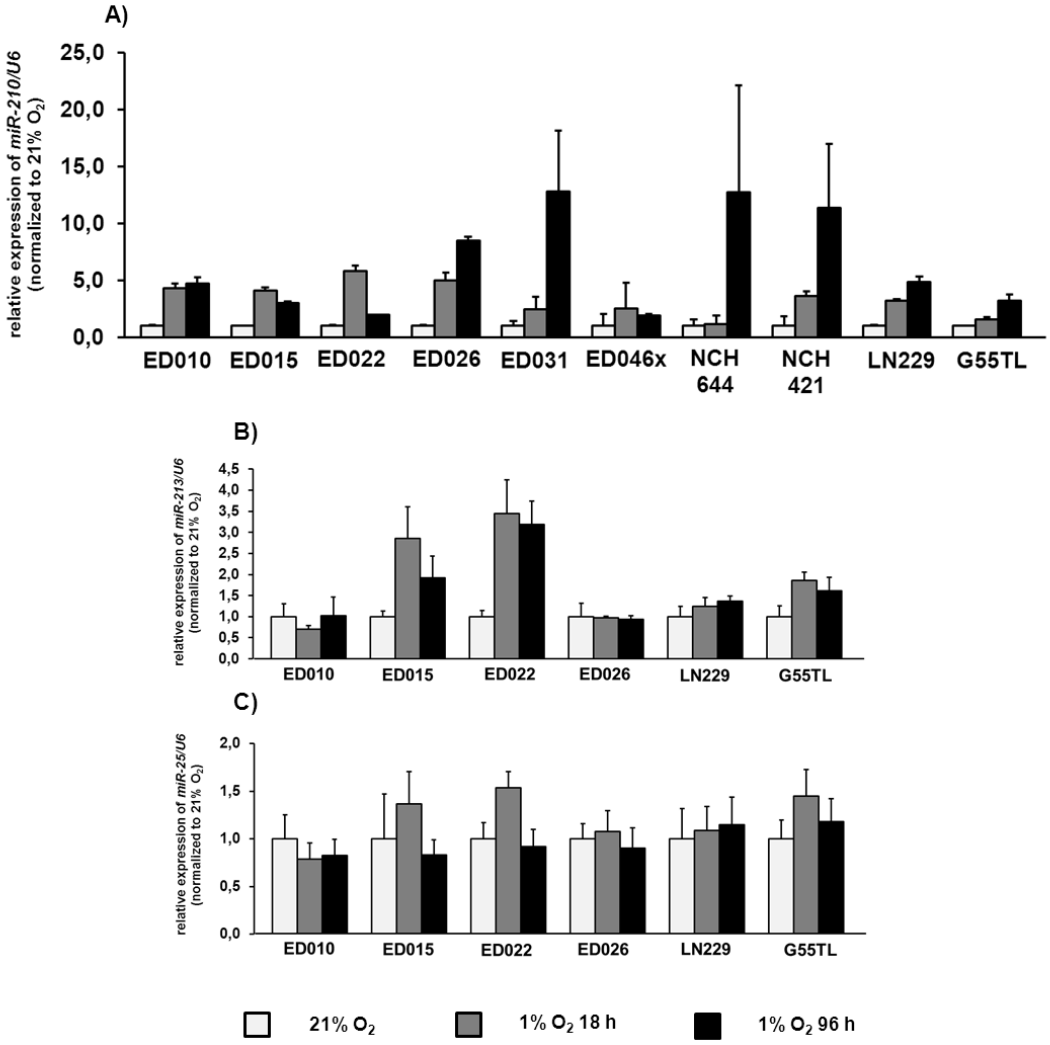

Figure 24: MiRNA expression analysis of *miR-210* (A), *miR-213* (B) and *miR-25* (C) in a panel of glioblastoma cell lines grown under hypoxia (1% O_2) relative to normoxia control cells (21% O_2). Glioblastoma cells were grown under hypoxia (1% O_2) for the indicated time points (18 h or 96 h). Control cells were incubated in normoxia (21% O_2). MiRNA expression levels were obtained using RT-PCR with U6 snRNA (U6) as an internal reference. Results are based on four (ED010, ED015, ED022, ED026, LN229, G55TL) or six technical replicates (ED031, ED046x, NCH644, NCH421) and presented in relative expression levels by setting the mean expression in normoxic control cells to 1. Standard deviations are illustrated as error bars. Statistical evaluations were not carried out because results were based on single experiments for each cell line and growth condition. **Note:** Hypoxia up-regulated the expression of *miR-210* at least 2-fold or higher in the vast majority of glioblastoma lines in relation to control cells grown under normoxia.

To determine whether the expression of the selected miRNAs is directly mediated through the hypoxia-inducible factor 1 alpha (HIF-1α) or HIF-2α transcription factors, RT-PCR analyses were performed for the three miRNAs in G55TL glioblastoma cells transfected with either HIF-1α or HIF-2α. Overexpression of HIF-1α rather than overexpression of HIF-2α robustly increased *miR-210* expression levels compared to control transfected cells (HIF-1α: 12.6-fold, HIF-2α: 4.2-fold). In contrast, *miR-213* and *miR-25* expression levels were not affected by HIF-1α or HIF-2α (Figure 25).

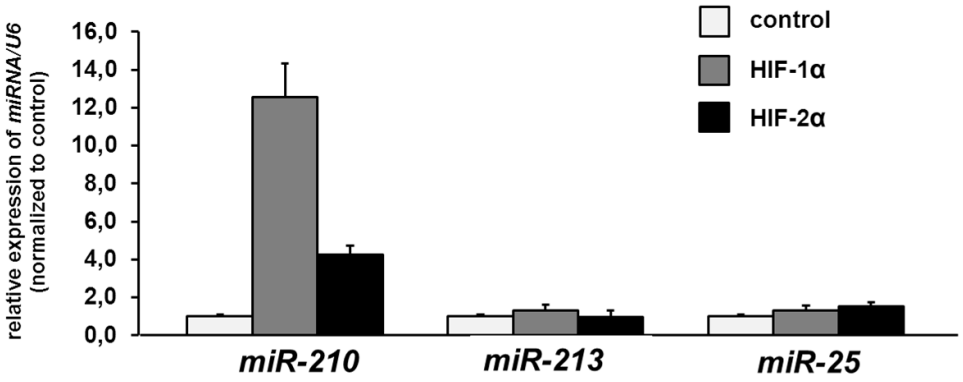

Figure 25: Expression analysis of *miR-210*, *miR-213* and *miR-25* in HIF-1α and HIF-2α overexpressing G55TL glioblastoma cells. For HIF-1α or HIF-2α overexpression, G55TL cells were stably transfected with pTetOff regulator plasmid (Clontech) as reported before (Seidel et al 2010). MiRNA expression levels were determined using RT-PCR with U6 snRNA (U6) as an internal reference. Results are based on four technical replicates and were presented in relative expression levels, with the mean result in the control cells set to 1. Standard deviations are illustrated as error bars. **Note:** Overexpression of HIF-1α strongly up-regulates the expression of *miR-210* in G55TL glioblastoma cells in relation to control cells. HIF-2α also upregulates *miR-210* expression, but to a lesser degree. No effect was seen on *miR-25* and *miR-213* expression levels.

In line with previous publications, these results suggested that HIF-1α plays a key role in mediating the hypoxia-induced *miR-210* expression in glioblastoma cells. To further validate this hypothesis, Sascha Seidel knocked down HIF-1α and HIF-2α in G55TL and ED010 glioblastoma cells (Seidel et al 2010). Afterwards, he incubated the cells under hypoxic conditions for the indicated time points (G55TL: 18 h, 96 h; ED010: 72 h). The effect of HIF-1α and HIF-2α knockdown (KD) on the *miR-210*, *miR-213* and *miR-25* expression levels was determined by real-time stem-loop RT-PCR (Figure 26). Importantly, knockdown of HIF-1α greatly suppressed the hypoxia-induced increase of *miR-210* expression levels (HIF-1α KD 18 h: 3.4-fold; HIF-1α KD 96 h: 1.9-fold; HIF-1α KD 72 h: 2.4-fold). Silencing of HIF-2α, on the other hand, had

only slight effects on *miR-210* expression levels (Figure 26 A). Notably, knockdown of HIF-2α resulted in a down-regulation of *miR-213* followed by hypoxia in G55TL glioblastoma cells (HIF-2α KD 18 h: 1.7-fold; HIF-2α KD 96 h: 1.6-fold) (Figure 26 B). HIF-1α/HIF-2α knockdown had no effect on *miR-25* expression in glioblastoma cells (Figure 26 C). Collectively, these results demonstrate that hypoxia induced expression of *miR-210* in glioblastoma cell lines preferentially via HIF-1α.

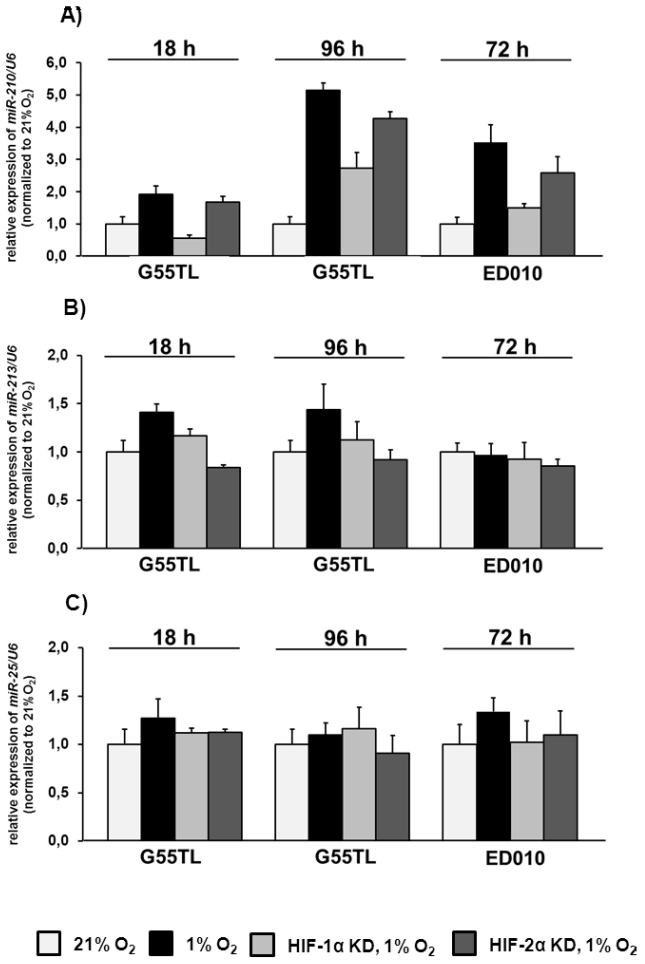

Figure 26: Expression analysis of *miR-210* (A), *miR-213* (B) and *miR-25* (C) in HIF-1α and HIF-2α knockdown G55TL and ED010 glioblastoma cells grown under hypoxia (1% O_2) relative to normoxic control cells (21% O_2). For HIF-1α or HIF-2α knockdown experiments, glioblastoma cells were transfected with small interfering RNAs. The next day, cells were incubated under hypoxia or normoxia for the indicated time points (18 h, 96 h, 72 h). Scrambled small interfering RNAs were used as control. Cell treatment has been carried out by Sascha Seidel (Seidel et al 2010). MiRNA expression levels were obtained using RT-PCR with U6 snRNA (U6) as an internal reference. Results are based on four technical replicates and presented in relative expression levels, with the mean result in the control cells set to 1. Standard deviations are illustrated as error bars. **Note:** Knockdown of HIF-1α profoundly ameliorated the induction of *miR-210* expression in G55TL and ED010 glioblastoma cells following hypoxia.

To evaluate whether the tumor stem cell phenotype influenced the expression of *miR-210*, *miR-213* and *miR-25* in primary ED010 glioblastoma stem cells grown under normoxic conditions, expression of these miRNAs was compared in CD133+ versus CD133- populations of this line. Sorted cell populations were provided by Sascha Seidel, Gießen. Reverse transcription of mature miRNA was carried out with stem-loop primers specific for *miR-210*, *miR-213* and *miR-25* (Figure 27). These analyses revealed a 2.2-fold up-regulation of *miR-210* expression in CD133+ cells in comparison to CD133- cells. The CD133+ subpopulations also showed a 1.6-fold higher *miR-213* expression and 1.4-fold higher *miR-25* expression.

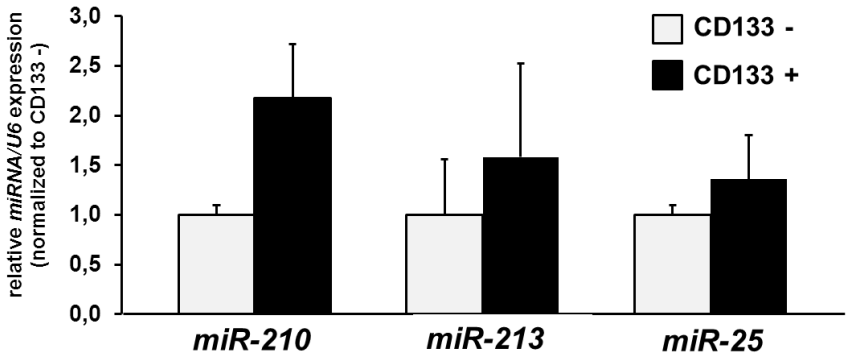

Figure 27: Expression analysis of *miR-210*, *miR-213* and *miR-25* in CD133+ versus CD133- subpopulations isolated from ED010 primary glioblastoma stem cells. CD133+ and CD133- populations had been isolated by FACS analysis. MiRNA expression levels were obtained using RT-PCR with U6 snRNA (U6) as an internal reference. Results are based on four technical replicates and were presented in relative expression levels, with the mean result in the CD133- cells set to 1. Standard deviations are illustrated as error bars. **Note:** CD133+ cells showed higher expression of these miRNAs as compared to CD133- cells, with the expression difference being highest for *miR-210* (2.2-fold).

4.4 Epigenetic changes of the 5`genomic region of *miR-132* and *miR-126* in gliomas and glioma cell lines

Several studies have highlighted conserved sequence motifs as well as GC-rich regions within 2000 bp in the upstream region of human miRNA genes (Inouchi et al 2007, Ohler et al 2004). Therefore, miRNA expression could be regulated by epigenetic alteration of the 5`genomic region like aberrant hypermethylation or histone modifications. Expression analysis of *miR-132* and *miR-126* in glioma cells treated with the demethylating agent 5'-aza-2'-deoxycytidine (5-Aza) and histone deacetylase inhibitor trichostatin A (TSA) showed increases of *miR-132* and *miR-126* expression in three and two out of five selected glioblastoma cell lines, respectively (Figure 23), thus providing evidence for a relationship between 5'-CpG island methylation, histone modifications and expression of these miRNAs in glioma cells. Therefore, *miR-132* and *miR-126* were selected for further molecular characterization using sequencing of sodium bisulfite-modified DNA and ChIP (chromatin immunoprecipitation) analysis of the 5´-genomic regions of each miRNA.

4.4.1 DNA methylation patterns in the 5`genomic region of *miR-132* and *miR-126*

4.4.1.1 DNA methylation patterns in the 5`genomic region of *miR-132*

The miRNA *miR-132* clusters together with *miR-212* and is located inside a large CpG island on chromosome 17p13.3 containing 886 CpG sites (Figure 28 A; UCSC Genome Browser-version February 2009). Down-regulation of *miR-132* by promoter hypermethylation was observed in pancreatic cancer samples around CpG sites 250-263 (Zhang et al 2011b). Therefore, the own studies were focused on the methylation patterns around the 5`CpG-rich genomic region of *miR-132/miR-212*. The methylation status of nine genomic regions within the large CpG island was investigated by using sodium bisulfite sequencing assay (Figure 28 B). Sodium bisulfite-modified DNA sequences of the investigated 5`genomic region of *miR-132/miR-212* as well as the corresponding primers are shown in the Materials, Table 13, Supplementary Figures 1a-1f.

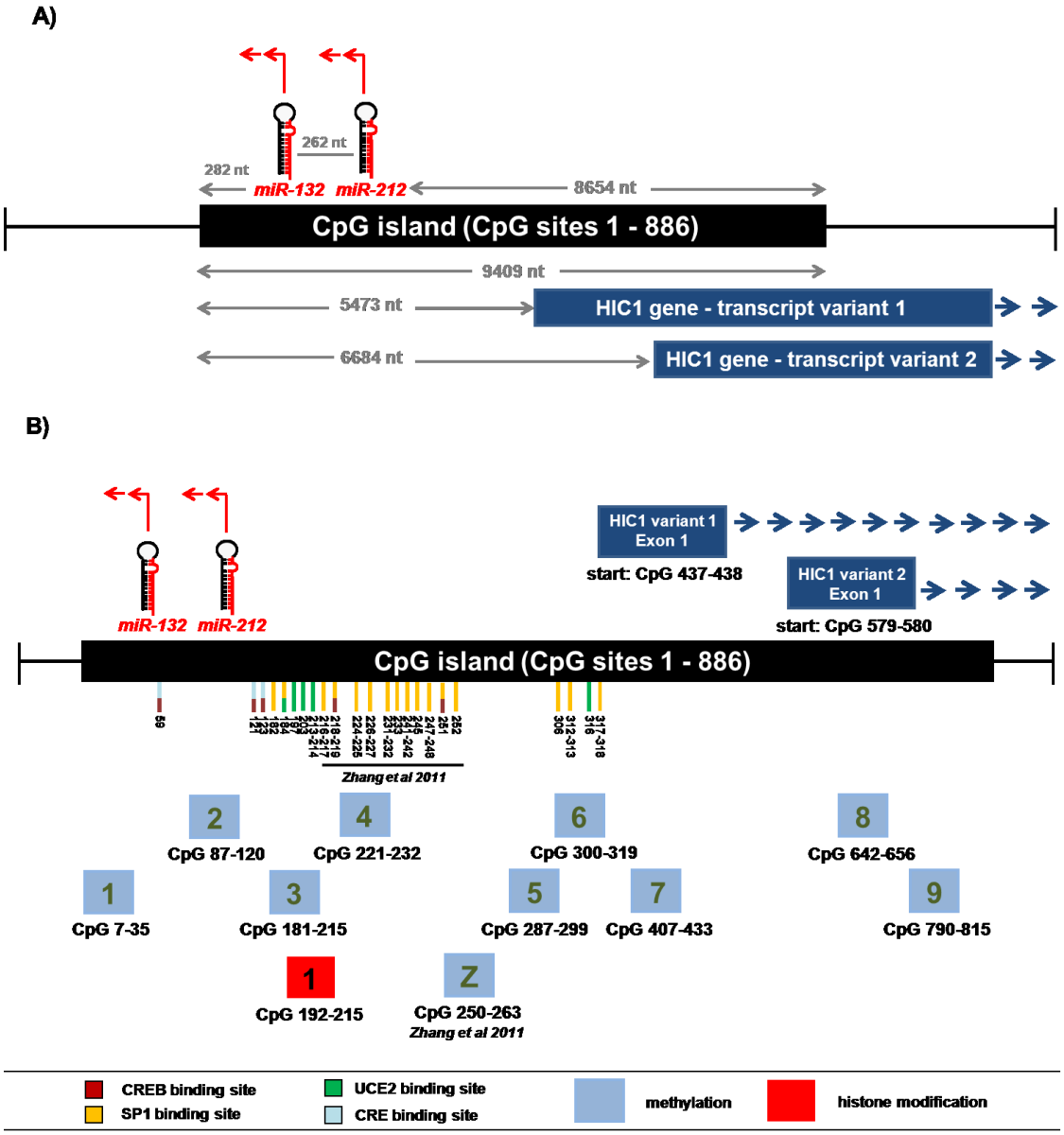

Figure 28: Schematic structure of the genomic region surrounding the *miR-132/miR-212* cluster. A) *MiR-132* and *miR-212* are embedded within a CpG island on chromosome band 17p13.3 (position: chr17:1952920-1962328; according to UCSC Genome Browser version February 2009). **B)** Nine DNA fragments were investigated for CpG methylation (1 to 9). The investigated genomic fragments cover the following CpG sites: (1) CpG 7 to 35 (29 CpG sites); (2) CpG 87 to 120 (34 CpG sites); (3) CpG 181 to 215 (35 CpG sites); (4) CpG 221-232 (12 CpGsites); (5) CpG287 to 299 (13 CpG sites); (6) CpG 300-319 (20 CpG sites); (7) CpG 407 to 433 (27 CpG sites); (8) CpG 642 to CpG 656 (15 CpG sites) and (9) CpG 790-815 (26 CpGs). **Note:** *Homo sapiens hypermethylated in cancer 1* (*HIC1*) gene and *miR-132/miR-212* have reading frames contrary to each other indicated by upright arrows. Furthermore, the diagram indicates the relative positions of selected transcription factor binding sites. CpG sites investigated for *miR-132/miR-212* hypermethylation are represented as blue boxes. The genomic region investigated for histone modification is represented as one red box.

The DNA methylation pattern of the *miR-132/miR-212* 5`CpG-rich region was evaluated in a tumor panel of AII, AAII, sGBIV and pGBIV as well as in 4 glioblastoma cell lines (A172, U138 MG, T98G and TP365MG) treated with 5-aza-2`-deoxycytidine (5-Aza) and trichostatin A (TSA) and untreated cells. Three commercially avalaible non-neoplastic brain tissue DNA samples were chosen as controls. Hypermethylated DNA served as an internal positive control.

Methylation analysis of the first two genomic regions (CpG 7 to 35 and CpG 87 to 120) revealed neither methylated CpG sites in the tumor tissues nor in the cell lines investigated. This observation argues against an involvement of this region in epigenetic regulation of *miR-132*/*miR-212* expression (Supplementary Figure 7A and 7B).

Methylation patterns and methylation scores of the third CpG promoter region spanning 35 CpGs (CpG 181-215) in the investigated 49 gliomas and three normal brain tissue samples are provided in Figure 29. Methylated CpG sites were detected in the majority of gliomas, as well as in four glioblastoma cell lines in comparison to respective non-cancerous tissues (NB1 to NB3). Interestingly, there is a difference in the percentage of methylated CpG sites between primary and secondary glioblastomas. For correlation between DNA methylation and *miR-132* expression, each tumor was assigned to one of two groups: (1) absent or low *miR-132* methylation (methylation score of 1, 2, or 3 in less than 50% of the investigated 35 CpG sites) or (2) *miR-132* hypermethylation (methylation score of 1, 2, or 3 in equal or more than 50% of the investigated 35 CpG sites). Comparison of *miR-132* expression and methylation around CpG sites 181- 215 revealed no statistical significance between the two groups (Mann-Whitney-test: $p = 0.17$) (Supplementary Figure 8).

This area was chosen as a crucial region within the putative *miR-132/miR-212* promoter containing binding sites of transcription factors like SP1 transcription factor (CCGCCC) and cAMP response element-binding protein (CREB) (CGTCA) (Zhang et al 2011a). Hypermethylation may compromise the accessibility of transcription factors to the *miR-132* promoter, resulting in the down-regulation of *miR-132* in gliomas. To examine this hypothesis, transcription factor binding sites within this CpG-rich region of *miR-132* were determined. SP1 binding sites were located around CpG sites 182 and 184 (Dynan and Tjian 1983, Guan et al 2012), upstream control elements (UCE2) binding sites (GGCCG) were located at CpG sites 184, 197 as well as CpG site 203 and CpG site 214. In the majority of AII, AAIII and sGBIV cases, the CpG sites 197 and 203 were methylated. CpG site 182, CpG site 184 as well as CpG site 214 revealed lower methylation levels in the majority of AII and AAIII tumors samples in relation to sGBIV.

Comparison of *miR-132* expression and methylation at each transcription binding site reached only significant methylation-dependent *miR-132* expression different for CpG site 184 (Mann-Whitney-test: $p = 0.04$) (Figure 30) (Supplementary Figure 9).

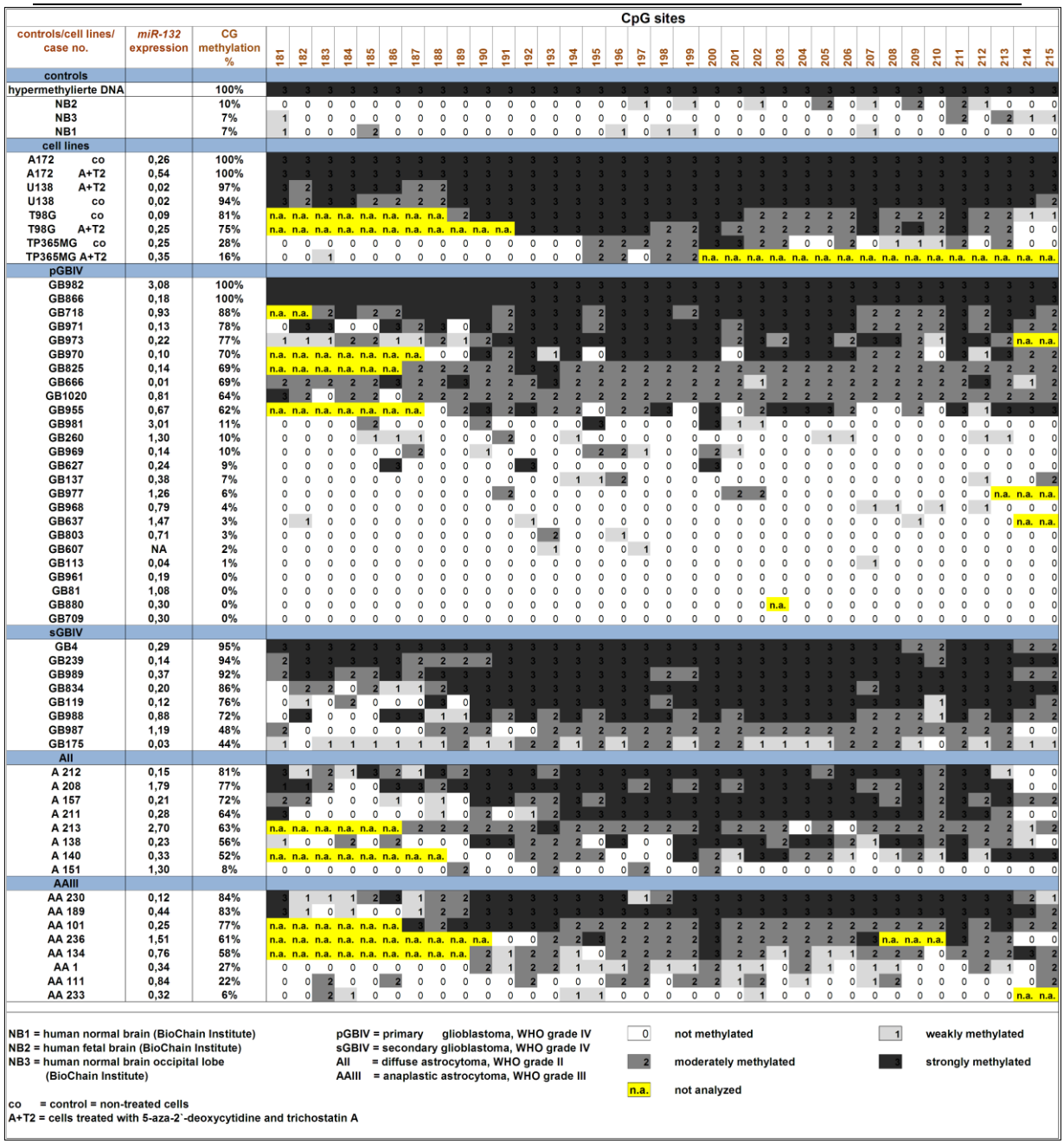

Figure 29: Methylation pattern of the genomic region (3) - CpG 181-215 - located in the CpG island on 17p13.3 in 49 gliomas and four glioblastoma cell lines as well as three non-neoplastic brain tissue samples (NB1 - NB3). Methylation analysis was performed by bisulfite sequencing of a PCR product covering 35 CpGs between nucleotides 1952920-1962328 on 17p13.3 (UCSC Genome Browser, version February 2009). The results of the DNA methylation analysis are represented in 4-tiered semi quantitative grey-scale pattern as indicated below the figure; white square: not methylated (0-25%), light grey: weakly methylated (26-50%), grey: moderately methylated (51-75%) and dark grey: strongly methylated (76-100%) (Tews et al 2007), n.a. = not analysed, hypermethylated DNA = *in vitro* methylated positive control. *MiR-132* expression levels obtained from the microRNA expression profile are indicated for each investigated astrocytic tumor and glioblastoma cell line. **Note:** Aberrant methylation was detected in astrocytic tumors and glioma cell lines when compared to the normal brain control samples. There is a significant higher percentage of methylated CpG sites in secondary glioblastomas compared to primary glioblastomas.

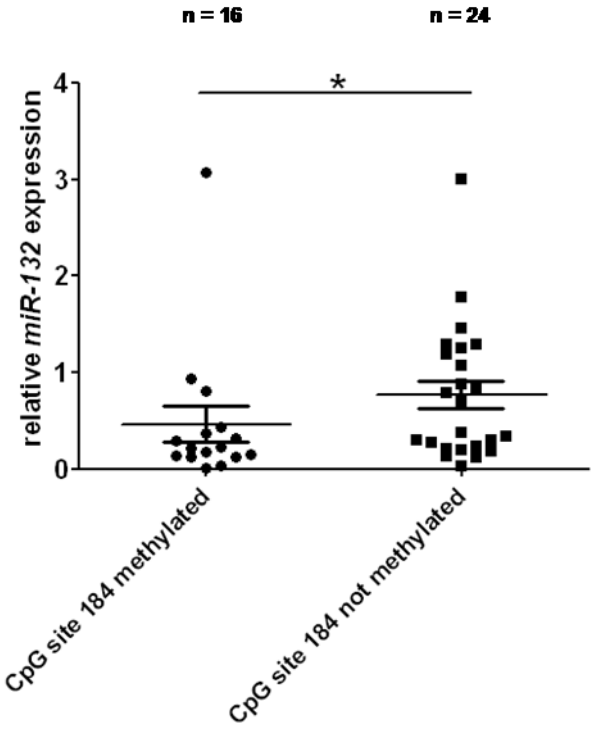

Figure 30: *MiR-132* expression analysis in human gliomas in relation to the methylation status of the CpG site 184 (SP1/UCE2 binding site). Statistics were made by Mann-Whitney-test, asterisks indicate significant expression differences (* $p < 0.05$). **Note:** Methylation at CpG site 184 was significantly associated with lower *miR-132* expression ($p = 0.04$).

The DNA methylation analysis of the fourth genomic region spanning 12 CpG sites (CpG 221 to CpG 232) was performed in 48 gliomas and four glioblastoma cell lines in comparison to three non-neoplastic brain tissue samples (NB1 to NB3). Direct sequencing of sodium bisulfite-modified DNA detected CpG methylation in the entire group of 48 patients as well as in all glioblastoma cell lines in comparison to non-neoplastic brain tissue samples. The data further suggested lower methylation in tumors from patients with pGBIV compared to patients with AII, AAIII or sGBIV (Figure 31). Comparison of *miR-132* expression and CpG methylation in this region revealed no statistically significant differences between hypermethylated and non-hypermethylated tumors (Mann-Whitney-test, $p = 0.84$; Supplementary Figure 10). Correlation of methylation at the SP1 transcription factor binding sites in this DNA segment with *miR-132* expression did not reveal significant methylation-dependent *miR-132* expression differences (Mann-Whitney-test: CpG sites 224-225: $p = 0.22$, CpG sites 226-227: $p = 0.88$, CpG sites 231-232: $p = 0.46$) (Supplementary Figure 11).

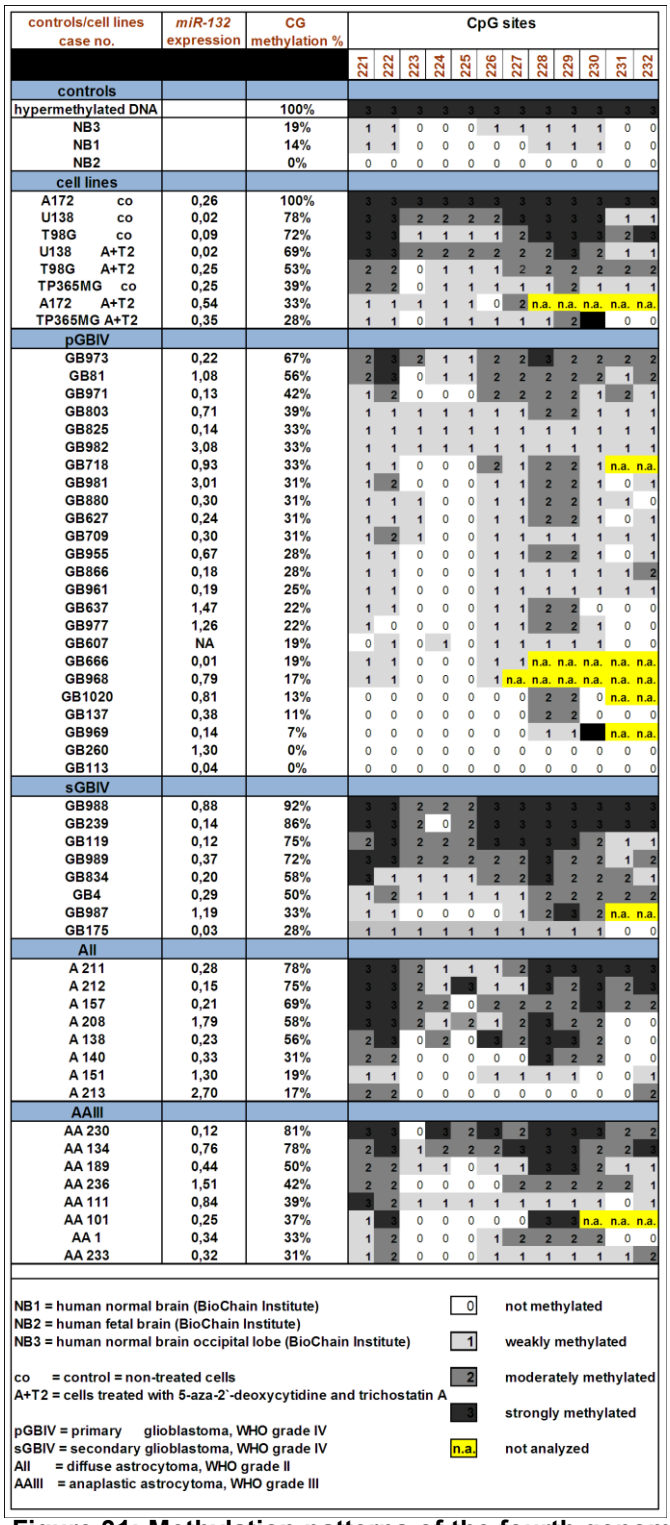

controls/cell lines case no.	*miR-132* expression	CG methylation %	CpG sites 221	222	223	224	225	226	227	228	229	230	231	232
controls														
hypermethylated DNA		100%	3	3	3	3	3	3	3	3	3	3	3	3
NB3		19%	1	1	0	0	0	1	1	1	1	1	0	0
NB1		14%	1	1	0	0	0	0	0	1	1	1	0	0
NB2		0%	0	0	0	0	0	0	0	0	0	0	0	0
cell lines														
A172 co	0,26	100%	3	3	3	3	3	3	3	3	3	3	3	3
U138 co	0,02	78%	3	3	2	2	2	2	3	3	3	3	1	1
T98G co	0,09	72%	3	3	1	1	1	1	2	3	3	3	2	3
U138 A+T2	0,02	69%	3	3	2	2	2	2	2	2	3	2	1	1
T98G A+T2	0,25	53%	2	2	0	1	1	1	2	2	2	2	2	2
TP365MG co	0,25	39%	2	2	0	1	1	1	1	1	2	1	1	1
A172 A+T2	0,54	33%	1	1	1	1	1	0	2	n.a.	n.a.	n.a.	n.a.	n.a.
TP365MG A+T2	0,35	28%	1	1	0	1	1	1	1	1	2	3	0	0
pGBIV														
GB973	0,22	67%	2	3	2	1	1	2	2	3	2	2	2	2
GB81	1,08	56%	2	3	0	1	1	2	2	2	2	2	1	2
GB971	0,13	42%	1	2	0	0	0	2	2	2	2	1	2	1
GB803	0,71	39%	1	1	1	1	1	1	1	2	2	1	1	1
GB825	0,14	33%	1	1	1	1	1	1	1	1	1	1	1	1
GB982	3,08	33%	1	1	1	1	1	1	1	1	1	1	1	1
GB718	0,93	33%	1	1	0	0	0	2	1	2	2	1	n.a.	n.a.
GB981	3,01	31%	1	2	0	0	0	1	1	2	2	1	0	1
GB880	0,30	31%	1	1	1	0	0	1	1	2	2	1	1	0
GB627	0,24	31%	1	1	1	0	0	1	1	2	2	1	0	1
GB709	0,30	31%	1	2	1	0	0	1	1	1	1	1	1	1
GB955	0,67	28%	1	1	0	0	0	1	1	2	2	1	0	1
GB866	0,18	28%	1	1	0	0	0	1	1	1	1	1	1	2
GB961	0,19	25%	1	1	0	0	0	1	1	1	1	1	1	1
GB637	1,47	22%	1	1	0	0	0	1	1	2	2	0	0	0
GB977	1,26	22%	1	0	0	0	0	1	1	2	2	1	0	0
GB607	NA	19%	0	1	0	1	0	1	1	1	1	1	0	0
GB666	0,01	19%	1	1	0	0	0	1	1	n.a.	n.a.	n.a.	n.a.	n.a.
GB968	0,79	17%	1	1	0	0	0	1	n.a.	n.a.	n.a.	n.a.	n.a.	n.a.
GB1020	0,81	13%	0	0	0	0	0	0	0	2	2	0	n.a.	n.a.
GB137	0,38	11%	0	0	0	0	0	0	0	2	2	0	0	0
GB969	0,14	7%	0	0	0	0	0	0	0	1	1	3	n.a.	n.a.
GB260	1,30	0%	0	0	0	0	0	0	0	0	0	0	0	0
GB113	0,04	0%	0	0	0	0	0	0	0	0	0	0	0	0
sGBIV														
GB988	0,88	92%	3	3	2	2	2	3	3	3	3	3	3	3
GB239	0,14	86%	3	3	2	0	2	3	3	3	3	3	3	3
GB119	0,12	75%	2	3	2	2	2	3	3	3	3	2	1	1
GB989	0,37	72%	3	3	2	2	2	2	2	3	2	2	1	2
GB834	0,20	58%	3	1	1	1	1	2	2	3	2	2	2	1
GB4	0,29	50%	1	2	1	1	1	1	1	2	2	2	2	2
GB987	1,19	33%	1	1	0	0	0	0	1	2	3	2	n.a.	n.a.
GB175	0,03	28%	1	1	1	1	1	1	1	1	1	1	0	0
AII														
A 211	0,28	78%	3	3	2	1	1	1	2	3	3	3	3	3
A 212	0,15	75%	3	3	2	1	3	1	1	3	2	3	2	3
A 157	0,21	69%	3	3	2	2	0	2	2	2	2	3	2	2
A 208	1,79	58%	3	3	2	1	2	1	2	3	2	2	0	0
A 138	0,23	56%	2	3	0	2	0	3	2	3	3	2	0	0
A 140	0,33	31%	2	2	0	0	0	0	0	3	2	2	0	0
A 151	1,30	19%	1	1	0	0	0	1	1	1	1	0	0	1
A 213	2,70	17%	2	2	0	0	0	0	0	0	0	0	0	2
AAIII														
AA 230	0,12	81%	3	3	0	3	2	3	2	3	3	3	2	2
AA 134	0,76	78%	2	3	1	2	2	2	3	3	3	2	2	3
AA 189	0,44	50%	2	2	1	1	0	1	1	3	3	2	1	1
AA 236	1,51	42%	2	2	0	0	0	0	2	2	2	2	2	1
AA 111	0,84	39%	3	2	1	1	1	1	1	1	1	1	0	1
AA 101	0,25	37%	1	3	0	0	0	0	0	3	3	n.a.	n.a.	n.a.
AA 1	0,34	33%	1	2	0	0	0	1	2	2	2	2	0	0
AA 233	0,32	31%	1	2	0	0	0	1	1	1	1	1	1	2

NB1 = human normal brain (BioChain Institute)
NB2 = human fetal brain (BioChain Institute)
NB3 = human normal brain occipital lobe (BioChain Institute)

co = control = non-treated cells
A+T2 = cells treated with 5-aza-2`-deoxycytidine and trichostatin A

pGBIV = primary glioblastoma, WHO grade IV
sGBIV = secondary glioblastoma, WHO grade IV
AII = diffuse astrocytoma, WHO grade II
AAIII = anaplastic astrocytoma, WHO grade III

0 not methylated
1 weakly methylated
2 moderately methylated
3 strongly methylated
n.a. not analyzed

Figure 31: Methylation patterns of the fourth genomic region (4) (CpG 221-232) located in the CpG island on 17p13.3 in 48 gliomas and four glioblastoma cell lines as well as three non-neoplastic brain tissue samples (NB1 - NB3). Methylation analysis was performed by bisulfite sequencing of the PCR product covering 12 CpGs between nucleotides 1952920-1962328 on chromosome band 17p13.3 (UCSC Genome Browser, version February 2009). *MiR-132* expression levels obtained from the microRNA expression profiling are also indicated for each investigated astrocytic tumor and glioblastoma cell line. **Note:** Aberrant methylation was detected in the majority of astrocytic tumors and glioma cell lines but not in the non-neoplastic brain tissue samples.

The methylation screening of DNA fragment 5 spanning 13 CpG sites (CpG sites 287 to 299) revealed methylated CpG sites in the majority of the nine investigated glioma samples as well as in four glioblastoma cell lines (treated with 5-Aza/TSA or non-treated) and three non-neoplastic brain tissues (NB1 to NB3) (Supplementary Figure 12). Fragment 6 spanning 20 CpG sites (CpG sites 300 to 319) in the 5´ genomic region of *miR-132*/*miR-212* was investigated for aberrant methylation in 49 gliomas and four glioblastoma cell lines as well as three non-neoplastic brain tissue samples (NB1 to NB3). Direct sequencing of sodium bisulfite-modified DNA detected only few methylated cytosines in this genomic region in gliomas as compared to the non-cancerous tissues (Figure 32). The correlation between DNA methylation and *miR-132* expression revealed no significant difference in miRNA expression between the groups with low versus high methylation (Mann-Whitney-test: $p = 0.08$) (Supplementary Figure 13). This area contains three binding sites for the transcription factor SP1 (with one nucleotide mismatch in SP1 binding sequence) (CpG sites 306, 313-314, 317-318) and one binding site for upstream control element UCE2 (CpG site 216). Comparison of *miR-132* expression and methylation at the SP1 transcription factor binding site CpG 306 did not reveal significant differences (Mann-Whitney-test: CpG sites 224-225: $p = 0.99$, (Supplementary Figure 14).

controls/cell lines case no.	*miR-132* expression	CG methylation %	CpG sites 300	301	302	303	304	305	306	307	308	309	310	311	312	313	314	315	316	317	318	319
controls																						
hypermethylated DNA		100%	3	3	3	3	3	3	3	3	3	3	3	3	3	3	3	3	3	3	3	3
NB1		0%	0	0	0	0	0	0	0	0	0	0	0	0	0	0	0	0	0	0	0	0
NB2		0%	0	0	0	0	0	0	0	0	0	0	0	0	0	0	0	0	0	0	0	0
NB3		0%	0	0	0	0	0	0	0	0	0	0	0	0	0	0	0	0	0	0	0	0
cell lines																						
A172 co	0,26	100%	3	3	3	3	3	3	3	3	3	3	3	3	3	3	3	3	3	3	3	3
A172 A+T2	0,54	100%	3	3	3	3	3	3	3	3	3	3	3	3	3	3	3	3	3	3	3	3
U138 A+T2	0,02	78%	3	3	3	3	2	3	3	3	2	3	2	2	2	2	2	2	2	2	1	2
U138 co	0,02	77%	3	3	3	3	3	3	3	3	2	3	3	2	1	2	2	2	1	1	1	2
TP365MG A+T2	0,35	43%	3	3	2	3	2	3	3	3	2	2	0	0	0	0	0	0	0	0	0	0
TP365MG co	0,25	40%	2	3	1	3	1	3	3	3	2	1	0	0	0	0	1	1	0	0	0	0
T98G co	0,09	25%	1	2	3	2	0	2	2	2	1	0	0	0	0	0	0	0	0	0	0	0
T98G A+T2	0,25	13%	1	2	1	2	1	1	0	0	0	0	0	0	0	0	0	0	0	0	0	0
pGBIV																						
GB970	0,10	45%	3	2	2	2	0	2	3	3	2	3	3	1	0	0	0	1	0	0	0	0
GB666	0,01	17%	2	1	1	1	0	0	2	0	0	1	2	0	0	0	0	0	0	0	0	0
GB637	1,47	15%	2	2	1	1	0	0	2	0	0	0	0	0	0	0	0	1	0	0	0	0
GB968	0,79	15%	1	1	1	1	0	0	2	1	1	0	1	0	0	0	0	0	0	0	0	0
GB825	0,14	13%	2	1	1	0	0	0	1	0	1	1	1	0	0	0	0	0	0	0	0	0
GB627	0,24	12%	2	1	0	1	0	0	1	0	0	0	1	0	0	0	0	1	0	0	0	0
GB709	0,30	12%	2	1	1	1	0	0	2	0	0	0	0	0	0	0	0	0	0	0	0	0
GB260	1,30	10%	1	1	1	1	0	0	1	0	1	0	0	0	0	0	0	0	0	0	0	0
GB718	0,93	10%	2	1	0	1	0	0	1	0	0	0	0	0	0	0	0	1	0	0	0	0
GB977	1,26	8%	1	1	0	0	0	0	0	0	0	0	0	1	1	0	0	1	0	0	0	0
GB81	1,08	8%	1	0	0	0	0	0	1	0	0	0	0	1	1	0	0	1	0	0	0	0
GB982	3,08	8%	1	1	1	1	0	0	1	0	0	0	0	0	0	0	0	0	0	0	0	0
GB969	0,14	8%	1	1	1	1	0	0	1	0	0	0	0	0	0	0	0	0	0	0	0	0
GB1020	0,81	7%	1	0	0	0	0	0	1	0	0	0	1	1	0	0	0	0	0	0	0	0
GB607	NA	6%	1	0	1	0	0	0	0	0	0	0	0	0	0	0	1	0	0	n.a.	n.a.	n.a.
GB880	0,30	5%	1	0	0	1	0	0	1	0	0	0	0	0	0	0	0	0	0	0	0	0
GB973	0,22	5%	1	1	0	0	0	0	1	0	0	0	0	0	0	0	0	0	0	0	0	0
GB866	0,18	5%	1	0	0	0	0	0	1	0	0	0	0	0	0	0	0	1	0	0	0	0
GB961	0,19	5%	2	0	0	0	0	0	1	0	0	0	0	0	0	0	0	0	0	0	0	0
GB955	0,67	3%	1	0	0	0	0	0	1	0	0	0	0	0	0	0	0	0	0	0	0	0
GB113	0,04	3%	1	0	0	0	0	0	1	0	0	0	0	0	0	0	0	0	0	0	0	0
GB137	0,38	2%	1	0	0	0	0	0	0	0	0	0	0	0	0	0	0	0	0	0	0	0
GB971	0,13	0%	0	0	0	0	0	0	0	0	0	0	0	0	0	0	0	0	0	0	0	0
GB981	3,01	0%	0	0	0	0	0	0	0	0	0	0	0	0	0	0	0	0	0	0	0	0
GB803	0,71	0%	0	0	0	0	0	0	0	0	0	0	0	0	0	0	0	0	0	0	0	0
sGBIV																						
GB119	0,12	100%	3	3	3	3	3	3	3	3	3	3	3	3	3	3	3	3	3	3	3	3
GB989	0,37	47%	2	2	1	2	1	3	3	3	2	3	3	2	1	0	0	0	0	0	0	0
GB239	0,14	43%	2	1	0	2	2	2	3	3	2	3	3	3	0	0	0	0	0	0	0	0
GB834	0,20	27%	1	2	1	2	0	2	2	2	1	2	1	0	0	0	0	0	0	0	0	0
GB988	0,88	25%	2	2	1	2	0	2	2	2	0	0	1	1	0	0	0	0	0	0	0	0
GB987	1,19	17%	1	1	1	1	0	1	2	2	1	0	0	0	0	0	0	0	0	0	0	0
GB4	0,29	2%	0	0	0	0	0	0	1	0	0	0	0	0	0	0	0	0	0	0	0	0
GB175	0,03	0%	0	0	0	0	0	0	0	0	0	0	0	0	0	0	0	0	0	0	0	0
AII																						
A 212	0,15	35%	1	2	2	2	2	2	2	2	2	2	2	0	0	0	0	0	0	0	0	0
A 140	0,33	28%	1	2	0	2	0	2	2	3	1	2	2	0	0	0	0	0	0	0	0	0
A 208	1,79	22%	1	1	0	1	0	1	2	2	1	2	2	0	0	0	0	0	0	0	0	0
A 211	0,28	20%	2	1	1	1	0	1	1	0	0	1	1	1	1	1	0	0	0	0	0	0
A 151	1,30	15%	2	1	1	1	0	0	1	1	1	0	1	0	0	0	0	0	0	0	0	0
A 157	0,21	8%	2	1	0	1	0	0	1	0	0	0	0	0	0	0	0	0	0	0	0	0
A 138	0,23	7%	2	1	0	0	0	0	0	0	0	0	1	0	0	0	0	0	0	0	0	0
A 213	2,70	7%	1	1	0	1	0	0	1	0	0	0	0	0	0	0	0	0	0	0	0	0
AAIII																						
AA 230	0,12	25%	2	1	0	2	0	2	2	2	1	1	2	0	0	0	0	0	0	0	0	0
AA 111	0,84	22%	1	1	1	1	0	0	2	1	1	2	2	1	0	0	0	0	0	0	0	0
AA 134	0,76	20%	1	2	0	2	0	0	1	0	0	1	2	2	0	0	0	1	0	0	0	0
AA 189	0,44	13%	1	1	1	1	0	1	1	1	0	0	1	0	0	0	0	0	0	0	0	0
AA 101	0,25	12%	3	1	0	1	0	0	1	1	0	0	0	0	0	0	0	0	0	0	0	0
AA 1	0,34	10%	1	1	1	1	0	0	1	0	0	0	0	0	0	0	0	1	0	0	0	0
AA 236	1,51	7%	0	1	0	1	0	1	1	0	0	0	0	0	0	0	0	0	0	0	0	0
AA 233	0,32	7%	1	1	1	1	0	0	0	0	0	0	0	0	0	0	0	0	0	0	0	0

NB1 = human normal brain (BioChain Institute)
NB2 = human fetal brain (BioChain Institute)
NB3 = human normal brain occipital lobe (BioChain Institute)

co = control = non-treated cells
A+T2 = cells treated with 5-aza-2´-deoxycytidine and trichostatin A

pGBIV = primary glioblastoma, WHO grade IV
sGBIV = secondary glioblastoma, WHO grade IV
AII = diffuse astrocytoma, WHO grade II
AAIII = anaplastic astrocytoma, WHO grade III

0 not methylated
1 weakly methylated
2 moderately methylated
3 strongly methylated
n.a. not analyzed

Figure 32: Methylation patterns of the sixth 5´-CpG-rich region (6) (CpG 300-319) of *miR-132/miR-212* in 49 gliomas and four glioblastoma cell lines as well as three samples of non-neoplastic brain tissue (NB1 - NB3). Methylation analysis was performed by bisulfite sequencing of the PCR product covering 20 CpGs between nucleotides 1952920-1962328 on 17p13.3 (UCSC Genome Browserversion February 2009). **Note:** Aberrant methylation was detected in pGBIV and sGBIV as well as in glioma cell lines, but not in the non-neoplastic brain tissue samples.

In the amplified fragment of the seventh (7) 5`genomic region of *miR-132/miR-212* covering 27 CpG sites (CpG 407 to 433), hypermethylation was neither detected in 5-Aza/TSA treated nor in non-treated glioma cell lines. Most cell lines and non-neoplastic brain tissue samples showed sporadic - or no methylation arguing against an involvement of this region in the epigenetic regulation of *miR-132* expression (Supplementary Figure 15). In contrast, hypermethylation was detected in the majority of the investigated gliomas and glioblastoma cells, as well as in non-neoplastic brain tissues in the two DNA fragments 8 and 9 (Supplementary Figure 16) located most upstream of the human *miR-132/miR-212* cluster on 17p13.3.

Taken together, three out of 9 selected CpG-rich 5`genomic regions of *miR-132/miR-212* showed evidence for hypermethylation in the investigated astrocytic tumors but not in the non-neoplastic brain tissue samples. Statistical analysis revealed no significant association between the global 5`CpG methylation status and *miR-132* expression. However, methylation at the SP1/UCE2 transcription factor binding site located around CpG site 184 was associated with reduced *miR-132* expression levels. Therefore, *miR-132* expression may to be regulated by SP1 and UCE2 binding to this site, which is compromised in case of CpG site 184 methylation.

4.4.1.2 DNA methylation patterns of the 5`genomic region of *miR-126*

The miRNA *miR-126* is located within intron 7 of the epidermal growth factor-domain gene (EGFL7). Interestingly, two CpG islands are mapping to the 5`genomic region of *miR-126* (Saito et al 2009) (Figure 33).

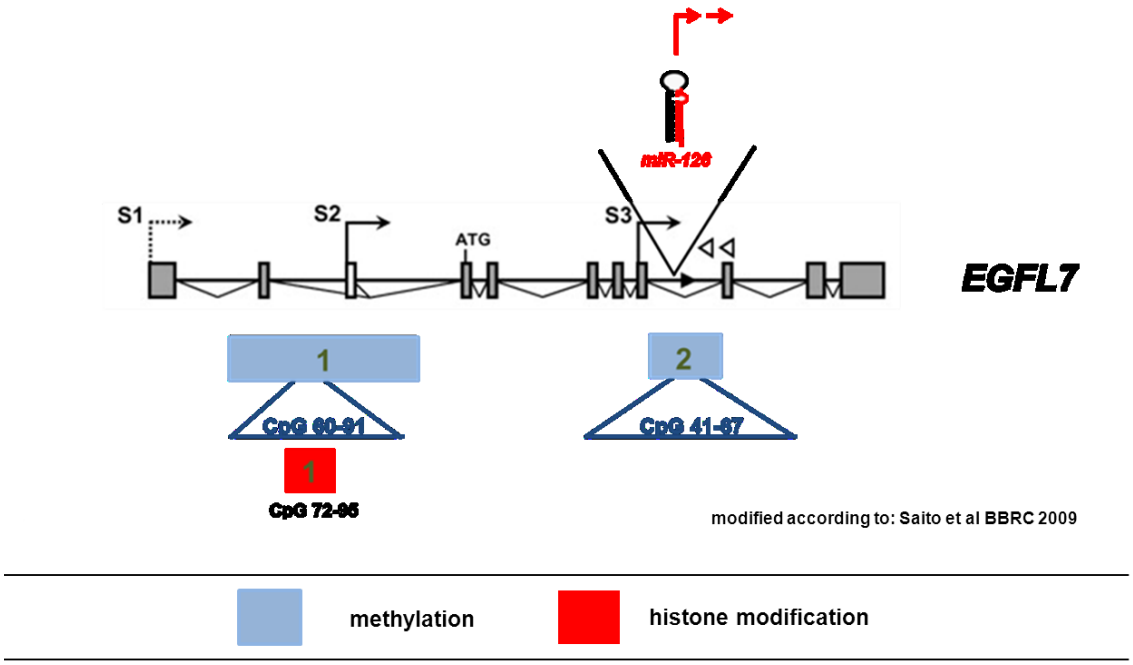

Figure 33: 5`CpG-rich genomic regions associated with *miR-126* and its host gene *EGFL7*. *MiR-126* is embedded within intron 7 of the *EGF-like-domain, multiple 7* (*EGFL7*) gene on 9 q34.3. CpG island 1 is located in intron 2 of *EGFL7* and CpG island 2, which contains *miR-126*, in intron 7, respectively (UCSC Genome Browser, version February 2009). Methylation analysis by direct sequencing was performed for two DNA fragments: the first fragment spans CpG sites 60-91 of CpG island 1, and the second fragment spans the entire CpG island 2 (2) (covering CpG sites from 41 to 67). The three transcription start sites are indicated (S1 to S3; Saito et al 2009). CpG sites investigated for *miR-126* promoter hypermethylation are represented as blue boxes. The genomic region investigated for histone modification is represented as one red box.

The methylation patterns in the *miR-126* - associated CpG islands 1 and 2 were determined in 50 gliomas, four glioblastoma cell lines, treated with 5-aza-2`-deoxycytidine and trichostatin (A+T2) in comparison to non-treated cells, as well as three non-neoplastic brain tissue samples (NB1-NB3). Hypermethylated DNA served as an internal positive control. Sodium bisulfite-modified DNA sequences of the investigated 5`genomic region of *miR-126* as well as the corresponding primers are shown in the Supplementary Figures 2-3.

Direct sequencing of sodium bisulfite-modified DNA covering 31 CpG sites from CpG 60 to CpG 91 in CpG-island 1 revealed an interesting methylation pattern. The CpG sites 60 to 71 were methylated in the tumors, cell lines and in the non-neoplastic brain tissue samples. In contrast, CpG sites 72 to 91 were not methylated in the non-neoplastic brain tissues (N1-N3) but methylated in the cell lines and tumor tissues, especially in the primary and secondary GBIV samples (Figure 34) (Supplementary Figure 17). Concerning CpG sites 76-91, methylation was observed in six out of 26 primary glioblastomas (pGBIV) (23.1%) and one out of eight secondary glioblastomas (sGBIV) (12.5%). Hypermethylation was absent in diffuse astrocytomas (AII) of eight patients, anaplastic astrocytomas (AAIII) of eight patients and the three investigated non-neoplastic brain tissue samples (NB1 to NB3) (Supplementary Figure 17). In summary, *miR-126* promoter hypermethylation was detected in seven out of 50 glioma patients (14%) and in two out of four investigated glioblastoma cell lines (Supplementary Figure 17). In order to identify methylation-dependent *miR-126* expression changes, each tumor was assigned to one of two groups: (1) absent or low *miR-126* promoter methylation (methylation score of 1, 2, or 3 in less than 50% of the investigated CpG1 sites) or (2) *miR-126* promoter hypermethylation (methylation score of 1, 2 or 3 in equal or more than 50% of the investigated CpG 1 sites). Comparison of *miR-126* expression and methylation around CpG sites 76-91 did not reveal significant differences in *miR-126* expression between the two groups (Mann-Whitney-test: $p = 0.87$, Supplementary Figure 18).

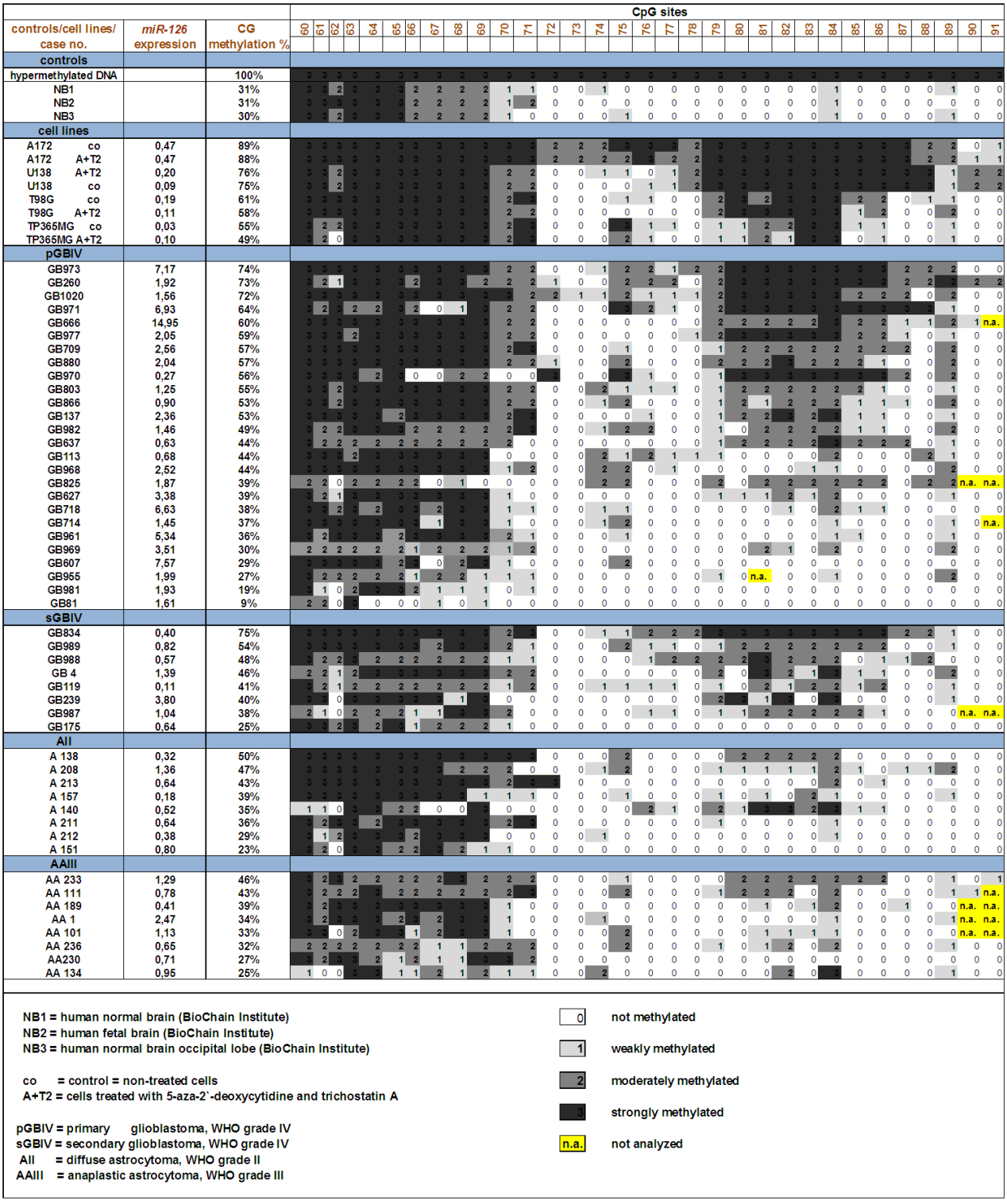

Figure 34: Methylation patterns and methylation scores of the 5´-CpG-rich genomic region 1 associated with *miR-126* in 50 gliomas and four glioblastoma cell lines as well as three non-neoplastic brain tissue samples (NB1 - NB3). Methylation patterns of 31 CpG sites (CpG 60 to 91) located in the 5´-CpG 1 genomic region of *miR-126* (nucleotides 139557805-139563005 on 9q34.3, UCSC Genome Browser, version February 2009) were determined by bisulfite sequencing. **Note:** The majority of pGBIV and sGBIV as well as the glioma cell lines were hypermethylated relative to the normal brain tissue samples in the region covering CpG sites 72 to 91.

The DNA methylation analysis of the second, *miR-126*-associated CpG-rich genomic region in 50 gliomas, four glioblastoma cell lines and three non-neoplastic brain tissue samples (NB1 to NB3) revealed methylated CpG nucleotides in all 27 CpG sites (CpG 41 to 67) in all samples investigated (Figure 35).

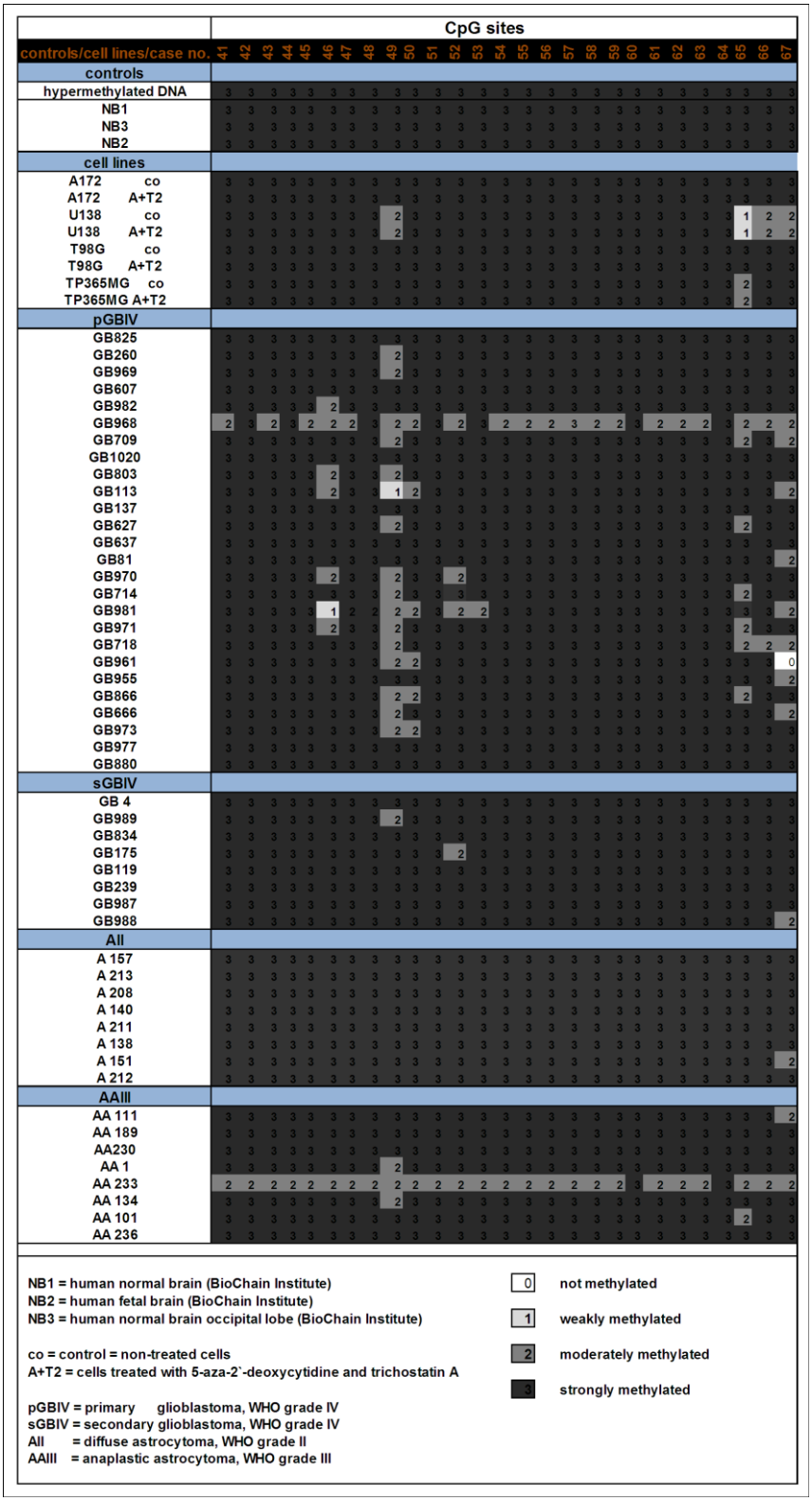

Figure 35: Methylation patterns of the CpG-rich genomic region 2 associated with *miR-126* in 50 gliomas and four glioblastoma cell lines as well as three non-neoplastic brain tissue samples (NB1 - NB3). Methylation analysis was performed by bisulfite sequencing of the PCR product covering 27 sites (CpG 41 to 67) located in CpG island 2 (nucleotides 139564000-139566286 on 9q34.3 UCSC Genome Browser, version February 2009). **Note:** Both, tumor and non-neoplastic brain tissue samples are strongly methylated in this region.

4.4.2 DNA methylation patterns of the 5`genomic region of *miR-210*

The stem loop of *miR-210* is located in an intron of a noncoding RNA and is embedded within one CpG island on chromosome 11p15.5. To examine *miR-210* promoter methylation in glioblastoma cells, the methylation patterns of 17 CpG sites (CpG sites 142 – 158) were determined (Figure 36). Sodium bisulfite-modified DNA sequences of the investigated 5`genomic region of *miR-210* as well as the corresponding primers are shown in the Supplementary Figure 4.

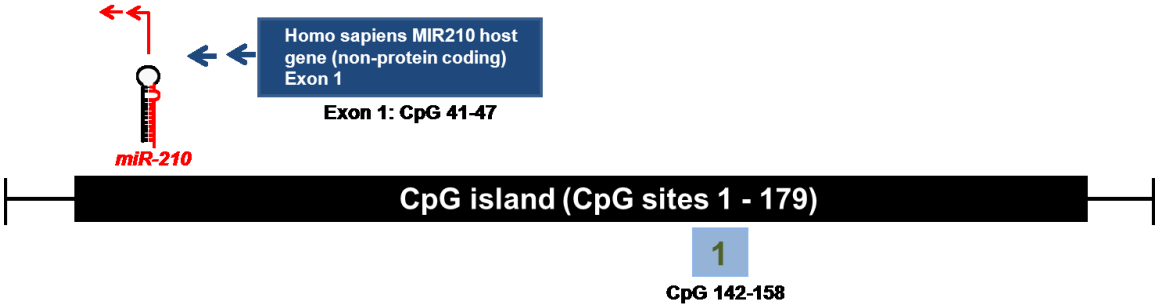

Figure 36: 5`CpG-rich region associated with *miR-210*. *MiR-210* is embedded within one CpG island (*miR-210* stem loop between CpG sites 13 to 23) on chromosome band 11p15.5 (UCSC Genome Browser, version February 2009). A DNA fragment spanning CpG sites 142 to 158 was investigated for methylation.

Bisulfite sequencing of this genomic region confirmed low or absent DNA methylation of the *miR-210*-associated CpG sites (nucleotides 567939-569461 on chromosome band 11p15.5) in four glioblastoma cell lines and three non-neoplastic brain tissue samples (Figure 37).

	CpG sites																
controls/cell lines	142	143	144	145	146	147	148	149	150	152	152	153	154	155	156	157	158
controls																	
hypermethylated DNA	3	3	3	3	3	3	3	3	3	3	3	3	3	3	3	3	3
NB1	1	1	0	0	0	0	0	0	0	1	0	0	0	2	0	1	1
NB2	0	0	0	0	0	0	0	0	0	0	0	0	0	0	0	0	1
NB3	0	0	0	0	0	0	0	0	0	0	0	0	0	0	0	0	0
cell lines																	
A172 co	0	0	0	0	0	0	0	0	0	0	0	0	1	1	2	2	3
A172 A+T2	0	1	0	0	0	0	0	0	0	0	0	1	2	2	2	2	3
U138 co	0	0	0	0	0	0	0	0	0	0	1	1	0	0	0	0	0
U138 A+T2	0	0	0	0	0	0	0	0	0	0	0	0	0	0	0	0	0
TP365MG co	0	0	0	0	0	0	0	0	0	0	0	0	0	0	2	3	1
TP365MG A+T2	0	0	0	0	0	0	0	0	0	0	0	0	0	1	1	2	1
T98G co	0	0	0	0	0	0	0	0	0	0	0	0	0	0	0	0	0
T98G A+T2	0	0	0	0	0	0	0	0	0	0	0	0	0	0	0	0	0

NB1 = human normal brain (BioChain Institute)
NB2 = human fetal brain (BioChain Institute)
NB3 = human normal brain occipital lobe (BioChain Institute)

co = control = non-treated cells
A+T2 = cells treated with 5-aza-2`-deoxycytidine and trichostatin A

0 not methylated
1 weakly methylated
2 moderately methylated
3 strongly methylated

Figure 37: Methylation patterns of the 5´-CpG-rich region (CpG sites 142-158) associated with *miR-210* in four glioblastoma cell lines as well as three non-neoplastic brain tissue samples (NB1 - NB3). Methylation analysis was performed by bisulfite sequencing of the PCR product covering 17 CpGs between nucleotides 567939-569461 on chromosome 11p15.5 (UCSC Genome Browser, version February 2009).

4.4.3 Chromatin immunoprecipitation (ChIP) analysis of the putative promoter regions of *miR-132* and *miR-126* in glioblastoma cell lines

In vitro treatment of five glioblastoma cell lines with TSA suggested that histone modifications contribute to *miR-132* and *miR-126* down-regulation in cultured glioma cells. TSA treatment increased *miR-132* expression in three out of five investigated cell lines relative to the untreated cells (Figure 23 A). Moreover, *miR-126* expression was up-regulated in two out of five cell lines after treatment (Figure 23 B). In collaboration with Dr. Natalie Schmidt (Department of Neuropathology, Düsseldorf, Germany), chromatin immunoprecipitation (ChIP) analyses were carried out to examine the effect of TSA treatment on histone H3 and histone H4 acetylation in the 5`genomic region of *miR-132* and *miR-126* in the T98G, U87MG and U138MG glioblastoma cell lines. *GAPDH* and *p21/CDKN1A* were used as controls. *GAPDH* is associated with euchromatin and is not regulated by histone modifications. Previous studies showed that *p21/CDKN1A* is inactivated by histone modifications in human T98G and U87MG glioblastoma cells (Schmidt et al 2012, Yin et al 2007). In fact, no significant increase was found for *GAPDH* mRNA expression l (T98G: 1.31-fold, p = 0.56; U87MG: 2.58-fold, p = 0.27; U138MG: 1.37-fold, p = 0.26) following TSA treatment (Figure 38 A). Significantly higher levels of *p21/CDKN1A* mRNA transcripts were detected in all three TSA-treated glioblastoma cell lines as compared to the non - treated control cells (T98G: 28.8-fold, p = 0.011; U87MG: 3.2-fold, p = 0.006; U138MG: 2.40-fold, p = 0.003) (Figure 38 B).

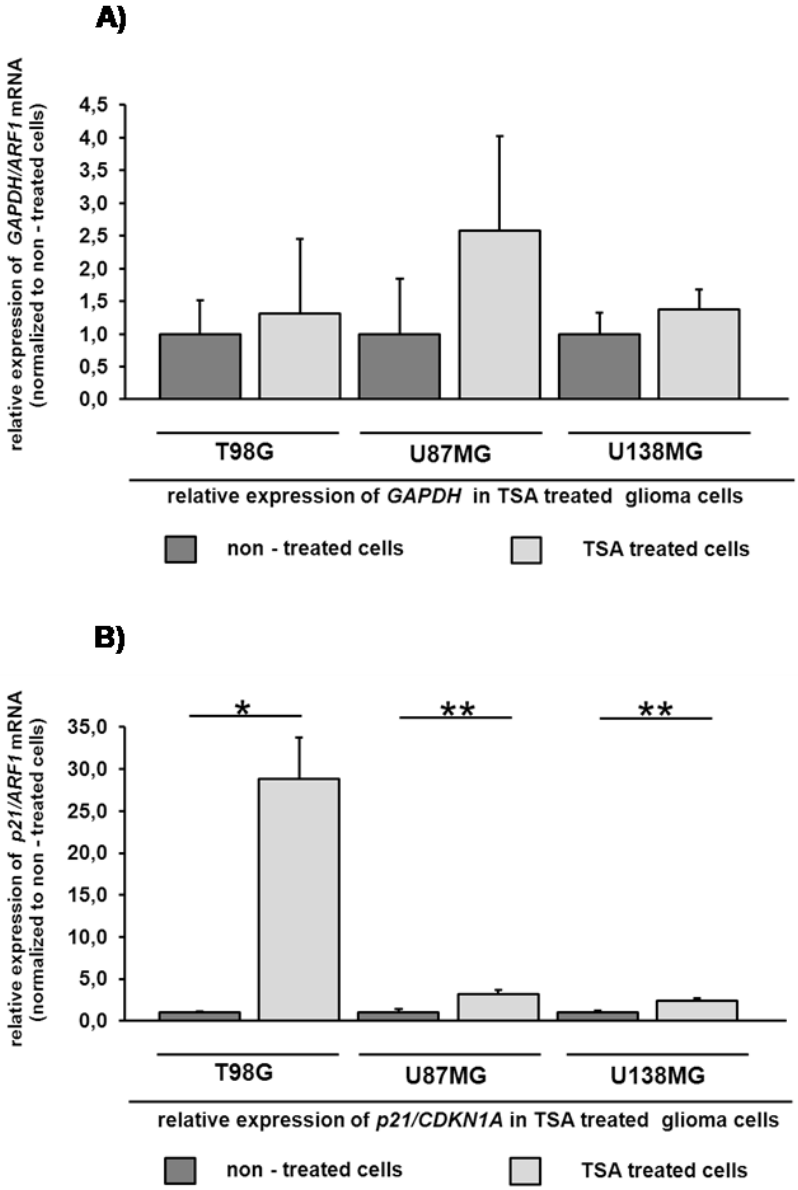

Figure 38: Expression analysis of *GAPDH* (A) and *p21/CDKN1A* (B) mRNA levels in glioblastoma cell lines after treatment with trichostatin A (TSA) relative to untreated control cells. T98G, U87MG and U138MG cells were treated with 1 µM histone deacetylase inhibitor trichostatin A (TSA). The mRNA expression of *GAPDH* and *p21/CDKN1A* were measured by real-time RT-PCR 36 h after treatment and normalized to the expression of *ARF1*. The experiments were done at least three times. Mean results in the non-treated cells were set to 1. Asterisks indicate significant expression differences determined by student`s t-test (* $p < 0.05$, ** $p < 0.01$). **Note:** Significant increase of *p21/CDKN1A* expression in all three investigated cell lines, particular in T98G cells, while the *GAPDH* expression levels remain only slightly affected in the three cell lines after treatment.

To determine the effects of the TSA treatment on the acetylation of histones H3 and H4, Tricin-SDS-PAGE was performed (Figure 39). The TSA treatment led to an increase of acetylated histone H3 as well as acetylated histone H4 in the unbound protein fraction compared to non-treated cells. Rabbit anti-human IgG (anti-IgG) fractions were used as a negative isotype control in both assays. In addition, the western-blot analysis demonstrated the specificity of the investigated antibodies. A strong signal was detected in the bound fraction of TSA treated U138MG and U87MG cells using anti - acetylated histone H4 (H4ac) as compared to the negative control antibody IgG fraction.

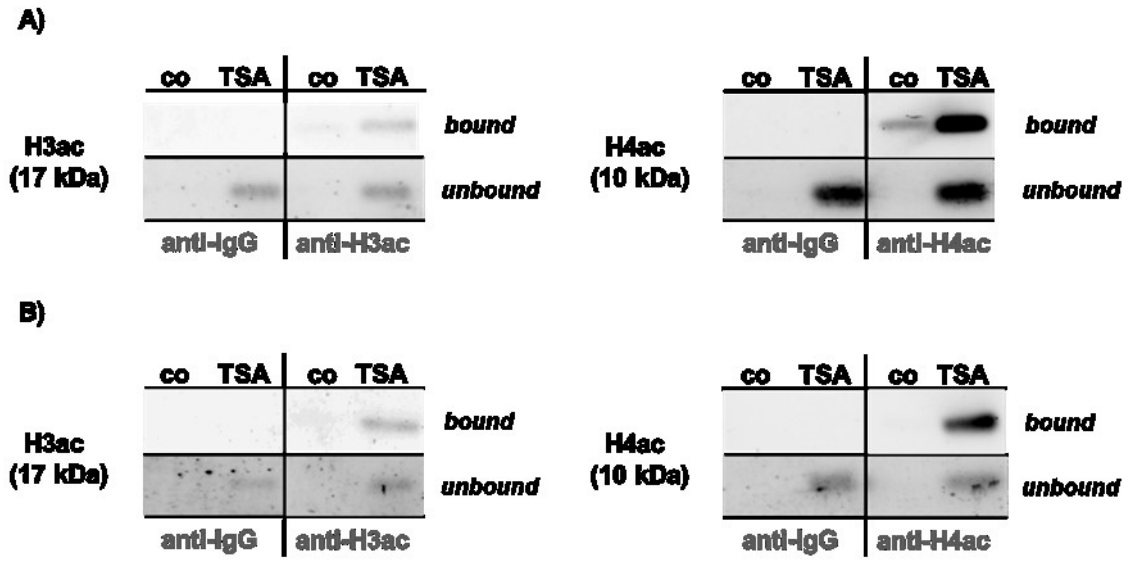

Figure 39: Western blot analysis with the antibodies against acetylated histone H3 (H3ac) (left) and acetylated histone H4 (H4ac) (right) after immunoprecipitation in U138MG (A) and U87MG (B) glioblastoma cells. A) U138MG cells and B) U87MG cells were cultured with (TSA) or without (co) 1 µM TSA for 36 h.

To address the relevance of acetylated histone H3 and acetylated histone H4 in the 5`genomic region of *miR-132* and *miR-126* for the regulation of miRNA expression quantitative real-time PCR analyses following chromatin immunoprecipitation were done with primers targeting the respective promoter regions of *miR-132* and *miR-126*. shown in the Supplementary Figures 5 and 6.

A DNA fragment spanning CpG sites 192 to 215 in the 5`genomic region of *miR-132* (Figure 28: B) was chosen as a crucial region within the *miR-132/miR-212* promoter, which contains transcription factor binding sites, namely upstream control element binding sites (UCE2) (GGCCG) located at CpG sites 197 as well as CpG site 203 and CpG site 214.

For the ChIP analysis of the *miR-126* putative promoter region a fragment located in the 5'-CpG 1 island covering 24 CpG sites (CpG 72 to CpG 95) spanning the reported 5`CpG region methylated in most glioma tumor samples was chosen (Figure 33, Figure 34). Primers for the *GAPDH* promoter were used as stated in the ChIP assay (-118 to -48 relative to the transcription start side). Interestingly, chromatin-immunoprecipitation after TSA treatment exhibited a significant increase of *miR-132* promoter DNA bound to acetylated histone H3 and histone H4 in T98G and U87MG glioblastoma cell lines (Figure 40 A and B). Furthermore, TSA treatment led to an increase of histone H3 and histone H4 acetylation in the 5´- genomic region of *miR-126* in U138MG cells compared to non-treated cells (co) (Figure 40 C). A 6.3-fold increase ($p = 0.0039$) was detected for T98G and a 10.8-fold increase ($p = 0.0064$) for U87MG of *miR-132* promoter DNA bound to acetylated histone H3 after treatment with TSA. A 5.8-fold increase ($p = 0.0037$) for T98G and an 8.1-fold increase ($p = 0.0261$) for U87MG were detected for *miR-132* promoter DNA bound to acetylated histone H4. Similarly, a significant 8.0-fold increase ($p = 0.0015$) of acetylated histone H3 and 17.9-fold increase ($p = 0.0066$) of acetylated histone H4 in the 5´- genomic regions of *miR-126* was detected in TSA-treated U138MG cells compared to non-treated cells.

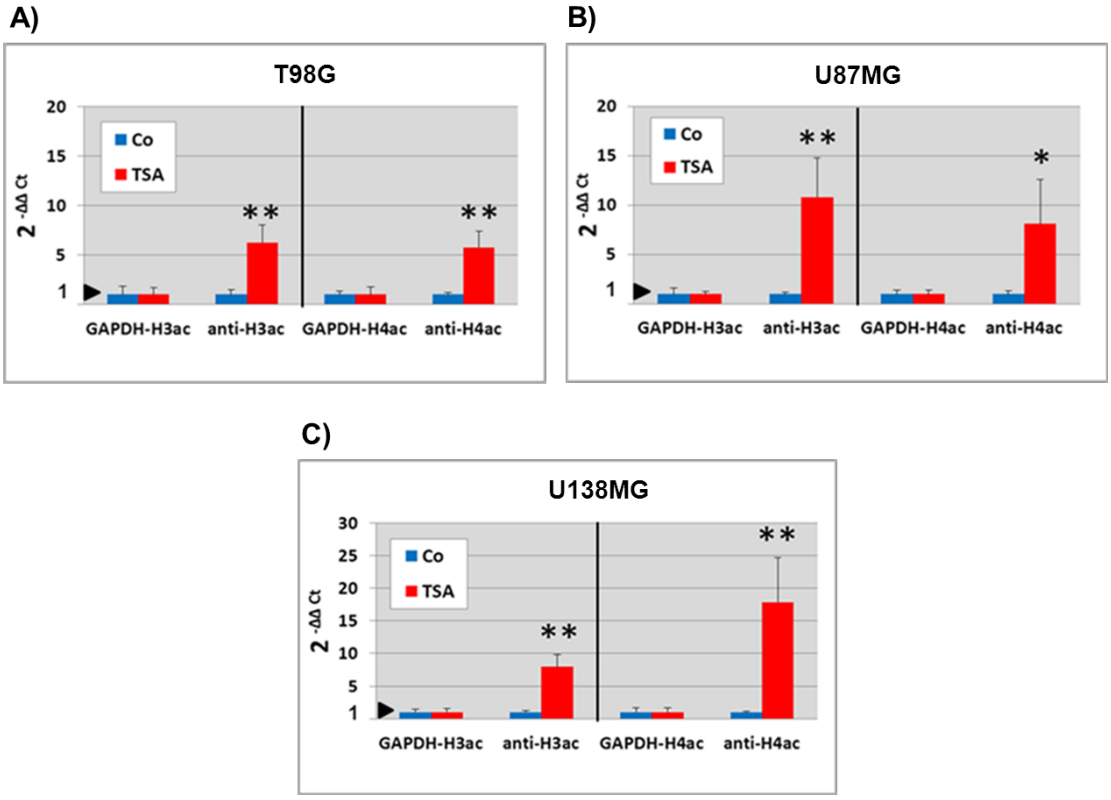

Figure 40: Quantitative real-time PCR analysis of *miR-132* (A, B) and *miR-126* (C) promoter DNA binding to anti-H3ac and anti-H4ac after treatment with trichostatin A (TSA). Glioblastoma cells were cultured with or without 1 µM TSA for 36 h. Acetylation of histone H3 and histone H4 in the 5`genomic region of *miR-132* (**A, B**) and *miR-126* (**C**) were analyzed by chromatin immunoprecipitation assay (ChIP) using anti-acetylated histone H3 (anti-H3ac) and anti-acetylated histone H4 (anti-H4ac) antibodies according to the manufacturer`s recommendations. Rabbit anti-human IgG fraction (anti-IgG) was used as a negative isotype control. *GAPDH* was used for normalization. The experiments were done three times. Abscissa: investigated acetylated DNA fractions; ordinate, DNA amount bound to the histones. Average results in the *GAPDH* acetylated H3 and H4 fractions (GAPDH-H3ac / GAPDH-H4ac) were set to 1. Untreated cells (co) were likewise set to 1. Asterisks indicate significant expression differences determined by student`s t-test (* $p < 0.05$, ** $p < 0.01$, *** $p < 0.001$). **Note:** TSA treatment led to an increase of histone H3 and histone H4 acetylation (anti-H3ac, anti-H4ac) in the 5´- genomic regions of *miR-132* and *miR-126* compared to non-treated cells (co).

These data suggest that the 5`genomic region of *miR-132* and *miR-126* are subjected to chromatin structural changes such as histone H3 and histone H4 acetylation in glioblastoma cells. *In vitro* treatment with TSA caused euchromatinization in the 5`promoter regions of *miR-132* and *miR-126* in glioblastoma cell lines. Thus, histone modifications might serve as an additional cause of *miR-132* and *miR-126* inactivation and either alone or in conjunction with *miR-132* 5`CpG island and *miR-126* 5`CpG island hypermethylation account for the frequent transcriptional down-regulation of these miRNAs in astrocytic tumors.

4.5 Functional *in vitro* analysis of *miR-132* and *miR-126* overexpression in glioma cells

To investigate the functional consequences of *miR-132* and *miR-126* overexpression, human glioblastoma T98G and A172 cells were transiently transfected with 10 nM and 25 nM pre-miR-132 (pre-132), pre-miR-126 (pre-126) or scrambled oligonucleotide molecules (pre-NC1) as a control. Afterwards, the effect of the miRNA overexpression was tested concerning caspase 3/7 activity, cell proliferation, and cell viability.

4.5.1 *MiR-132* and *miR-126* overexpression increased caspase 3/7 activity in glioblastoma cells

To study the biological significance of *miR-132* and *miR-126* overexpression on the induction of apoptosis in transiently transfected glioblastoma cells, the Apo-ONE® homogeneous caspase 3/7 assay (Promega, Madison, WI) was used. Caspases 3 and caspase 7 are key mediators of apoptosis, and therefore activities of these enzymes indirectly reflect levels of apoptosis (Chan et al 2005). Pre-miR-132 and pre-miR-126 transfected T98G and A172 cells showed significantly increased caspase 3/7 activity at 72 h post transfection (Figure 41). Caspase 3/7 activity increased significantly in A172 and T98G cells transfected with 25 nM pre-miR-132 compared to the respective control transfected cells (pre-NC1) (Figure 41 A). Up-regulation of *miR-126* expression significantly increased caspase 3/7 activity of T98G cells transfected with 25 nM pre-miR-126 and of A172 cells transfected with either 10 nM or 25 nM pre-miR-126, relative to cells treated with control oligonucleotides (Figure 41 B).

These results show that overexpression of *miR-132* and *miR-126* increased capase 3 and caspase 7 activity in glioblastoma cells.

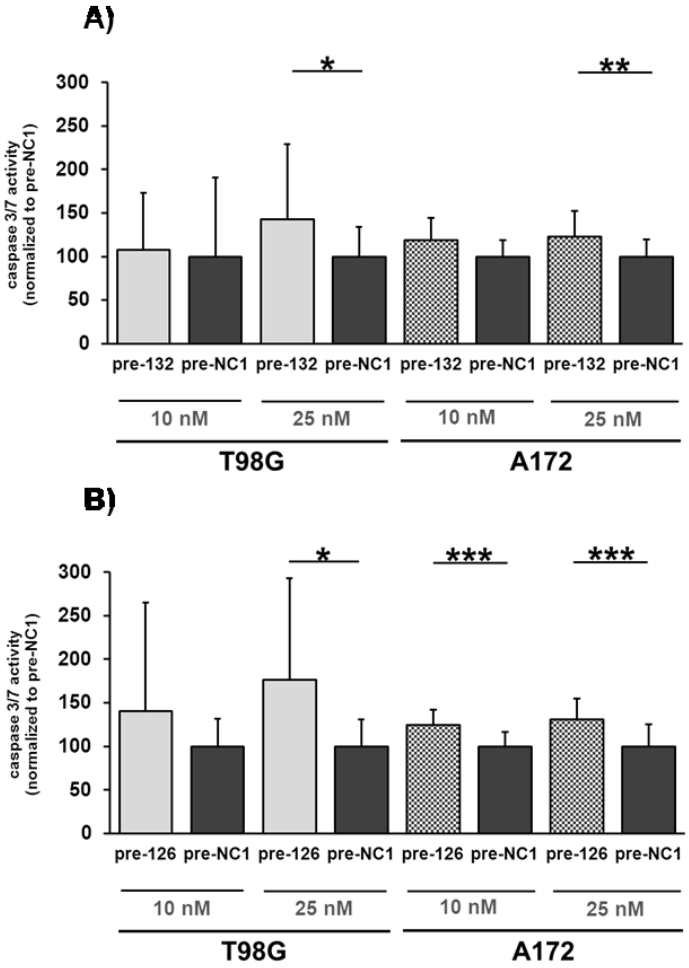

Figure 41: Caspase- 3/7 -activity of T98G and A172 glioblastoma cells after pre-miR-132 (A) and pre-miR-126 (B) transient transfection. For detection of caspase 3/7 activity, T98G and A172 cells were plated in replicates of five in 96-well plates, transfected with 10 nM or 25 nM pre-miR-132 (pre-132), pre-miR-126 (pre-126) molecules or scrambled oligonucleotides as control (pre-NC1). 72 h after transfection caspase activity was measured using the ApoONE homogeneous caspase 3/7 assay (Promega). The experiments were done four times. Average results in the scrambled control cells (pre-NC-1) were set to 100%. Asterisks indicate significant differences determined by student`s t-test (* $p < 0.05$, ** $p < 0.01$, *** $p < 0.001$). **Note:** Overexpression of both miRNAs by transfection of 25 mM pre-miRNAs significantly increased caspase 3/7 activity relative to control transfected cells.

4.5.2 *MiR-126* negatively influences cell proliferation of A172 glioblastoma cells

The effect of *miR-132* and *miR-126* overexpression on glioma cell proliferation was assessed by using BrdU assays. As shown in Figure 42 B, the 10 nM and 25 nM pre-miR-126 transfected A172 cells exhibited significantly lower proliferation compared to the pre-NC1-transfected cells 72h after transfection. In contrast, transfection of T98G cells with pre-miR-126 or pre-miR-132 did not influence the cell proliferation rate. A172 cells transfected with 10 nM pre-miR-132 showed a significant increase in cell proliferation, which was not evident after transfection of 25 mM pre-miR-132. Taken together, these data indicate that *miR-126* inhibits cell growth of A172 cells *in vitro.*

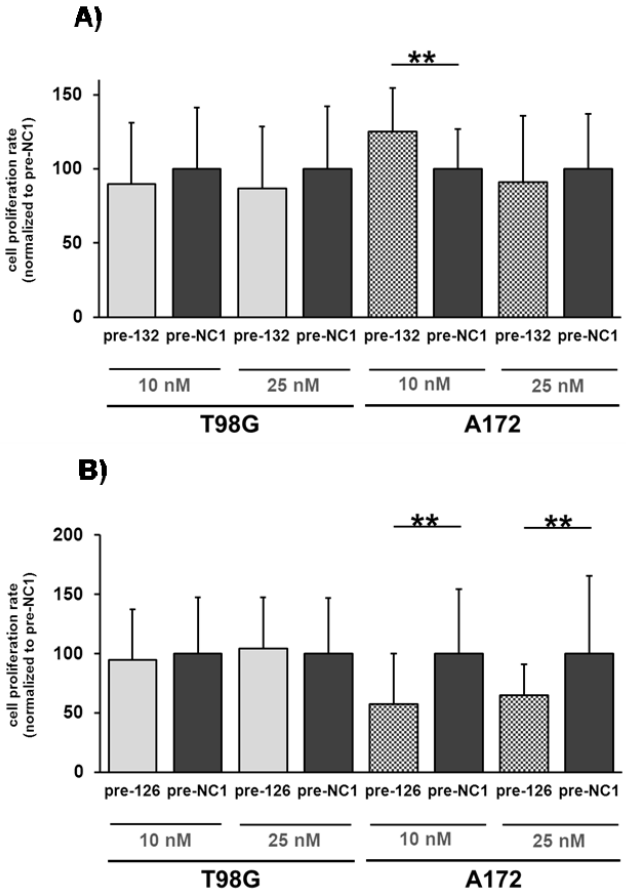

Figure 42: Cell proliferation rate of T98G and A172 glioblastoma cells after pre-miR-132 (A) and pre-miR-126 (B) transient transfection. T98G and A172 cells were plated in replicates of five in 96-well plates, transfected with 10 nM or 25 nM pre-miR-132 (pre-132), pre-miR-126 (pre-126) molecules or scrambled oligonucleotides as control (pre-NC1). 72 h after transfection proliferation rate was measured using the cell proliferation ELISA, BrdU (chemiluminescence) assay (Roche). The experiments were done four times, except for the analysis of 25 nM pre-miR-132 transfected A172 cells, which was performed 3 times. Mean results obtained in the scrambled control cells (pre-NC-1) were set to 100%. Asterisks indicate significant differences determined by student`s t-test ** $p < 0.01$).

4.5.3 *MiR-132* reduced cell viability of T98G glioblastoma cells

Cell viability of *miR-132* or *miR-126* transfected glioma cells was determined by CellTiter-Glo® luminescent cell viability assay (Promega, Madison, WI). Therefore, the two glioblastoma cell lines were transiently transfected with 10 nM or 25 nM pre-miR-132 or pre-miR-126 in comparison to control transfected cells (Figure 43). Up-regulation of *miR-132* expression significantly reduced the number of viable T98G cells (10 nM) while cell viability remained unaffected by *miR-132* up-regulation in A172 cells (Figure 43 A). Measuring the cell viability characteristics of *miR-126* overexpressing T98G and A172 cells revealed increased cell viability in T98G cells after 25 nM transfection but not 10 mM transfection, while pre-126 transfected A172 cells showed no changes in cell viability (Figure 43 B).

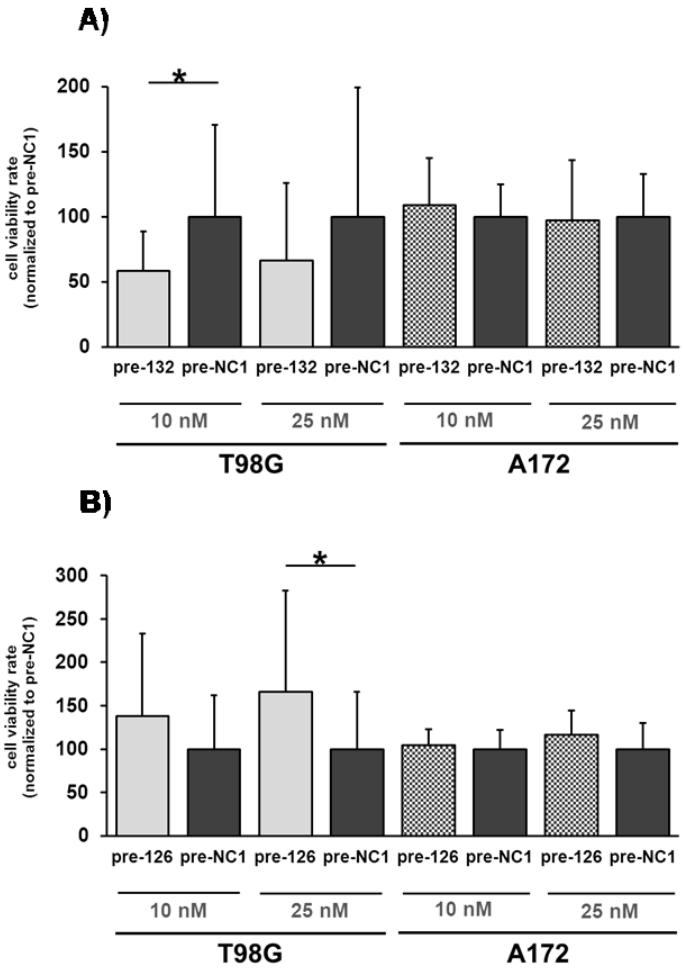

Figure 43: Cell viability of T98G and A172 glioblastoma cells after pre-miR-132 (A) and pre-miR-126 (B) transient transfection. To determine the number of viable cells, T98G and A172 cells were plated in replicates of five in 96-well plates, transfected with 10 nM or 25 nM pre-miR-132 (pre-132), pre-miR-126 (pre-126) molecules or scrambled oligonucleotides as control (pre-NC1). 72 h after transfection cell viability rate was measured using CellTiter-Glo® luminescent cell viability assay (Promega). The experiments were done four times. Mean results in the scrambled control cells (pre-NC-1) were set to 100%. Asterisks indicate significant differences determined by student`s t-test (* $p < 0.05$). **Note:** *MiR-132* up-regulation resulted in decreased cell viability rate of T98G cells.

4.6 Identification and validation of putative *miR-132/miR-212*, *miR-126* and *miR-210* targets

The identification of target genes directly regulated by the selected miRNAs *miR-132/212*, *miR-126* and *miR-210* may help to characterize the functions of these miRNAs in gliomas. As a starting point, candidate target gene for *miR-132/212*, *miR-126* and *miR-210* were retrieved using publically available miRNA databases and target prediction programs. The search was limited to the 3`UTR of human mRNAs extracted from the annotated Reference mRNA Sequences (Ref-Seq) database (Kiriakidou et al 2004, Pruitt et al 2003). The prediction tool miRGen (http://diana.pcbi.upenn.edu/miRGen/v3/miRGen.html) (version v3) was used for target recognition. miRGen is an integrated database that provides access to unions and intersections of four widely used target prediction programs (Union (DIANA-microT), miRanda (microrna.org-miRBase), PicTar (4-way-5-way), TargetScanS) and experimentally supported targets from TarBase (Megraw et al 2007). These *in silico* searches revealed conserved target sites of human *miR-132/212*, *miR-126* and *miR-210* within the 3`UTR of of large number of putative target mRNAs. To narrow down the number of putative target mRNAs, the search was focused on candidate genes that have a miRNA binding site for the seed-sequence (nucleotides 2-8 of the miRNA) of *miR-132/212*, *miR-126* or *miR-210* in their 3´UTR (Lewis et al 2003), that were predicted by all four algorithms and/or were supported by existing literature concerning a functional link with cancer pathogenesis. Eventually, three putative *miR-132* targets were selected for further analysis: *SIRT1* (NAD-dependent deacetylase sirtuin-1), *BTG2* (BTG family member 2) and *JARID1A* (Jumonji, AT-rich interactive domain 1A). *PLAGL2* (pleiomorphic adenoma gene-like 2) was selected as a putative target of *miR-126. GPD1L* (glycerol-3-phosphate dehydrogenase 1-like) and *COX10* (COX10 homolog, cytochrome c oxidase assembly protein, heme A: farnesyltransferase (yeast)) represented two putative targets for *miR-210* that were chosen for further analysis.

4.6.1 Expression analysis of *SIRT1*, *BTG2 and JARID1A*, three putative mRNA targets of *miR-132,* in astrocytic gliomas

MiR-132 was significantly down-regulated in the astrocytic tumors in comparison to normal brain tissue samples (Figure 44 A). In case that *miR-132* directly regulates *SIRT1*, *BTG2* and *JARID1A* through binding to their 3`UTRs, the mRNA expression level of these putative targets should be up-regulated in astrocytic tumors.

To address this hypothesis, the expression of the putative targets was studied in a series of 70 human astrocytic gliomas of different WHO grades (AII, diffuse astrocytoma; AAIII, anaplastic astrocytoma, WHO grade III; sGBIV, secondary glioblastoma, WHO grade IV; pGBIV, primary glioblastoma, WHO grade IV) and compared to four normal brain tissue samples (NB) using microarray analysis in collaboration with Dr. Bernhard Radlwimmer (Molecular Genetics, DKFZ, Heidelberg). Interestingly, the expression of *SIRT1* and *BTG2* was significantly up-regulated in the astrocytic tumors compared to the non-neoplastic brain tissue samples (Figure 44 B and C). For *JARID1A*, three probes located on three different positions on chromosome 12p13.33, ENSG00000073614 according to UCSC Genome Browser (created by the Genome Bioinformatics Group of UC Santa Cruz – version February 2009) were spotted on the microarray. The investigated astrocytic tumors showed an up-regulation of *JARID1A* - mRNA expression for probes 2 and 3 (Figure 44 E and F), whereas the expression level detected by *JARID1A* probe 1 revealed no differences as compared to normal brain tissue samples (Figure 44 D). Thus, all three candidate genes, that are *SIRT1*, *BTG2* and *JARID1A,* appeared to be overexpressed in astrocytic tumors relative to control brain tissue, pointing to a possible oncogenic role of the respective gene products in gliomas.

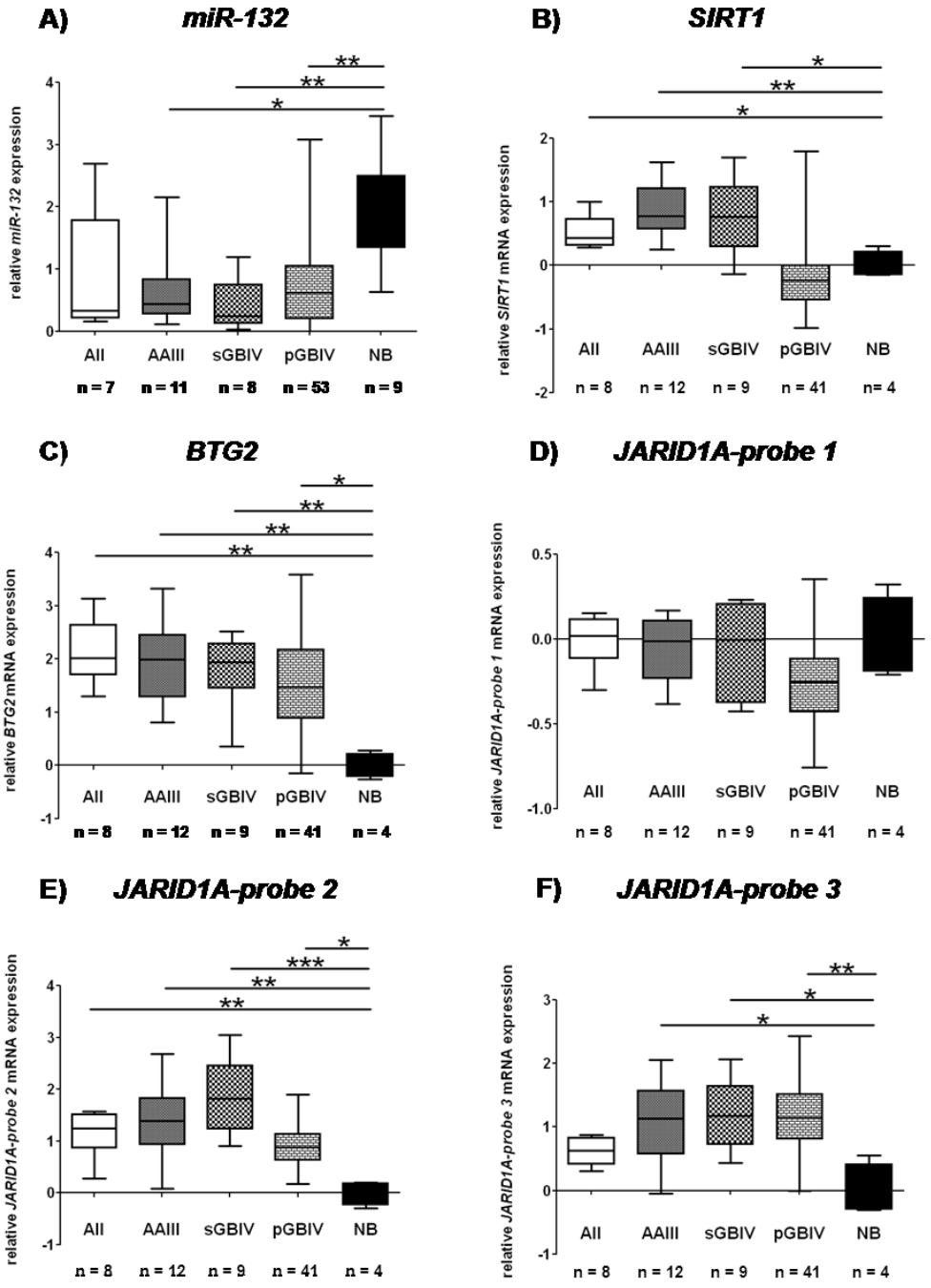

Figure 44: Expression of *miR-132* (A) and its putative target genes *SIRT1* (B), *BTG2* (C), and *JARID1A* (D-F) in astrocytic gliomas. Box plots are depicted indicating median, lower and upper quartile as well as sample maximum and sample minimum of normalized miRNA expression values **(A)** and normalized sample mRNA expression values **(B-F)**. AII, diffuse astrocytoma, WHO grade II; AAIII, anaplastic astrocytoma, WHO grade III; sGBIV, secondary glioblastoma, WHO grade IV; pGBIV, primary glioblastoma, WHO grade IV; NB, normal brain tissue. Asterisks indicate significant expression differences **B)** Mann-Whitney-test; **A, C-F)** Kruskal-Wallis test with Dunn`s Multiple Comparison test of AII vs. NB; AAIII vs. NB; sGBIV vs. NB; pGBIV vs. NB) (* $p < 0.05$, ** $p < 0.01$, *** $p < 0.001$. **Note:** The expression of *SIRT1* (B), *BTG2* (C), and *JARID1A (probes 2 and 3)* (E and F) is upregulated in the tumors while the expression of *miR-132* is down-regulated in the tumors relative to the control brain tissue.

4.6.2 Expression analysis of *PLAGL2*, a putative target of *miR-126*, in astrocytic gliomas

The expression of *miR-126* was significantly lower in AII, AAIII and sGBIV in comparison to normal brain tissue samples (Figure 45 A). The *in silico* target search revealed *pleiomorphic adenoma gene-like 2* (*PLAGL2*) as a putative target of *miR-126*. *PLAGL2* mRNA expression was strongly increased in all groups of astrocytic tumors compared to normal brain tissue (NB, mean: -0.02), with the highest level in AAIII (mean: 1.47), sGBIV (mean: 1.41) and pGBIV (mean: 1.37) followed by AII (mean: 0.96) (Figure 45 B).

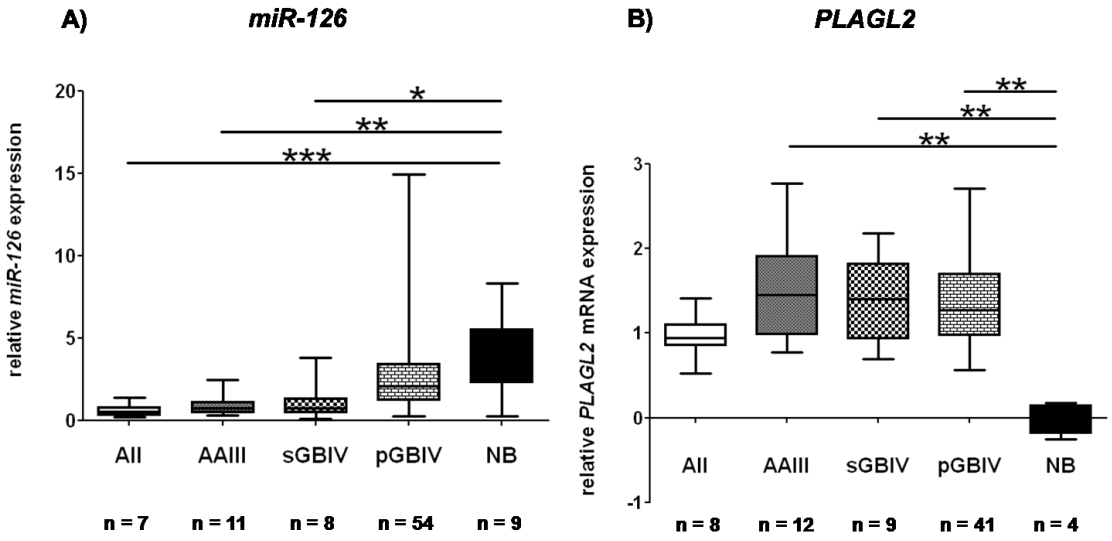

Figure 45: Expression of *miR-126* (A) and its putative target gene *PLAGL2* (B) in astrocytic gliomas. A) Box plots are depicted indicating median, lower and upper quartile as well as sample maximum and sample minimum of normalized miRNA expression values **(A)** and normalized sample mRNA expression values **(B)**. AII, diffuse astrocytoma, WHO grade II; AAIII, anaplastic astrocytoma, WHO grade III; sGBIV, secondary glioblastoma, WHO grade IV; pGBIV, primary glioblastoma, WHO grade IV; NB, normal brain tissue. Asterisks indicate significant expression differences (Kruskal-Wallis test with Dunn`s Multiple Comparison test of AII vs. NB; AAIII vs. NB; sGBIV vs. NB; pGBIV vs. NB (* $p < 0.05$, ** $p < 0.01$, *** $p < 0.001$). **Note:** *PLAGL2* is overexpressed while *miR-126* expression is decreased in astrocytic tumors relative to normal brain tissue.

4.6.3 Expression analysis of putative mRNA targets of *miR-210*

The expression of *miR-210* increased with higher grade of malignancy in astrocytic gliomas. In particular, a significant up-regulation of *miR-210* expression was detected in pGBIV compared to normal brain tissue (Figure 46 A). Two *miR-210* targets predicted by the miRGen prediction programm, *COX10* (*cytochrome c oxidase assembly protein*) and *GPD1L* (*glycerol-3-phosphate dehydrogenase 1-like*), were selected for further analysis. The mRNA levels of *COX10* were slightly but not significantly down-regulated in astrocytic tumors (pGBIV mean: -0.36; AII mean: -0.28; AAIII mean: -0.20; sGBIV mean: -0.11) compared to the reference tissue (mean: -0.93) (Figure 46 B). The mRNA levels of *GPD1L* were significantly down-regulated in the astrocytic tumors (sGBIV mean: -1.41; pGBIV mean: -1.26; AII mean: -1.19; AAIII mean: -0.80) in comparison to normal brain tissue (mean: -0.01) (Figure 46 C).

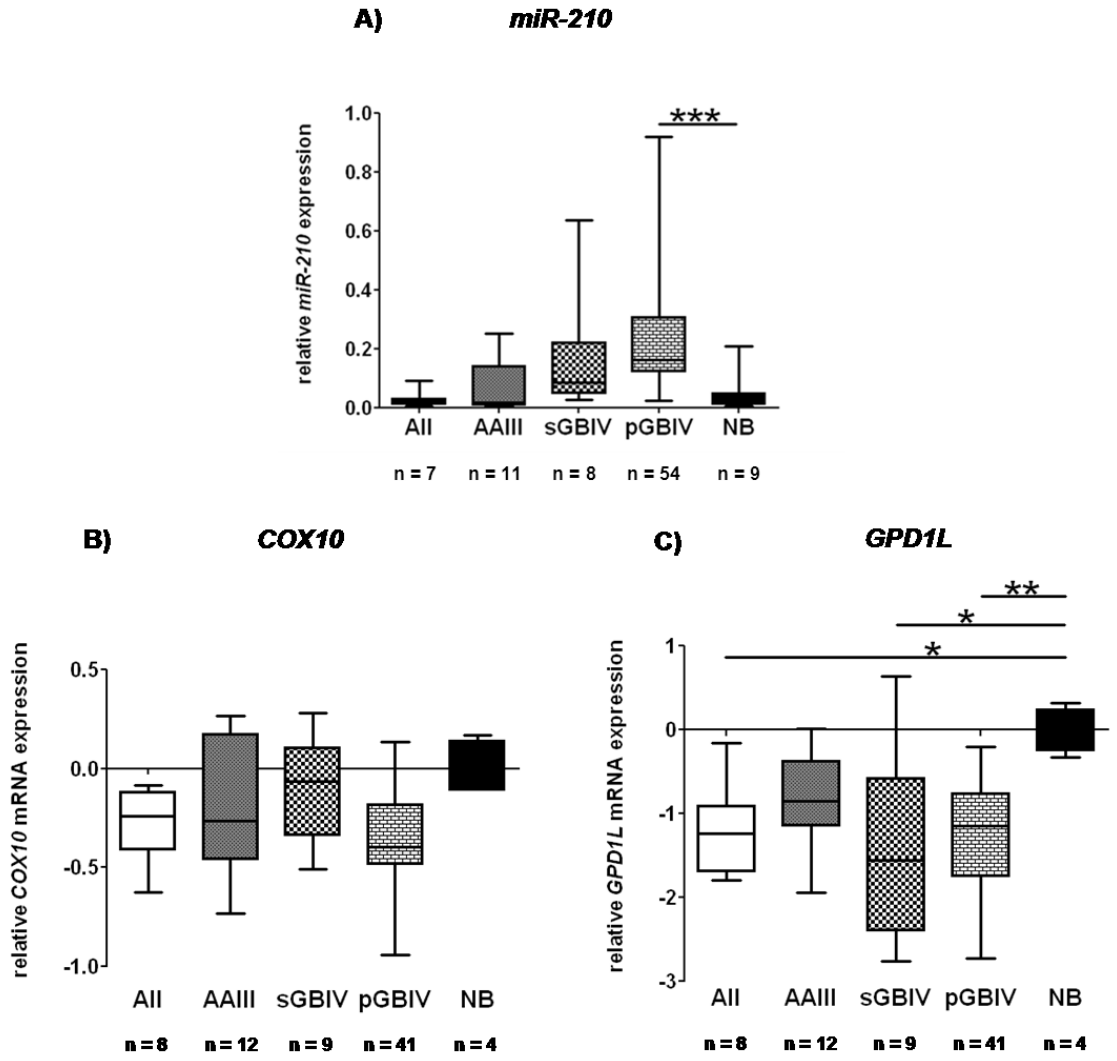

Figure 46: Expression of *miR-210* (A) and its putative targets *COX10* (B) and *GPD1L* (C) in astrocytic tumors. Box plots are depicted indicating median, lower and upper quartile as well as sample maximum and sample minimum of normalized miRNA expression values **(A)** and normalized sample mRNA expression values **(B and C)**. AII, diffuse astrocytoma, WHO grade II; AAIII, anaplastic astrocytoma, WHO grade III; sGBIV, secondary glioblastoma, WHO grade IV; pGBIV, primary glioblastoma, WHO grade IV; NB, normal brain tissue. Asterisks indicate significant expression differences (Kruskal-Wallis test with Dunn`s Multiple Comparison test of AII vs. NB; AAIII vs. NB; sGBIV vs. NB; pGBIV vs. NB (* $p < 0.05$, ** $p < 0.01$, *** $p < 0.001$). Note: While *miR-210* shows elevated expression in the tumors, in particular in the group of pGBIV, the two putative target genes *COX10* and *GPD1L* show lower expression levels in the gliomas as compared to normal brain tissue, with expression of *GPDL1* being significantly reduced in AII, sGBIV and pGBIV.

4.7 Expression analysis of the selected putative mRNA targets in precursor-miR transfected glioma cell lines

As a first step in the functional evaluation of the selected genes as pontential targets of *miR-132/miR-212, miR-126* or *miR-210*, their mRNA levels were determined in glioma cell lines after transient transfection of the respective precursor-miR molecules or scrambled oligonucleotide molecules (pre-NC1) using qRT-PCR.

4.7.1 Overexpression of *miR-132* results in decreased *SIRT1* mRNA levels

The three human glioma cell lines T98G, A172 and U251MG were transfected with 10 nM, 25 nM and 50 nM pre-miR-132 molecules (pre-132) or with the negative control molecules (pre-NC1). All three pre-miR-132 transfected cell lines exhibited a significant decrease in *SIRT1* mRNA expression compared to the respective control transfected cells (Figure 47). Thus, it seems that *miR-132* may directly influence the mRNA level of *SIRT1*.

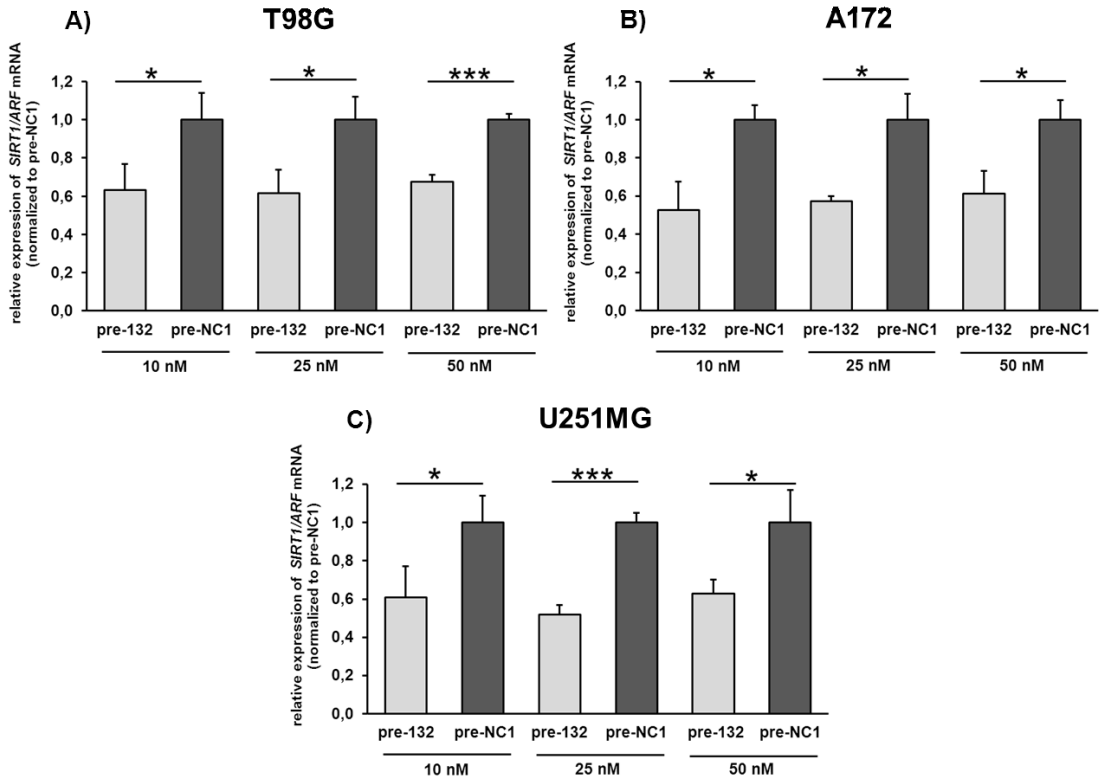

Figure 47: *SIRT1* mRNA expression analysis in pre-miR-132 transfected human glioblastoma cells. A) T98G (50,000 cells/well), **B)** A172 (75,000 cells/well) and **C)** U251MG (60,000 cells/well) cells were plated in 6-well plates. After 24 h cells, were transfected with 10 nM, 25 nM or 50 nM pre-miR-132 molecules (pre-132) or scrambled oligonucleotide molecules (pre-NC1) as a control. Total RNAs were extracted 72 h after transfection. *SIRT1* mRNA levels were detected using real-time RT-PCR. Data represent the mean of three independent experiments. Error bars show standard deviations. Statistics were made by student´s t-test, asteriks indicate significant expression differences: * $p < 0.05$; *** $p < 0.001$.

4.7.2 *MiR-132* down-regulates the expression of *BTG2* in U251MG glioma cells

Overexpression of *miR-132* did not result in decreased *BTG2* mRNA expression levels in A172 and T98G cells. In contrast, *BTG2* mRNA levels were significantly lower in pre-miR-132 transfected U251MG cells of at least 65 % compared to control transfected cells (Figure 48 C). These data suggest that *miR-132* regulates *BTG2* on the mRNA level in U251MG cells, but not in A172 and T98G cells.

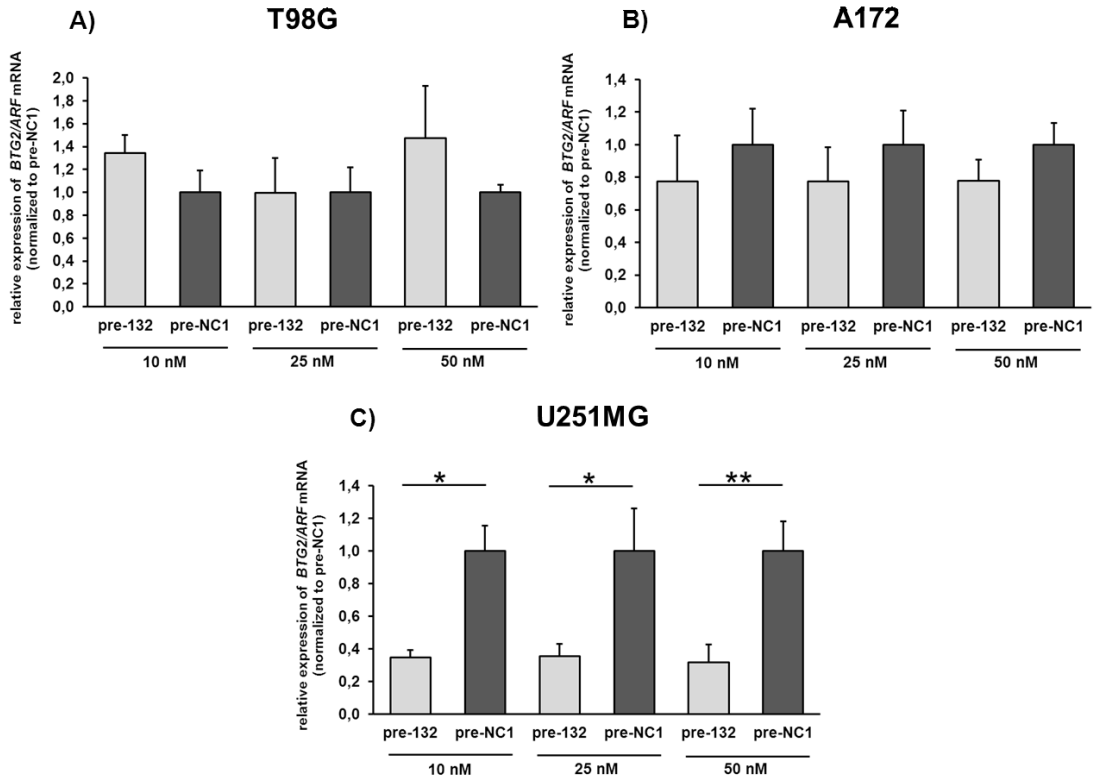

Figure 48: *BTG2* mRNA expression analysis in pre-miR-132 transfected human glioblastoma cells. A) T98G (50,000 cells/well), **B)** A172 (75,000 cells/well) and **C)** U251MG (60,000 cells/well) cells were plated in 6-well plates. After 24 h, cells were transfected with 10 nM, 25 nM or 50 nM pre-miR-132 molecules (pre-132) or scrambled oligonucleotide molecules (pre-NC1) as a control. Total RNAs were extracted 72 h after transfection. *BTG2* mRNA levels were detected using real-time RT-PCR. Data represent the mean of three independent transfection experiments. Error bars show standard deviations. Statistics were made by student´s t-test, asteriks indicate significant expression differences: * $p < 0.05$; ** $p < 0.01$.

4.7.3 Down-regulation of *JARID1A* expression in pre-miR-132 transfected human glioma cells

Reduction of *JARID1A* mRNA expression was observed in all three investigated glioma cell lines transfected with pre-miR-132 (Figure 49). In T98G cells transfected with 25 nM pre-miR-132 and in A172 cells transfected with 50 nM pre-miR-132, significant down-regulation of about 25 % of *JARID1A* expression was detected when compared to the control transfected cells (Figure 49 A and B). In addition, U251MG cells transfected with either 25 nM or 50 nM pre-miR-132 exhibited a significant down-regulation of approximately 25 % of *JARID1A* mRNA expression (Figure 49 C). The data support the hypothesis that *miR-132* may influence the mRNA level of *JARID1A*.

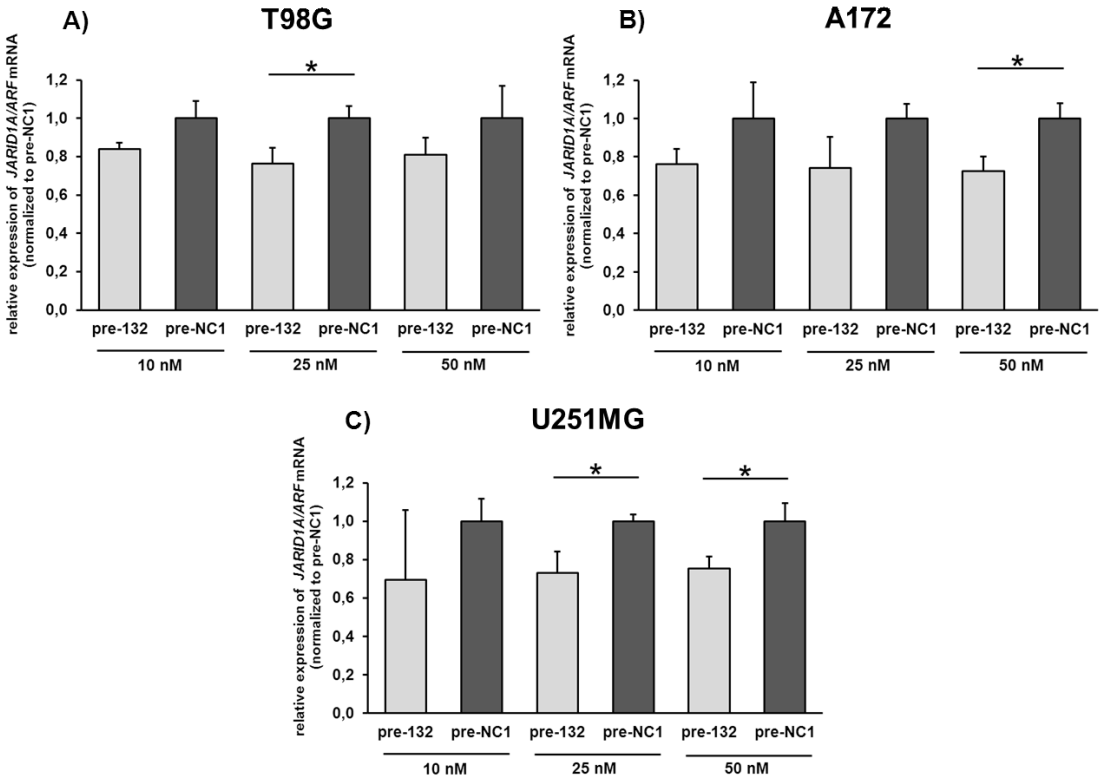

Figure 49: *JARID1A* mRNA expression analysis in pre-miR-132 transfected human glioblastoma cells. A) T98G (50,000 cells/well), **B)** A172 (75,000 cells/well) and **C)** U251 (60,000 cells/well) cells were plated in 6-well plates. After 24 h, cells were transfected with 10 nM, 25 nM or 50 nM pre-miR-132 molecules (pre-132) or scrambled oligonucleotide molecules (pre-NC1) as a control. Total RNAs were extracted 72 h after transfection. *JARID1A* mRNA levels were detected using real-time RT-PCR. Data represent the mean of three independent transfection experiments. Error bars show standard deviations. Statistics were made by student´s t-test, asteriks indicate significant expression differences: * $p < 0.05$.

4.7.4 Down-regulation of *SIRT1* and *JARID1A* expression in pre-miR-212 transfected human glioma cells

Determination of *SIRT1*, *BTG2* and *JARID1A* mRNA expression in glioma cells after pre-miR-212 transfection revealed reduced *SIRT1* and *JARID1A* transcript levels in A172 cells more than in T98G cells transfected with 10 nM or 25 nM pre-miR-212 molecules as compared to control-transfected cells (pre-NC1). However, these data were derived from single experiments and therefore not statistically evaluated (Figure 50 A and C). Transfection of pre-miR-212 did increased *BTG2* mRNA levels in T98G glioma cells and caused only slightly lower *BTG2* transcript levels in A172 cells (Figure 50 C). Collectively, these rather preliminary data would be in line with *miR-212* reducing the mRNA levels of *SIRT1* and *JARID1A*.

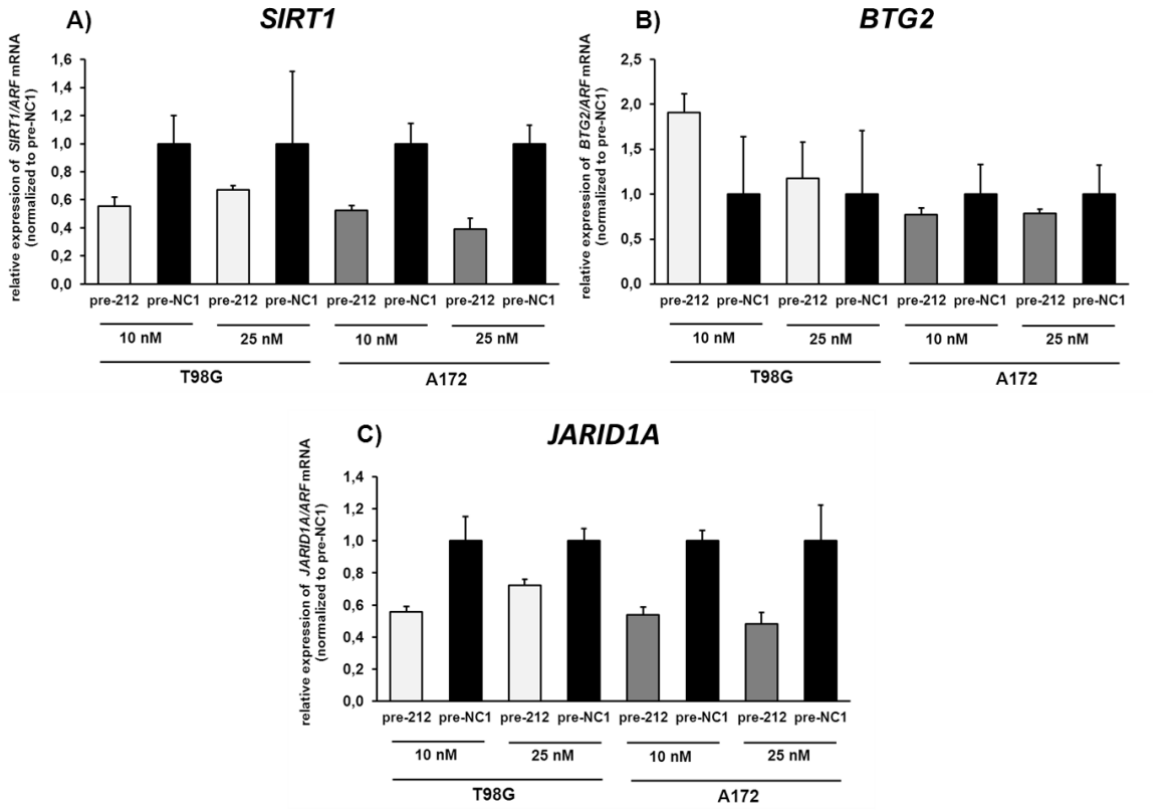

Figure 50: *SIRT1* (A) *BTG2* (B) and *JARID1A* (C) mRNA expression analysis in pre-miR-212 transfected human glioblastoma cells. T98G (50,000 cells/well) and A172 (75,000 cells/well) - were plated in 6-well plates. After 24 h cells, were transfected with 10 nM and 25 nM pre-miR-212 molecules (pre-212) or scrambled oligonucleotide molecules (pre-NC1) as a control. Total RNAs were extracted 72 h after transfection. MRNA levels were detected using real-time RT-PCR. Each bar represents the mean data of three technical replicates. Error bars show standard deviations.

4.7.5 *PLAGL2* mRNA expression is not influenced by *miR-126* overexpression in human glioma cells

The mRNA levels of the proto-oncogene *PLAGL2* were not changed in pre-miR-126 transfected glioma cells when compared to control transfected cells (pre-NC1) (Figure 51).

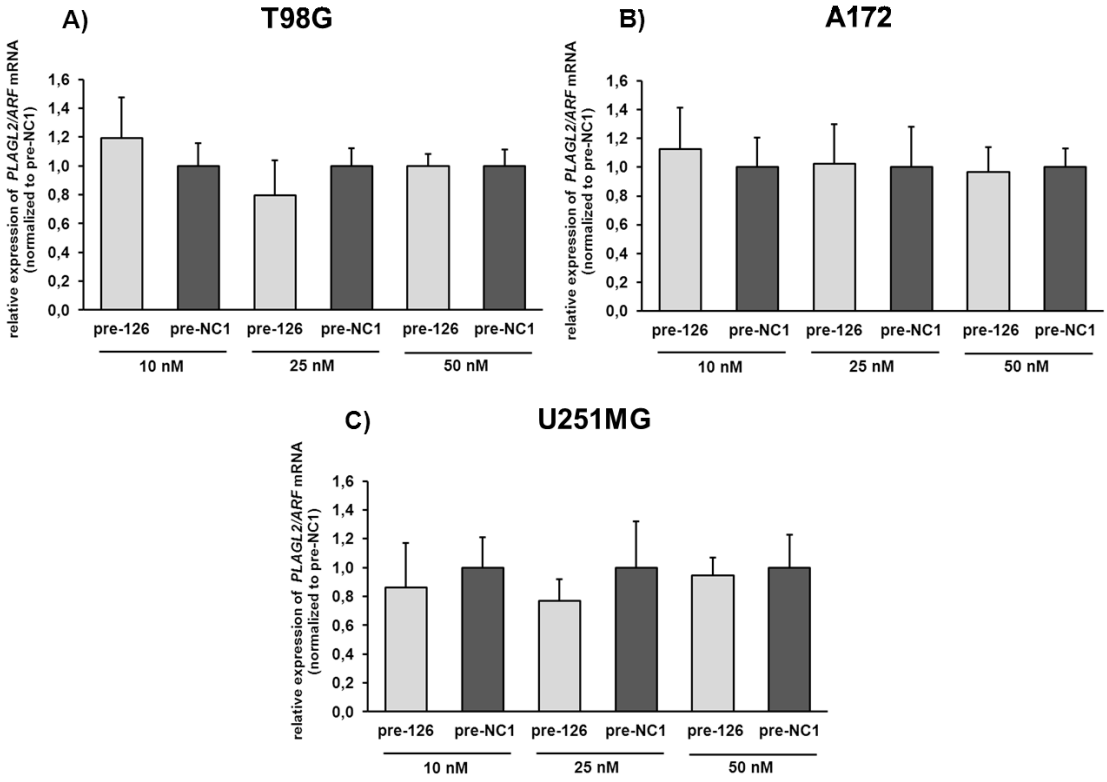

Figure 51: *PLAGL2* mRNA expression analysis in pre-miR-126 transfected human glioblastoma cells. A) T98G (50,000 cells/well), **B)** A172 (75,000 cells/well) and **C)** U251MG (60,000 cells/well) cells were plated in 6-well plates. After 24 h, cells were transfected with 10 nM, 25 nM or 50 nM pre-miR-126 molecules (pre-126) or scrambled oligonucleotide molecules (pre-NC1) as a control. Total RNAs were extracted 72 h after transfection. *PLAGL2* mRNA levels were detected using real-time RT-PCR. Data represent the mean of three independent transfection experiments. Error bars show standard deviations.

4.8 3`UTR luciferase reporter gene assays

To experimentally validate the selected miRNA targets predicted by the miRGen prediction program, the 3`UTR regions of the respective transcripts were cloned into the luciferase reporter plasmid psiCHECK^{TM}-2. Human glioma cells were transfected with each of the reporter constructs in combination with a synthetic precursor-miRNA molecules or a negative control (pre-NC1). Binding of the investigated miRNA to its target sequence in the 3´-UTR of the selected mRNA should result in a decrease of luciferase activity.

4.8.1 Binding of *miR-132*/*miR-212* to the 3'-UTRs of *SIRT1, JARID1A* and *BTG2*

The 3`UTR-regions of *SIRT1*, *JARID1A* and *BTG2* containing potential *miR-132/miR-212* binding sites were cloned into the psiCHECK^{TM}-2 vector. *MiR-132* and *miR-212* exhibit similar mature sequences and both miRNAs share the same seed-sequence. Therefore, they may target the same mRNAs (Wanet et al 2012). Therefore, the following transfection experiments were performed with both miRNAs, respectively.

4.8.1.1 *MiR-132* and *miR-212* repressed *SIRT1* expression through binding to complementary sequences in the 3`UTR of the gene

The *NAD+-dependent protein deacetylase* (*SIRT1*) is evolutionarily conserved across mammals (Hirschey et al 2011). Both isoforms of *SIRT1* (isoform a and b; according to http://genome.ucsc.edu/; version: February 2009) contain the same 3`UTR with two putative binding sites for *miR-132/212* (microRNA.org software (version: august 2010). As shown in Figure 52 A, *miR-132/212* can bind to two sequences in the 3`UTR of *SIRT1* that are complementary to their seed sequence "AACAGUC". Luciferase reporter constructs containing a part of the *SIRT1* 3`UTR were cloned to assess the binding of *miR-132/miR-212* to these sequences (Figure 52 B). The wild-type construct "wt-luc-SIRT1" contained the part of *SIRT1* 3`UTR with the two putative *miR-132/miR-212* binding sites, whereas the mutant "mut1-luc-SIRT1" had deleted the first binding site of *miR-132/miR-212* and retained only the second binding site. The mutant "mut2-luc-SIRT1" contained the first binding site of *miR-132/miR-212* and had deleted the second one. In the full mutant "mut(1+2)-luc-SIRT1", both *miR-132/miR-212*-binding sites had been deleted.

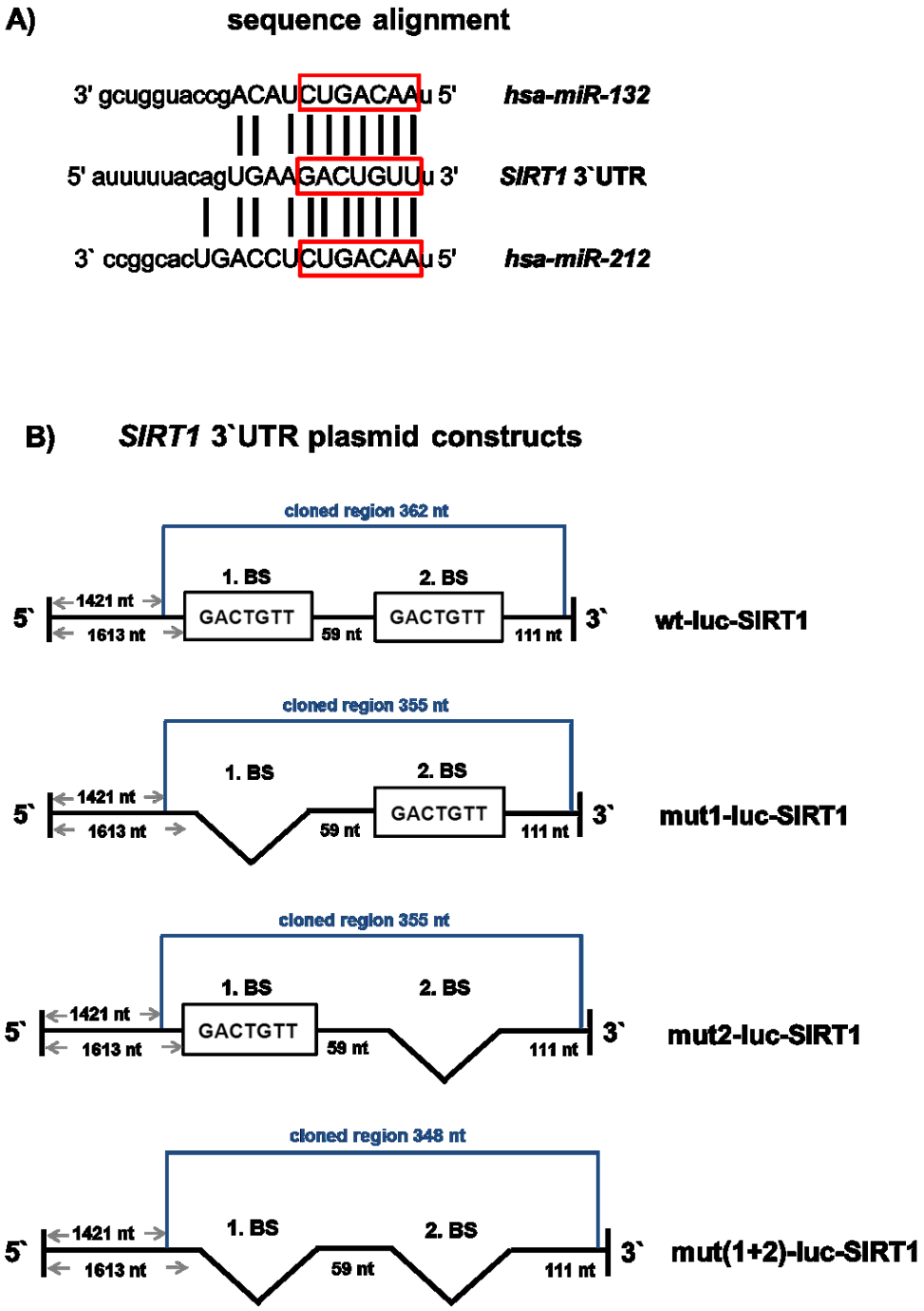

Figure 52: Sequence alignment of *miR-132/miR-212* on *SIRT1* 3`UTR (A) and plasmid constructs (B). A)** Diagram of the *miR-132/miR-212* binding sites in the *SIRT1* 3`UTR. **B) In order to evaluate *miR-132/miR-212* binding, four 3`-UTR constructs were generated and cloned into psiCHECK$^{TM}$-2. The "wt-luc-SIRT1" contained the part of the *SIRT1* 3`UTR with the two *miR-132/miR-212* sites (wild-type construct); "mut1-luc-SIRT1" had deleted the first binding site of *miR-132/miR-212* and retained only the second binding site of *miR132/miR-212*. "mut2-luc-SIRT1" contained the first binding site of *miR-132/miR-212* but had deleted the second one. "mut(1+2)-luc-SIRT1" - the full mutant – had deleted both putative binding sites of *miR-132/miR-212*. 1. BS = binding site 1; 2. BS = binding site 2

To validate the interaction between *miR-132/miR-212* and complementary sequences in the *SIRT1* 3`UTR, T98G cells were co-transfected with the psiCHECK^{TM}-2-*SIRT1* vector and either pre-miR-132, pre-miR-212, or control molecules (Figure 53 A and B). These experiments demonstrated that *miR-132* or *miR-212* up-regulation led to a significant decrease of at least 38 % in luciferase activity of the reporter vector "wt-luc-SIRT1" containing both binding sites of *miR-132/miR-212,* compared to control transfected cells. To verify the binding of *miR-132* or *miR-212* to the two binding sites in the *SIRT1*-3´UTR, either the first ("mut1-luc-SIRT1") or the second binding site ("mut2-luc-SIRT1") were deleted. With either of the two deleted constructs, an inhibitory effect of *miR-132* (Figure 53 A) or *miR-212* (Figure 53 B) on the luciferase activity in T98G cells was still detectable. In contrast, deletion of both putative binding sites ("mut(1+2)-luc-SIRT1") completely abrogated the inhibitory effect of *miR-132* or *miR-212* on luciferase activity. Furthermore, in this context, overexpression of a combination of *miR-132* and *miR-212* resulted in significantly decreased luciferase activity about 30% using "wt-luc-SIRT1" whereas this effect was no longer detectable after deletion of both binding sites (data not shown). These findings indicate that both *miR-132*/*miR-212* binding sites in the 3´UTR of *SIRT1* are functionally important and provide experimental evidence that *miR-132* and *miR-212* directly target and inhibit *SIRT1* expression.

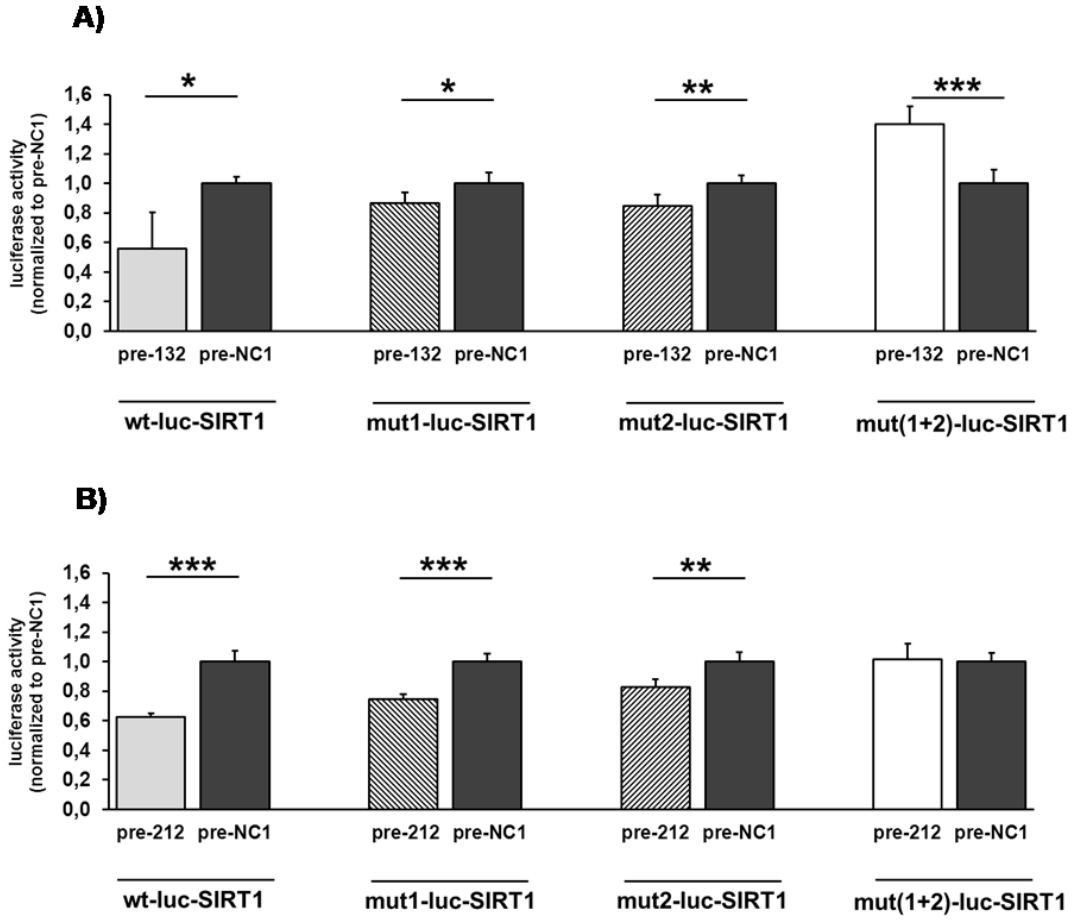

Figure 53: *MiR-132* (A) and *miR-212* (B) directly bind to the 3-UTR of *SIRT1*. Human T98G cells (8000 cells/well) were plated in 96-well plates and co-transfected with 200 ng psiCHECK^{TM}-2 luciferase vector and 50 nM pre-miR-132 (pre-132) or 50 nM scrambled oligonucleotide molecules (pre-NC1) as a control. The Dual-Glo® Luciferase Assay System was performed 24 h after transfection. Renilla luciferase counts were normalized to Firefly luciferase counts. Data represent the mean of three independent transfection experiments. Error bars show standard deviations. Statistics were carried out with the student´s t-test, asteriks indicate significant expression differences: * $p < 0.05$; ** $p < 0.01$; *** $p < 0.001$. wt-luc-SIRT1, wild-type *SIRT1*-3`UTR vector containing both *miR-132/miR-212* binding sites; mut1-luc-SIRT1, mutant *SIRT1*-3`UTR vector with first *miR-132/miR-212* binding site deleted; mut2-luc-SIRT1, mutant *SIRT1*-3`UTR vector with second *miR-132/miR-212* binding site deleted; mut(1+2)-luc-SIRT1, mutant *SIRT1*-3`UTR with both *miR-132/miR-212* binding sites deleted.

4.8.1.2 Down-regulation of *SIRT1* expression in DAOY cells

The identification of *SIRT1* as a direct target of *miR-132/miR-212* emphazises a role of the *miR-132/miR-212* cluster as tumor-suppressive miRNAs in gliomas. As noted above, *miRNA-132* overexpression directly influences the mRNA level of *SIRT1* and represses its expression through binding to the 3`UTR of *SIRT1* transcripts at the post-transcriptional level. To investigate the influence of *miR-132* overexpression on SIRT1 protein levels, the SIRT1- expressing human medulloblastoma cell line DAOY was used, as SIRT1 protein expression in T98G and A172 glioblastoma cells is constitutively very low (data not shown). These experiments were carried out in collaboration with Anneliese Forchmann and Petra Zipper (Department of Neuropathology, Düsseldorf, Germany). Real-time RT-PCR analyses confirmed a 35 % decrease of *SIRT1* mRNA expression in pre-miR-132 transfected DAOY cells as compared to cells transfected with control oligonucleotides (pre-NC1) (Figure 54 A). Western blot analyses revealed significantly decreased expression of SIRT1 of about 32 % in DAOY cells after transfection of miR-132 precursors in three independent biological experiments. Quantification of the Western blots was performed with ß-actin as the loading control and normalization standard (Figure 54 B and C).

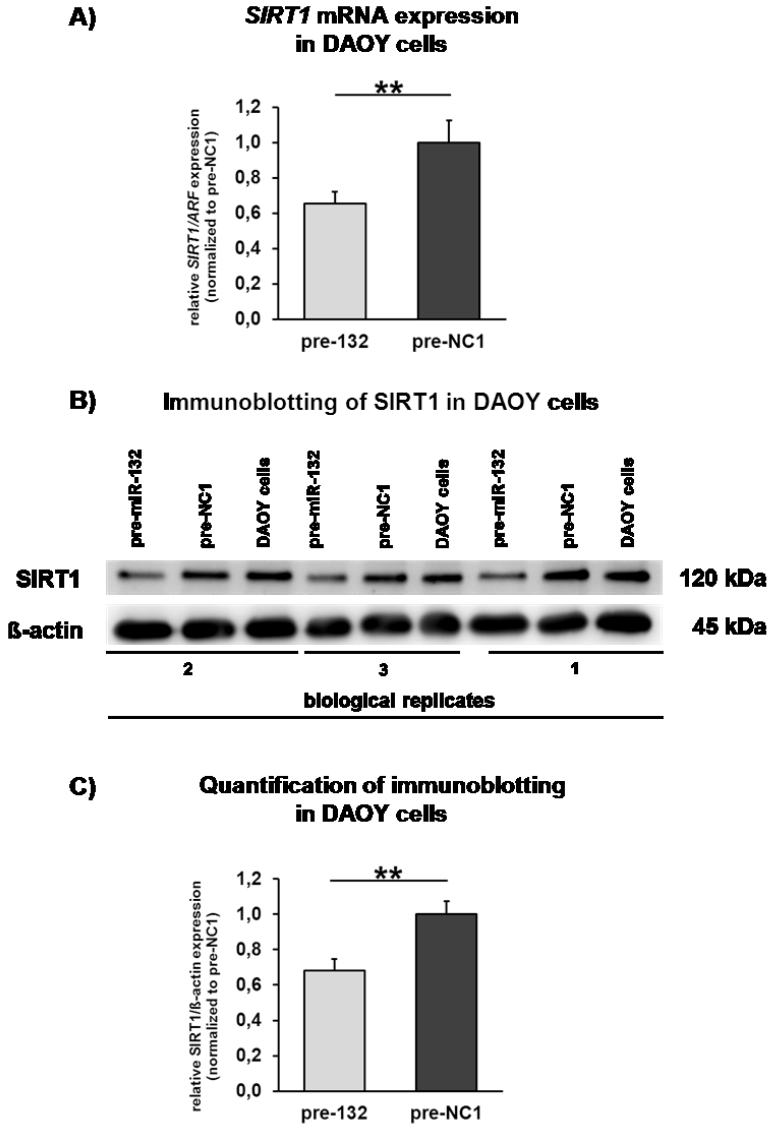

Figure 54: Down-regulation of *SIRT1* mRNA (A) and SIRT1 protein (B, C) expression in human DAOY medulloblastoma cells following transfection of pre-miR-132. A) Human DAOY medulloblastoma cells were plated in 6-well plates. After 24 h, cells were transfected with 50 nM pre-miR-132 molecules (pre-132) or scrambled oligonucleotide molecules (pre-NC1) as a control. Total RNAs were extracted 72 h after transfection. *SIRT1* mRNA levels were detected using real-time RT-PCR. Data represent the mean of four independent transfection experiments. Error bars show standard deviations. Statistics were made by student´s t-test, asterisks indicate significant expression differences: ** $p < 0.01$. **B)** Western blotting analysis of SIRT1 protein expression. DAOY cells were transfected with 50 nM miR-132 precursors or corresponding controls. 50 µg nuclear protein was separated electrophoretically on polyacrylamide gels. Western blots were probed with antibodies against SIRT1 (120 kDa, Santa Cruz, 1:100 in 5 % BSA in TBS-Tween20) and ß-actin (45 kDa, Cell Signaling, 1:500 in 5 % BSA in TBS-Tween20) as a loading control. **C)** Quantification of Western blotting results of SIRT1 proteins normalized to ß-actin; Data represent the mean of three independent experiments. Error bars show standard deviations. Statistics were made by student´s t-test, asteriks indicate significant expression differences: ** $p < 0.01$.

4.8.1.3 *MiR-132* and *miR-212* regulate *JARID1A* expression through one binding site in the *JARID1A* 3`UTR

To determine whether *miR-132/miR-212* targets the expression of *JARID1A* via the predicted *miR-132/miR-212* binding sequence within the 3`UTR (Figure 55 A), luciferase reporter construct bearing the part of the *JARID1A* 3`UTR region with the putative *miR-132/miR-212* binding site ("wt-luc-JARID1A", Figure 55 B) were cloned and analysed.

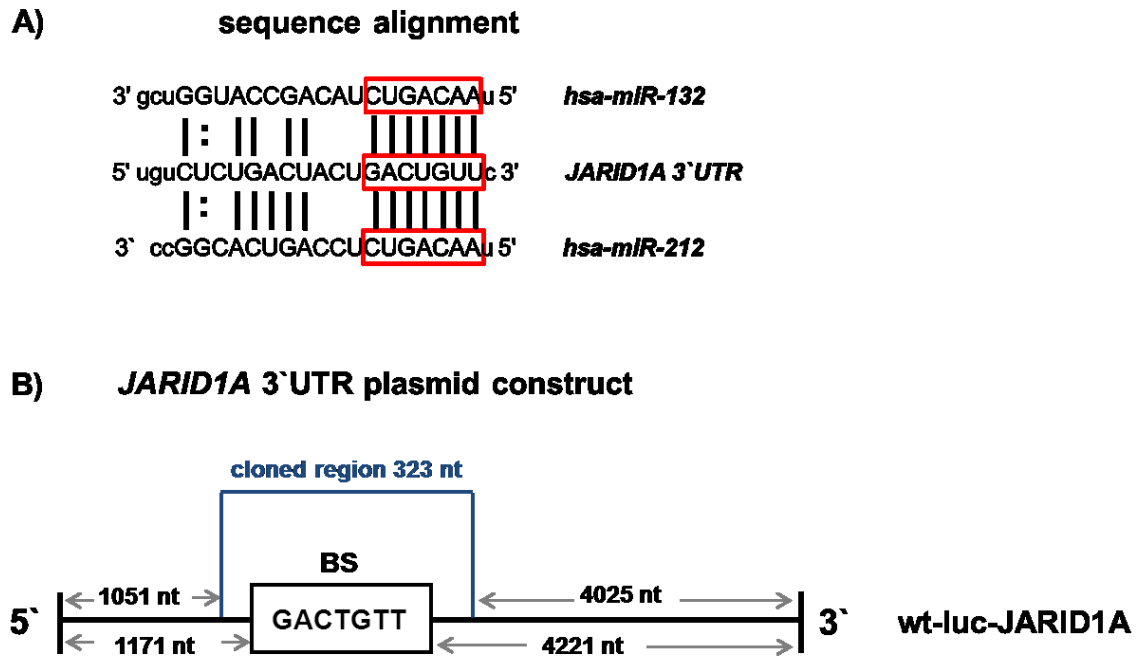

Figure 55: Sequence alignment of *miR132/miR-212* to the *JARID1A* 3`UTR (A) and plasmid construct (B). A)** Diagram of the *miR-132* binding site in the *JARID1A* 3`UTR. **B) The "wt-luc-JARID1A" retained a segment of *JARID1A* 3`UTR with the putative binding region of *miR-132/miR-212* (wild-type construct). BS = binding site

The luciferase activity of the "wt-luc-JARID1A" construct was significantly repressed by the miR-132 mimic (pre-132), with a 26 % mean reduction 72 h after transfection relative to the control-transfected cells (Figure 56). By combining *in silico* miRNA target prediction and target validation by 3`UTR luciferase assays, *JARID1A* thus was confirmed as a direct target of *miR-132*.

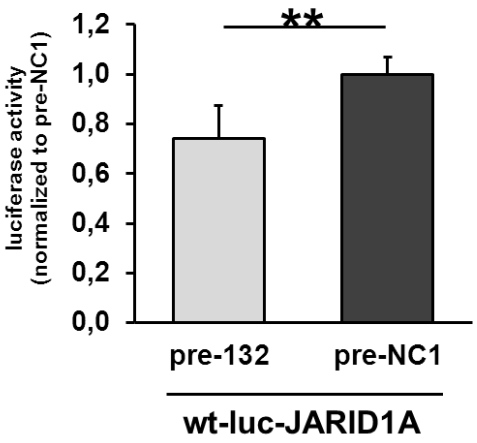

Figure 56: *MiR-132* targets *JARID1A* through its binding site in the *JARID1A* 3`UTR. Human T98G glioma cells (8000 cells/well) were plated in 96-well plates and co-transfected with 200 ng psiCHECK™-2 luciferase vector and 50 nM pre-miR-132 (pre-132) or 50 nM scrambled oligonucleotide molecules (pre-NC1) as a control. The Dual-Glo® Luciferase Assay was performed 72 h after transfection. Renilla luciferase counts were normalized to Firefly luciferase counts. Data represent the mean of three independent experiments. Error bars show standard deviations. Statistics were made by student´s t-test, asteriks indicate significant expression differences: ** $p < 0.01$. "wt-luc-JARID1A", wild-type *JARID1A* 3`UTR vector containing the binding site for *miR-132/miR-212*.

4.8.1.4 *BTG2* does not appear to be directly regulated by *miR-132* or *miR-212*

To determine the direct effect of *miR-132* and *miR-212* on *BTG2* 3`UTR, a "wt-luc-BTG2" plasmid construct was cloned that carried the part of *BTG2* 3`UTR with the predicted binding site of *miR-132/miR-212* (Figure 57).

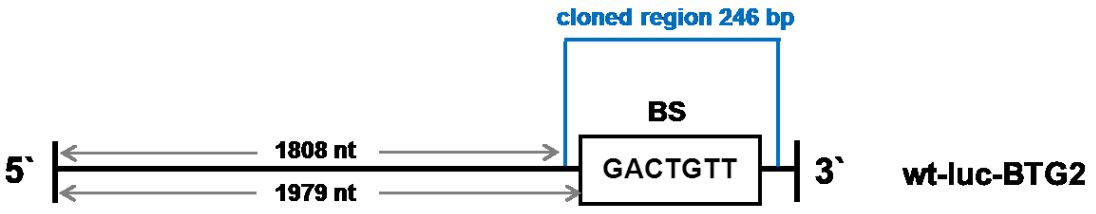

**Figure 57: *MiR-132/miR-212* binding sites in the *BTG2* 3`UTR.** The "wt-luc-BTG2" covered the part of the *BTG2* 3`UTR containing the putative binding region of *miR-132/miR-212* (wild-type construct). BS = binding site.

Transfection of T98G cells with synthetic pre-miR-132 or pre-miR-212 molecules and the psiCHECK^{TM}-2-*BTG2* 3`UTR luciferase reporter construct (wt-luc-BTG2) did not result in a reduction of luciferase activity compared to control-transfected cells (pre-NC1) (Figure 58 A and B). To exclude that this result depends on the cell line the experiment was repeated with another human glioma cell line (U251MG), but again revealed no reduction in luciferase activity (data not shown). These results indicate that neither *miR-132* nor *miR-212* directly regulate *BTG2* mRNA expression by binding to the predicted seed sequence in its 3`UTR.

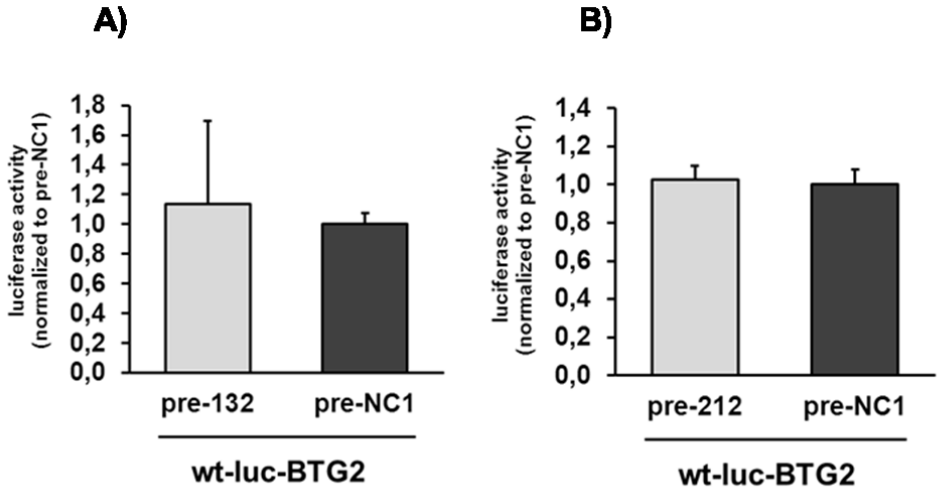

Figure 58: *BTG2* is not directly regulated by *miR-132* (A) and *miR-212* (B). Human glioma T98G cells (8000 cells/well) were plated in 96-well plates and co-transfected with 200 ng psiCHECK^{TM}-2 luciferase vector -and either 50 nM pre-miR-132 **(**pre-132) **(A)**; 50 nM pre-miR-212 (pre-212) **(B)**, or 50 nM scrambled oligonucleotide molecules (pre-NC1) as a control. The Dual-Glo® Luciferase Assay was performed 24 h **(A)** or 72 h after transfection **(B)**. Renilla luciferase counts were normalized to Firefly luciferase counts. Data represent the mean of three independent transfection experiments. Error bars show standard deviations. "wt-luc-BTG2", wild-type *BTG2*-3`UTR vector containing the binding site for *miR-132/miR-212*.

4.8.2 *MiR-210* influences *GPD1L and COX10* in human glioma cells

To experimentally validate and confirm *GPD1L* and *COX10* as *miR-210* targets, the activity of luciferase vector contructs with either the 3`UTR of *GPD1L* or the 3`UTR of *COX10* (Figure 59 B) fused to the *Renilla* luciferase gene were co-transfected with pre-miR-210 molecules. Most importantly, the luciferase activity of the "wt-luc-GPD1L" construct was significantly repressed by pre-miR-210 transfection (pre-210) compared to control-transfected T98G cells (Figure 60 A). In addition, *miR-210* also regulated *COX10* expression directly through binding to the complementary sequence in the 3`UTR, which resulted in 45 % reduction in luciferase activity 72 h after transfection (Figure 60 B). To verify the binding of *miR-210* to the binding site in the *GPD1L* 3`UTR and *COX10* 3`UTR, constructs were cloned in collaboration with Anneliese Forchmann, Department of Neuropathology, Heinrich Heine University, in which the predicted binding sites were deleted. The deletions abolished the *miR-210*-induced reduction in luciferase activity (Figure 60). Therefore, *GPD1L* and *COX10* are direct targets of *miR-210*.

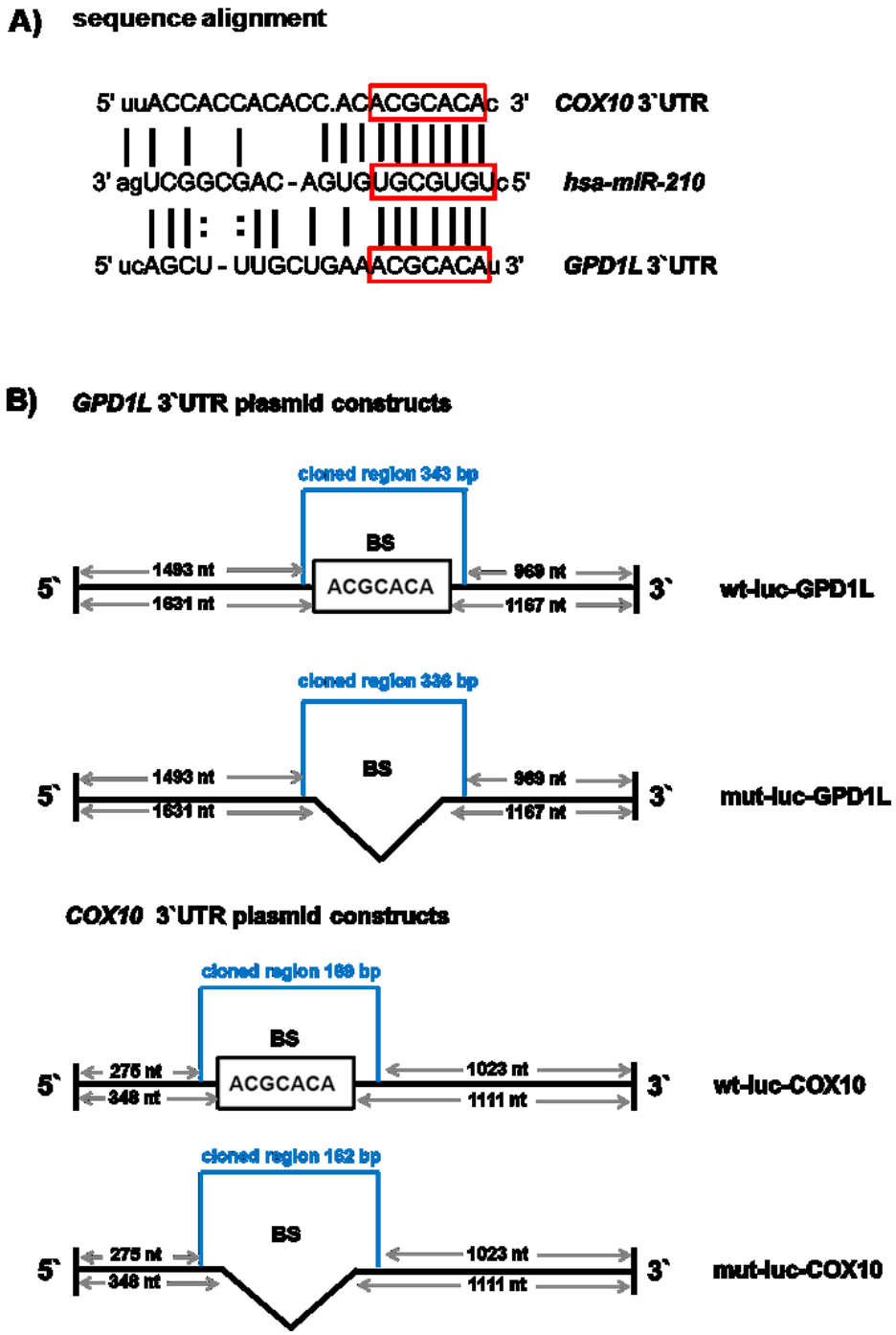

Figure 59: Sequence alignment of *miR-210* to *GPD1L* 3`UTR and *COX10* 3`UTR (A) as well as *miR-210* binding sites in the *GPD1L* 3`UTR (B) and *COX10* 3`UTR (C). A) Sequence alignment of *miR-210* to the *GPD1L* 3`UTR and *COX10* 3`UTR according to microRNA.org software (version: august 2010). **B)** In order to evaluate *miR-210* binding, four psiCHECK^{TM}-2 constructs were produced. The "wt-luc-GPD1L" retained the part of *GPD1L* 3`UTR containing the putative binding region of *miR-210* (wild-type construct) whereas the "mut-luc-GPD1L" had deleted the putative binding site of *miR-210* (full mutant construct). "wt-luc-COX10" retained the part of *COX10* 3`UTR containing the putative binding region of *miR-210* (wild-type construct) whereas the "mut-luc-COX10" had deleted the putative binding site of *miR-210* (full mutant construct). BS = binding site.

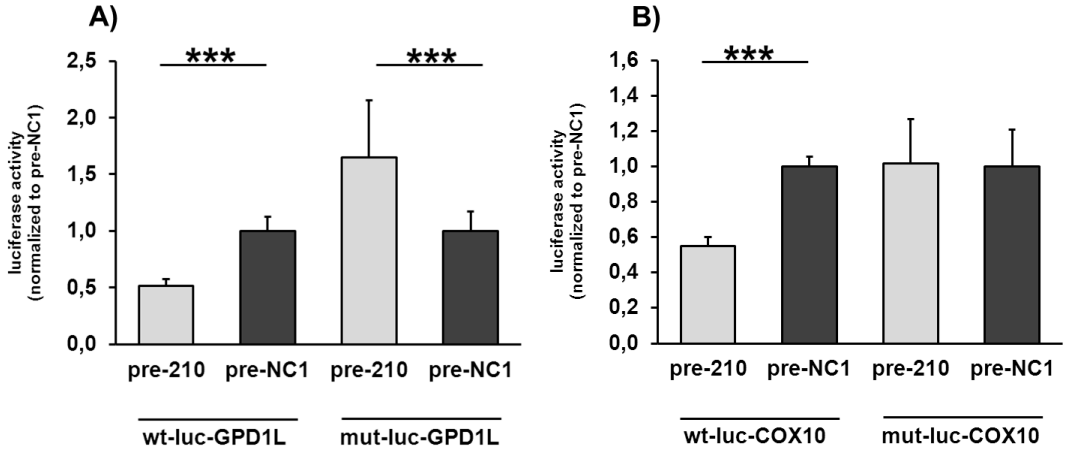

Figure 60: *GPD1L* (A) and *COX10* (B) are direct targets of *miR-210* in T98G cells. Human glioma T98G cells (8000 cells/well) were plated in 96-well plates and co-transfected with 200 ng psiCHECK^{TM}-2 luciferase vector and 50 nM pre-miR-210 (pre-210) or 50 nM scrambled oligonucleotide molecules (pre-NC1) as a control. The Dual-Glo® Luciferase Assay System was performed 72 h after transfection. Renilla luciferase counts were normalized to Firefly luciferase counts. Data represent the mean of three biological replicates. Error bars show standard deviations. Statistics were made by student´s t-test, asteriks indicate significant expression differences: *** $p < 0.001$. "wt-luc-GPD1L", *GPD1L*-3`UTR vector containing the binding site for *miR-210*; "wt-luc-COX10", *COX10*-3`UTR vector containing the binding site for *miR-210*; mut-luc-GPD1L, mutant *GPD1L*-3`UTR vector with deleted *miR-210* binding site; mut-luc-COX10, mutant *COX10*-3`UTR vector with deleted *miR-210* binding site.

5 Discussion

5.1 Retrospective view

Malignant adult brain tumors are associated with a poor clinical outcome and are one of the most feared diseases that afflict human beings (Salacz et al 2011). Anaplastic astrocytoma, anaplastic oligodendroglioma, anaplastic oligoastrocytoma (WHO III) and glioblastoma multiforme (WHO IV) - one of the most deadly forms of cancer - belong to the group of malignant gliomas representing the most common primary tumors of the central nervous system (Louis et al 2007b, Wehming et al 2012). Tremendous efforts have been undertaken to improve patient outcome by multimodality treatment regimens, including surgery, radiotherapy and chemotherapy, thereby offering new hopes for patients, families and clinicians. Glioblastoma is characterized by its aggressive growth behavior including diffuse infiltration into neighboring brain tissue, thereby rendering the tumors unsuitable for complete surgical resection. A further important point is the inherent resistance of these tumors to both radiation and chemotherapy. Due to this fact, the prognosis remains poor (Hadziahmetovic et al 2011, Nieder et al 2004). It has been shown that primary glioblastoma and secondary glioblastoma constitute distinct entities characterized by different genetic pathways and molecular profiles (Pollo 2011). The complex signaling networks in glioma are overwhelming, but relevant molecular characteristics were identified over the last decades (Hu and Kesari 2012, Louis et al 2007b, Riemenschneider and Reifenberger 2009). An important finding was that the formation of cancer can be explained by disturbances in the complex crosstalk between tumor suppressors and tumor promoters. In this context, oncogenes and tumor suppressor genes have been identified as key regulators in tumor development and progression (Zhang et al 2007). Recently, a class of non-protein-coding small RNAs (microRNAs) has been found to be involved in glioma formation and growth (Zhang et al 2012). Most interestingly, human gliomas, glioma cells and glioma stem cells exhibit deregulated miRNA expression compared to normal tissue and cells (Chan et al 2005, Ciafre et al 2005, Hummel et al 2011, Malzkorn et al 2010, Shi et al 2012, Silber et al 2009). However, so far the investigations on the role of miRNAs expression in glioma are still in its infancy, with the vast majority of publications refering to glioblastoma. It has to be clearified whether miRNA expression patterns will prove useful as potential biomarkers of glioma diagnosis, prognosis and may one day also have therapeutic implications.

This project aimed at the identification of miRNAs regulated by epigenetic changes in gliomas and those induced under hypoxic conditions in glioma cells *in vitro*.

5.2 *MiR-132* acts as a putative tumor suppressor gene in gliomas

MiR-132 expression is regulated by histone modification rather than by DNA methylation in its 5`genomic region

The regulation of cell growth and cell differentiation is influenced by epigenetic mechanisms in mammals. It is well known that epigenetic alterations affect the expression of cancer genes either alone or in combination with genetic mechanisms (Egger et al 2004, Jones and Baylin 2002, Nagarajan and Costello 2009). Several miRNA-regulated genes are involved in apoptosis and cell proliferation. Therefore, changes in miRNA expression could promote or suppress tumorigenesis (Cai et al 2009, Hummel et al 2011, Weber et al 2007). Recent studies have reported that locus-specific DNA hypermethylation and histone modifications - mostly at 5'-CpG islands and CpG shores in gene promoter regions - are important in the molecular pathology of glioblastoma (Baeza et al 2003, Bello and Rey 2006, Watanabe et al 2001). Indeed, in the last few years, increasing evidence has been found that a large number of miRNAs are subjected to epigenetic alterations like DNA methylation and histone modifications, which could result in a dysregulated expression of key miRNAs and finally contribute to tumorigenesis (Guil and Esteller 2009, Weber et al 2007). In fact, the regulation of several tumor-suppressive miRNAs was closely associated with DNA methylation of the respective 5`genomic regions in human cancers including gliomas (Bandres et al 2009, Corney et al 2010, Grady et al 2008, Lujambio et al 2007, Silber et al 2008). Inouchi and colleagues identified specific sequence motifs 500 bp to 2000 bp upstream of several human and mouse miRNAs that might be involved in the transcriptional regulation of miRNA precursors (Inouchi et al 2007).

To identify those miRNAs that are silenced in gliomas by epigenetic mechanisms, glioma cell lines were treated with the demethylating agent 5-aza-2'-deoxycytidine (5-Aza) as well as the histone deacetylase inhibitor trichostatin A (TSA). Fifty miRNAs, including *miR-132,* were up-regulated after treatment. Interestingly, *miR-132* was significantly down-regulated in primary astrocytic tumors in relation to non-neoplastic brain tissue samples, suggesting a tumor-suppressive function in gliomas. In line with this observation, Lages and co-workers also detected low levels of *miR-132* in glioma (Lages et al 2011). Several studies revealed increased *miR-132* expression after 5-Aza

treatment in prostate cancer (Formosa et al 2012) and pancreatic cancer ((Zhang et al 2011a). *MiR-132* is known as a brain-enriched or brain-specific miRNA (Cao et al 2006) and is important for the proper development, maturation and function of neurons. Deregulation of *miR-132* expression was associated with neurological disorders, such as Alzheimer's disease and tauopathies (Wanet et al 2012). Due to these findings, *miR-132* was further studied in greater detail to investigate the causes and consequences of epigenetic *miR-132* dysregulation in glioma. In accordance with the array results, simultaneous *in vitro* treatment with 5-Aza and TSA induced expression of *miR-132* at least 2-fold or higher in two glioblastoma cell lines compared to non-treated cells. However, statistically significant up-regulation of *miR-132* was detected in only one of the investigated cell lines used for the validation experiments due to high deviations in the expression of *miR-132* between the three biological replicates. *MiR-132* expression differences in glioma cells between microRNA array (2-fold increase in A172 and T98G cells) and independent validation (increased expression in T98G and TP365MG cells) could be due to the use of different charges of glioma cells for array analysis and validation experiments as well as the fact that only one biological replicate was used for miRNA expression array analysis. To gain insights in the epigenetic mechanism contributing to *miR-132* down-regulation in gliomas, five glioblastoma cell lines were either treated with the demethylating agent 5-Aza or the histone deacetylase inhibitor trichostatin A (TSA). A significant increase in *miR-132* expression levels was only found in TP365MG cells after 5-Aza treatment. Interestingly, *in vitro* treatment of the five glioblastoma cell lines with TSA only led to increased *miR-132* expression levels of 1.5-fold or higher in A172, U138MG, T98G and U87MG cells, suggesting a direct effect of histone modifications on the regulation of *miR-132* expression in glioma cells. Stronger up-regulation of *miR-132* following TSA treatment could be caused by different duration of TSA treatment on the cells. For the combined 5-AZA/TSA-treatment the glioblastoma cell lines were incubated with 1 µM TSA for 24 h whereas for the TSA-treatment, cells were incubated with 1 µM TSA for 36 h. Longer treatment of these two glioblastoma cells with TSA seems to increase expression of the *miR-132*.

To clarify the extent to which either DNA hypermethylation or histone modifications play a role in the regulation of *miR-132* expression, the DNA methylation status around the 5`-genomic region of *miR-132* was determined by sequencing of sodium bisulfite-modified DNA. The *miR-132* is located on chromosome 17p13.3, approximately 260 bp from a closely related miRNA, *miR-212*. Recent studies have reported that microRNAs

can be regulated from their own promoters by CpG island promoter hypermethylation. This epigenetic silencing mechanism is based on the methylation of the C5 position of cytosine, which has been recognized as mutational hotspots (Egger et al 2004, Holliday and Pugh 1975, Lujambio et al 2007). Zhang and co-workers demonstrated that promoter hypermethylation in the 5`genomic region of *miR-132* contributes to the down-regulation of *miR-132* in human pancreatic tumors (Zhang et al 2011a). Contrary to these observations, the own investigations did not reveal 5`CpG methylation-dependent *miR-132* expression in gliomas, with the exception of one CpG site where the methylation significantly correlated with the expression of *miR-132*. Nevertheless, three parts of the investigated *miR-132* 5`genomic region, revealed hypermethylation in samples of glioma patients compared to non-neoplastic brain tissue samples. Moreover, tumor samples from patients with sGBIV, AAIII and AII showed hypermethylation in these *miR-132* parts of the 5`genomic region whereas lower fractions of methylated cytosines were detected in the majority of pGBIV. Interestingly, this CpG methylation pattern correlated with the presence of somatic mutations in codon 132 of the gene encoding isocitrate dehydrogenase 1 (*IDH1*). *IDH1* and its homolog *IDH2* are mutated in 50-80% of astrocytomas, oligodendrogliomas and oligoastrocytomas of WHO grades II and III, as well as secondary glioblastomas and glioblastomas of younger patients, and coincident with increased patient survival. They are, however, rarely mutated in primary glioblastomas and never in other types of glioma (Balss et al 2008, Hartmann et al 2009, Ichimura 2012, Parsons et al 2008, Yan et al 2009). Therefore, it seemed that *IDH1/2* mutations generally occurred in the progressive form of diffuse glioma, rather than in *de novo* glioblastoma. Gliomas with *IDH1/2* mutations frequently carry either additional *TP53* mutations (in diffuse astrocytic gliomas) or total 1p/19q loss (in oligodendrogliomas). Therefore, these two types of tumors may develop from common progenitor cells that have *IDH1/2* mutations and subsequently evolved into each tumor type by the acquisition of *TP53* mutations or total 1p/19q loss (Ichimura 2012). The finding that global DNA hypermethylation is frequent in tumor samples with *IDH1/2* mutations prompted the designation of this phenomenon as d glioma CpG Island Methylator Phenotype (G-CIMP). CIMP was first identified in human colorectal cancer as cancer-specific CpG island hypermethylation of multiple genes in a subset of tumors (Toyota et al 1999). Noushmehr and colleagues found that G-CIMP status stratified gliomas into two distinct subgroups with different molecular and clinical phenotypes (Noushmehr et al 2010). In line with the own results, Noushmehr and colleagues found that *IDH1* somatic mutations were tightly associated

with G-CIMP within a group of 300 genes with significant DNA hypermethylation in G-CIMP-positive tumors compared to G-CIMP-negative tumors. They also identified 20 miRNAs that showed significant differences in their gene expression between proneural G-CIMP-positive and proneural g-CIMP negative tumors.

One important explanation for the limited association between DNA methylation and expression of *miR-132* in gliomas may be the fact that different CpG regions were investigated by Zhang and co-workers as compared to the own studies. Zhang and colleagues demonstrated 5`CpG methylation-dependent *miR-132* expression within CpG sites 250-263 (Zhang et al 2011b). The own studies revealed hypermethylation in the 5`genomic region of *miR-132* around CpG sites in front of or behind these CpG sites 250-263 (CpG sites 181-215, CpG sites 221-232 and CpG sites 300-319). However, the own data clearly demonstrate significant association between *miR-132* expression and methylation at CpG site 184 located within the *miR-132* 5` genomic region (CpG 181 to 215). Moreover, *miR-132* expression in *miR-132* 5` hypermethylated astrocytic tumors might be due to contaminating non-neoplastic cell populations, such as microglial or lymphocytic cells. In addition, such differences may also be explained by subpopulations of unmethylated tumor cells. In line with my observations, Felsberg and co-workers described similar mismatches in the correlation of methylation and expression data for other hypermethylated genes, such as *MGMT*, in gliomas (Felsberg et al 2009). Zhang and co-workers reported that hypermethylation eliminated SP1 binding in the *miR-132* 5`genomic region, thereby resulting in decreased *miR-132* expression in pancreatic tumor tissues (Zhang et al 2011a). In this thesis, several SP1 and UCE2 transcription factor binding sites within the 5`genomic region of *miR-132/miR-212* were investigated in glioma patient samples. One SP1/UCE2 transcription factor binding site at CpG site 184 revealed methylation-dependent *miR-132* expression in gliomas. Thus, SP1 and UCE2 could play an important role in controlling *miR-132* expression through methylation-dependent binding in this particular CpG-rich region in glioma. However, to examine whether SP1, UCE2 or yet unidentified transcriptional factors regulate the expression of *miR-132*, especially around CpG site 184, further research on the *miR-132* 5`genomic region and approaches on transcription factor binding sites are needed. One further experiment may be the cloning of the SP1/UCE2 transcription factor binding site sequence and deleted binding site constructs into a luciferase reporter plasmid to analyze the expression of the reporter after co-transfection with different transcription factors in glioma cells. If the binding of SP1/UCE2 transcription factors will take place then the

expression of the reporter should be up-regulated in glioma cells. In addition, it should also be investigated whether the expression levels of SP1/UCE2 correlate with that of *miR-132* in glioma tissue samples. A further experiment could be the treatment of the luciferase-transcription factor binding site constructs with methylase SssI to mimic the hypermethylation status of the *miR-132/miR-212* 5`genomic region *in vivo* to analyze if hypermethylation eliminates SP1/UCE2 binding in the 5`genomic region of *miR-132/miR-212* based on reduced luciferase activities relative to the unmethylated reporter.

Histone modifications around the 5`genomic region of miR-132

Gene expression may be modulated by global changes in histone acetylation and promoter-specific histone acetylation (Vaissiere et al 2008). Interestingly, evidence has been obtained for inhibition of cancer cell growth *in vitro* and *in vivo* by treatment with the histone deacetylase inhibitor trichostatin A (TSA) (Vigushin et al 2001, Yoshida et al 1990). In this thesis, glioblastoma cell lines were treated *in vitro* with TSA, leading to an euchromatinization of gene promoters, and as a consequence to increased expression of genes silenced by histone deacetylation. Indeed, TSA treatment increased the expression level of *miR-132* at least 2-fold in T98G and U87MG glioma cells in relation to untreated cells, suggesting that histone modifications contribute to the down-regulation of *miR-132* in gliomas. Chromatin-immunoprecipitation after TSA-treatment corroborated a significant increase of *miR-132* promoter DNA bound to acetylated histone H3 (H3ac) and histone H4 (H4ac) in T98G and U87MG glioblastoma cell lines. Histone modifications associated with light exposure have been demonstrated to regulate *miR-132/miR-212* transcription at CREB transcription binding sites within the 5`genomic region of *miR-132/212* in the visual cortex of juvenile mice, a mechanism that has been implicated in the plasticity of dendrites and spines (Tognini et al 2011, Wanet et al 2012). CREB (cAMP response element-binding) is a cellular transcription factor that binds to several DNA sequences called cAMP response elements (CRE), thereby increasing or decreasing the transcription of the downstream genes (Fusco et al 2012). In line with these findings, the own data would be compatible with the hypothesis that histone modification, in particular histone de-acetylation, may contribute to the down-regulation of *miR-132* expression in glioma cells. Further experiments - concerning chromatin immunoprecipitation in a separate subset of glioblastoma tissue samples - are necessary to confirm that the *miR-132* 5`genomic region is indeed regulated by histone modifications in primary gliomas *in situ*.

Collectively, this study highlights two epigenetic alterations in the 5`genomic region of *miR-132* in glioma cells. Both, histone modifications as well as DNA methylation at the CpG island promoter likely contribute to *miR-132* down-regulation in human gliomas. Thus, the epigenetic dysregulation of *miR-132* in gliomas constitutes an emerging scientific field that eventually may have consequences for cancer patients undergoing treatment with DNA-demethylating and histone-deacetylase inhibitor drugs in the clinical setting.

MiR-132 and miR-212 promote SIRT1 mRNA expression in glioblastoma cells

In most instances, miRNAs interact with their target mRNA by perfect or imperfect matching between miRNA "seed"-sequence and the mRNA 3`-untranslated region leading to cleavage and degradation or to translational inhibition of their mRNA targets (Breving and Esquela-Kerscher 2010). Until now, over 1500 miRNAs have been identified in the human genome (Wanet et al 2012). A single miRNA might control hundreds of distinct targets (Filipowicz et al 2008). *MiR-132* and *miR-212* share the same seed sequences, which are highly conserved in vertebrates (Park et al 2011, Remenyi et al 2010, Wanet et al 2012). Until now, it is not well described if *miR-132* and *miR-212* have specific targets and if they exert numerous and overlapping functions (Wanet et al 2012). In this study, *miR-132/miR-212* target genes were identified initially by computational analyses predicting the presence of putative binding sites for both miRNAs. One of the putative targets with bindings sites for *miR-132/miR-212* in its 3`UTR was *SIRT1*, the major mammalian member of the sirtuin family, which deacetylates histones and nonhistone proteins, including p53, Ku70 and FOXO (Audrito et al 2011). *SIRT1* has been implicated in the regulation of circadian rhythm, endocrine signaling and aging (Hursting and Berger 2010). Further studies revealed an upregulation of *SIRT1* in several human tumor types, including breast and colon cancers (Liu et al 2009b). In these tumors *SIRT1* may act as an oncogene by suppressing p53 functions. In line with these findings, the own data revealed an inverse association between *miR-132* expression and *SIRT1* mRNA expression. Microarray analysis revealed significant overexpression of *SIRT1* in tumors of patients with AII, AAIII and sGBIV in relation to non-neoplastic brain tissue samples. The tumor suppressor gene product p53 has been observed to play an important role in G1 cell cycle arrest and apoptosis (Fueyo et al 1998). An increase in *SIRT1* expression and function is followed by decreasing p53 active form, thereby leading to genome instability and resistance to apoptosis (Audrito et al 2011, Vaziri et al 2001). In addition, it was shown that Sirtuin inhibitors (NAD+ analogs or direct kinase inhibitors) could be

useful for the treatment of cancers through the inhibition of tumor-formation and induction of apoptosis (Kucinska and Murias 2010, Marks and Xu 2009).

This thesis addressed the biological significance of *miR-132* overexpression on the induction of apoptosis in transiently transfected glioblastoma cells. Interestingly, overexpression of *miR-132* can promote caspase 3/7 activity and inhibits cell viability, suggesting a tumor suppressive role of this miRNA in gliomas. Cell proliferation rate seems to be unaffected after transfection with *miR-132* precursors in human T98G glioblastoma cells. In contrast, Zhang and co-workers reported that *miR-132* mimics significantly repressed the proliferation of pancreatic tumor cells (Zhang et al 2011a). Particularly noticeable in all functional experiments were the high standard deviations obtained with T98G cells. This observation might be due to the fact that T98G cells aggregated more quickly than A172 cells. Therefore, homogeneous seeding of T98G cells was more difficult. As outlined above, these experiments suggested that the effect of pre-miR transfection can differ between T98G and A172 cells, e.g. concerning increased caspase 3/7 activities after pre-miR-132 transfection. One explanation for this observation might be the different *p53* status of the investigated glioma cell lines (A172: p53 wild type; T98G: p53 defective; (Jane et al 2007). A closer look to the T98G cells revealed that additional biological pathways might be activated by *miR-132* overexpression. The own experiments focused on the potential *p53/miR-132/SIRT1* tumor suppressor network, with the hypothesis that *miR-132* overexpression repressed *SIRT1* mRNA, thereby resulting in the activation of the *p53* pathway and the onset of apoptosis in glioma cells. Luan and colleagues demonstrated that overexpression of *miR-34a* decreased SIRT1 protein levels but not mRNA expression in p53-mutant U251MG glioma cells (Luan et al 2010). With respect to *SIRT1* as a putative target of *miR-132*, the own results revealed reduced *SIRT1* mRNA levels in glioma cell lines after transient transfection of the precursor-miR-132/miR-212 molecules in all investigated cell lines. To determine whether or not the predicted target sites for *miR-132/miR-212* in the 3`UTR of *SIRT1* mRNA are responsible for the mRNA down-regulation, 3'-UTR luciferase reporter assays were carried out. These experiments indicated that both binding sites are important for *miR-132* and *miR-212* binding to the *SIRT1* 3`UTR. On the contrary, Strum and colleagues demonstrated translational repression of *SIRT1* through one binding site in *SIRT1* 3′-UTR after *miR-132* overexpression in the case of human preadipocytes (Strum et al 2009). The own results illustrate the potential role of the *p53/miR-132/SIRT1* tumor suppressor network in glioma. In line with the own data, Audrito and co-workers demonstrated that

nicotinamide blocks proliferation and induces apoptosis of chronic lymphocytic leukemia cells through activation of p53, which in turn induced *miR-34a* and this miRNA repressed *SIRT1* (Audrito et al 2011). With regard to SIRT1 protein expression in glioma, the own Western analyses of glioma cell lines did not reveal high amounts of SIRT1 protein expression in T98G, A172 and U251MG glioma cells (data not shown). Saunders and co-workers reported that miRNAs post-transcriptionally downregulated protein expression during mouse embryonic stem cell differentiation and maintain low SIRT1 protein levels in differentiated adult mouse tissues (Saunders et al 2010). They clearly demonstrated repressed SIRT1 protein expression levels by *miR-181a, miR-181b, miR-9, miR-204, miR-135a, and miR-199b*. Recent work has shown that SIRT1 protein is expressed at lower levels in the DAOY human medulloblastoma cell line (Baxter and Milner 2010). In line with this observation, SIRT1 protein expression was detected in DAOY cells. Furthermore, *miR-132* overexpression decreased *SIRT1* mRNA expression and SIRT1 protein expression in DAOY cells. These results indicated that *miR-132* promoted *SIRT1* mRNA instability and regulated SIRT1 at the posttranscriptional level in DAOY cells.

In agreement with the own results, a recent publication revealed relatively low amounts of SIRT1 protein expression in glioblastoma and oligodendrogliomas tissue samples (Lages et al 2011) demonstrate that *miR-132* and *miR-212* may directly regulate *SIRT1* expression in glioma cells. However, a significant relationship between *miR-132* expression and SIRT1 protein expression could not be demonstrated in primary gliomas, suggesting more complex mechanisms of *SIRT1* regulation in gliomas in situ. Moreover, regulation other target genes may contribute to the functional effects of *miR-132*. Therefore, other putative targets of *miR-132* with putative oncogenic functions were investigated.

MiR-132 promotes JARID1A mRNA expression in glioblastoma cells

An additional *miR-132/miR-212* effector gene was identified initially by computational analyses predicting the presence of putative binding sites for *miR-132/miR-212* in the 3`UTR of the *Jumonji, AT-rich interactive domain 1A (JARID1A)* gene, also called *RBP2* or *KDM5A*. Moreover, microarray-based expression profiling revealed significant overexpression of *JARID1A* in astrocytic tumors in relation to non-neoplastic brain tissue samples. In line with these findings, Zeng and colleagues reported that *JARID1A* is up-regulated in primary gastric cancer (Zeng et al 2010). Therefore, this gene may function as an oncogene in glioma. Further investigation revealed that *JARID1A* is a

newly identified member of JARID family proteins with histone demethylase (HDM) activity (Christensen et al 2007, Klose et al 2007, Secombe et al 2007). JARID1A acts as a transcriptional repressor by inhibiting tri- and dimethylated lysine 4 of histone H3 (H3-K4) methylation at its target promoters (Zeng et al 2010). Furthermore, *JARID1A* was described as a binding partner for the retinoblastoma tumor suppressor protein (*RB1*) (Defeo-Jones et al 1991), and its expression is required to repress the transcription of multiple cyclin-dependent kinase inhibitors (CDKIs), thereby sustaining the proliferation of cancer cells (Zeng et al 2010). Interestingly, *JARID1A* binds to c-Myc, an oncoprotein that is a potent inducer of cell growth, cell cycle progression, and apoptosis (Secombe et al 2007). *C-Myc* and wild-type *p53* have been shown to play important roles in the regulation of cellular proliferation and oncogenic transformation (Reisman et al 1993). High levels of c-Myc induce the expression of endogenous *p53* (Hermeking and Eick 1994, Roy et al 1994) resulting in cell cycle arrest and apoptosis (Lowe et al 1993, Woods and Vousden 2001). Furthermore, Lin and colleagues reported that loss of *JARID1A* impaired proliferation, promoted senescence and enhanced differentiation in mice lacking the retinoblastoma gene (*RB1*) (Lin et al 2011). *RB1* is a tumor suppressor gene that is frequently inactivated in a variety of cancers, including gliomas (2008, Sellers and Kaelin 1997). Thus, overexpression of *miR-132* may cause *JARID1A* downregulation through the predicted *miR-132* target site in the *JARID1A* 3`UTR.

Transfection of T98G, A172 and U251MG glioma cells with miR-132 mimics resulted in significant down-regulation of *JARID1A* expression in all investigated cell lines relative to control-transfected cells. Furthermore, expression of *JARID1A* was down-regulated in T98G and A172 glioma cells after transfection with miR-212 precursors. To determine whether or not the predicted target sites for *miR-132/212* in the 3`UTR of *JARID1A* mRNA are responsible for the mRNA down-regulation, 3'-UTR luciferase reporter assays were carried out. In line with the own observations, Alvarez-Saavedra and colleagues demonstrated that *miR-132* regulated *JARID1A* mRNA, which was found to be associated with chromatin remodeling in the murine suprachiasmatic nucleus (SCN) (Alvarez-Saavedra et al 2011). Further studies are needed to investigate if the inhibition of *miR-132/miR-212* binding site has an impact on the luciferase activity of *JARID1A* 3`UTR vector compared with control transfected glioma cells. To validate the potential regulatory relationship between *miR-212* and *JARID1A*, it has furthermore to be clarified if *miR-212* overexpression has a significantly negative effect on the luciferase activity in the presence of *miR-212* on the *JARID1A* 3`UTR. In

addition, Western blot analyses are necessary to confirm that JARID1A protein expression is decreased in *miR-132* or *miR-212* overexpressing glioma cells. Nevertheless, an inhibition of *JARID1A* by *miR-132* or *miR-212* likely contributes to the pro-apoptotic effects observed in glioma cells that overexpress *miR-132*.

MiR-132 did not directly regulate BTG2 mRNA expression by binding to its 3`UTR in human glioma cells.

Further *in silico* screens revealed a conserved target site of human *miR-132/miR-212* within the 3`UTR of *B-cell translocation gene-2* (*BTG2*). *BTG2* is a member of the BTG/Tob antiproliferative protein family. Microarray analysis revealed that *BTG2* was significantly upregulated in astrocytic tumors in relation to non-neoplastic brain tissue samples. *BTG2* was an interesting candidate because it has been suggested to act as an onco-suppressor in medulloblastoma (Farioli-Vecchioli et al 2007). In contrary to the own results, *BTG2* was reported to play a tumor suppressive role in mice and humans (Lim 2006, Liu et al 2009a). Moreover, *BTG2* was strongly down-regulated in high-grade glioma compared to low-grade glioma derived from murine embryonic neural progenitors (Calzolari et al 2008), in melanoma cells (Yang et al 2011) and in human breast cancer (Takahashi et al 2011). However, *BTG2* seems to function as either an oncogene or a tumor suppressor gene depending on the investigated tissue.

Recent reports have found that the p53-inducible gene *BTG2*, a pan-cell cycle regulator, induces G1-S arrest via pRB-dependent and pRB-independent pathways (Guardavaccaro et al 2000, Liu et al 2009a). *BTG2* has been described as a transcriptional co-regulator, a differentiation and anti-apoptotic factor in neurogenesis as well as a key mediator of the stage-specific expansion of thymocytes and a negative regulator of hematopoietic progenitor expansion. Interestingly, Alvarez-Saavedra and colleagues demonstrated that *BTG2* is direct target of *miR-132* in the murine suprachiasmatic nucleus (SCN).

Transient transfection of T98G, A172 and U251MG glioma cells with *miR-132* mimics revealed significant down-regulation of *BTG2* expression relative to control-transfected cells only in U251 cells. In addition, overexpression of *miR-212* molecules did not affect *BTG2* expression levels. A further approach was to determine whether *miR-132* or *miR-212* target the expression of *BTG2* via the predicte *miR-132/miR-212* binding site within *BTG2* 3`UTR by 3'UTR-luciferase assays. These experiments revealed that neither *miR-132* nor *miR-212* did directly regulate *BTG2* by binding to its 3`UTR in glioma cells. These observations were in line with the lack of decreased *BTG2* mRNA

expression levels after *miR-132* or *miR-212* overexpression in T98G and A172 cells. These findings suggest an indirect effect of *miR-132* overexpression on BTG2 mRNA expression through other involved genes. In contrast to the own observations, the wild-type 3`UTR of *BTG2* was significantly repressed by the *miR-132* mimic in murine neuroblastoma cell line (Alvarez-Saavedra et al 2011). These contrasting results suggest that the regulation of *BTG2* mRNA expression through *miR-132* may vary in different cellular types and further experiments are necessary to clarify whether *miR-132* post-transcriptionally downregulates BTG2 protein expression in glioma cells or not.

5.3 *MiR-126* acts as putative tumor-suppressor gene in gliomas

MiR-126 expression is regulated by histone modification rather than by DNA methylation around the miR-126 5`genomic region

TaqMan-based miRNA expression analysis identified 50 miRNAs, including *miR-126*, which were significantly up-regulated after treatment with the demethylating agent 5-aza-2'-deoxycytidine (5-Aza) as well as the histone deacetylase inhibitor trichostatin A (TSA). Interestingly, *miR-126* was significantly down-regulated in astrocytic tumors in relation to non-neoplastic brain tissue, suggesting a tumor suppressive function in gliomas. Increased expression of *miR-126* was observed in bladder, breast and cervical cancer cell lines after treatment with 5-Aza and the histone deacetylase inhibitor 4-phenylbutyric acid (PBA) (Saito et al 2009). In line with the own findings, *miR-126* expression was reported to be down-regulated in relapsing breast cancer, cervical cancer, myeloid lineage leukemic cell lines, bladder and prostate tumors (Saito et al 2009, Shen et al 2008, Tavazoie et al 2008, Wang et al 2008). Increased expression of *miR-126* has been reported in human brain and endothelial cells (Kuehbacher et al 2007, Landgraf et al 2007). It is also worth noting that there are very limited functional data available concerning the role of *miR-126* in the CNS. Divergent results may be related to the heterogeneity of the tumor samples investigated in the different studies and to the methodological approaches. However, oncogenic and tumor suppressive functions can represent two different features of one and the same miRNA, depending on cell type and molecular context (Fabbri et al 2007). Based on the own proflling results and literature data, *miR-126* was studied in greater detail to investigate the causes and consequences of epigenetic *miR-126* dysregulation in gliomas. In accordance with the array results, simultaneous *in vitro* treatment with

5-Aza and TSA induced expression of *miR-126* to 2-fold or higher in two glioblastoma cell lines compared to the respective non-treated controls. Due to high deviations in the expression of *miR-126* between the three biological replicates, the expression differences in the investigated cell lines did only reach significance in the TP365 cells, which showed a 2-fold-upregulation of *miR-126* following treatment To gain further insights into the epigenetic mechanism contributing to *miR-126* down-regulation in gliomas, five glioblastoma cell lines were either treated with the demethylating agent 5-Aza or the histone deacetylase inhibitor trichostatin A (TSA). *MiR-126* expression levels turned out to be unaffected after treatment with 5-Aza. Thus, it seems unlikely to suggest a relationship between *miR-126* 5'-CpG island methylation and decreased expression in glioma. Interestingly, *in vitro* treatment of the five glioblastoma cell lines with TSA led to increased *miR-126* expression levels at least 1.5-fold or higher in A172, U138MG, T98G and U87MG cells, suggesting a direct effect of histone modifications on the regulation of *miR-126* expression in glioma cells. Stronger up-regulation of *miR-126* following TSA treatment alone, as compared to combined 5-Aza/TSA treatment, could be caused by the different duration of the TSA treatment (24 h vs. 36 h). To further address the putative role of DNA methylation in the regulation of *miR-126* expression, the DNA methylation status in the 5`-genomic region of *miR-126* was determined by sequencing of sodium bisulfite-modified DNA. The primary transcript of *miR-126* corresponds to an alternative transcript of *EGFL7* (S2) with two CpG island promoters (Li et al 2008, Saito et al 2009). Saito and co-workers reported low levels of DNA methylation corresponding to CpG sites 76-91 of *miR-126* CpG island 1 in human urinary bladder carcinoma cells as well as in primary bladder and prostate tumors (Saito et al 2009). Interestingly, methylation analysis of this genomic region revealed hypermethylation in astrocytic gliomas in comparison to non-neoplastic brain tissue sample. These findings are in line with the miRNA array expression data uncovering significantly reduced *miR-126* expression levels in AII, AAIII and sGBIV compared to non-neoplastic brain tissue samples. However, methylation analysis of the *miR-126* 5`genomic region also showed hypermethylation in the investigated pGBIV patient samples, which was not significantly associated with reduced *miR-126* expression in these samples. However, a more detailed consideration indicated methylation of the *miR-126* 5`CpG 1 region rather in a subset of pGBIV and sGBIV than in AII and AAIII tumors, thus suggesting a progression-associated *miR-126* 5`CpG methylation. The fact that hypermethylation occurred more commonly in pGBIV, which are characterized by rare *IDH1/2* mutations, as compared

to sGBIV, which show frequent *IDH1/2* mutation, suggests that this methylation is independent from the *IDH1* mutation-associated glioma CpG Island Methylator Phenotype (G-CIMP). Thus, these findings were in contrast to those obtained for the *miR-132* 5`genomic region. In diffuse astrocytic gliomas. The pronounced molecular and cellular heterogeneity of astrocytic tumors might explain the lack of a significant association between *miR-126* and expression in gliomas, e.g. retained *miR-126* expression in *miR-126* 5`hypermethylated astrocytic tumors might be caused by contaminating non-neoplastic cell populations. Moreover, the own data suggest an additional role of histone modifications in the regulation of *miR-126* expression in human gliomas (see below), which adds another level of complexity and may also contribute to the missing correlation between hypermethylation of 5`genomic regions and expression of the miRNA.

Histone modifications around the 5`genomic region of miR-126

As stated above, an at least 1.5-fold up-regulation of *miR-126* expression was detected in U138MG, T98G and U87MG glioma cells after TSA treatment, suggesting that histone modifications contribute to the down-regulation of *miR-126* in gliomas. Aberrant patterns of histone modifications in the 5`genomic region of *miR-126* were further investigated in U138MG glioma cells by ChIP analyses. TSA treatment led to an increase of histone H3 and histone H4 acetylation in the 5´- genomic regions of *miR-126* around CpG sites 72-95 in these cells compared to non-treated cells. This observation is in line with data by Saito and co-workers who also reported on higher levels of acetylated histone H3 in the same 5`genomic region of *miR-126* in HeLa (cervical cancer) and T24 (bladder cancer) cells after treatment with the histone deacetylase inhibitor 4-phenylbutyric acid (PBA) and 5-Aza (Saito et al 2009). To this end, additional experiments using chromatin immunoprecipitation analyses of a wider range of glioblastoma cell lines and separate subset of glioblastoma tissue samples are necessary to validate the hypothesis that histone acetylation indeed constitutes a major epigenetic mechanism for the transcriptional regulation of *miR-126* in gliomas.

PLAGL2, a putative target of miR-126

Putative *miR-126* target genes were identified initially by *in silico* analyses predicting the presence of putative binding sites for *miR-126* in the 3`UTR of certain genes, including the proto-oncogene *pleomorphic adenoma gene-like 2* (*PLAGL2*). Amplification of the chromosomal region 20q11.21 containing *PLAGL2* identified this gene as a suspect cancer gene in human malignant gliomas and colon cancer (Hanks and Gauss 2011). *PLAGL2* belongs to the small PLAG family of zinc-finger transcription factors (Abdollahi 2007) and its expression may contribute to the progression of a subset of human malignant gliomas by regulating cell proliferation and differentiation (Zeng et al 2010, Zheng et al 2010). Both, oncogenic and tumor suppressor activities have been reported for *PLAGL2* (Hanks and Gauss 2011). Nevertheless, functional data on the regulation of its expression by certain miRNAs in cancer are still sparse.

Microarray-based expression profiling data revealed an inverse association between *PLAGL2* mRNA expression and *miR-126* expression in astrocytic gliomas. A closer look revealed that *PLAGL2* mRNA expression was upregulated in tumors of patients with AAIII, sGBIV and pGBIV in relation to non-neoplastic brain tissue samples. Overexpression of mouse *PLAGL2* in fibroblasts and neuroblastoma cells caused an increase in the pro-apoptotic factor, bNip3, followed by apoptosis (Furukawa et al 2001, Mizutani et al 2002). Furthermore, *PLAGL2* was demonstrated to inhibit neural stem cell differentiation and promoted self-renewal through Wnt/ß-catenin signaling (Zheng et al 2010). Hanks and colleagues revealed a role for *PLAGL2* in cell cycle regulation and apoptosis via activation of the p53 homologue p73 and its respective target genes in histocytic lymphomas (Hanks and Gauss 2011).

In the own studies, the effect of *miR-126* overexpression on caspase 3/7 activity, cell proliferation and cell viability of glioma cells was investigated. Cell-based functional assays revealed effects of *miR-126* overexpression on caspase 3/7 activity and a significant negative impact on cell proliferation, while cell viability appeared uneffected in human A172 glioblastoma cells containing wild-type *p53* gene. Based on these findings, overexpression of *miR-126* may inhibit *PLAGL2,* which in turn may lead to apoptosis by activation of the p53 pathway. To confirm this hypothesis, the mRNA expression of *PLAGL2* was determined in glioma cells following transfection with pre-miR-126 molecules. However, these experiments revealed that *miR-126* overexpression apparently does not affect *PLAGL2* mRNA level in human glioma cells. In further studies, it will be necessary to clarifiy whether *miR-126* directly targets

PLAGL2 and thereby could potentially downregulate PLAGL2 protein expression through translational inhibition rather than enhanced mRNA degradation. Moreover, further investigation of *miR-126* overexpression in gliomas is required to address the question of its biological relevance for the regulation of apoptosis.

5.4 *MiR-210* is up-regulated in astrocytic tumors and directly targets *GPD1L* and *COX10* in glioma cells

One of the prominent features of rapidly growing malignant tumors are regions of low oxygen concentration (hypoxia) frequently found around necrotic areas (Seidel et al 2010, Silber et al 2009). Unfortunately, hypoxic/necrotic tumors are more resistant to chemotherapy and radiation therapy, and are associated with a poorer prognosis (Bertout et al 2008, Laurenti et al 2011). The importance of hypoxia-regulated miRNAs for cell survival in a hypoxic microenvironment has been demonstrated in previous studies (Camps et al 2008, Rane et al 2009, Taguchi et al 2008). In order to determine the possible roles of miRNAs in hypoxic gene regulation and to identify miRNAs induced by hypoxia in gliomas, changes in miRNA expression levels were profiled in response to hypoxia in several glioblastoma stem cell lines using a TaqMan array-based approach. *MiR-210* was identified in a group of eight miRNAs that exhibited an increased expression under hypoxia in glioblastoma stem cells. Moreover, *miR-210* showed an increased expression in the primary glioblastoma group of astrocytic tumors compared to non-neoplastic brain tissue samples. These findings are in line with other studies pointing out that *miR-210* is up-regulated in brain tumor tissue samples (Lages et al 2011, Malzkorn et al 2010). In addition, *miR-210* expression is frequently elevated in melanoma (Zhang et al 2009b), lung cancer (Donnem et al 2012, Puissegur et al 2011), pancreatic cancer (Ho et al 2010) and clear cell renal cell carcinoma (Nakada et al 2011). Overexpression of *miR-210* protected breast cancer cells from hypoxia-induced apoptosis (Kulshreshtha et al 2007). *MiR-210* has also been reoorted to have a role in cell cycle regulation (Giannakakis et al 2008) and DNA damage and repair (Crosby et al 2009).

The own array results were validated by performing RT-PCR on RNA from several glioblastoma cell lines grown grown under hypoxia versus normoxia. These experiments showed that *miR-210* was the predominant miRNA gene up-regulated in primary glioblastoma stem cells grown under hypoxia, suggesting an important tumor-

promoting function of *miR-210* in gliomas. Previous studies reported that the hypoxic tumor microenvironment controls tumor stem cells through the transcription factor hypoxia-inducible factor-1 alpha (HIF-1α) (Seidel et al 2010, Silber et al 2009, Zhong et al 1999). HIFs are well-documented regulators of the hypoxia response. They are stabilized during hypoxia and coordinate the transcription of a variety of genes that are important for survival under conditions of low oxygen (Giatromanolaki and Harris 2001). A fascinating recent discovery was that HIF-1α-mediated regulation of miRNA transcription seems to be important for tumorigenesis. *MiR-210* overexpression is induced by hypoxia in HIF-1α-dependent manner in breast cancer cell lines, hepatocellular carcinoma samples (HCC), and in clear cell renal cell carcinoma (Camps et al 2008, Valera et al 2011, Ying et al 2011). In line with these data, expression analysis of *miR-210* in either HIF-1α/HIF-2α overexpressing - or in HIF-1α/HIF-2α knockdown glioblastoma cells, revealed that HIF-1α rather than HIF-2α robustly increased *miR-210* expression levels compared to control transfected cells. In addition, knockdown of HIF-1α suppressed the increase of *miR-210* expression levels following hypoxia in the investigated cell lines.

Collectively, these results demonstrate that hypoxia induced expression of *miR-210* in glioblastoma cell lines via HIF-1α. The data presented in this study are complementary to those of Kulshreshtha and co-workers, who reported that HIF-1α induces *miR-210* expression in HT-29 cells (human colon adenocarcinoma grade II cell line) (Kulshreshtha et al 2007).

Recent studies elucidated the presence of cell populations with stem cell-like properties, including self-renewal and multilineage differentiation potential, in a variety of human tumors (Lobo et al 2007). Cancer stem cells are able to initiate tumor growth, whereas other, non-stem cell tumor cells fail to form new tumors when injected into nude mice (Schraivogel et al 2011). Previous studies demonstrated that cancer stem cells can be enriched in cell fractions expressing specific surface proteins, such as the adhesion molecule CD44 in breast cancer or CD133 in colorectal cancer and primary glioblastoma (Gilbertson and Rich 2007, Lobo et al 2007, Tabatabai and Weller 2011, Visvader and Lindeman 2008). Interestingly, several miRNA expression profiling studies revealed evidence of a relationship between miRNA expression and the tumor stem cell phenotype (Liu et al 2011, Schraivogel et al 2011, Yu et al 2007). Until now, a detailed characterization of miRNA expression in glioblastoma stem cells has not been demonstrated. The own experiments revealed robust up-regulation of *miR-210* in CD133 positive (CD133 +) G55 glioma cells in comparison to CD133 negative cells

(CD133 -). Further research is needed to determine if inhibition of *miR-210* may functionally influence the CD133 positive tumor cell population or whether up-regulation of both, *miR-210* and CD133 is a consequence of hypoxia-induced activation of HIFs.
A recent paper by Lages and co-workers reported that higher expression of *miR-210* in glioblastoma than in oligodendrogliomas may not only be due to hypoxia but also to a higher DNA methylation rate of the *miR-210* locus in oligodendrogliomas (Lages et al 2011). In accordance with Lages and co-workers, the own experiments revealed low or absent DNA methylation of the *miR-210*-associated CpG sites in glioblastoma cell lines and non-neoplastic brain tissue samples. Thus, at least in glioblastomas *miR-210* expression is not regulated by DNA methylation.
In order to identify which *miR-210* targets are directly regulated by this miRNA and may elicit a stabilizing effect on HIF-1α, target prediction databases were consulted, which revealed *glycerol-3-phosphate dehydrogenase 1-like (GPD1L)*, and *iron-sulfur cluster scaffold homolog (COX10)* as promising putative *miR-210* target genes. *GPD1L* was selected for further studies because of the established link between glycolytic enzymes and hypoxia. Overexpression of *miR-210* resulted in increased HIF-1α accumulation during hypoxia through decreased expression of GPD1L protein in HEK 293A cells (human embryonic kidney cells) (Kelly et al 2011). Moreover, Fasanaro and colleagues confirmed that *miR-210* directly regulated the expression of *GPD1L* in MCF7 cells (human breast adenocarcinoma cell line) (Fasanaro et al 2009). *COX10* encodes a protoheme: heme O farnesyl transferase that is involved in the biosynthesis of heme-α, an essential component of cytochrome c oxidase, complex IV (COX). The loss of function of *COX10* may result in suppression of mitochondrial function at the level of complex I and IV (Diaz et al 2006). Chen and colleagues reported that *COX10* was under direct regulation of *miR-210* in HCT-116 (colon adenocarcinoma cell line), indicating that *miR-210* may have a role in regulation of the mitochondria electron transport chain and tricarboxylic acid cycle (Chen et al 2010b). Microarray analysis revealed significantly lower expression levels of *GPD1L* in the astrocytic tumors in relation to non-neoplastic brain tissue, whereas the mRNA level of *COX10* was slightly but not significant down-regulated. Using Luciferase reporter gene assays both putative *miR-210* target genes could be validated.
Taken together, these data indicate that *GPD1L* and *COX10* are bona fide targets of *miR-210*. Further experiments are required to validate that *miR-210* regulates GPD1L and COX10 protein levels through direct interaction with the mRNA 3`UTR in glioma cells and to analyze the causative role of *COX10* in *miR-210* modulated mitochondrial

functions. In addition, the functional connection between HIF-1α inducible *miR-210* and the glycolytic enzyme *GPD1L* needs to be explored in greater detail. Interestingly, Ostro and co-workers reported that glycerol phosphate dehydrogenase activity has an inverse correlation with tumor growth rate (Ostro and Fondy 1977). In this context, it is possible that inducing the expression of *GPD1L* and *COX10*, possibly through inhibition of *miR-210* in gliomas, may be advantageous for glioma treatment.

In addition to *miR-210*, the TaqMan-based microRNA profiling revealed significantly increased expression of *miR-213* and *miR-25* in response to hypoxia in several glioblastoma stem cell lines. The miRNA *miR-25* also showed increased expression at least in the primary glioblastoma group as compared to non-neoplastic brain tissue samples. These array-based screening results were validated in independent experiments by using RT-PCR. The own findings are in line with previous studies reporting that *miR-25* was up-regulated in brain tumor tissue samples (Malzkorn et al 2010), pediatric brain tumors (Birks et al 2011), as well as ovarian cancer samples and cell lines (Zhang et al 2012a), prostate carcinoma (Poliseno et al 2010) and gastric adenocarcinoma (Petrocca et al 2008). Up-regulation of *miR-213* was observed in squamous cell carcinoma (SCC) of the tongue (Wong et al 2008). Additional studies investigating CD133-positive subpopulations of glioma cells revealed only slight differences in *miR-213* and *miR-25* expression levels in CD133 + versus CD133 - cells. Moreover, both miRNA did not appear to be consistently regulated by HIF-1α or HIF-2α in glioma cells. In contrast, Kulshreshtha and colleagues reported that HIF-1α increased *miR-213* expression levels in HT-29 cells (human colon adenocarcinoma grade II cell line) and that HIF-2α increased the expression of *miR-213* in MCF-7 cells (human breast adenocarcinoma cell line) (Kulshreshtha et al 2007). Further experiments are necessary to clarify the precise roles of *miR-213* and *miR-25* in glioma stem cells and the response of glioma cells to hypoxia.

6 Abstract

MicroRNAs (miRNAs) are small, non-coding RNAs that are effective post-transcriptional regulators of gene expression. Binding of miRNAs to the 3`-untranslated region (3`-UTR) of messenger RNAs (mRNAs) results in translational inhibition or enhanced mRNA cleavage. MiRNAs play an important role in the regulation of fundamental cellular mechanisms, such as cell proliferation, differentiation, apoptosis, cell migration and metabolism. They are also involved in the pathogenesis of human diseases including cancer. In this study, the expression of 365 distinct human miRNAs was determined by stem-loop real-time reverse transcriptase PCR in four established glioblastoma cell lines (A172, U138MG, T98G, TP365MG) treated with the demethylating agent 5-aza-2`-deoxycytidine (5-Aza) and the histone deacetylase inhibitor trichostatin A (TSA), and compared to the miRNA expression profiles in the respective untreated control cell lines. Thereby, 50 miRNAs were identified that demonstrated an increased expression (fold change ≥ 2) in at least two of the four 5-Aza/TSA-treated glioma cell lines compared to the non-treated control cells. Two of these miRNAs, *miR-132* and *miR-126*, were significantly down-regulated in astrocytic tumors relative to non-neoplastic brain tumors and were therefore selected for independent validation and further molecular characterization using sequencing of sodium bisulfite-modified DNA and chromatin immunoprecipitation analysis of the 5´-genomic regions of each miRNA. These studies revealed that modified acetylation of the core histones H3 and H4 might cause reduced expression of *miR-132* and *miR-126* in gliomas either alone or in conjunction with 5`CpG island hypermethylation of the miRNAs. Overexpression of *miR-132* and *miR-126* precursors in glioma cells increased apoptotic activity. Gene expression profiling was carried out to identify *miR-132* and *miR-126* regulated targets. Using Western-blot analysis and 3'-UTR luciferase assays, *SIRT1* and *JARID1A* were identified as direct targets of *miR-132*.

The second part of this doctoral thesis addressed the identification of miRNAs induced by hypoxia that may have relevance in glioma pathogenesis. A total of eight miRNAs were found to be significantly up-regulated by hypoxia in a study of four glioblastoma stem cell lines grown under hypoxic versus normoxic conditions. Independent validation experiments revealed that hypoxia induced expression of *miR-210* in glioblastoma cell lines via HIF-1α. *MiR-210* down-regulated the expression of *GPD1L* and *COX10* by directly binding to their 3`UTRs.

Taken together, the results summarized in this thesis provide new insights into the involvement of miRNAs in the pathogenesis of human gliomas. The epigenetic alterations leading to transcriptional downregulation of *miR-132* and *miR-126* in gliomas were clarified and *SIRT1* was validated as a direct target of these miRNAs Moreover, hypoxia-mediated regulation of *miR-210* via HIF-1α was characterized in glioma cells, and *GPD1L* and *COX10* were identified as immediate targets of *miR-210*.

7 Zusammenfassung

MicroRNAs (miRNAs) sind kleine, nicht-kodierende RNAs, welche die Genexpression auf post-transkriptionaler Ebene regulieren. Die Genregulation erfolgt dabei durch die Bindung der miRNA an die 3'-untranslatierte Region (3'-UTR) der mRNA von Zielgenen, welche je nach Komplementarität der Bindesequenz und der beteiligten Proteine entweder an der Translation gehemmt oder vorzeitig abgebaut werden. Aktuelle Studien belegen die kritische Rolle von miRNAs für die Regulierung fundamentaler zellulärer Mechanismen wie Entwicklung, Zellwachstum, Proliferation, Differenzierung von Zell - oder Gewebetypen, Migration von Zellpopulationen und Stoffwechselprozessen. Dysfunktionen von miRNAs können verschiedene Krankheiten zur Folge haben, darunter Tumoren unterschiedlichen Ursprungs einschließlich der glialen Hirntumoren. Hinsichtlich der Tumorigenese können miRNAs entweder eine tumorhemmende (tumorsuppressive) oder tumorfördernde (onkogene) Wirkung zeigen. In der vorliegenden Arbeit wurde die Expression von 365 miRNAs mittels quantitativer PCR-Analysen in vier Glioblastomzelllinien (A172, U138MG, T98G, TP365MG) nach Behandlung der Zellen mit dem DNA-demethylierenden Agens 5-Aza-2'- Deoxycytidin (5-Aza) und dem Histondeacetylase-Inhibitor Trichostatin A (TSA) im Vergleich zu unbehandelten Zellen untersucht. Insgesamt wiesen 50 der untersuchten miRNAs ein signifikant erhöhtes Expressionsniveau in mindestens zwei von vier behandelten Zelllinien im Vergleich zu den zugehörigen nicht behandelten Zelllinien auf. Zwei dieser miRNAs, *miR-132* und *miR-126*, zeigten ein signifikant reduziertes Expressionsniveau in astrozytären Tumoren im Vergleich zu nicht-neoplastischem Hirngewebe. Deshalb wurden diese beiden miRNAs für weitere Analysen ausgewählt und zunächst die verstärkte Expression von *miR-132* und *miR-126* in unabhängigen Validierungsgruppen 5-Aza/TSA-behandelter Glioblastomzellen bestätigt. Zur Identifizierung epigenetischer Veränderungen, die zu einer verminderten Expression dieser miRNAs in astrozytären Tumoren führen könnten, wurden die 5`genomischen Regionen der beiden miRNAs auf eine aberrante DNA-Methylierung sowie Veränderungen der Histonacetylierung hin untersucht. Mittels Chromatin-Immunopräzipitation (ChIP) und Natriumbisulfit-Sequenzierung konnte nachgewiesen werden, dass sowohl eine veränderte Acetylierung der Histone H3 und H4 sowie eine aberrante DNA Methylierung in der 5`genomischen Region beider untersuchten microRNAs zu einer transkriptionellen Herunterregulation von *miR-132* und *miR-126* in Glioblastomzellen führte. Funktionelle Analysen der beiden miRNAs *in vitro* erbrachten einen miRNA-spezifischen Einfluss auf die Apoptoserate von transient mit entsprechenden Vorläufer-miRNAs transfizierten A172 und T98G Gliomzelllen. Für *miR-132* wurden *JARID1A* und *SIRT1* als direkt durch *miR-132* regulierte Zielgene identifiziert und mittels 3´UTR Luciferase-Reportergen-Assays validiert.

Darüber hinaus wurden Hypoxie-bedingte Veränderungen im Expressionsniveau von 365 miRNAs in vier verschiedenen Glioblastom-Stammzelllinien untersucht. Eine signifikant verstärkte Expression unter Hypoxie wurde für acht miRNAs nachgewiesen.

Unabhängige Validierungsexperimente bestätigten einen Hypoxie-induzierten Expressionsanstieg von *miR-210*, welcher durch HIF-1α vermittelt wurde. *GPD1L* und *COX10* wurden als unmittelbare Zielgene von *miR-210* in Gliomzellen identifiziert und mit Hilfe von 3`UTR Luciferase-Reportergen-Assays bestätigt.

Zusammenfassend unterstützen die eigenen Ergebnisse eine wichtige Rolle von miRNAs in der Pathogenese von Gliomen. Es wurde gezeigt, dass eine aberrante DNA-Methylierung und Histonmodifikationen zu einer verminderten Expression von *miR-132* und *miR-126* in Gliomen führen. Zusätzlich konnten mit *SIRT1* und *JARID1A* zwei interessante Zielgene von *miR-132* in Gliomen charakterisiert werden. Des Weiteren wurde eine über HIF-1a vermittelte Hochregulation von *miR-210* in Gliomen gefunden, die wiederum zu einer verminderten Expression der *miR-210* Zielgene *GPD1L* und *COX10* führt. Die immer offensichtlicher werdende Rolle von miRNAs in der Entstehung und Progression von Gliomen rechtfertigt weiterführende Untersuchungen, um ein besseres molekulares Verständnis, eine genauere Diagnostik und neue Therapieansätze für diese bislang unheilbaren Tumoren zu finden.

8 References

(2008). Comprehensive genomic characterization defines human glioblastoma genes and core pathways. *Nature* **455:** 1061-1068.

Abdollahi A (2007). LOT1 (ZAC1/PLAGL1) and its family members: mechanisms and functions. *Journal of cellular physiology* **210:** 16-25.

Abounader R (2009). Interactions between PTEN and receptor tyrosine kinase pathways and their implications for glioma therapy. *Expert Rev Anticancer Ther* **9:** 235-245.

Agirre X, Vilas-Zornoza A, Jimenez-Velasco A, Martin-Subero JI, Cordeu L, Garate L *et al* (2009). Epigenetic silencing of the tumor suppressor microRNA Hsa-miR-124a regulates CDK6 expression and confers a poor prognosis in acute lymphoblastic leukemia. *Cancer Res* **69:** 4443-4453.

Altuvia Y, Landgraf P, Lithwick G, Elefant N, Pfeffer S, Aravin A *et al* (2005). Clustering and conservation patterns of human microRNAs. *Nucleic Acids Res* **33:** 2697-2706.

Alvarez-Saavedra M, Antoun G, Yanagiya A, Oliva-Hernandez R, Cornejo-Palma D, Perez-Iratxeta C *et al* (2011). miRNA-132 orchestrates chromatin remodeling and translational control of the circadian clock. *Hum Mol Genet* **20:** 731-751.

Audrito V, Vaisitti T, Rossi D, Gottardi D, D'Arena G, Laurenti L *et al* (2011). Nicotinamide blocks proliferation and induces apoptosis of chronic lymphocytic leukemia cells through activation of the p53/miR-34a/SIRT1 tumor suppressor network. *Cancer Res* **71:** 4473-4483.

Baeza N, Weller M, Yonekawa Y, Kleihues P, Ohgaki H (2003). PTEN methylation and expression in glioblastomas. *Acta Neuropathol* **106:** 479-485.

Balss J, Meyer J, Mueller W, Korshunov A, Hartmann C, von Deimling A (2008). Analysis of the IDH1 codon 132 mutation in brain tumors. *Acta Neuropathol* **116:** 597-602.

Bandres E, Agirre X, Bitarte N, Ramirez N, Zarate R, Roman-Gomez J *et al* (2009). Epigenetic regulation of microRNA expression in colorectal cancer. *Int J Cancer* **125:** 2737-2743.

Bartel DP (2004). MicroRNAs: genomics, biogenesis, mechanism, and function. *Cell* **116:** 281-297.

Bartel DP (2009). MicroRNAs: target recognition and regulatory functions. *Cell* **136:** 215-233.

Baskerville S, Bartel DP (2005). Microarray profiling of microRNAs reveals frequent coexpression with neighboring miRNAs and host genes. *RNA* **11:** 241-247.

Baxter EW, Milner J (2010). p53 Regulates LIF expression in human medulloblastoma cells. *J Neurooncol* **97:** 373-382.

Behm-Ansmant I, Rehwinkel J, Doerks T, Stark A, Bork P, Izaurralde E (2006). mRNA degradation by miRNAs and GW182 requires both CCR4:NOT deadenylase and DCP1:DCP2 decapping complexes. *Genes Dev* **20:** 1885-1898.

Bello MJ, Rey JA (2006). The p53/Mdm2/p14ARF cell cycle control pathway genes may be inactivated by genetic and epigenetic mechanisms in gliomas. *Cancer Genet Cytogenet* **164:** 172-173.

Bertout JA, Patel SA, Simon MC (2008). The impact of O2 availability on human cancer. *Nat Rev Cancer* **8:** 967-975.

Birks DK, Barton VN, Donson AM, Handler MH, Vibhakar R, Foreman NK (2011). Survey of MicroRNA expression in pediatric brain tumors. *Pediatric blood & cancer* **56:** 211-216.

Bohnsack MT, Czaplinski K, Gorlich D (2004). Exportin 5 is a RanGTP-dependent dsRNA-binding protein that mediates nuclear export of pre-miRNAs. *RNA* **10:** 185-191.

Bradford MM (1976). A rapid and sensitive method for the quantitation of microgram quantities of protein utilizing the principle of protein-dye binding. *Analytical biochemistry* **72:** 248-254.

Breving K, Esquela-Kerscher A (2010). The complexities of microRNA regulation: mirandering around the rules. *Int J Biochem Cell Biol* **42:** 1316-1329.

Brueckner B, Stresemann C, Kuner R, Mund C, Musch T, Meister M *et al* (2007). The human let-7a-3 locus contains an epigenetically regulated microRNA gene with oncogenic function. *Cancer Res* **67:** 1419-1423.

Burnette WN (1981). "Western blotting": electrophoretic transfer of proteins from sodium dodecyl sulfate--polyacrylamide gels to unmodified nitrocellulose and radiographic detection with antibody and radioiodinated protein A. *Anal Biochem* **112:** 195-203.

Cai X, Hagedorn CH, Cullen BR (2004). Human microRNAs are processed from capped, polyadenylated transcripts that can also function as mRNAs. *RNA* **10:** 1957-1966.

Cai Y, Yu X, Hu S, Yu J (2009). A brief review on the mechanisms of miRNA regulation. *Genomics Proteomics Bioinformatics* **7:** 147-154.

Calin G (1994). Oncogenes and tumor-suppressor genes - 2 different looks of the same gene. *Oncology reports* **1:** 987-991.

Calin GA, Dumitru CD, Shimizu M, Bichi R, Zupo S, Noch E *et al* (2002). Frequent deletions and down-regulation of micro- RNA genes miR15 and miR16 at 13q14 in chronic lymphocytic leukemia. *Proc Natl Acad Sci U S A* **99:** 15524-15529.

Calin GA, Sevignani C, Dumitru CD, Hyslop T, Noch E, Yendamuri S *et al* (2004). Human microRNA genes are frequently located at fragile sites and genomic regions involved in cancers. *Proc Natl Acad Sci U S A* **101:** 2999-3004.

Calin GA, Ferracin M, Cimmino A, Di Leva G, Shimizu M, Wojcik SE *et al* (2005). A MicroRNA signature associated with prognosis and progression in chronic lymphocytic leukemia. *The New England journal of medicine* **353:** 1793-1801.

Calin GA, Croce CM (2006a). MicroRNA-cancer connection: the beginning of a new tale. *Cancer Res* **66:** 7390-7394.

Calin GA, Croce CM (2006b). MicroRNA signatures in human cancers. *Nat Rev Cancer* **6:** 857-866.

Calzolari F, Appolloni I, Tutucci E, Caviglia S, Terrile M, Corte G *et al* (2008). Tumor progression and oncogene addiction in a PDGF-B-induced model of gliomagenesis. *Neoplasia* **10:** 1373-1382, following 1382.

Camps C, Buffa FM, Colella S, Moore J, Sotiriou C, Sheldon H *et al* (2008). hsa-miR-210 Is induced by hypoxia and is an independent prognostic factor in breast cancer. *Clin Cancer Res* **14:** 1340-1348.

Cao X, Yeo G, Muotri AR, Kuwabara T, Gage FH (2006). Noncoding RNAs in the mammalian central nervous system. *Annu Rev Neurosci* **29:** 77-103.

Chan JA, Krichevsky AM, Kosik KS (2005). MicroRNA-21 is an antiapoptotic factor in human glioblastoma cells. *Cancer Res* **65:** 6029-6033.

Chen G, Zhu W, Shi D, Lv L, Zhang C, Liu P *et al* (2010a). MicroRNA-181a sensitizes human malignant glioma U87MG cells to radiation by targeting Bcl-2. *Oncology reports* **23:** 997-1003.

Chen Y, Meltzer PS (2005). Gene expression analysis via multidimensional scaling. *Curr Protoc Bioinformatics* **Chapter 7:** Unit 7 11.

Chen Y, Liu W, Chao T, Zhang Y, Yan X, Gong Y *et al* (2008). MicroRNA-21 down-regulates the expression of tumor suppressor PDCD4 in human glioblastoma cell T98G. *Cancer letters* **272:** 197-205.

Chen Z, Li Y, Zhang H, Huang P, Luthra R (2010b). Hypoxia-regulated microRNA-210 modulates mitochondrial function and decreases ISCU and COX10 expression. *Oncogene* **29:** 4362-4368.

Christensen J, Agger K, Cloos PA, Pasini D, Rose S, Sennels L *et al* (2007). RBP2 belongs to a family of demethylases, specific for tri-and dimethylated lysine 4 on histone 3. *Cell* **128:** 1063-1076.

Christenson LK, Stouffer RL, Strauss JF, 3rd (2001). Quantitative analysis of the hormone-induced hyperacetylation of histone H3 associated with the steroidogenic acute regulatory protein gene promoter. *J Biol Chem* **276:** 27392-27399.

Ciafre SA, Galardi S, Mangiola A, Ferracin M, Liu CG, Sabatino G *et al* (2005). Extensive modulation of a set of microRNAs in primary glioblastoma. *Biochem Biophys Res Commun* **334:** 1351-1358.

Cimmino A, Calin GA, Fabbri M, Iorio MV, Ferracin M, Shimizu M *et al* (2005). miR-15 and miR-16 induce apoptosis by targeting BCL2. *Proc Natl Acad Sci U S A* **102:** 13944-13949.

Conrad ME, Barton JC (1978). Factors affecting the absorption and excretion of lead in the rat. *Gastroenterology* **74:** 731-740.

Conti A, Aguennouz M, La Torre D, Tomasello C, Cardali S, Angileri FF *et al* (2009). miR-21 and 221 upregulation and miR-181b downregulation in human grade II-IV astrocytic tumors. *J Neurooncol* **93:** 325-332.

Corney DC, Hwang CI, Matoso A, Vogt M, Flesken-Nikitin A, Godwin AK *et al* (2010). Frequent downregulation of miR-34 family in human ovarian cancers. *Clin Cancer Res* **16:** 1119-1128.

Corsten MF, Miranda R, Kasmieh R, Krichevsky AM, Weissleder R, Shah K (2007). MicroRNA-21 knockdown disrupts glioma growth in vivo and displays synergistic cytotoxicity with neural precursor cell delivered S-TRAIL in human gliomas. *Cancer Res* **67:** 8994-9000.

Crocetti E, Trama A, Stiller C, Caldarella A, Soffietti R, Jaal J *et al* (2012). Epidemiology of glial and non-glial brain tumours in Europe. *Eur J Cancer*.

Crosby ME, Kulshreshtha R, Ivan M, Glazer PM (2009). MicroRNA regulation of DNA repair gene expression in hypoxic stress. *Cancer Res* **69:** 1221-1229.

Datta J, Kutay H, Nasser MW, Nuovo GJ, Wang B, Majumder S *et al* (2008). Methylation mediated silencing of MicroRNA-1 gene and its role in hepatocellular carcinogenesis. *Cancer Res* **68:** 5049-5058.

Defeo-Jones D, Huang PS, Jones RE, Haskell KM, Vuocolo GA, Hanobik MG *et al* (1991). Cloning of cDNAs for cellular proteins that bind to the retinoblastoma gene product. *Nature* **352:** 251-254.

Deng S, Calin GA, Croce CM, Coukos G, Zhang L (2008). Mechanisms of microRNA deregulation in human cancer. *Cell Cycle* **7:** 2643-2646.

Denli AM, Tops BB, Plasterk RH, Ketting RF, Hannon GJ (2004). Processing of primary microRNAs by the Microprocessor complex. *Nature* **432:** 231-235.

Diaz F, Fukui H, Garcia S, Moraes CT (2006). Cytochrome c oxidase is required for the assembly/stability of respiratory complex I in mouse fibroblasts. *Mol Cell Biol* **26:** 4872-4881.

Dong JT, Boyd JC, Frierson HF, Jr. (2001). Loss of heterozygosity at 13q14 and 13q21 in high grade, high stage prostate cancer. *The Prostate* **49:** 166-171.

Donnem T, Fenton CG, Lonvik K, Berg T, Eklo K, Andersen S *et al* (2012). MicroRNA signatures in tumor tissue related to angiogenesis in non-small cell lung cancer. *PLoS One* **7:** e29671.

Dynan WS, Tjian R (1983). The promoter-specific transcription factor Sp1 binds to upstream sequences in the SV40 early promoter. *Cell* **35:** 79-87.

Egger G, Liang G, Aparicio A, Jones PA (2004). Epigenetics in human disease and prospects for epigenetic therapy. *Nature* **429:** 457-463.

Esquela-Kerscher A, Slack FJ (2006). Oncomirs - microRNAs with a role in cancer. *Nat Rev Cancer* **6:** 259-269.

Eulalio A, Behm-Ansmant I, Izaurralde E (2007). P bodies: at the crossroads of post-transcriptional pathways. *Nature reviews Molecular cell biology* **8:** 9-22.

Fabbri M, Ivan M, Cimmino A, Negrini M, Calin GA (2007). Regulatory mechanisms of microRNAs involvement in cancer. *Expert opinion on biological therapy* **7:** 1009-1019.

Farioli-Vecchioli S, Tanori M, Micheli L, Mancuso M, Leonardi L, Saran A *et al* (2007). Inhibition of medulloblastoma tumorigenesis by the antiproliferative and pro-differentiative gene PC3. *FASEB journal : official publication of the Federation of American Societies for Experimental Biology* **21:** 2215-2225.

Fasanaro P, Greco S, Lorenzi M, Pescatori M, Brioschi M, Kulshreshtha R *et al* (2009). An integrated approach for experimental target identification of hypoxia-induced miR-210. *J Biol Chem* **284:** 35134-35143.

Fazi F, Racanicchi S, Zardo G, Starnes LM, Mancini M, Travaglini L *et al* (2007). Epigenetic silencing of the myelopoiesis regulator microRNA-223 by the AML1/ETO oncoprotein. *Cancer Cell* **12:** 457-466.

Feinberg AP, Tycko B (2004). The history of cancer epigenetics. *Nat Rev Cancer* **4:** 143-153.

Felsberg J, Rapp M, Loeser S, Fimmers R, Stummer W, Goeppert M *et al* (2009). Prognostic significance of molecular markers and extent of resection in primary glioblastoma patients. *Clin Cancer Res* **15:** 6683-6693.

Ferlay J, Shin HR, Bray F, Forman D, Mathers C, Parkin DM (2010). Estimates of worldwide burden of cancer in 2008: GLOBOCAN 2008. *Int J Cancer* **127:** 2893-2917.

Filipowicz W (2005). RNAi: the nuts and bolts of the RISC machine. *Cell* **122:** 17-20.

Filipowicz W, Bhattacharyya SN, Sonenberg N (2008). Mechanisms of post-transcriptional regulation by microRNAs: are the answers in sight? *Nat Rev Genet* **9:** 102-114.

Formosa A, Lena AM, Markert EK, Cortelli S, Miano R, Mauriello A *et al* (2012). DNA methylation silences miR-132 in prostate cancer. *Oncogene*.

Fraga MF, Ballestar E, Villar-Garea A, Boix-Chornet M, Espada J, Schotta G *et al* (2005). Loss of acetylation at Lys16 and trimethylation at Lys20 of histone H4 is a common hallmark of human cancer. *Nat Genet* **37:** 391-400.

Fueyo J, Gomez-Manzano C, Yung WK, Kyritsis AP (1998). The functional role of tumor suppressor genes in gliomas: clues for future therapeutic strategies. *Neurology* **51:** 1250-1255.

Furukawa T, Adachi Y, Fujisawa J, Kambe T, Yamaguchi-Iwai Y, Sasaki R *et al* (2001). Involvement of PLAGL2 in activation of iron deficient- and hypoxia-induced gene expression in mouse cell lines. *Oncogene* **20:** 4718-4727.

Fusco S, Ripoli C, Podda MV, Ranieri SC, Leone L, Toietta G *et al* (2012). A role for neuronal cAMP responsive-element binding (CREB)-1 in brain responses to calorie restriction. *Proc Natl Acad Sci U S A* **109:** 621-626.

Gabriely G, Wurdinger T, Kesari S, Esau CC, Burchard J, Linsley PS *et al* (2008). MicroRNA 21 promotes glioma invasion by targeting matrix metalloproteinase regulators. *Mol Cell Biol* **28:** 5369-5380.

Giannakakis A, Sandaltzopoulos R, Greshock J, Liang S, Huang J, Hasegawa K *et al* (2008). miR-210 links hypoxia with cell cycle regulation and is deleted in human epithelial ovarian cancer. *Cancer biology & therapy* **7:** 255-264.

Giatromanolaki A, Harris AL (2001). Tumour hypoxia, hypoxia signaling pathways and hypoxia inducible factor expression in human cancer. *Anticancer research* **21:** 4317-4324.

Gilbertson RJ, Rich JN (2007). Making a tumour's bed: glioblastoma stem cells and the vascular niche. *Nat Rev Cancer* **7:** 733-736.

Gillies JK, Lorimer IA (2007). Regulation of p27Kip1 by miRNA 221/222 in glioblastoma. *Cell Cycle* **6:** 2005-2009.

Grady WM, Parkin RK, Mitchell PS, Lee JH, Kim YH, Tsuchiya KD *et al* (2008). Epigenetic silencing of the intronic microRNA hsa-miR-342 and its host gene EVL in colorectal cancer. *Oncogene* **27:** 3880-3888.

Gregory RI, Yan KP, Amuthan G, Chendrimada T, Doratotaj B, Cooch N *et al* (2004). The Microprocessor complex mediates the genesis of microRNAs. *Nature* **432:** 235-240.

Grishok A, Pasquinelli AE, Conte D, Li N, Parrish S, Ha I *et al* (2001). Genes and mechanisms related to RNA interference regulate expression of the small temporal RNAs that control C. elegans developmental timing. *Cell* **106:** 23-34.

Guan H, Cai J, Zhang N, Wu J, Yuan J, Li J *et al* (2012). Sp1 is upregulated in human glioma, promotes MMP-2-mediated cell invasion and predicts poor clinical outcome. *Int J Cancer* **130:** 593-601.

Guardavaccaro D, Corrente G, Covone F, Micheli L, D'Agnano I, Starace G *et al* (2000). Arrest of G(1)-S progression by the p53-inducible gene PC3 is Rb dependent and relies on the inhibition of cyclin D1 transcription. *Mol Cell Biol* **20:** 1797-1815.

Guil S, Esteller M (2009). DNA methylomes, histone codes and miRNAs: tying it all together. *Int J Biochem Cell Biol* **41:** 87-95.

Hadziahmetovic M, Shirai K, Chakravarti A (2011). Recent advancements in multimodality treatment of gliomas. *Future Oncol* **7:** 1169-1183.

Han J, Lee Y, Yeom KH, Nam JW, Heo I, Rhee JK *et al* (2006). Molecular basis for the recognition of primary microRNAs by the Drosha-DGCR8 complex. *Cell* **125:** 887-901.

Hanahan D (1983). Studies on transformation of Escherichia coli with plasmids. *J Mol Biol* **166:** 557-580.

Hanks TS, Gauss KA (2011). Pleomorphic adenoma gene-like 2 regulates expression of the p53 family member, p73, and induces cell cycle block and apoptosis in human promonocytic U937 cells. *Apoptosis*.

Harfe BD (2005). MicroRNAs in vertebrate development. *Current opinion in genetics & development* **15:** 410-415.

Harris AL (2002). Hypoxia--a key regulatory factor in tumour growth. *Nat Rev Cancer* **2:** 38-47.

Hartmann C, Meyer J, Balss J, Capper D, Mueller W, Christians A *et al* (2009). Type and frequency of IDH1 and IDH2 mutations are related to astrocytic and oligodendroglial differentiation and age: a study of 1,010 diffuse gliomas. *Acta Neuropathol* **118:** 469-474.

Hatziapostolou M, Iliopoulos D (2011). Epigenetic aberrations during oncogenesis. *Cellular and molecular life sciences : CMLS* **68:** 1681-1702.

Hayashita Y, Osada H, Tatematsu Y, Yamada H, Yanagisawa K, Tomida S *et al* (2005). A polycistronic microRNA cluster, miR-17-92, is overexpressed in human lung cancers and enhances cell proliferation. *Cancer Res* **65:** 9628-9632.

Hayatsu H, Shiragami M (1979). Reaction of bisulfite with the 5-hydroxymethyl group in pyrimidines and in phage DNAs. *Biochemistry* **18:** 632-637.

He L, Hannon GJ (2004). MicroRNAs: small RNAs with a big role in gene regulation. *Nat Rev Genet* **5:** 522-531.

He L, Thomson JM, Hemann MT, Hernando-Monge E, Mu D, Goodson S *et al* (2005). A microRNA polycistron as a potential human oncogene. *Nature* **435:** 828-833.

Hebbes TR, Thorne AW, Crane-Robinson C (1988). A direct link between core histone acetylation and transcriptionally active chromatin. *The EMBO journal* **7:** 1395-1402.

Hebert C, Norris K, Scheper MA, Nikitakis N, Sauk JJ (2007). High mobility group A2 is a target for miRNA-98 in head and neck squamous cell carcinoma. *Mol Cancer* **6:** 5.

Hermanson M, Funa K, Hartman M, Claesson-Welsh L, Heldin CH, Westermark B *et al* (1992). Platelet-derived growth factor and its receptors in human glioma tissue: expression of messenger RNA and protein suggests the presence of autocrine and paracrine loops. *Cancer Res* **52:** 3213-3219.

Hermeking H, Eick D (1994). Mediation of c-Myc-induced apoptosis by p53. *Science* **265:** 2091-2093.

Hiroi H, Christenson LK, Strauss JF, 3rd (2004). Regulation of transcription of the steroidogenic acute regulatory protein (StAR) gene: temporal and spatial changes in transcription factor binding and histone modification. *Molecular and cellular endocrinology* **215:** 119-126.

Hirschey MD, Shimazu T, Capra JA, Pollard KS, Verdin E (2011). SIRT1 and SIRT3 deacetylate homologous substrates: AceCS1,2 and HMGCS1,2. *Aging (Albany NY)* **3:** 635-642.

Ho AS, Huang X, Cao H, Christman-Skieller C, Bennewith K, Le QT *et al* (2010). Circulating miR-210 as a Novel Hypoxia Marker in Pancreatic Cancer. *Translational oncology* **3:** 109-113.

Holliday R, Pugh JE (1975). DNA modification mechanisms and gene activity during development. *Science* **187:** 226-232.

Hu J, Kesari S (2012). The molecular basis for novel therapies. *Cancer J* **18:** 32-39.

Hummel R, Maurer J, Haier J (2011). MicroRNAs in brain tumors : a new diagnostic and therapeutic perspective? *Mol Neurobiol* **44:** 223-234.

Hursting SD, Berger NA (2010). Energy balance, host-related factors, and cancer progression. *Journal of clinical oncology : official journal of the American Society of Clinical Oncology* **28:** 4058-4065.

Huse JT, Brennan C, Hambardzumyan D, Wee B, Pena J, Rouhanifard SH *et al* (2009). The PTEN-regulating microRNA miR-26a is amplified in high-grade glioma and facilitates gliomagenesis in vivo. *Genes Dev* **23:** 1327-1337.

Ichimura K, Ohgaki H, Kleihues P, Collins VP (2004). Molecular pathogenesis of astrocytic tumours. *J Neurooncol* **70:** 137-160.

Ichimura K (2012). Molecular pathogenesis of IDH mutations in gliomas. *Brain tumor pathology*.

Iliou MS, Lujambio A, Portela A, Brustle O, Koch P, Andersson-Vincent PH *et al* (2011). Bivalent histone modifications in stem cells poise miRNA loci for CpG island hypermethylation in human cancer. *Epigenetics : official journal of the DNA Methylation Society* **6**.

Inouchi A, Shinohara S, Inoue H, Kita K, Itakura M (2007). Identification of specific sequence motifs in the upstream region of 242 human miRNA genes. *Comput Biol Chem* **31:** 207-214.

Iorio MV, Ferracin M, Liu CG, Veronese A, Spizzo R, Sabbioni S *et al* (2005). MicroRNA gene expression deregulation in human breast cancer. *Cancer Res* **65:** 7065-7070.

Jane EP, Premkumar DR, Pollack IF (2007). AG490 influences UCN-01-induced cytotoxicity in glioma cells in a p53-dependent fashion, correlating with effects on BAX cleavage and BAD phosphorylation. *Cancer letters* **257:** 36-46.

Jones PA, Baylin SB (2002). The fundamental role of epigenetic events in cancer. *Nat Rev Genet* **3:** 415-428.

Kaatsch P (2010). Epidemiology of childhood cancer. *Cancer treatment reviews* **36:** 277-285.

Karius T, Schnekenburger M, Dicato M, Diederich M (2012). MicroRNAs in cancer management and their modulation by dietary agents. *Biochemical pharmacology*.

Kelly TJ, Souza AL, Clish CB, Puigserver P (2011). A hypoxia-induced positive feedback loop promotes hypoxia-inducible factor 1alpha stability through miR-210 suppression of glycerol-3-phosphate dehydrogenase 1-like. *Mol Cell Biol* **31:** 2696-2706.

Kim H, Huang W, Jiang X, Pennicooke B, Park PJ, Johnson MD (2010). Integrative genome analysis reveals an oncomir/oncogene cluster regulating glioblastoma survivorship. *Proc Natl Acad Sci U S A* **107:** 2183-2188.

Kim YK, Yu J, Han TS, Park SY, Namkoong B, Kim DH *et al* (2009). Functional links between clustered microRNAs: suppression of cell-cycle inhibitors by microRNA clusters in gastric cancer. *Nucleic Acids Res* **37:** 1672-1681.

Kiriakidou M, Nelson PT, Kouranov A, Fitziev P, Bouyioukos C, Mourelatos Z *et al* (2004). A combined computational-experimental approach predicts human microRNA targets. *Genes Dev* **18:** 1165-1178.

Klose RJ, Yan Q, Tothova Z, Yamane K, Erdjument-Bromage H, Tempst P *et al* (2007). The retinoblastoma binding protein RBP2 is an H3K4 demethylase. *Cell* **128:** 889-900.

Kouzarides T (2007). Chromatin modifications and their function. *Cell* **128:** 693-705.

Kozaki K, Imoto I, Mogi S, Omura K, Inazawa J (2008). Exploration of tumor-suppressive microRNAs silenced by DNA hypermethylation in oral cancer. *Cancer Res* **68:** 2094-2105.

Kucinska M, Murias M (2010). [Sirtuins--way to longevity or just a fad?]. *Polski merkuriusz lekarski : organ Polskiego Towarzystwa Lekarskiego* **28:** 158-161.

Kuehbacher A, Urbich C, Zeiher AM, Dimmeler S (2007). Role of Dicer and Drosha for endothelial microRNA expression and angiogenesis. *Circ Res* **101:** 59-68.

Kulshreshtha R, Ferracin M, Wojcik SE, Garzon R, Alder H, Agosto-Perez FJ *et al* (2007). A microRNA signature of hypoxia. *Mol Cell Biol* **27:** 1859-1867.

Kwak PB, Iwasaki S, Tomari Y (2010). The microRNA pathway and cancer. *Cancer science* **101:** 2309-2315.

Laemmli UK (1970). Cleavage of structural proteins during the assembly of the head of bacteriophage T4. *Nature* **227:** 680-685.

Lages E, Guttin A, El Atifi M, Ramus C, Ipas H, Dupre I *et al* (2011). MicroRNA and target protein patterns reveal physiopathological features of glioma subtypes. *PLoS One* **6:** e20600.

Lagos-Quintana M, Rauhut R, Lendeckel W, Tuschl T (2001). Identification of novel genes coding for small expressed RNAs. *Science* **294:** 853-858.

Landgraf P, Rusu M, Sheridan R, Sewer A, Iovino N, Aravin A *et al* (2007). A mammalian microRNA expression atlas based on small RNA library sequencing. *Cell* **129:** 1401-1414.

Landthaler M, Yalcin A, Tuschl T (2004). The human DiGeorge syndrome critical region gene 8 and Its D. melanogaster homolog are required for miRNA biogenesis. *Current biology : CB* **14:** 2162-2167.

Laurenti G, Benedetti E, D'Angelo B, Cristiano L, Cinque B, Raysi S *et al* (2011). Hypoxia induces peroxisome proliferator-activated receptor alpha (PPARalpha) and lipid metabolism peroxisomal enzymes in human glioblastoma cells. *J Cell Biochem* **112:** 3891-3901.

Lee RC, Feinbaum RL, Ambros V (1993). The C. elegans heterochronic gene lin-4 encodes small RNAs with antisense complementarity to lin-14. *Cell* **75:** 843-854.

Lee RC, Ambros V (2001). An extensive class of small RNAs in Caenorhabditis elegans. *Science* **294:** 862-864.

Lee Y, Ahn C, Han J, Choi H, Kim J, Yim J *et al* (2003). The nuclear RNase III Drosha initiates microRNA processing. *Nature* **425:** 415-419.

Lehmann U, Hasemeier B, Christgen M, Muller M, Romermann D, Langer F *et al* (2008). Epigenetic inactivation of microRNA gene hsa-mir-9-1 in human breast cancer. *The Journal of pathology* **214:** 17-24.

Lewis BP, Shih IH, Jones-Rhoades MW, Bartel DP, Burge CB (2003). Prediction of mammalian microRNA targets. *Cell* **115:** 787-798.

Li W, Xie L, He X, Li J, Tu K, Wei L *et al* (2008). Diagnostic and prognostic implications of microRNAs in human hepatocellular carcinoma. *Int J Cancer* **123:** 1616-1622.

Li Y, Guessous F, DiPierro C, Zhang Y, Mudrick T, Fuller L *et al* (2009). Interactions between PTEN and the c-Met pathway in glioblastoma and implications for therapy. *Molecular cancer therapeutics* **8:** 376-385.

Liang G, Lin JC, Wei V, Yoo C, Cheng JC, Nguyen CT *et al* (2004). Distinct localization of histone H3 acetylation and H3-K4 methylation to the transcription start sites in the human genome. *Proc Natl Acad Sci U S A* **101:** 7357-7362.

Lim IK (2006). TIS21 (/BTG2/PC3) as a link between ageing and cancer: cell cycle regulator and endogenous cell death molecule. *J Cancer Res Clin Oncol* **132:** 417-426.

Lin W, Cao J, Liu J, Beshiri ML, Fujiwara Y, Francis J *et al* (2011). Loss of the retinoblastoma binding protein 2 (RBP2) histone demethylase suppresses tumorigenesis in mice lacking Rb1 or Men1. *Proc Natl Acad Sci U S A* **108:** 13379-13386.

Liu C, Kelnar K, Liu B, Chen X, Calhoun-Davis T, Li H *et al* (2011). The microRNA miR-34a inhibits prostate cancer stem cells and metastasis by directly repressing CD44. *Nat Med* **17:** 211-215.

Liu J, Carmell MA, Rivas FV, Marsden CG, Thomson JM, Song JJ *et al* (2004). Argonaute2 is the catalytic engine of mammalian RNAi. *Science* **305:** 1437-1441.

Liu M, Wu H, Liu T, Li Y, Wang F, Wan H *et al* (2009a). Regulation of the cell cycle gene, BTG2, by miR-21 in human laryngeal carcinoma. *Cell Res* **19:** 828-837.

Liu T, Liu PY, Marshall GM (2009b). The critical role of the class III histone deacetylase SIRT1 in cancer. *Cancer Res* **69:** 1702-1705.

Livak KJ, Schmittgen TD (2001). Analysis of relative gene expression data using real-time quantitative PCR and the 2(-Delta Delta C(T)) Method. *Methods* **25:** 402-408.

Lobo NA, Shimono Y, Qian D, Clarke MF (2007). The biology of cancer stem cells. *Annual review of cell and developmental biology* **23:** 675-699.

Louis DN, Ohgaki H, Wiestler OD, Cavenee WK (2007a). WHO Classification of Tumours of the Central Nervous System, 4th edn. IARC Press: Lyon.

Louis DN, Ohgaki H, Wiestler OD, Cavenee WK, Burger PC, Jouvet A *et al* (2007b). The 2007 WHO classification of tumours of the central nervous system. *Acta Neuropathol* **114:** 97-109.

Lowe SW, Schmitt EM, Smith SW, Osborne BA, Jacks T (1993). p53 is required for radiation-induced apoptosis in mouse thymocytes. *Nature* **362:** 847-849.

Luan S, Sun L, Huang F (2010). MicroRNA-34a: a novel tumor suppressor in p53-mutant glioma cell line U251. *Arch Med Res* **41:** 67-74.

Lujambio A, Ropero S, Ballestar E, Fraga MF, Cerrato C, Setien F *et al* (2007). Genetic unmasking of an epigenetically silenced microRNA in human cancer cells. *Cancer Res* **67:** 1424-1429.

Lund E, Guttinger S, Calado A, Dahlberg JE, Kutay U (2004). Nuclear export of microRNA precursors. *Science* **303:** 95-98.

Ma L, Teruya-Feldstein J, Weinberg RA (2007). Tumour invasion and metastasis initiated by microRNA-10b in breast cancer. *Nature* **449:** 682-688.

Macrae IJ, Zhou K, Li F, Repic A, Brooks AN, Cande WZ *et al* (2006). Structural basis for double-stranded RNA processing by Dicer. *Science* **311:** 195-198.

Malzkorn B, Wolter M, Liesenberg F, Grzendowski M, Stuhler K, Meyer HE *et al* (2010). Identification and functional characterization of microRNAs involved in the malignant progression of gliomas. *Brain Pathol* **20:** 539-550.

Marks PA, Xu WS (2009). Histone deacetylase inhibitors: Potential in cancer therapy. *J Cell Biochem* **107:** 600-608.

Megraw M, Sethupathy P, Corda B, Hatzigeorgiou AG (2007). miRGen: a database for the study of animal microRNA genomic organization and function. *Nucleic Acids Res* **35:** D149-155.

Meister G, Tuschl T (2004). Mechanisms of gene silencing by double-stranded RNA. *Nature* **431:** 343-349.

Michael MZ, SM OC, van Holst Pellekaan NG, Young GP, James RJ (2003). Reduced accumulation of specific microRNAs in colorectal neoplasia. *Molecular cancer research : MCR* **1:** 882-891.

Mizutani A, Furukawa T, Adachi Y, Ikehara S, Taketani S (2002). A zinc-finger protein, PLAGL2, induces the expression of a proapoptotic protein Nip3, leading to cellular apoptosis. *J Biol Chem* **277:** 15851-15858.

Moorthy K, Mohamad MS (2011). Random forest for gene selection and microarray data classification. *Bioinformation* **7:** 142-146.

Nagarajan RP, Costello JF (2009). Epigenetic mechanisms in glioblastoma multiforme. *Semin Cancer Biol* **19:** 188-197.

Nakada C, Tsukamoto Y, Matsuura K, Nguyen TL, Hijiya N, Uchida T *et al* (2011). Overexpression of miR-210, a downstream target of HIF1alpha, causes centrosome amplification in renal carcinoma cells. *The Journal of pathology* **224:** 280-288.

Nieder C, Andratschke N, Wiedenmann N, Busch R, Grosu AL, Molls M (2004). Radiotherapy for high-grade gliomas. Does altered fractionation improve the outcome? *Strahlenther Onkol* **180:** 401-407.

Noushmehr H, Weisenberger DJ, Diefes K, Phillips HS, Pujara K, Berman BP *et al* (2010). Identification of a CpG island methylator phenotype that defines a distinct subgroup of glioma. *Cancer Cell* **17:** 510-522.

O'Donnell KA, Wentzel EA, Zeller KI, Dang CV, Mendell JT (2005). c-Myc-regulated microRNAs modulate E2F1 expression. *Nature* **435:** 839-843.

Ohgaki H, Kleihues P (2007). Genetic pathways to primary and secondary glioblastoma. *The American journal of pathology* **170:** 1445-1453.

Ohler U, Yekta S, Lim LP, Bartel DP, Burge CB (2004). Patterns of flanking sequence conservation and a characteristic upstream motif for microRNA gene identification. *RNA* **10:** 1309-1322.

Ohno M, Natsume A, Kondo Y, Iwamizu H, Motomura K, Toda H *et al* (2009). The modulation of microRNAs by type I IFN through the activation of signal transducers and activators of transcription 3 in human glioma. *Molecular cancer research : MCR* **7:** 2022-2030.

Ostro MJ, Fondy TP (1977). Isolation and characterization of multiple molecular forms of cytosolic NAD-linked glycerol-3-phosphate dehydrogenase from normal and neoplastic rabbit tissues. *J Biol Chem* **252:** 5575-5583.

Ota A, Tagawa H, Karnan S, Tsuzuki S, Karpas A, Kira S *et al* (2004). Identification and characterization of a novel gene, C13orf25, as a target for 13q31-q32 amplification in malignant lymphoma. *Cancer Res* **64:** 3087-3095.

Papagiannakopoulos T, Shapiro A, Kosik KS (2008). MicroRNA-21 targets a network of key tumor-suppressive pathways in glioblastoma cells. *Cancer Res* **68:** 8164-8172.

Parasramka MA, Ho E, Williams DE, Dashwood RH (2012). MicroRNAs, diet, and cancer: new mechanistic insights on the epigenetic actions of phytochemicals. *Molecular carcinogenesis* **51:** 213-230.

Park JK, Henry JC, Jiang J, Esau C, Gusev Y, Lerner MR *et al* (2011). miR-132 and miR-212 are increased in pancreatic cancer and target the retinoblastoma tumor suppressor. *Biochem Biophys Res Commun* **406:** 518-523.

Parsons DW, Jones S, Zhang X, Lin JC, Leary RJ, Angenendt P *et al* (2008). An integrated genomic analysis of human glioblastoma multiforme. *Science* **321:** 1807-1812.

Petrocca F, Visone R, Onelli MR, Shah MH, Nicoloso MS, de Martino I *et al* (2008). E2F1-regulated microRNAs impair TGFbeta-dependent cell-cycle arrest and apoptosis in gastric cancer. *Cancer Cell* **13:** 272-286.

Poliseno L, Salmena L, Riccardi L, Fornari A, Song MS, Hobbs RM *et al* (2010). Identification of the miR-106b~25 microRNA cluster as a proto-oncogenic PTEN-targeting intron that cooperates with its host gene MCM7 in transformation. *Science signaling* **3:** ra29.

Pollo B (2011). Neuropathological diagnosis of brain tumours. *Neurol Sci* **32 Suppl 2:** S209-211.

Porstmann T, Ternynck T, Avrameas S (1985). Quantitation of 5-bromo-2-deoxyuridine incorporation into DNA: an enzyme immunoassay for the assessment of the lymphoid cell proliferative response. *Journal of immunological methods* **82:** 169-179.

Pruitt KD, Tatusova T, Maglott DR (2003). NCBI Reference Sequence project: update and current status. *Nucleic Acids Res* **31:** 34-37.

Puissegur MP, Mazure NM, Bertero T, Pradelli L, Grosso S, Robbe-Sermesant K *et al* (2011). miR-210 is overexpressed in late stages of lung cancer and mediates mitochondrial alterations associated with modulation of HIF-1 activity. *Cell death and differentiation* **18:** 465-478.

Rane S, He M, Sayed D, Vashistha H, Malhotra A, Sadoshima J *et al* (2009). Downregulation of miR-199a derepresses hypoxia-inducible factor-1alpha and Sirtuin 1 and recapitulates hypoxia preconditioning in cardiac myocytes. *Circ Res* **104:** 879-886.

Reisman D, Elkind NB, Roy B, Beamon J, Rotter V (1993). c-Myc trans-activates the p53 promoter through a required downstream CACGTG motif. *Cell growth & differentiation : the molecular biology journal of the American Association for Cancer Research* **4:** 57-65.

Remenyi J, Hunter CJ, Cole C, Ando H, Impey S, Monk CE *et al* (2010). Regulation of the miR-212/132 locus by MSK1 and CREB in response to neurotrophins. *Biochem J* **428:** 281-291.

Riemenschneider MJ, Reifenberger G (2009). Molecular neuropathology of gliomas. *Int J Mol Sci* **10:** 184-212.

Riemenschneider MJ, Jeuken JW, Wesseling P, Reifenberger G (2010). Molecular diagnostics of gliomas: state of the art. *Acta Neuropathol* **120:** 567-584.

Rodriguez A, Griffiths-Jones S, Ashurst JL, Bradley A (2004). Identification of mammalian microRNA host genes and transcription units. *Genome Res* **14:** 1902-1910.

Roldo C, Missiaglia E, Hagan JP, Falconi M, Capelli P, Bersani S *et al* (2006). MicroRNA expression abnormalities in pancreatic endocrine and acinar tumors are associated with distinctive pathologic features and clinical behavior. *Journal of clinical oncology : official journal of the American Society of Clinical Oncology* **24:** 4677-4684.

Roman-Gomez J, Agirre X, Jimenez-Velasco A, Arqueros V, Vilas-Zornoza A, Rodriguez-Otero P *et al* (2009). Epigenetic regulation of microRNAs in acute lymphoblastic leukemia. *Journal of clinical oncology : official journal of the American Society of Clinical Oncology* **27:** 1316-1322.

Roy B, Beamon J, Balint E, Reisman D (1994). Transactivation of the human p53 tumor suppressor gene by c-Myc/Max contributes to elevated mutant p53 expression in some tumors. *Mol Cell Biol* **14:** 7805-7815.

Ryazansky SS, Gvozdev VA (2008). Small RNAs and cancerogenesis. *Biochemistry Biokhimiia* **73:** 514-527.

Saito Y, Liang G, Egger G, Friedman JM, Chuang JC, Coetzee GA *et al* (2006). Specific activation of microRNA-127 with downregulation of the proto-oncogene BCL6 by chromatin-modifying drugs in human cancer cells. *Cancer Cell* **9:** 435-443.

Saito Y, Friedman JM, Chihara Y, Egger G, Chuang JC, Liang G (2009). Epigenetic therapy upregulates the tumor suppressor microRNA-126 and its host gene EGFL7 in human cancer cells. *Biochem Biophys Res Commun* **379:** 726-731.

Salacz ME, Watson KR, Schomas DA (2011). Glioblastoma: Part I. Current state of affairs. *Mo Med* **108:** 187-194.

Sanger F, Nicklen S, Coulson AR (1977). DNA sequencing with chain-terminating inhibitors. *Proc Natl Acad Sci U S A* **74:** 5463-5467.

Saunders LR, Sharma AD, Tawney J, Nakagawa M, Okita K, Yamanaka S *et al* (2010). miRNAs regulate SIRT1 expression during mouse embryonic stem cell differentiation and in adult mouse tissues. *Aging (Albany NY)* **2:** 415-431.

Schagger H (2006). Tricine-SDS-PAGE. *Nat Protoc* **1:** 16-22.

Schmidt N, Windmann S, Reifenberger G, Riemenschneider MJ (2012). DNA hypermethylation and histone modifications downregulate the candidate tumor suppressor gene RRP22 on 22q12 in human gliomas. *Brain Pathol* **22:** 17-25.

Schmittgen TD, Jiang J, Liu Q, Yang L (2004). A high-throughput method to monitor the expression of microRNA precursors. *Nucleic Acids Res* **32:** e43.

Schraivogel D, Weinmann L, Beier D, Tabatabai G, Eichner A, Zhu JY *et al* (2011). CAMTA1 is a novel tumour suppressor regulated by miR-9/9* in glioblastoma stem cells. *The EMBO journal* **30:** 4309-4322.

Scott GK, Mattie MD, Berger CE, Benz SC, Benz CC (2006). Rapid alteration of microRNA levels by histone deacetylase inhibition. *Cancer Res* **66:** 1277-1281.

Secombe J, Li L, Carlos L, Eisenman RN (2007). The Trithorax group protein Lid is a trimethyl histone H3K4 demethylase required for dMyc-induced cell growth. *Genes Dev* **21:** 537-551.

Seidel S, Garvalov BK, Wirta V, von Stechow L, Schanzer A, Meletis K *et al* (2010). A hypoxic niche regulates glioblastoma stem cells through hypoxia inducible factor 2 alpha. *Brain* **133:** 983-995.

Seitz H, Royo H, Bortolin ML, Lin SP, Ferguson-Smith AC, Cavaille J (2004). A large imprinted microRNA gene cluster at the mouse Dlk1-Gtl2 domain. *Genome Res* **14:** 1741-1748.

Sellers WR, Kaelin WG, Jr. (1997). Role of the retinoblastoma protein in the pathogenesis of human cancer. *Journal of clinical oncology : official journal of the American Society of Clinical Oncology* **15:** 3301-3312.

Shen WF, Hu YL, Uttarwar L, Passegue E, Largman C (2008). MicroRNA-126 regulates HOXA9 by binding to the homeobox. *Mol Cell Biol* **28:** 4609-4619.

Shi L, Cheng Z, Zhang J, Li R, Zhao P, Fu Z *et al* (2008). hsa-mir-181a and hsa-mir-181b function as tumor suppressors in human glioma cells. *Brain research* **1236:** 185-193.

Shi L, Zhang S, Feng K, Wu F, Wan Y, Wang Z *et al* (2012). MicroRNA-125b-2 confers human glioblastoma stem cells resistance to temozolomide through the mitochondrial pathway of apoptosis. *Int J Oncol* **40:** 119-129.

Silber J, Lim DA, Petritsch C, Persson AI, Maunakea AK, Yu M *et al* (2008). miR-124 and miR-137 inhibit proliferation of glioblastoma multiforme cells and induce differentiation of brain tumor stem cells. *BMC Med* **6:** 14.

Silber J, James CD, Hodgson JG (2009). microRNAs in gliomas: small regulators of a big problem. *Neuromolecular Med* **11:** 208-222.

Slaby O, Lakomy R, Fadrus P, Hrstka R, Kren L, Lzicarova E *et al* (2010). MicroRNA-181 family predicts response to concomitant chemoradiotherapy with temozolomide in glioblastoma patients. *Neoplasma* **57:** 264-269.

Standart N, Jackson RJ (2007). MicroRNAs repress translation of m7Gppp-capped target mRNAs in vitro by inhibiting initiation and promoting deadenylation. *Genes Dev* **21:** 1975-1982.

Strum JC, Johnson JH, Ward J, Xie H, Feild J, Hester A *et al* (2009). MicroRNA 132 regulates nutritional stress-induced chemokine production through repression of SirT1. *Mol Endocrinol* **23:** 1876-1884.

Suzuki H, Yamamoto E, Nojima M, Kai M, Yamano HO, Yoshikawa K *et al* (2010). Methylation-associated silencing of microRNA-34b/c in gastric cancer and its involvement in an epigenetic field defect. *Carcinogenesis* **31:** 2066-2073.

Tabatabai G, Weller M (2011). Glioblastoma stem cells. *Cell and tissue research* **343:** 459-465.

Taguchi A, Yanagisawa K, Tanaka M, Cao K, Matsuyama Y, Goto H *et al* (2008). Identification of hypoxia-inducible factor-1 alpha as a novel target for miR-17-92 microRNA cluster. *Cancer Res* **68:** 5540-5545.

Takahashi F, Chiba N, Tajima K, Hayashida T, Shimada T, Takahashi M *et al* (2011). Breast tumor progression induced by loss of BTG2 expression is inhibited by targeted therapy with the ErbB/HER inhibitor lapatinib. *Oncogene* **30:** 3084-3095.

Takai D, Jones PA (2002). Comprehensive analysis of CpG islands in human chromosomes 21 and 22. *Proc Natl Acad Sci U S A* **99:** 3740-3745.

Tanzer A, Stadler PF (2004). Molecular evolution of a microRNA cluster. *J Mol Biol* **339:** 327-335.

Tavazoie SF, Alarcon C, Oskarsson T, Padua D, Wang Q, Bos PD *et al* (2008). Endogenous human microRNAs that suppress breast cancer metastasis. *Nature* **451:** 147-152.

Tepel M, Roerig P, Wolter M, Gutmann DH, Perry A, Reifenberger G *et al* (2008). Frequent promoter hypermethylation and transcriptional downregulation of the NDRG2 gene at 14q11.2 in primary glioblastoma. *Int J Cancer* **123:** 2080-2086.

Tews B, Roerig P, Hartmann C, Hahn M, Felsberg J, Blaschke B *et al* (2007). Hypermethylation and transcriptional downregulation of the CITED4 gene at 1p34.2 in oligodendroglial tumours with allelic losses on 1p and 19q. *Oncogene* **26:** 5010-5016.

Toedt G, Barbus S, Wolter M, Felsberg J, Tews B, Blond F *et al* (2011). Molecular signatures classify astrocytic gliomas by IDH1 mutation status. *Int J Cancer* **128:** 1095-1103.

Tognini P, Putignano E, Coatti A, Pizzorusso T (2011). Experience-dependent expression of miR-132 regulates ocular dominance plasticity. *Nat Neurosci* **14:** 1237-1239.

Towbin H, Staehelin T, Gordon J (1979). Electrophoretic transfer of proteins from polyacrylamide gels to nitrocellulose sheets: procedure and some applications. *Proc Natl Acad Sci U S A* **76:** 4350-4354.

Toyota M, Ahuja N, Ohe-Toyota M, Herman JG, Baylin SB, Issa JP (1999). CpG island methylator phenotype in colorectal cancer. *Proc Natl Acad Sci U S A* **96:** 8681-8686.

Toyota M, Suzuki H, Sasaki Y, Maruyama R, Imai K, Shinomura Y *et al* (2008). Epigenetic silencing of microRNA-34b/c and B-cell translocation gene 4 is associated with CpG island methylation in colorectal cancer. *Cancer Res* **68:** 4123-4132.

Tusher VG, Tibshirani R, Chu G (2001). Significance analysis of microarrays applied to the ionizing radiation response. *Proc Natl Acad Sci U S A* **98:** 5116-5121.

Vaissiere T, Sawan C, Herceg Z (2008). Epigenetic interplay between histone modifications and DNA methylation in gene silencing. *Mutat Res* **659:** 40-48.

Valera VA, Walter BA, Linehan WM, Merino MJ (2011). Regulatory Effects of microRNA-92 (miR-92) on VHL Gene Expression and the Hypoxic Activation of miR-210 in Clear Cell Renal Cell Carcinoma. *J Cancer* **2:** 515-526.

Valeri N, Vannini I, Fanini F, Calore F, Adair B, Fabbri M (2009). Epigenetics, miRNAs, and human cancer: a new chapter in human gene regulation. *Mammalian genome : official journal of the International Mammalian Genome Society* **20:** 573-580.

van den Boom J, Wolter M, Kuick R, Misek DE, Youkilis AS, Wechsler DS *et al* (2003). Characterization of gene expression profiles associated with glioma progression using oligonucleotide-based microarray analysis and real-time reverse transcription-polymerase chain reaction. *The American journal of pathology* **163:** 1033-1043.

Vandesompele J, De Preter K, Pattyn F, Poppe B, Van Roy N, De Paepe A *et al* (2002). Accurate normalization of real-time quantitative RT-PCR data by geometric averaging of multiple internal control genes. *Genome Biol* **3:** RESEARCH0034.

Varkonyi-Gasic E, Wu R, Wood M, Walton EF, Hellens RP (2007). Protocol: a highly sensitive RT-PCR method for detection and quantification of microRNAs. *Plant methods* **3:** 12.

Varkonyi-Gasic E, Hellens RP (2011). Quantitative stem-loop RT-PCR for detection of microRNAs. *Methods Mol Biol* **744:** 145-157.

Vaziri H, Dessain SK, Ng Eaton E, Imai SI, Frye RA, Pandita TK *et al* (2001). hSIR2(SIRT1) functions as an NAD-dependent p53 deacetylase. *Cell* **107:** 149-159.

Vigushin DM, Ali S, Pace PE, Mirsaidi N, Ito K, Adcock I *et al* (2001). Trichostatin A is a histone deacetylase inhibitor with potent antitumor activity against breast cancer in vivo. *Clin Cancer Res* **7:** 971-976.

Visvader JE, Lindeman GJ (2008). Cancer stem cells in solid tumours: accumulating evidence and unresolved questions. *Nat Rev Cancer* **8:** 755-768.

Volinia S, Calin GA, Liu CG, Ambs S, Cimmino A, Petrocca F *et al* (2006). A microRNA expression signature of human solid tumors defines cancer gene targets. *Proc Natl Acad Sci U S A* **103:** 2257-2261.

Wanet A, Tacheny A, Arnould T, Renard P (2012). miR-212/132 expression and functions: within and beyond the neuronal compartment. *Nucleic Acids Res*.

Wang X, Tang S, Le SY, Lu R, Rader JS, Meyers C *et al* (2008). Aberrant expression of oncogenic and tumor-suppressive microRNAs in cervical cancer is required for cancer cell growth. *PLoS One* **3:** e2557.

Watanabe T, Yokoo H, Yokoo M, Yonekawa Y, Kleihues P, Ohgaki H (2001). Concurrent inactivation of RB1 and TP53 pathways in anaplastic oligodendrogliomas. *J Neuropathol Exp Neurol* **60:** 1181-1189.

Weber B, Stresemann C, Brueckner B, Lyko F (2007). Methylation of human microRNA genes in normal and neoplastic cells. *Cell Cycle* **6:** 1001-1005.

Wehming FM, Wiese B, Nakamura M, Bremer M, Karstens JH, Meyer A (2012). Malignant glioma grade 3 and 4: How relevant is timing of radiotherapy? *Clin Neurol Neurosurg*.

Wong TS, Liu XB, Wong BY, Ng RW, Yuen AP, Wei WI (2008). Mature miR-184 as Potential Oncogenic microRNA of Squamous Cell Carcinoma of Tongue. *Clin Cancer Res* **14:** 2588-2592.

Woods DB, Vousden KH (2001). Regulation of p53 function. *Experimental cell research* **264:** 56-66.

Wyllie AH, Kerr JF, Currie AR (1980). Cell death: the significance of apoptosis. *Int Rev Cytol* **68:** 251-306.

Yan H, Parsons DW, Jin G, McLendon R, Rasheed BA, Yuan W *et al* (2009). IDH1 and IDH2 mutations in gliomas. *The New England journal of medicine* **360:** 765-773.

Yanaihara N, Caplen N, Bowman E, Seike M, Kumamoto K, Yi M *et al* (2006). Unique microRNA molecular profiles in lung cancer diagnosis and prognosis. *Cancer Cell* **9:** 189-198.

Yang CH, Yue J, Pfeffer SR, Handorf CR, Pfeffer LM (2011). MicroRNA miR-21 regulates the metastatic behavior of B16 melanoma cells. *J Biol Chem* **286:** 39172-39178.

Yi R, Qin Y, Macara IG, Cullen BR (2003). Exportin-5 mediates the nuclear export of pre-microRNAs and short hairpin RNAs. *Genes Dev* **17:** 3011-3016.

Yin D, Ong JM, Hu J, Desmond JC, Kawamata N, Konda BM *et al* (2007). Suberoylanilide hydroxamic acid, a histone deacetylase inhibitor: effects on gene expression and growth of glioma cells in vitro and in vivo. *Clin Cancer Res* **13:** 1045-1052.

Ying Q, Liang L, Guo W, Zha R, Tian Q, Huang S *et al* (2011). Hypoxia-inducible microRNA-210 augments the metastatic potential of tumor cells by targeting vacuole membrane protein 1 in hepatocellular carcinoma. *Hepatology* **54:** 2064-2075.

Yoshida M, Kijima M, Akita M, Beppu T (1990). Potent and specific inhibition of mammalian histone deacetylase both in vivo and in vitro by trichostatin A. *J Biol Chem* **265:** 17174-17179.

Yu F, Yao H, Zhu P, Zhang X, Pan Q, Gong C *et al* (2007). let-7 regulates self renewal and tumorigenicity of breast cancer cells. *Cell* **131:** 1109-1123.

Zeng J, Ge Z, Wang L, Li Q, Wang N, Bjorkholm M *et al* (2010). The histone demethylase RBP2 Is overexpressed in gastric cancer and its inhibition triggers senescence of cancer cells. *Gastroenterology* **138:** 981-992.

Zhang B, Pan X, Cobb GP, Anderson TA (2007). microRNAs as oncogenes and tumor suppressors. *Dev Biol* **302:** 1-12.

Zhang C, Kang C, You Y, Pu P, Yang W, Zhao P *et al* (2009a). Co-suppression of miR-221/222 cluster suppresses human glioma cell growth by targeting p27kip1 in vitro and in vivo. *Int J Oncol* **34:** 1653-1660.

Zhang C, Han L, Zhang A, Yang W, Zhou X, Pu P *et al* (2010). Global changes of mRNA expression reveals an increased activity of the interferon-induced signal transducer and activator of transcription (STAT) pathway by repression of miR-221/222 in glioblastoma U251 cells. *Int J Oncol* **36:** 1503-1512.

Zhang H, Kolb FA, Jaskiewicz L, Westhof E, Filipowicz W (2004). Single processing center models for human Dicer and bacterial RNase III. *Cell* **118:** 57-68.

Zhang S, Hao J, Xie F, Hu X, Liu C, Tong J *et al* (2011a). Downregulation of miR-132 by promoter methylation contributes to pancreatic cancer development. *Carcinogenesis*.

Zhang S, Hao J, Xie F, Hu X, Liu C, Tong J *et al* (2011b). Downregulation of miR-132 by promoter methylation contributes to pancreatic cancer development. *Carcinogenesis* **32:** 1183-1189.

Zhang Y, Dutta A, Abounader R (2012). The role of microRNAs in glioma initiation and progression. *Front Biosci* **17:** 700-712.

Zhang Z, Sun H, Dai H, Walsh RM, Imakura M, Schelter J *et al* (2009b). MicroRNA miR-210 modulates cellular response to hypoxia through the MYC antagonist MNT. *Cell Cycle* **8:** 2756-2768.

Zheng H, Ying H, Wiedemeyer R, Yan H, Quayle SN, Ivanova EV *et al* (2010). PLAGL2 regulates Wnt signaling to impede differentiation in neural stem cells and gliomas. *Cancer Cell* **17:** 497-509.

Zhong H, De Marzo AM, Laughner E, Lim M, Hilton DA, Zagzag D *et al* (1999). Overexpression of hypoxia-inducible factor 1alpha in common human cancers and their metastases. *Cancer Res* **59:** 5830-5835.

Zhou X, Ren Y, Moore L, Mei M, You Y, Xu P *et al* (2010). Downregulation of miR-21 inhibits EGFR pathway and suppresses the growth of human glioblastoma cells independent of PTEN status. *Laboratory investigation; a journal of technical methods and pathology* **90:** 144-155.

References to web pages

3.1.2.2 Real-time PCR analysis using TaqMan® miRNA assays.

https://products.appliedbiosystems.com 02.02.2012

Table 17: SYBR® Green Dye assay chemistry.

http://www.appliedbiosystems.com/absite/us/en/home/applications-technologies/real-time-pcr/taqman-and-sybr-green-chemistries.html 22.03.2012

Figure 5: Conversion of unmethylated cytosine to uracil by sodium bisulfite treatment.

http://www.cmmt.ubc.ca/sites/default/files/pdf_methylseqr_protocol.pdf 29.03.2012

Figure 7: Schematic representation of the SDS-PAGE.

http://www.imb-jena.de/~rake/Bioinformatics_WEB/proteins_purification.html 01.04.2012

Figure 8: Schematic representation of a western blot transfer.

http://technologyinscience.blogspot.de/2011/12/western-blot-protein-immunoblot.html 03.04.2012

Figure 9: Chemiluminescent detection of Western blot.

http://advansta.com/Chemiluminescent_Western_Detection.html 13.04.2012

Figure 10: Cleavage of the non - fluorescent caspase substrate Z-DEVD-R110.

http://www.promega.com
Apo-ONE® Homogeneous Caspase-3/7 Assay Technical Bulletin 14.04.2012

Figure 11: Reaction of Luciferin and ATP to Oxyluciferin, ADP and light.

http://www.promega.com
CellTiter-Glo® Luminescent Cell Viability Assay Technical Bulletin 14.04.2012

Figure 14: Schematic representation of the bioluminescent reaction catalyzed by Firefly and Renilla luciferases

http://www.promega.com

Dual-Glo® Luciferase Assay System Technical Manual 14.04.2012

4.6 Identification and validation of putative *miR-132/miR-212*, *miR-126* and *miR-210* targets

http://diana.pcbi.upenn.edu/miRGen/v3/miRGen.html (version v3) 01.05.2012

microRNA.org software (version: August 2010) 01.05.2012

4.1.2 Epigenetically regulated miRNAs in gliomas

4.1.3 MiRNAs induced by hypoxia in glioblastoma stem cell lines

http://genome.ucsc.edu/ (version: February 2009) 07.04.2012

3.5 3`- Luciferase reporter gene assay system

http://www.starseq.com 05.04.2012

9 Supplementary Figures

5`genomic region of *miR-132/miR-212* (CpG sites 1 to 886)

Position: chr17 :1952920-1962328; band: 17p13.3 according to UCSC Genome Browser, created by the Genome Bioinformatics Group of UC Santa Cruz; version February 2009.

Sodium bisulfite-modified DNA sequence and investigated primers used for bisulfite sequencing according to Figure 28: Schematic structure of the genomic region surrounding the *miR-132/miR-212* cluster. Additionally, primers used by Zhang and colleagues are indicated in green (Zhang et al 2011).

Location of the *miR-132/miR-212 stem-loop* cluster is indicated in red.

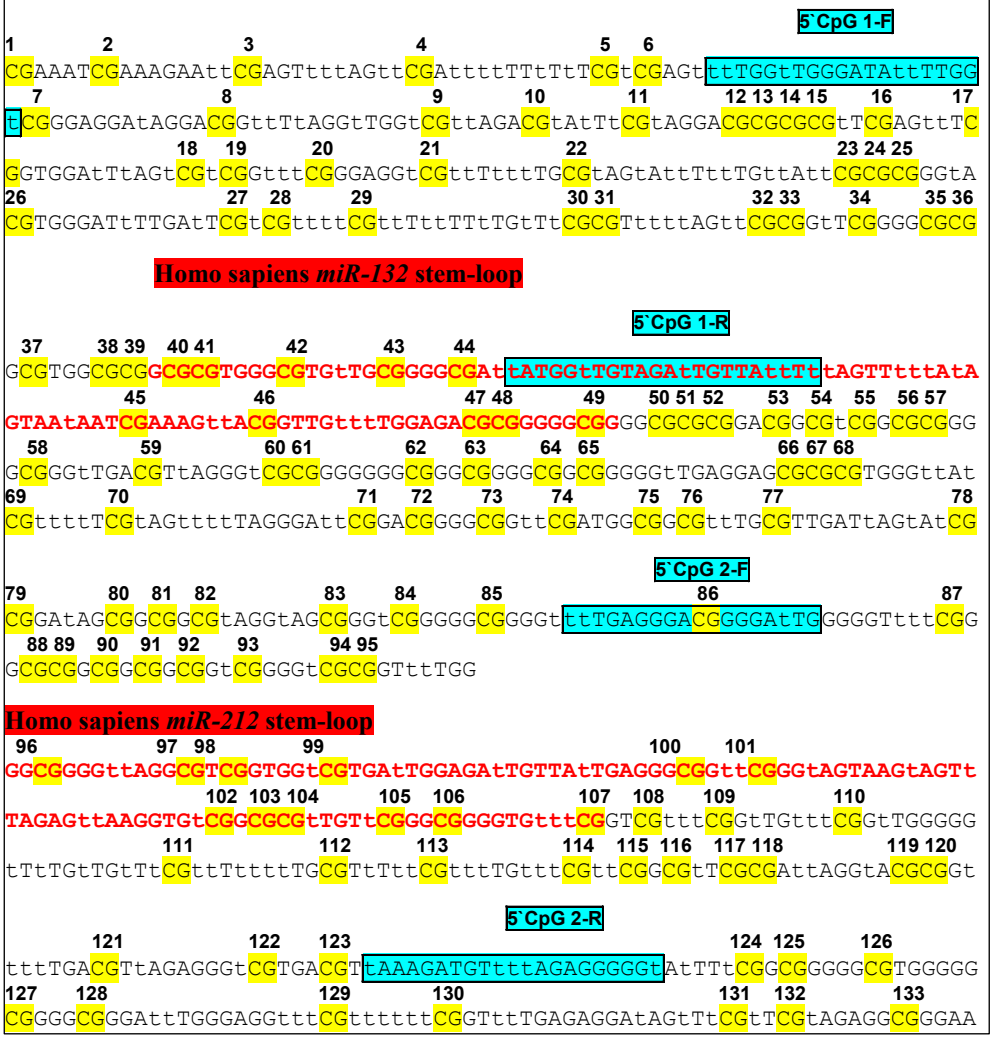

Supplementary Figure 1a: Sodium bisulfite-modified DNA sequence of the 5`genomic region of *miR-132/miR-212* indicating CpG sites 1 to 133.

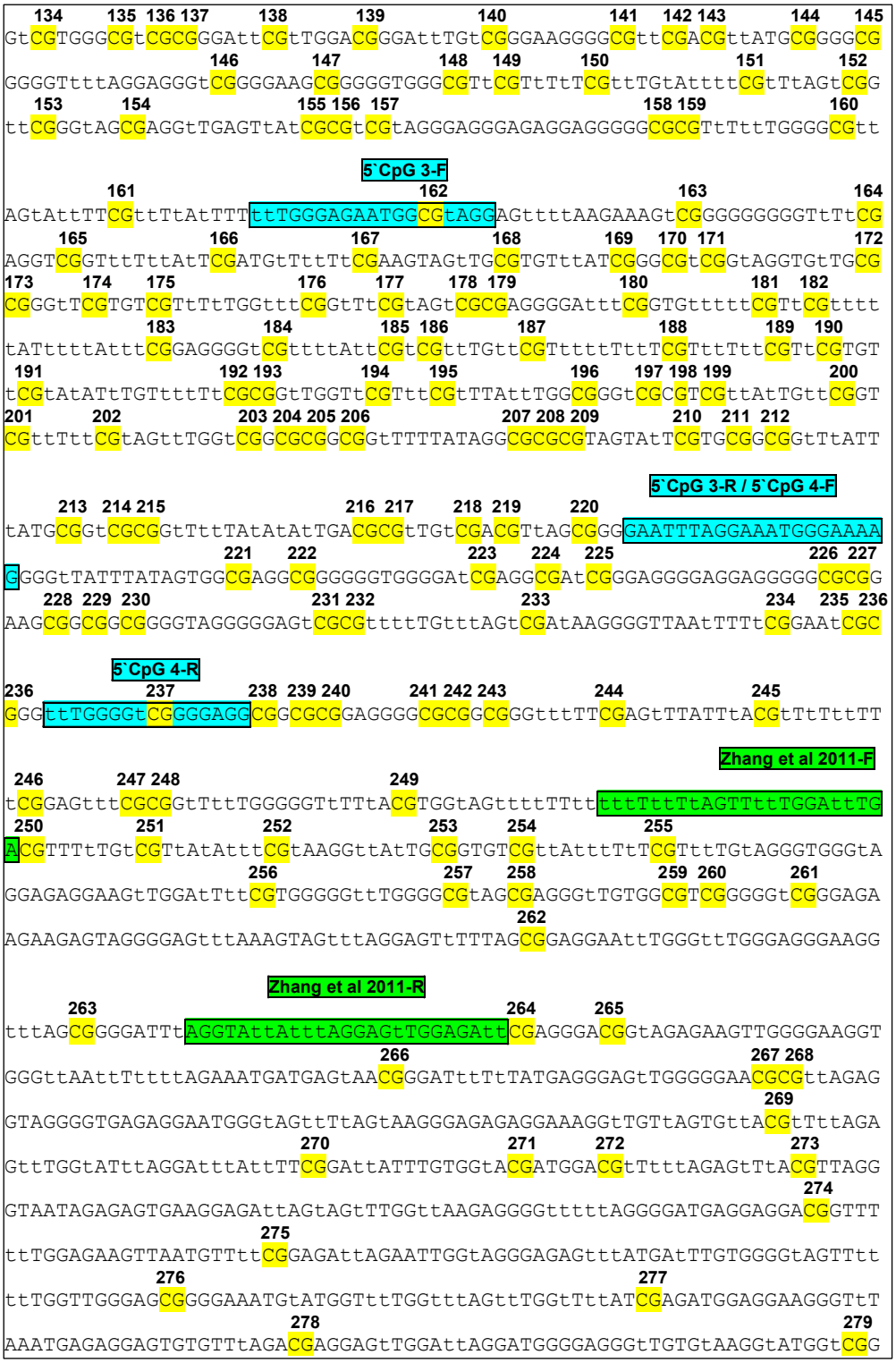

Supplementary Figure 1b: Sodium bisulfite-modified DNA sequence of the 5`genomic region of *miR-132/miR-212* indicating CpG sites 134 to 279.

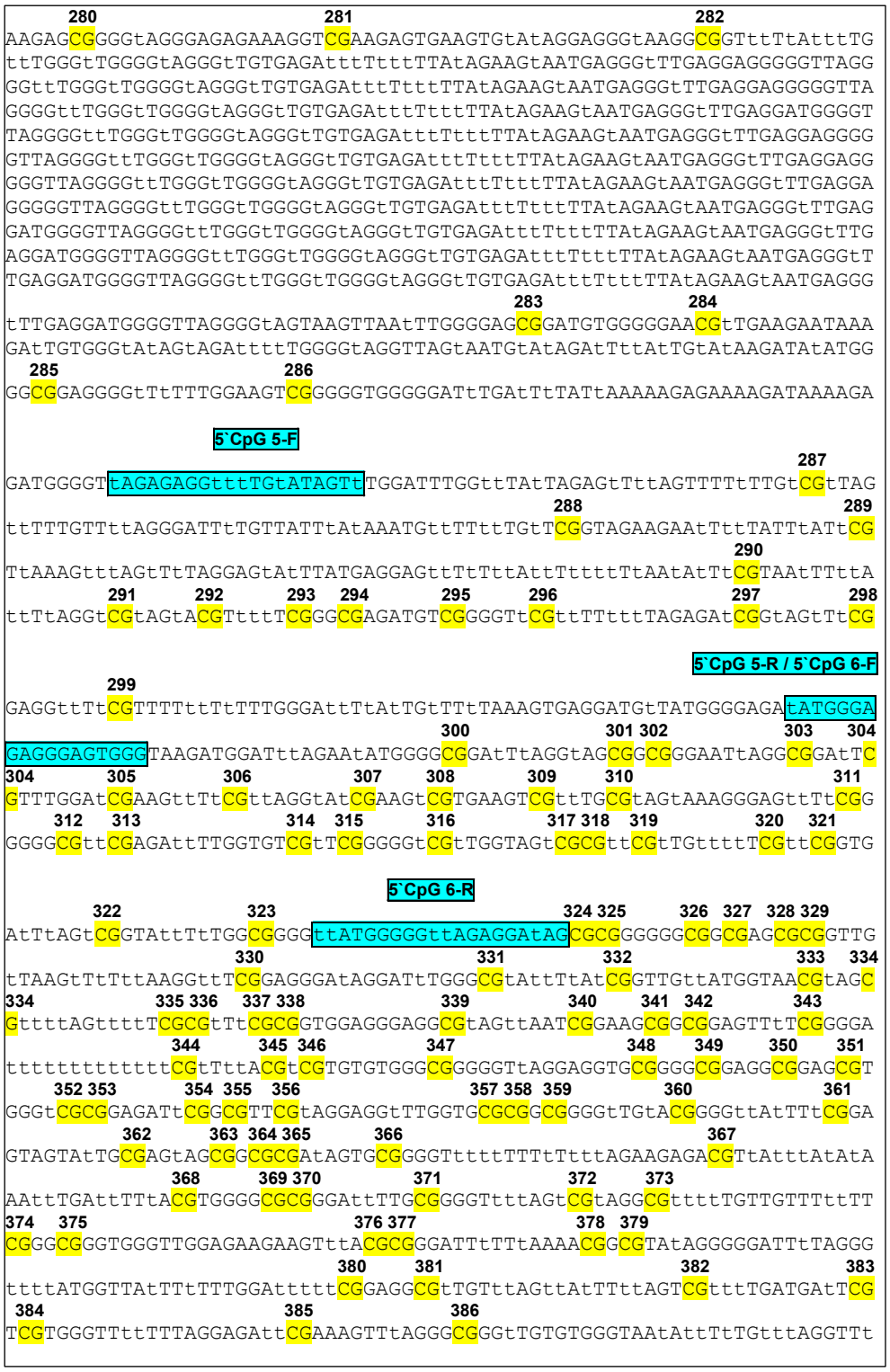

Supplementary Figure 1c: Sodium bisulfite-modified DNA sequence of the 5`genomic region of *miR-132/miR-212* indicating CpG sites 280 to 386.

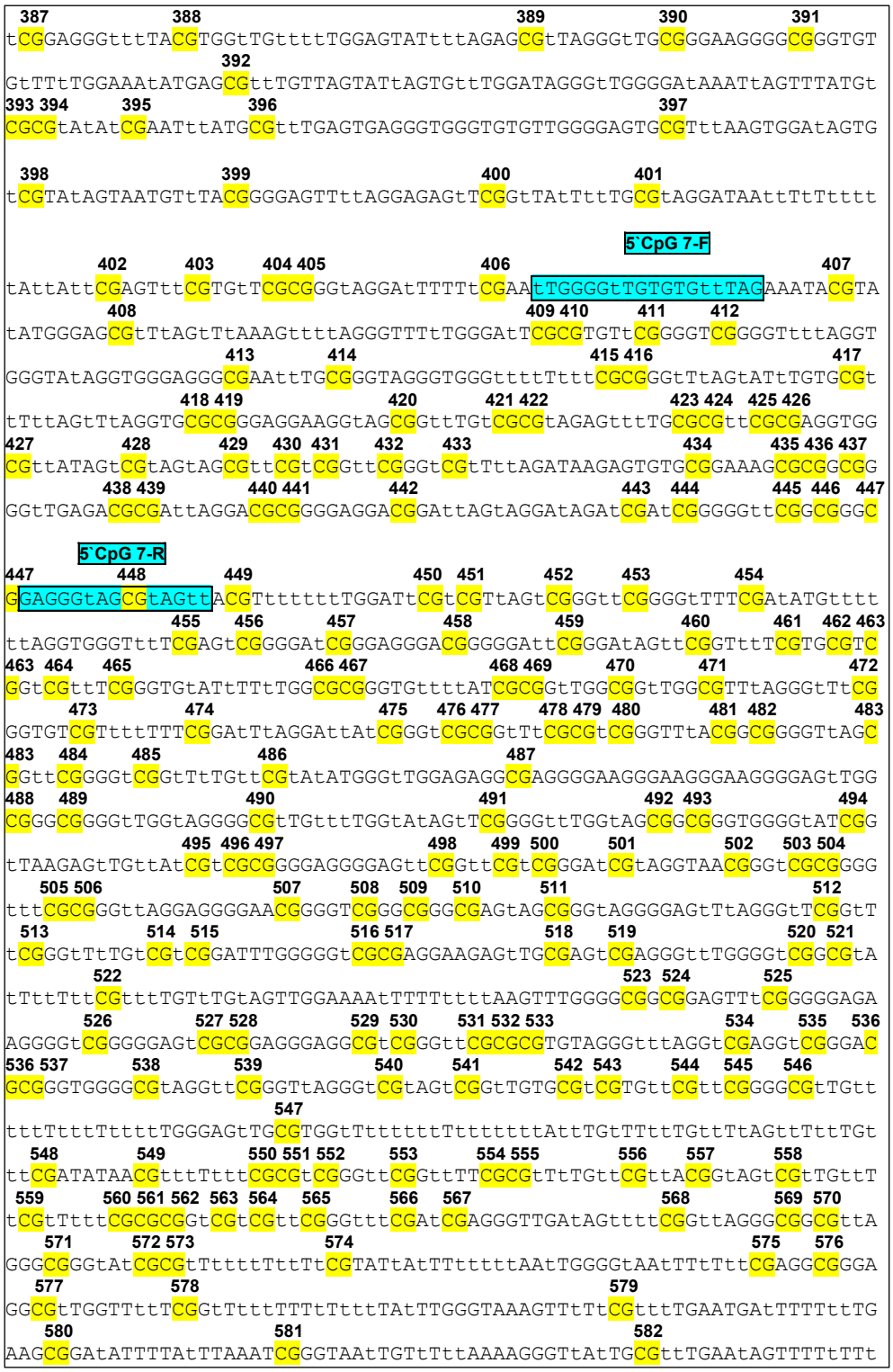

Supplementary Figure 1d: Sodium bisulfite-modified DNA sequence of the 5`genomic region of *miR-132/miR-212* indicating CpG sites 387 to 582.

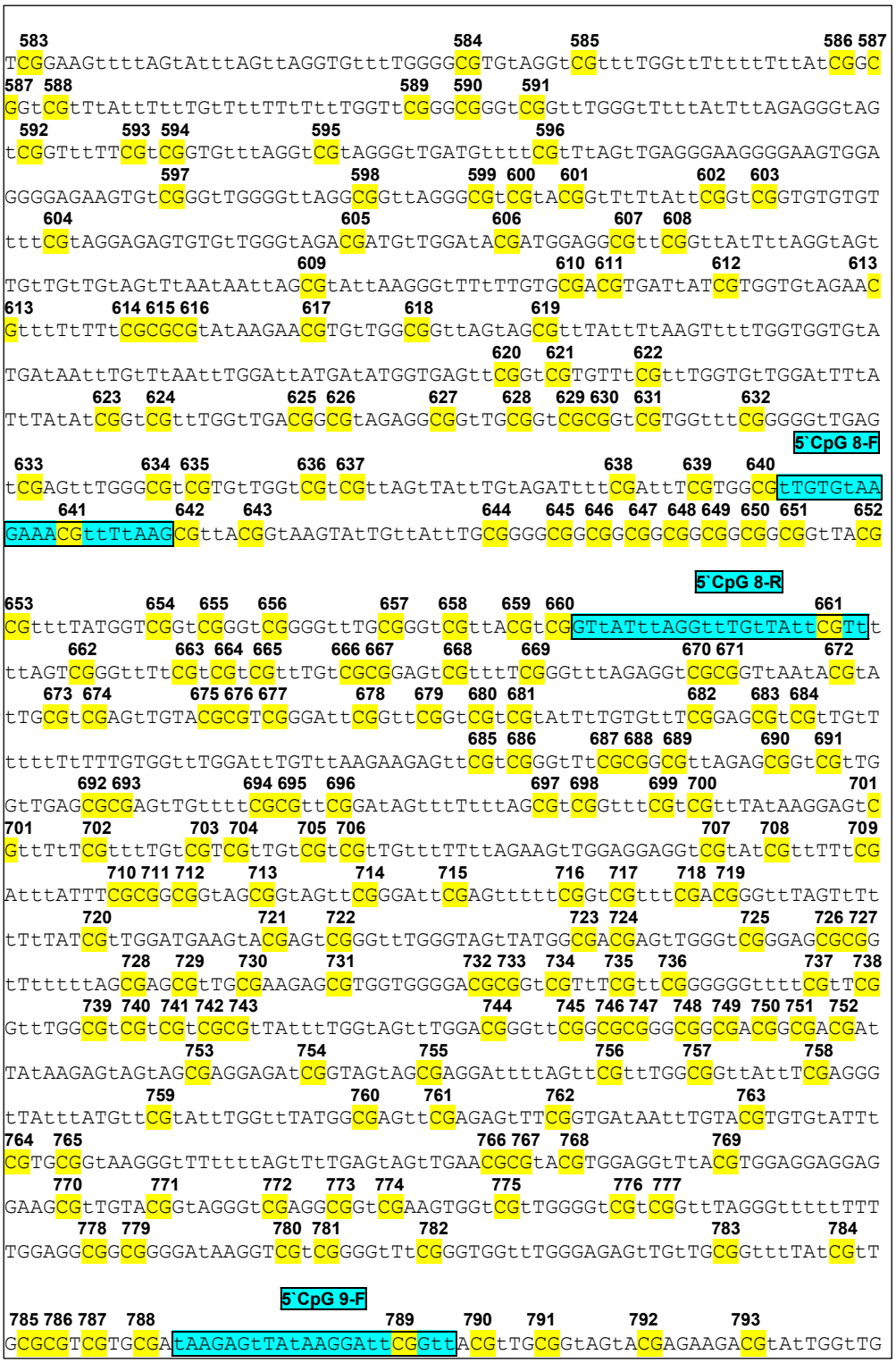

Supplementary Figure 1e: Sodium bisulfite-modified DNA sequence of the 5`genomic region of *miR-132/miR-212* indicating CpG sites 583 to 793.

Supplementary Figure 1f: Sodium bisulfite-modified DNA sequence of the 5`genomic region of *miR-132/miR-212* indicating CpG sites 794 to 886.

5`genomic region of *miR-126 (CpG island 1)* (CpG sites 1 to 294)

Position:chr9:139557805-139563005 band: 9q34.3 (2000 extra bases upstream 5`and upstream 3`) according to UCSC Genome Browser, created by the Genome Bioinformatics Group of UC Santa Cruz; version February 2009

Sodium bisulfite-modified DNA sequence and investigated primers used for bisulfite sequencing according to Figure 33: 5`CpG-rich genomic region of *miR-126* and its host gene *EGFL7*.

```
          1                                                    2
ttttAGTCGttttTttttTGAAttttAtttTtTGGttTTTtTtTtttTtCGtAGAGtAGttttTGTG
                                    3                  4 5   6      7       8
GTTGGtAGtAAAGTTtAGtTTGGtTGGGttCGtTGTGAGGGGtTTCGCGtTACGtttTGCGGTGTttC
8                                                   9          10
GAGGGtTGAGGTtTttTtATtTTtTtttTAGtAGTGGATGAGtAAtttAACGGGGGttCGGGAGGGG
          11
AAtTGGtttCGAGGGAGAGGAAttttAAAGttAtATtTGTAGttAGGATGAGtAGTGTGAATttAGGG
   12   13        14                              15
TGCGGGACGTGGGGtTCGGGtTTAGGGATGAtTTGtTGGGTGCGGTGGGtAAATGGGTGAtTtTGTGG
                  16
Gttttttt TTGGAtttTGGAGACGtttTTGTTtTtttTtTttttAGttTtATGtAGAGTGGtTGAAGtt
                                                                  17
ttATtttAAAGttttttAAAAttAtAGTGGGTttTAGAAGGttttAtTTTTTGTtTtATACGTttAtAt
                                                                  18
tAAGAAGttTGTtTGAGAAttttttAtTTTttAAATGGTGttTAGttAGGATGGGGGtAGCGAGGGtTG
    19                        20
AGTCGGGGtAGtttTGGAGtTGtttTTTtTGtTttATCGttTtTTttAGAtTtAGGtAGGAGAGGTGG
                  21
GGAGGtAGGTtAAAGGGTTAAGTGAtCGtAGATttAGAGATGAGGttAGGGGtAGGGGAtAGGGAGGG
    22
TGGCGGTGGtTtTttttAtttAGAGGtttttTAGGttttAtTtTGAAtAtTTtAtTGtTGGGGGtTAGG
                  23                  24                              25
TAAGAGtTGttttTGCGTGGGtTtAGGGCGttAGGAGGttTAGGAtTttttAGTtAGATGAGGAACGtt
                            26                  27
tttTGAtAGtAGtTGtTtTGGTCGTtttTTGGAttACGTGttAGGGGtTTttAGGGttttTGGTttAG
                                    28
AGtAGTGGttAtTGGATTGtAGGGTGGGGCGGtttTtATTTTGGGGAtTttTtTttAGGGAttTGGGtt
                                                        29
ttTtttTTttTttAGtTtttATGtAttAAGGTAGGAttAAGtTGGTGGtttTtTCGGAtttATtTGtA
GGttttTTGtttAGtAtttTGGGTTAtATGGAGAGAttTttAGtTttAtTtAtAGtAGttTtttATtt
                                                                30      31
ttATGttAGGGAGTttAGGGtTGGAGGtAATAAttttATTTTAtTGAGGttAGGGGtTGCGGATtCGA
                                    32
GAGGAtAATtAGtTtAGGAtAGGATGGGGTCGGGGTAGGTGtAGGAtAGGGGttTGTAGGttTAGTGt
    33                  34              35
AGGCGGAGGTtttAtAGtAGtAtCGAAAGtTGGTttCGGGttttTTtttAGtttttAGAtATtAGGGT
                                                              36
GAttAGGAtTGTGtATAGGtAtTAAtttAtAAtTttTtTttAAttAGtAGtttttAGGAtCGGGAGG
                          37                        38                  39
tAtAGGTGGtttttAttAttCGGAGGAGtAGtTttTGttttTGTtCGGGGGATGAtTGATTtTttTtC
39                                  40                        41 42    43 44
GttAGGTGAGTtttAGtAAAttttTTGtTtCGAGGGAAtAtTTtTtAtAtCGGCGtttACGCGGGTTA
              45          46                                      47      48
TGAtAtAGGGCGtTGGtTtCGGtTGGGGTtTGAGGGGtTGtTGAATTGGGtTGGttCGAGttttACGT
```

Supplementary Figure 2a: Sodium bisulfite-modified DNA sequence of the 5`genomic region of *miR-126* (CpG island 1) indicating CpG sites 1 to 48.

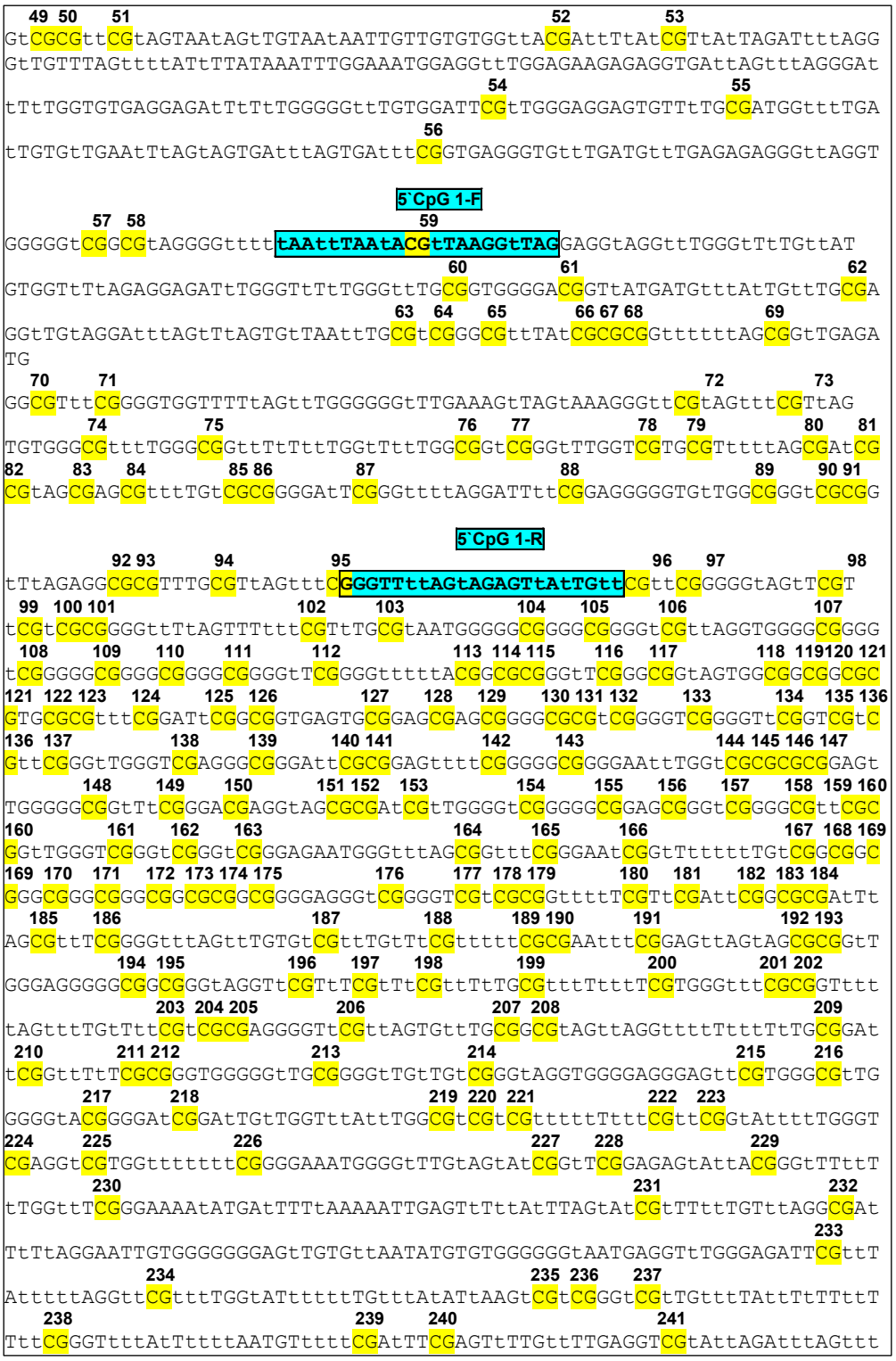

Supplementary Figure 2b: Sodium bisulfite-modified DNA sequence of the 5`genomic region of *miR-126* (CpG island 1) indicating CpG sites 49 to 241.

Supplementary Figure 2c: Sodium bisulfite-modified DNA sequence of the 5`genomic region of *miR-126* (CpG island 1) indicating CpG sites 242 to 294.

5`genomic region of *miR-126 (CpG island 2)* (CpG sites 1 to 95)

Position:139564000-139565286, band: 9q34.3 (1000 extra bases upstream 5`and upstream 3`) according to UCSC Genome Browser, created by the Genome Bioinformatics Group of UC Santa Cruz; version February 2009.

Sodium bisulfite-modified DNA sequence and investigated primers used for bisulfite sequencing according to Figure 33: 5`CpG-rich genomic region of *miR-126* and its host gene *EGFL7*.

Location of the *miR-126 stem-loop* is indicated in red.

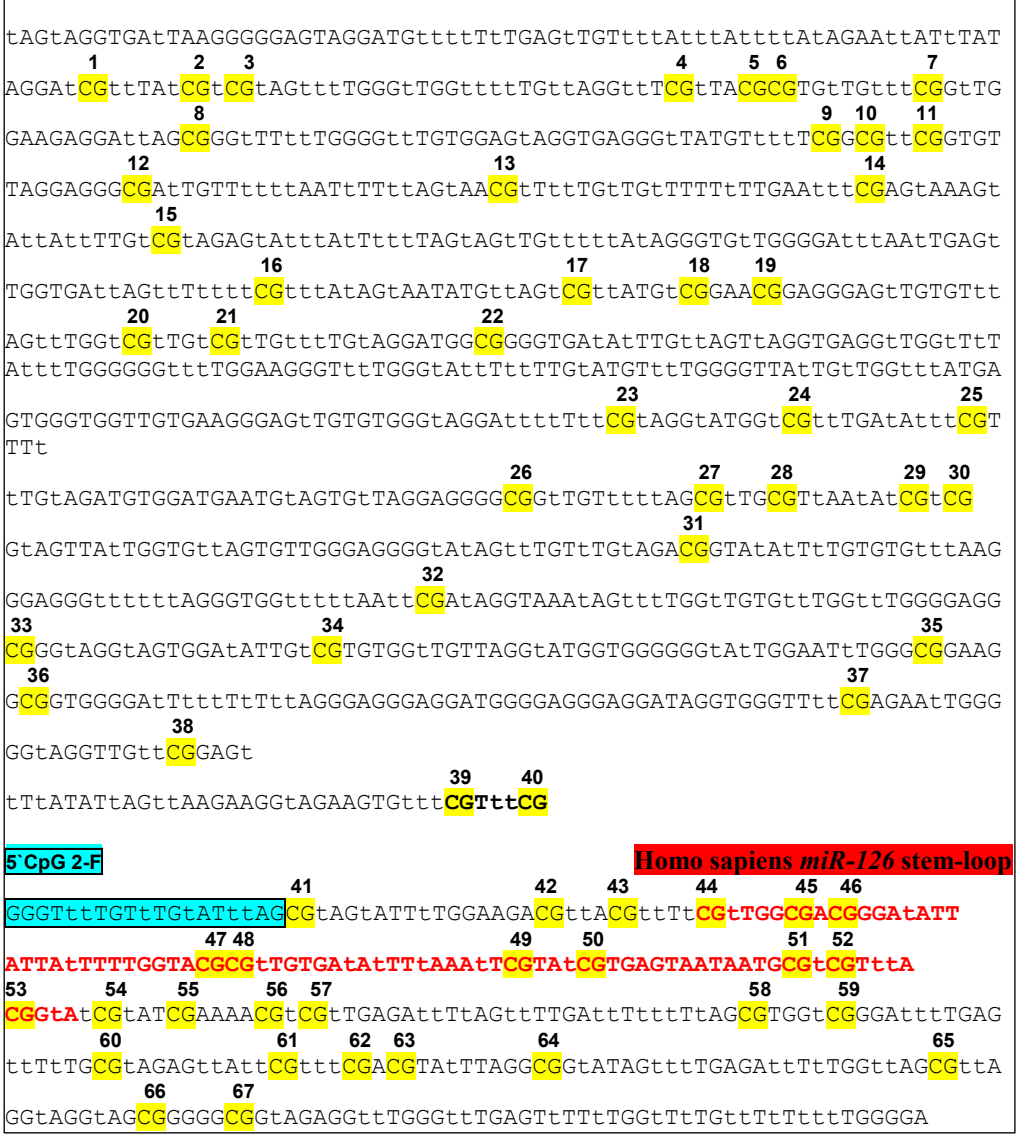

Supplementary Figure 3a: Sodium bisulfite-modified DNA sequence of the 5`genomic region of *miR-126* (CpG island 2) indicating CpG sites 1 to 67.

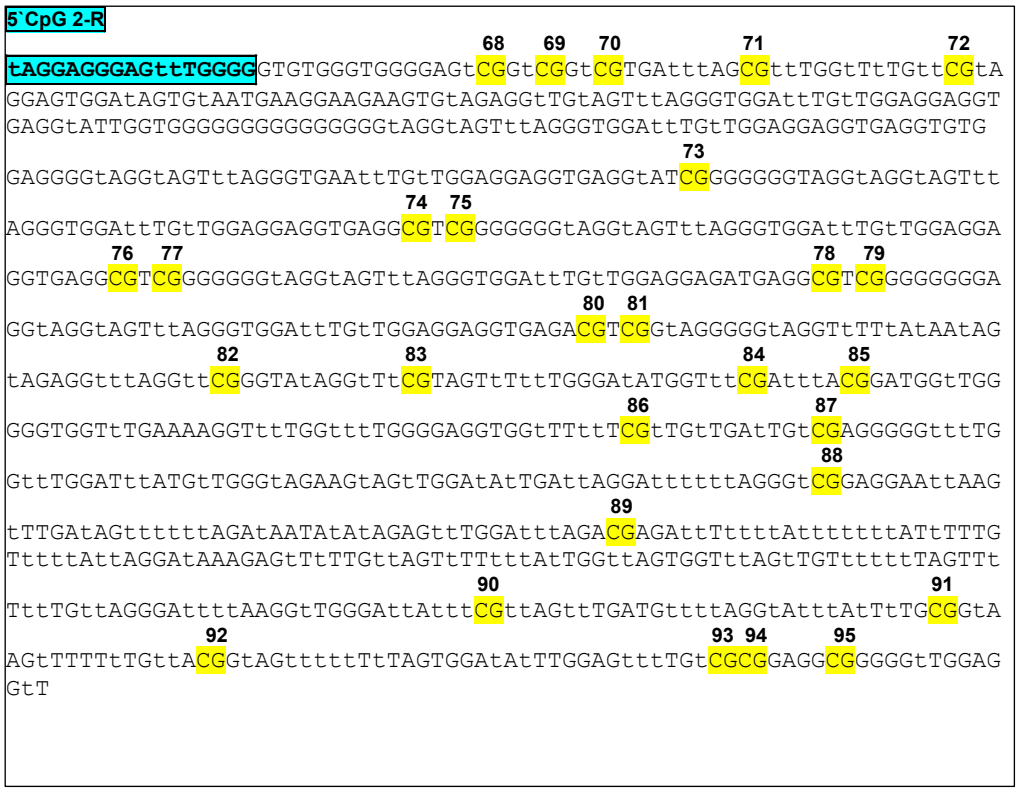

Supplementary Figure 3b: Sodium bisulfite-modified DNA sequence of the 5`genomic region of *miR-126* (CpG island 2) indicating CpG sites 68 to 95.

5`genomic region of *miR-210* (CpG sites 1 to 179)

Position: 567939-569461, band: 11p15.5 according to UCSC Genome Browser, created by the Genome Bioinformatics Group of UC Santa Cruz; version February 2009.

Sodium bisulfite-modified DNA sequence and investigated primers used for bisulfite sequencing according to Figure 36: 5`CpG-genomic region of *miR-210*.

Location of the *miR-210 stem-loop* is indicated in red.

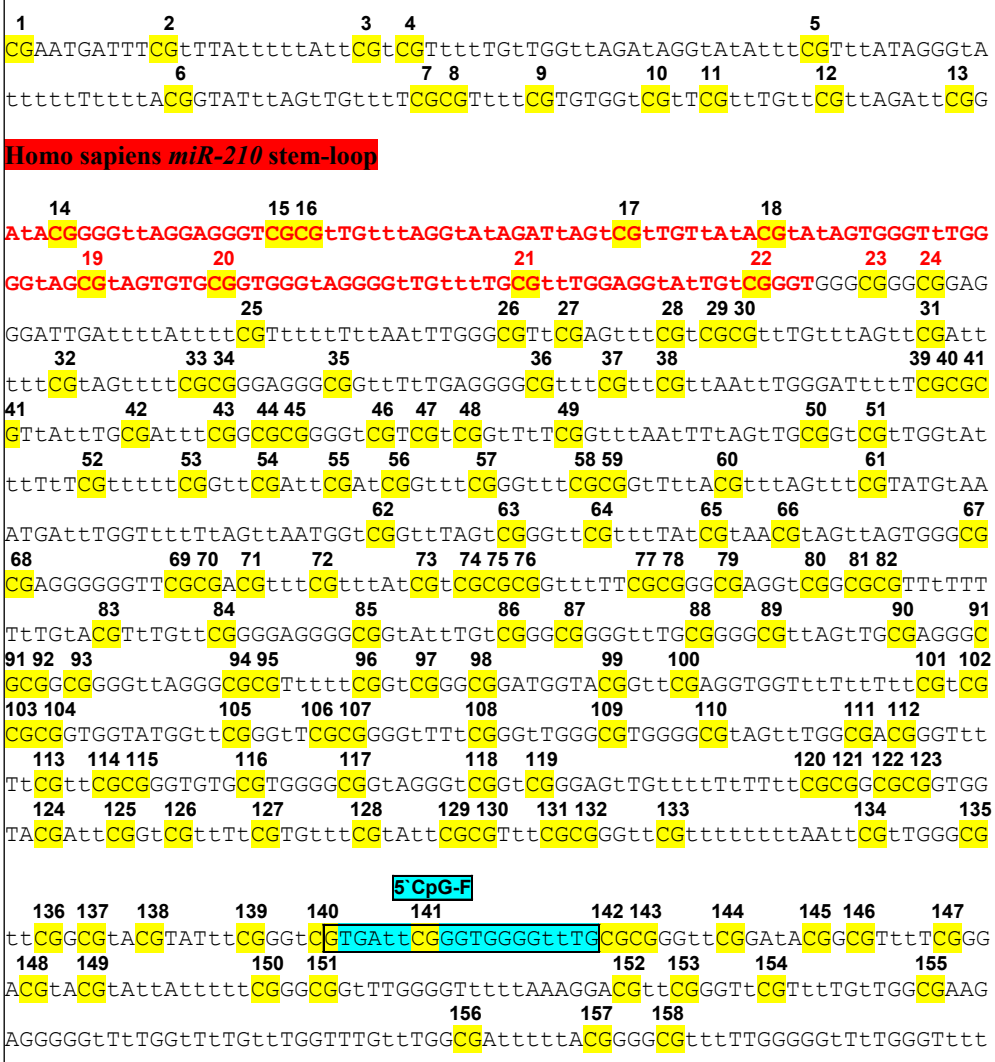

Supplementary Figure 4a: Sodium bisulfite-modified DNA sequence of the 5`genomic region of *miR-210* indicating CpG sites 1 to 158.

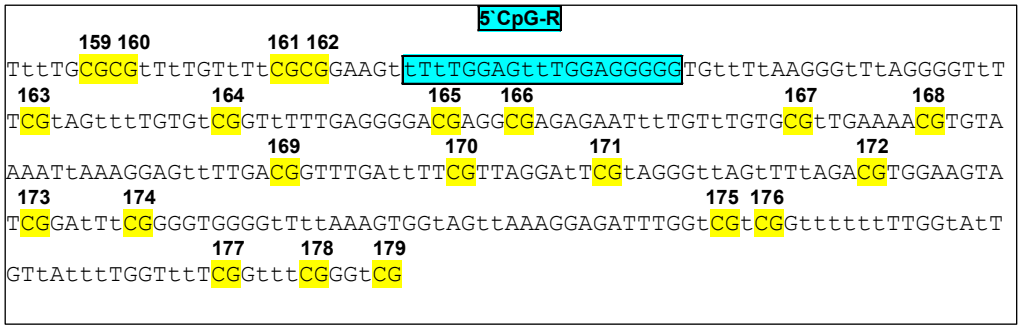

Supplementary Figure 4b: Sodium bisulfite-modified DNA sequence of the 5`genomic region of *miR-210* indicating CpG sites 159 to 179.

5`genomic region of *miR-132/miR-212* (CpG island spanning CpG sites 1 to 886; investigated DNA region from CpG site 1 to CpG site 253 are listed below

Position: chr17 :1952920-1962328; band: 17p13.3 according to UCSC Genome Browser, created by the Genome Bioinformatics Group of UC Santa Cruz; version February 2009.

Genomic DNA sequence and investigated primers used for quantitative real-time PCR analysis following ChIP analysis according to Figure 28: Schematic structure of the genomic region surrounding the *miR-132/miR-212* cluster.

Location of the *miR-132/miR-212 stem-loop* cluster is indicated in red.

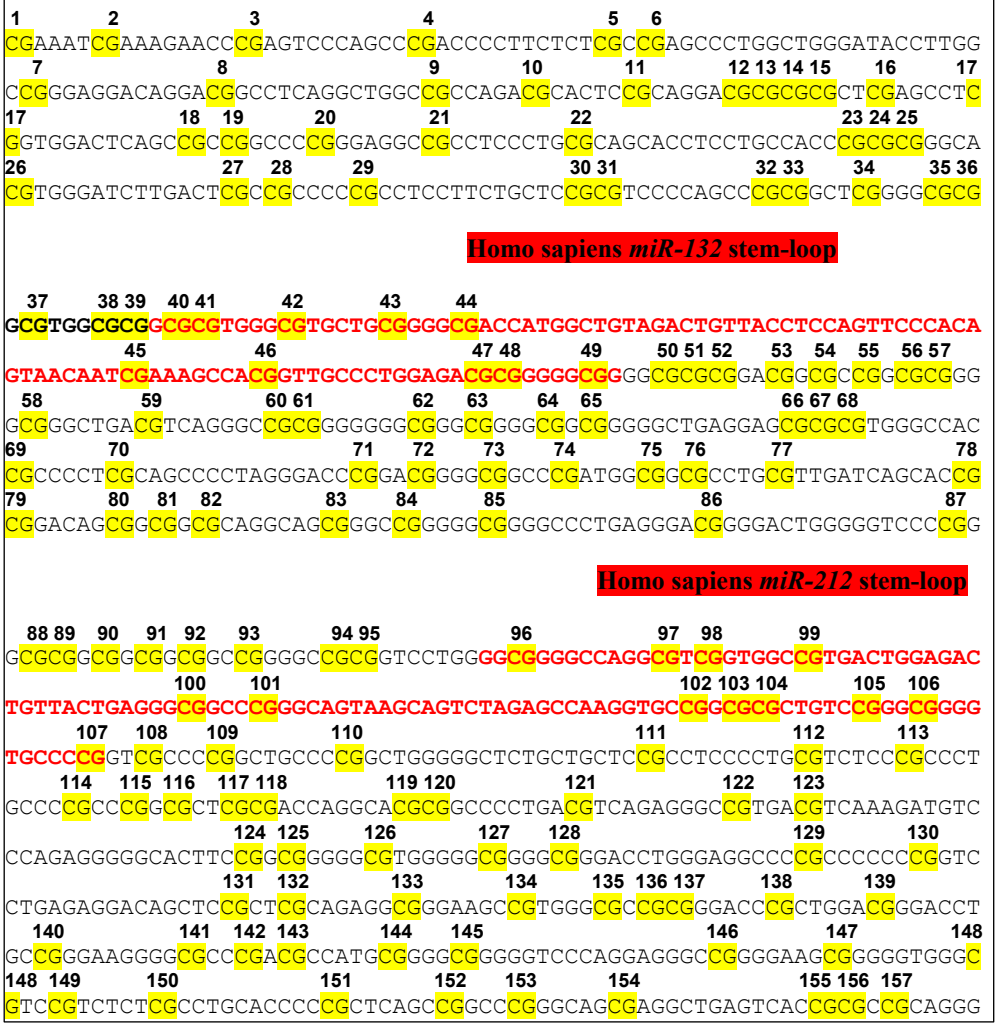

Supplementary Figure 5a: Sodium bisulfite-modified DNA sequence of the 5`genomic region of *miR-132/miR-212* indicating CpG sites 1 to 157.

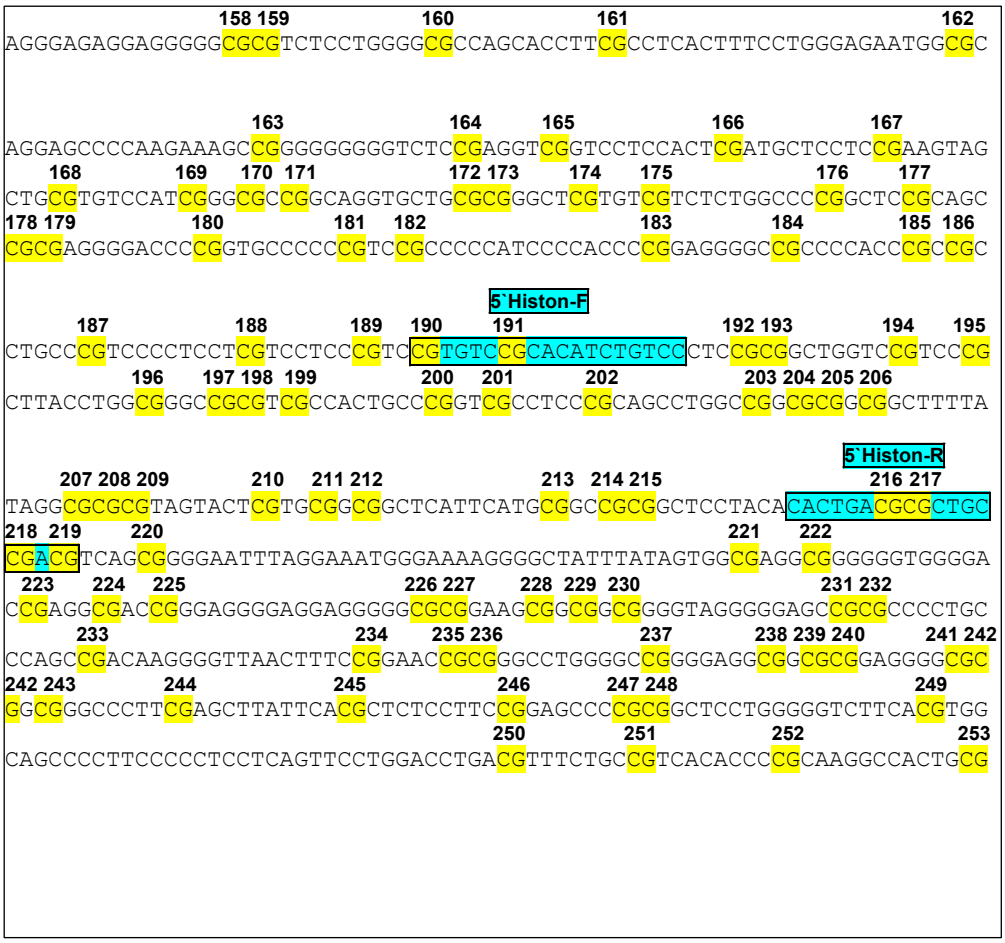

Supplementary Figure 5b: Sodium bisulfite-modified DNA sequence of the 5`genomic region of *miR-132/miR-212* indicating CpG sites 158 to 253.

5`genomic region of *miR-126 (CpG island 1)* (CpG sites 1 to 294)

Position:chr9:139557805-139563005 band: 9q34.3 (2000 extra bases upstream 5`and upstream 3`) according to UCSC Genome Browser, created by the Genome Bioinformatics Group of UC Santa Cruz; version February 2009.

Genomic DNA sequence and investigated primers used for quantitative real-time PCR analysis following ChIP analysis according to Figure 33: 5`CpG-rich genomic region of *miR-126* and its host gene *EGFL7*. Additionally, primers used by Saito and colleagues are indicated in pink (Saito et al 2009).

```
          1                                                    2
CCCCCAGTCGCCCTTCCCCTGAACCCCACCCTCTGGCCTTTCTCTCCCTCCGCAGAGCAGCCCCTGTG
                                    3                 4 5    6       7       8
GTTGGCAGCAAAGTTCAGCTTGGCTGGGCCCGCTGTGAGGGGCTTCGCGCTACGCCCTGCGGTGTCCC
8                                                     9       10
GAGGGCTGAGGTCTCCTCATCTTCTCCCTAGCAGTGGATGAGCAACCCAACGGGGGCCCGGGGAGGGG
          11
AACTGGCCCCGAGGGAGAGGAACCCCAAAGCCACATCTGTAGCCAGGATGAGCAGTGTGAATCCAGGG
   12    13         14                              15
TGCGGGACGTGGGGCTCGGCTTAGGGATGACTTGCTGGGTGCGGTGGGCAAATGGGTGACTCTGTGG
                        16
GCCCCCCTTGGACCCTGGAGACGCCCTTGTTCTCCCTCTCCCCAGCCTCATGCAGAGTGGCTGAAGCC
                                                                  17
CCATCCCAAAGCCCCCAAAACCACAGTGGGTCCTAGAAGGCCCCACTTTTTGTCTCATACGTCCACAC
                                                                  18
CAAGAAGCCTGTCTGAGAACCCCCACTTTCCAAATGGTGCCTAGCCAGGATGGGGGCAGCGAGGGCTG
    19                                    20
AGTCGGGGCAGCCCTGGAGCTGCCCTTTCTGCTCCATCGCCTCTTCCAGACTCAGGCAGGAGAGGTGG
                                  21
GGAGGCAGGTCAAAGGGTTAAGTGACCGCAGATCCAGAGATGAGGCCAGGGGCAGGGGACAGGGAGGG
    22
TGGCGGTGGCTCTCCCACCCAGAGGCCCCCTAGGCCCCACTCTGAACACTTCACTGCTGGGGGCTAGG
                23                  24                                  25
TAAGAGCTGCCCTGCGTGGGCTCAGGGCGCCAGGAGGCCTAGGACTCCCCAGTCAGATGAGGAACGCC
                              26                27
CCCTGACAGCAGCTGCTCTGGTCGTCCCTTGGACCACGTGCCAGGGGCTTCCAGGGCCCCTGGTCCAG
                                        28
AGCAGTGGCCACTGGATTGCAGGGTGGGGCGGCCTCATTTTGGGGACTCCTCTCCAGGGACCTGGGCC
                                                            29
CCTCCCTTCCTCCAGCTCCCATGCACCAAGGTAGGACCAAGCTGGTGGCCCTCTCGGACCCATCTGCA
GGCCCCTTGCCCAGCACCCTGGGTTACATGGAGAGACCTCCAGCTCCACTCACAGCAGCCTCCCATCC
                                                                30      31
CCATGCCAGGGAGTCCAGGGCTGGAGGCAATAACCCCATTTTACTGAGGCCAGGGGCTGCGGATCCGA
                                        32
GAGGACAATCAGCTCAGGACAGGATGGGGTCGGGGTAGGTGCAGGACAGGGGCCTGTAGGCCTAGTGC
    33                        34              35
AGGCGGAGGTCCCACAGCAGCACCGAAAGCTGGTCCCGGGCCCCTTCCCAGCCCCCAGACATCAGGGT
                                                                  36
GACCAGGACTGTGCATAGGCACTAACCCACAACTCCTCTCCAACCAGCAGCCCCCAGGACCGGGGAGG
```

Supplementary Figure 6a: Sodium bisulfite-modified DNA sequence of the 5`genomic region of *miR-126* (CpG island 1) indicating CpG sites 1 to 36.

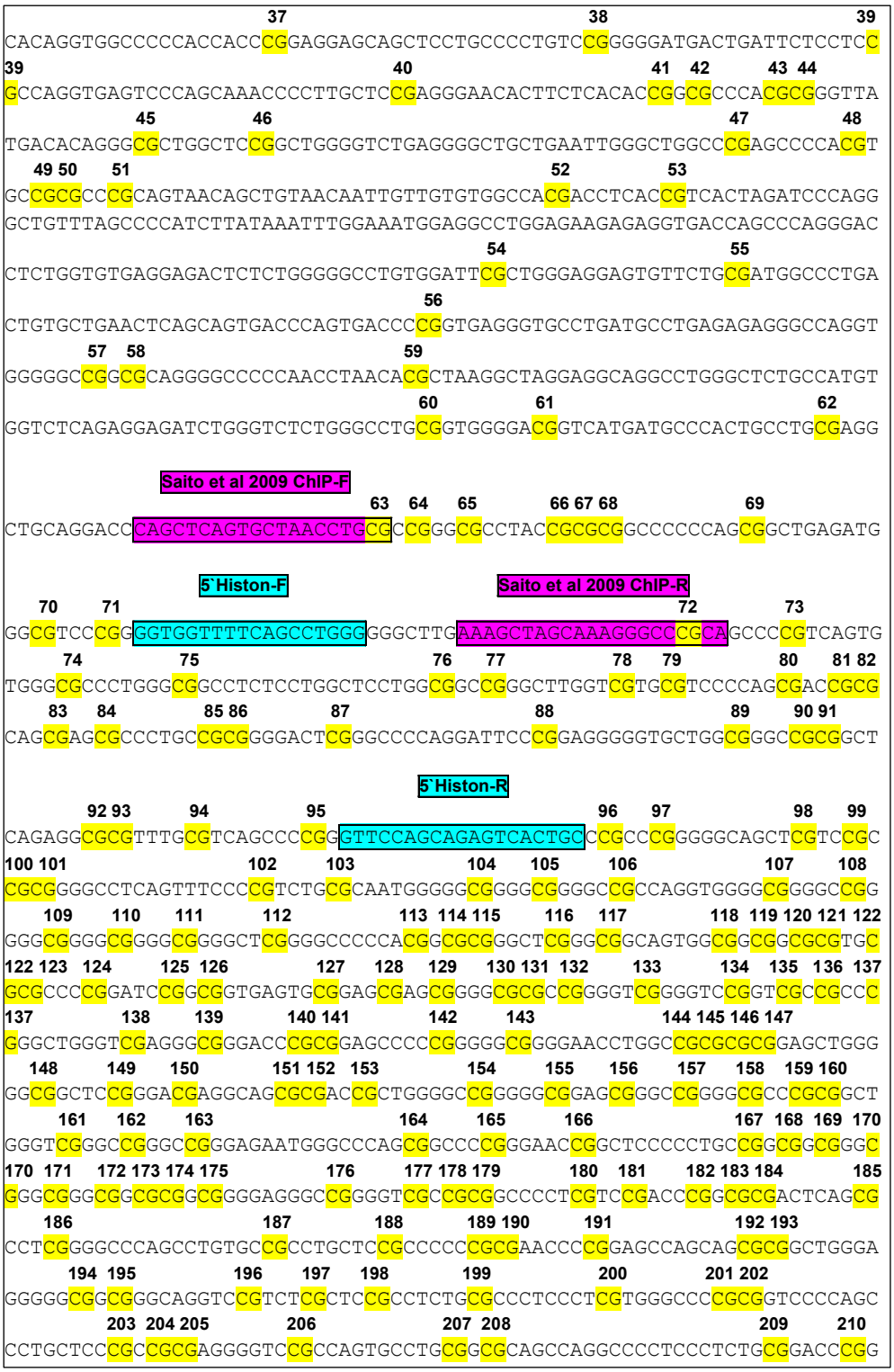

Supplementary Figure 6b: Sodium bisulfite-modified DNA sequence of the 5`genomic region of *miR-126* (CpG island 1) indicating CpG sites 37 to 210.

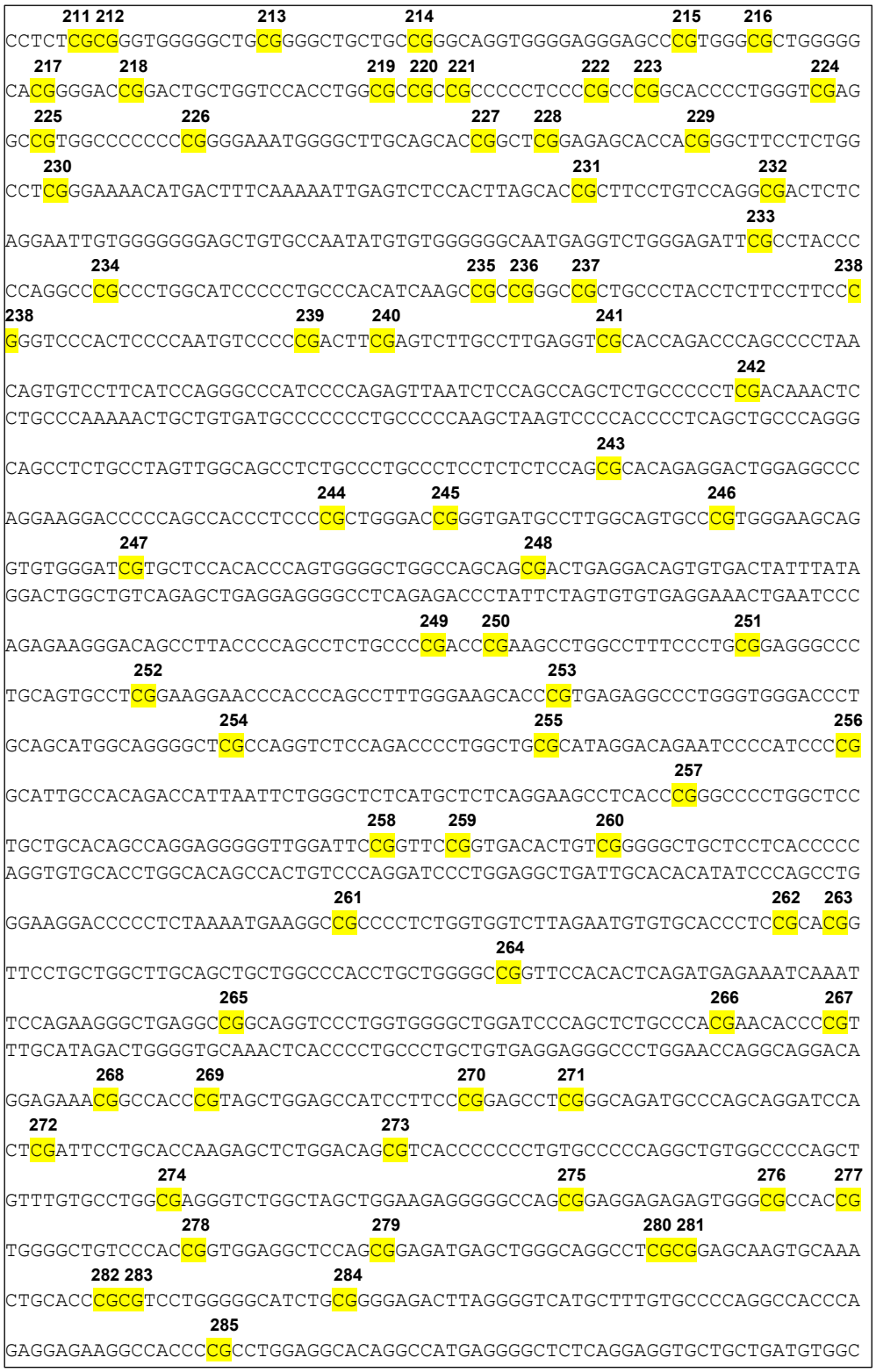

Supplementary Figure 6c: Sodium bisulfite-modified DNA sequence of the 5`genomic region of *miR-126* (CpG island 1) indicating CpG sites 211 to 285.

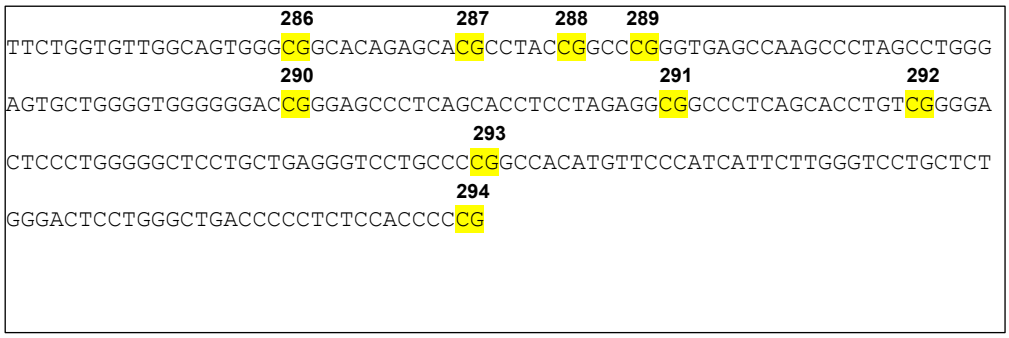

Supplementary Figure 6d: Sodium bisulfite-modified DNA sequence of the 5`genomic region of *miR-126* (CpG island 1) indicating CpG sites 286 to 294.

A)

controls/cell lines	CpG sites 7	8	9	10	11	12	13	14	15	16	17	18	19	20	21	22	23	24	25	26	27	28	29	30	31	32	33	34	35
controls																													
hypermethylated DNA	3	3	3	3	3	3	3	3	3	3	3	3	3	3	3	3	3	3	3	3	3	3	3	3	3	3	3	3	3
NB1	0	0	0	0	0	0	0	0	0	0	0	0	0	0	0	0	0	0	0	0	0	0	0	0	0	0	0	0	0
NB3	0	0	0	0	0	0	0	0	0	0	0	0	0	0	0	0	0	0	0	0	0	0	0	0	0	0	0	0	0
NB2	0	0	0	0	0	0	0	0	0	0	0	0	0	0	0	0	0	0	0	0	0	0	0	0	0	0	0	0	0
cell lines																													
A172 co	0	0	0	0	0	0	0	0	0	0	0	0	0	0	0	0	0	0	0	0	0	0	0	0	0	0	n.a.	n.a.	n.a.
A172 A+T2	0	0	0	0	0	0	0	0	0	0	0	0	0	0	0	0	0	0	0	0	0	0	0	0	0	0	0	0	0
U138 co	0	0	0	0	0	0	0	0	0	0	0	0	0	0	0	0	0	0	0	0	0	0	0	n.a.	n.a.	n.a.	n.a.	n.a.	n.a.
U138 A+T2	0	0	0	0	0	0	0	0	0	0	0	0	0	0	0	0	0	0	0	0	0	0	0	0	n.a.	n.a.	n.a.	n.a.	n.a.
T98G co	0	0	0	0	0	0	0	0	0	0	0	0	0	0	0	0	0	0	0	0	0	0	0	n.a.	n.a.	n.a.	n.a.	n.a.	n.a.
T98G A+T2	0	0	0	0	0	0	0	0	0	0	0	0	0	0	0	0	0	0	0	0	0	0	0	n.a.	n.a.	n.a.	n.a.	n.a.	n.a.
TP365MG co	0	0	0	0	0	0	0	0	2	0	0	0	0	0	0	0	0	0	0	0	0	0	0	n.a.	n.a.	n.a.	n.a.	n.a.	n.a.
TP365MG A+T2	0	0	0	0	0	0	0	0	2	0	0	0	0	0	0	0	0	0	0	0	0	0	0	n.a.	n.a.	n.a.	n.a.	n.a.	n.a.

NB1 = human normal brain (BioChain Institute)
NB2 = human fetal brain (BioChain Institute)
NB3 = human normal brain occipital lobe (BioChain Institute)

co = control = non-treated cells
A+T2 = cells treated with 5-aza-2`-deoxycytidine and trichostatin A

0 not methylated
2 moderately methylated
3 strongly methylated
n.a. not analyzed

B)

controls/cell lines	CpG sites 87	88	89	90	91	92	93	94	95	96	97	98	99	100	101	102	103	104	105	106	107	108	109	110	111	112	113	114	115	116	117	118	119	120
controls																																		
hypermethylated DNA	3	3	3	3	3	3	3	3	3	3	3	3	3	3	3	3	3	3	3	3	3	3	3	3	3	3	3	3	3	3	3	3	3	3
NB1	0	0	0	0	0	0	0	2	0	0	0	0	0	0	0	0	0	0	0	0	0	0	0	0	0	0	0	0	0	0	0	0	0	0
NB2	0	0	0	0	0	0	0	0	0	0	0	0	0	0	0	0	0	0	0	0	0	0	0	0	0	0	0	0	0	n.a.	n.a.	n.a.	n.a.	n.a.
cell lines																																		
A172 co	0	0	0	0	0	0	0	0	0	0	0	0	0	0	0	0	0	0	0	0	0	0	0	0	0	0	0	0	0	0	0	0	0	0
A172 A+T2	0	0	0	0	0	0	0	0	0	0	0	0	0	0	0	0	0	0	0	0	0	0	0	0	0	0	0	0	0	0	0	0	0	0
T98G co	0	0	0	0	0	0	0	0	0	0	0	0	0	0	0	0	0	0	0	0	0	0	0	0	0	0	0	0	0	0	0	0	0	0
T98G A+T2	0	0	0	0	0	0	0	0	0	0	0	0	0	0	0	0	0	0	0	0	0	0	0	0	0	0	0	0	0	0	0	0	0	0
TP365MG co	0	0	0	0	0	0	0	0	0	0	0	0	0	0	0	0	0	0	1	0	0	0	0	0	0	0	0	0	0	0	0	0	0	0
TP365MG A+T2	n.a.	n.a.	n.a.	1	0	1	0	0	0	0	0	0	0	0	0	0	0	0	0	0	0	0	0	0	0	0	0	0	0	n.a.	n.a.	n.a.	n.a.	n.a.

NB1 = human normal brain (BioChain Institute)
NB2 = human fetal brain (BioChain Institute)

co = control = non-treated cells
A+T2 = cells treated with 5-aza-2`-deoxycytidine and trichostatin A

0 not methylated
1 weakly methylated
2 moderately methylated
3 strongly methylated
n.a. not analyzed

Supplementary Figure 7: Methylation patterns in the two genomic regions (CpG 7-35 (A) and CpG 87-120 (B)) located in the *miR-132/miR-212*-associated CpG island on 17p13.3 in glioblastoma cell lines as well as samples of non-neoplastic brain tissue samples (NB1 - NB3). Methylation analysis was performed by bisulfite sequencing of the respective PCR products. **A)** Fragment 1 covers 29 CpGs (CpG 7 to 35),and **B)** fragment 2 covers 34 CpGs (CpG 87 to 120) between 1952920-1962328 on chromosome band 17p13.3 (UCSC Genome Browser, version February 2009). The results of the DNA methylation analysis are represented in a 4-tiered semi quantitative grey-scale pattern as indicated below the figure; white square: not methylated (0-25%), light grey: weakly methylated (26-50%), grey: moderately methylated (51-75%) and dark grey: strongly methylated (76-100%) (Tews et al 2007), n.a. = not analysed, hypermethylated DNA = *in vitro* methylated positive control. **Note:** There was no methylation in both investigated DNA fragments in control brain tissues and glioma cell lines.

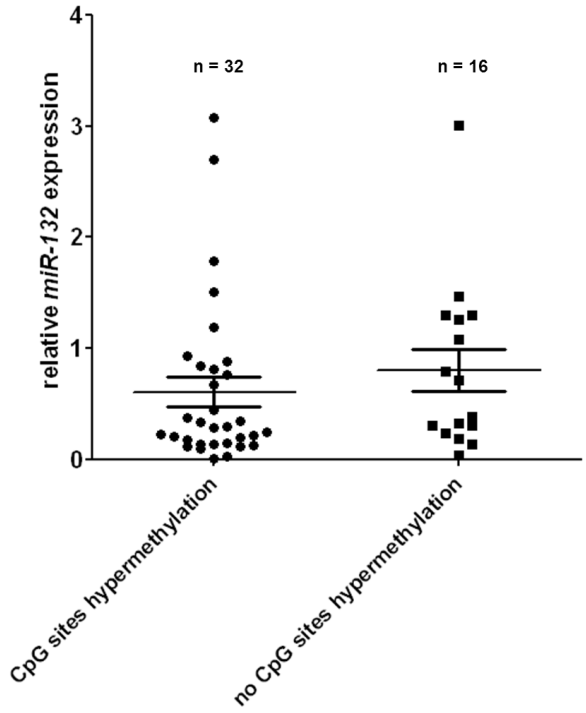

Supplementary Figure 8: *MiR-132* expression analysis in human gliomas in relation to the methylation status of the genomic region 3 (CpG 181-215). Each tumour was assigned to one of two groups: low, no *miR-132/miR-212* hypermethylation (methylation score 1, 2 or 3 in < 50% of the investigated CpG sites) or high, *miR-132/miR-212* hypermethylation (methylation score 1, 2 or 3 in ≥ 50% of the investigated CpGsites). **Note:** methylation at CpG sites 181-215 was not significantly associated with lower *miR-132* expression.

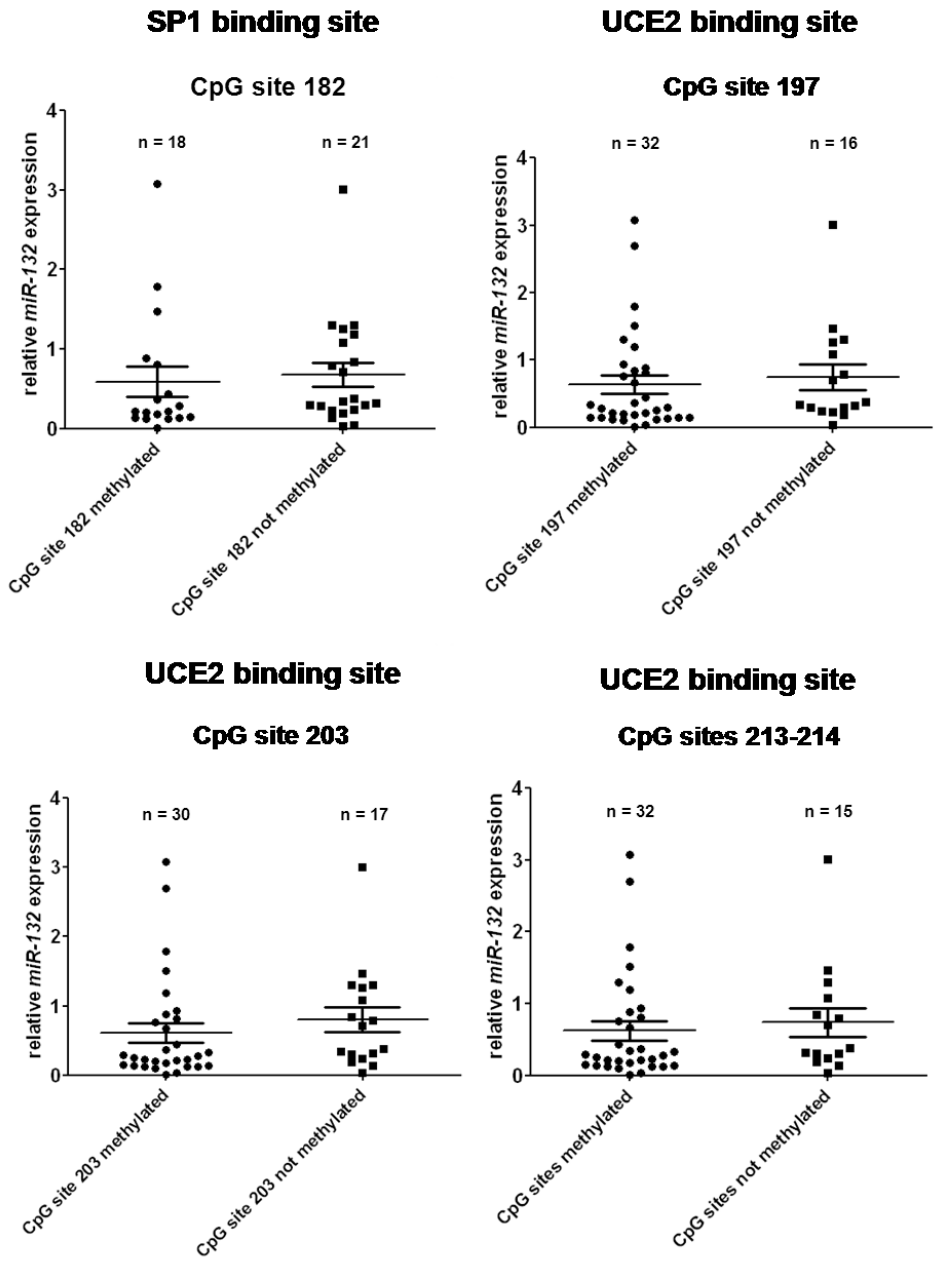

Supplementary Figure 9: *MiR-132* expression analysis in human gliomas in relation to the methylation status of the CpG sites 182, 197, 203 and 213-214. Note: There was no association between methylation at any of the four transcription factor binding sites and *miR-132* expression.

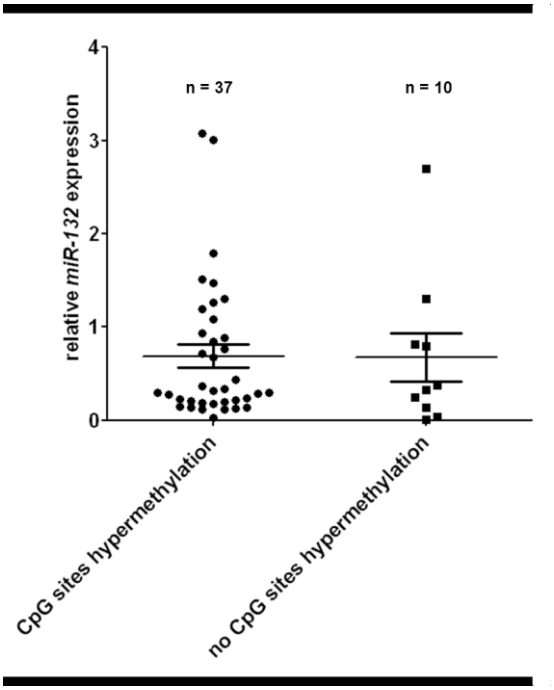

Supplementary Figure 10: *MiR-132* expression analysis in human gliomas in relation to the methylation status of the genomic region 4 (CpG sites 221-232). Each tumour was assigned to one of two groups: low, no *miR-132/miR-212* hypermethylation (methylation score 1, 2 or 3 in < 50% of the investigated CpG sites) or high, *miR-132/miR-212* hypermethylation (methylation score 1, 2 or 3 in ≥ 50% of the investigated CpGsites). **Note:** There was no association between methylation and *miR-132* expression.

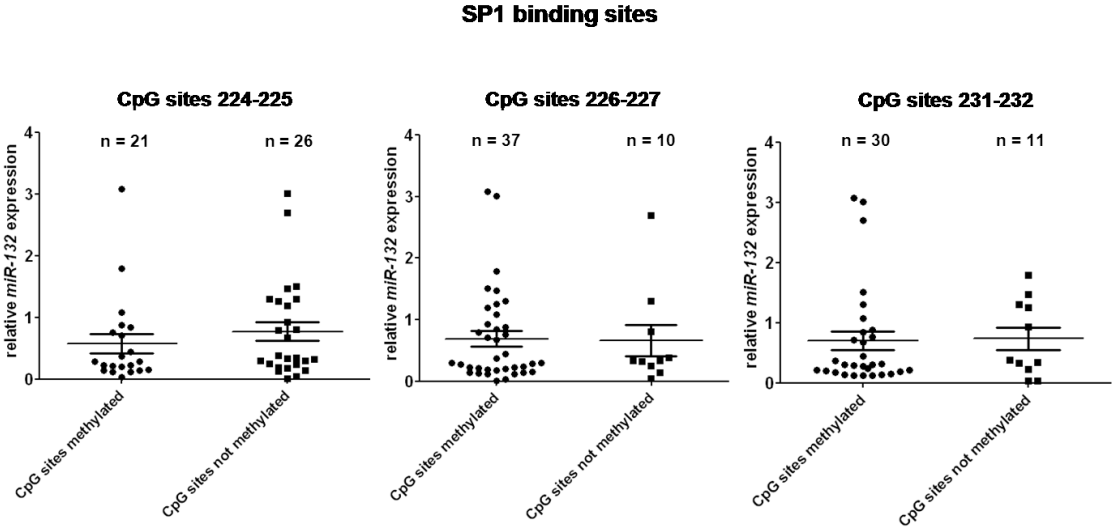

Supplementary Figure 11: *MiR-132* expression analysis in human gliomas in relation to the methylation status of CpG sites 224-225, CpG sites 226-227 and CpG sites 231-232. Note: There was no association between methylation at any of the three SP1 transcription factor binding sites and *miR-132* expression.

	CpG sites												
controls/cell lines/case no.	287	288	289	290	291	292	293	294	295	296	297	298	299
controls													
hypermethylated DNA	3	3	3	3	3	3	3	3	3	3	3	3	3
NB1	3	3	2	3	2	2	2	2	3	3	2	2	0
NB3	3	3	2	3	2	2	2	3	3	3	2	2	0
NB2	3	2	1	2	2	1	1	2	2	3	1	0	0
cell lines													
A172 co	3	3	3	3	3	3	3	3	3	3	3	3	3
A172 A+T2	3	3	3	3	3	3	3	3	3	3	3	3	n.a.
U138 co	3	3	2	3	3	3	3	3	3	3	3	n.a.	n.a.
U138 A+T2	3	3	2	3	3	3	3	3	3	3	3	3	3
T98G co	3	3	2	3	3	3	3	3	3	3	3	3	2
T98G A+T2	3	3	2	3	3	3	3	3	3	3	3	3	2
TP365MG co	3	2	1	3	3	3	3	3	3	3	3	2	2
TP365MG A+T2	3	2	1	3	3	3	2	3	3	3	n.a.	n.a.	n.a.
pGBIV													
GB825	3	3	0	2	2	2	2	2	2	2	3	2	2
GB260	3	3	2	3	2	2	2	3	3	3	3	2	2
GB969	3	2	1	2	2	2	2	2	2	2	2	1	n.a.
GB982	3	3	2	2	2	3	2	3	3	3	3	2	2
sGBIV													
GB4	3	2	2	3	2	2	2	3	3	2	3	2	2
GB989	3	3	2	3	3	3	3	3	3	3	3	3	3
GB834	3	3	3	3	3	3	3	3	3	3	3	3	2
GB175	3	2	2	3	3	2	2	3	3	3	n.a.	n.a.	n.a.
GB119	3	3	3	3	3	3	3	3	3	3	3	3	2

NB1 = human normal brain (BioChain Institute)
NB2 = human fetal brain (BioChain Institute)
NB3 = human normal brain occipital lobe (BioChain Institute)

co = control = non-treated cells
A+T2 = cells treated with 5-aza-2`-deoxycytidine and trichostatin A

pGBIV = primary glioblastoma, WHO grade IV
sGBIV = secondary glioblastoma, WHO grade IV

0	not methylated
1	weakly methylated
2	moderately methylated
3	strongly methylated
n.a.	not analyzed

Supplementary Figure 12: Methylation pattern of the 5´-CpG genomic region 5 (CpG 287-299) of *miR-132/miR-212* in nine gliomas and four glioblastoma cell lines as well as three non-neoplastic brain tissue samples (NB1 - NB3). Note: All investigated gliomas, glioblastoma cell lines as well as the non-neoplastic brain tissue samples showed methylated CpG sites in the investigated region.

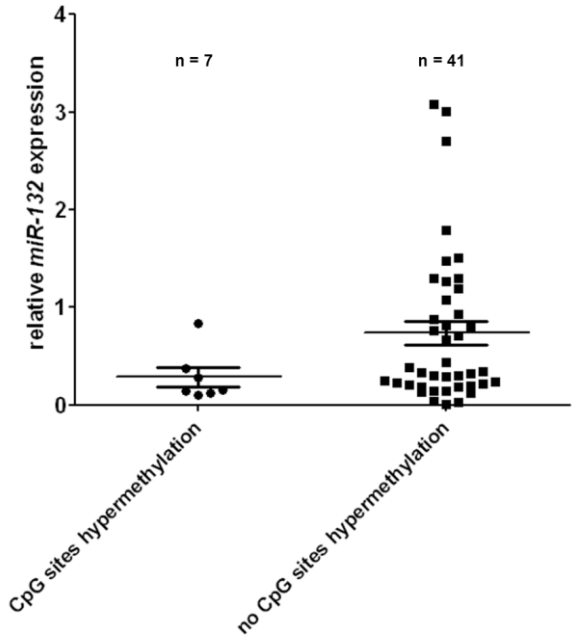

Supplementary Figure 13: *MiR-132* expression analysis in human gliomas in relation to the methylation status of genomic region 6 (CpG sites 300-319). Each tumour was assigned to one of two groups: low, no *miR-132/miR-212* hypermethylation (methylation score 1, 2 or 3 in < 50% of the investigated CpG sites) or high, *miR-132/miR-212* hypermethylation (methylation score 1, 2 or 3 in ≥ 50% of the investigated CpG sites). **Note:** There was no association between methylation and *miR-132* expression.

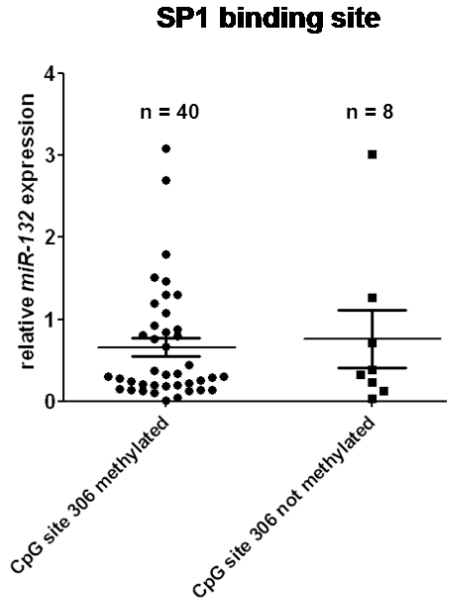

Supplementary Figure 14: *MiR-132* expression analysis in human gliomas in relation to the methylation status of CpG site 306. Note: There was no association between methylation and *miR-132* expression.

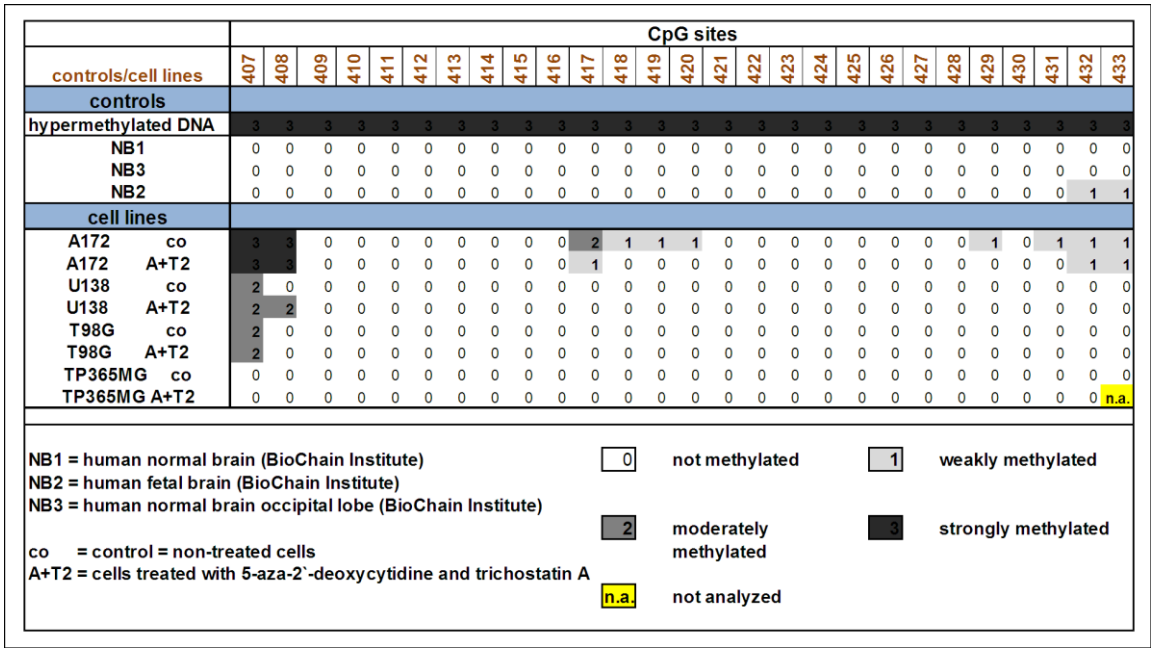

	CpG sites																												
controls/cell lines	407	408	409	410	411	412	413	414	415	416	417	418	419	420	421	422	423	424	425	426	427	428	429	430	431	432	433
controls																											
hypermethylated DNA	3	3	3	3	3	3	3	3	3	3	3	3	3	3	3	3	3	3	3	3	3	3	3	3	3	3	3
NB1	0	0	0	0	0	0	0	0	0	0	0	0	0	0	0	0	0	0	0	0	0	0	0	0	0	0	0
NB3	0	0	0	0	0	0	0	0	0	0	0	0	0	0	0	0	0	0	0	0	0	0	0	0	0	0	0
NB2	0	0	0	0	0	0	0	0	0	0	0	0	0	0	0	0	0	0	0	0	0	0	0	0	0	1	1
cell lines																											
A172 co	3	3	0	0	0	0	0	0	0	0	2	1	1	1	0	0	0	0	0	0	0	0	1	0	1	1	1
A172 A+T2	3	3	0	0	0	0	0	0	0	0	1	0	0	0	0	0	0	0	0	0	0	0	0	0	0	1	1
U138 co	2	0	0	0	0	0	0	0	0	0	0	0	0	0	0	0	0	0	0	0	0	0	0	0	0	0	0
U138 A+T2	2	2	0	0	0	0	0	0	0	0	0	0	0	0	0	0	0	0	0	0	0	0	0	0	0	0	0
T98G co	2	0	0	0	0	0	0	0	0	0	0	0	0	0	0	0	0	0	0	0	0	0	0	0	0	0	0
T98G A+T2	2	0	0	0	0	0	0	0	0	0	0	0	0	0	0	0	0	0	0	0	0	0	0	0	0	0	0
TP365MG co	0	0	0	0	0	0	0	0	0	0	0	0	0	0	0	0	0	0	0	0	0	0	0	0	0	0	0
TP365MG A+T2	0	0	0	0	0	0	0	0	0	0	0	0	0	0	0	0	0	0	0	0	0	0	0	0	0	0	n.a.

NB1 = human normal brain (BioChain Institute)
NB2 = human fetal brain (BioChain Institute)
NB3 = human normal brain occipital lobe (BioChain Institute)

co = control = non-treated cells
A+T2 = cells treated with 5-aza-2`-deoxycytidine and trichostatin A

0 not methylated
1 weakly methylated
2 moderately methylated
3 strongly methylated
n.a. not analyzed

Supplementary Figure 15: Methylation pattern associated with the 5´-CpG-rich genomic region 7 (CpG sites 407- 433) of *miR-132/miR-212* in four glioblastoma cell lines as well as three non-neoplastic brain tissue samples (NB1 - NB3). Note: No hypermethylation in the investigated DNA fragment.

A)

controls/cell lines	CpG sites 642	643	644	645	646	647	648	649	650	651	652	653	654	655	656
controls															
hypermethylated DNA	3	3	3	3	3	3	3	3	3	3	3	3	3	3	3
NB1	3	2	3	3	3	3	2	3	3	3	3	3	2	3	2
NB2	2	1	2	2	2	2	2	2	2	2	2	2	2	2	2
cell lines															
A172 co	3	3	3	3	3	3	3	3	3	3	3	3	3	3	3
A172 A+T2	3	3	3	3	3	3	3	3	3	3	3	3	3	3	3
U138 co	3	3	3	3	3	3	3	3	3	3	3	3	3	3	3
U138 A+T2	3	3	3	3	3	3	3	3	3	3	3	3	3	3	n.a.
TP365MG co	3	3	3	3	3	3	3	3	3	3	3	3	3	3	3
TP365MG A+T2	3	3	3	3	3	3	3	3	3	3	3	3	3	3	3
T98G co	3	3	3	3	3	3	3	3	3	3	3	3	3	3	3
T98G A+T2	3	3	3	3	3	3	3	3	3	3	3	3	3	3	3

NB1 = human normal brain (BioChain Institute)
NB2 = human fetal brain (BioChain Institute)

co = control = non-treated cells
A+T2 = cells treated with 5-aza-2`-deoxycytidine and trichostatin A

n.a. not analyzed
1 weakly methylated
2 moderately methylated
3 strongly methylated

B)

controls/cell lines/ case no.	CpG sites 790	791	792	793	794	795	796	797	798	799	800	801	802	803	804	805	806	807	808	809	810	811	812	813	814	815
controls																										
hypermethylated DNA	3	3	3	3	3	3	3	3	3	3	3	3	3	3	3	3	3	3	3	3	3	3	3	3	3	3
NB1	3	3	3	3	3	3	3	3	3	3	3	3	2	3	3	3	3	3	3	3	3	3	3	3	3	3
NB2	2	3	2	2	2	2	2	1	2	2	3	2	1	1	1	2	2	2	2	2	2	2	2	2	2	2
NB3	3	3	3	3	3	3	3	3	3	3	3	3	2	3	3	2	3	3	3	3	3	3	3	2	2	2
cell lines																										
A172 co	3	3	3	3	3	3	3	3	3	3	3	3	3	3	3	3	3	3	3	3	3	3	3	3	3	3
A172 A+T2	3	3	3	3	3	3	3	3	3	3	3	3	3	3	3	3	3	3	3	3	3	3	3	3	3	3
U138 co	3	3	3	3	3	3	3	3	3	3	3	3	3	3	3	3	3	3	3	3	3	3	3	3	3	3
U138 A+T2	3	3	3	3	3	3	3	3	3	3	3	3	3	3	3	3	3	3	3	3	3	3	3	3	3	3
TP365MG co	3	3	3	3	3	3	3	3	3	3	3	3	3	3	3	3	3	3	3	3	3	3	3	3	3	3
TP365MG A+T2	3	3	3	3	3	3	3	3	3	3	3	3	3	3	3	3	3	3	3	3	3	3	3	3	3	3
T98G co	3	3	3	3	3	3	3	3	3	3	3	3	3	3	3	3	3	3	3	3	3	3	3	3	3	3
T98G A+T2	3	3	3	3	3	3	3	3	3	3	3	3	3	3	3	3	3	3	3	3	3	3	3	3	2	3
pGBIV																										
GB825	3	3	3	3	3	3	3	3	3	3	3	3	3	3	3	3	3	3	3	3	3	3	3	3	3	3
GB260	3	3	3	3	3	3	3	3	3	3	3	3	3	3	3	3	3	3	3	3	3	3	3	3	3	3
GB969	3	3	3	3	3	3	3	3	3	3	3	3	3	3	3	3	3	3	3	3	3	3	3	3	3	3
GB607	3	3	3	3	3	3	3	3	3	3	3	3	3	3	3	3	3	3	3	3	3	3	3	3	3	3
GB982	3	3	3	3	3	3	3	3	3	3	3	3	3	3	3	3	3	3	3	3	3	3	3	3	3	3
sGBIV																										
GB989	3	3	3	3	3	3	3	3	3	3	3	3	3	3	3	3	3	3	3	3	3	3	3	3	3	3
GB834	3	3	3	3	3	3	3	3	3	3	3	3	3	3	3	3	3	3	3	3	3	3	3	3	3	3
GB119	3	3	3	3	3	3	3	3	3	3	3	3	3	3	3	3	3	3	3	3	3	3	3	3	3	3

NB1 = human normal brain (BioChain Institute)
NB2 = human fetal brain (BioChain Institute)
NB3 = human normal brain occipital lobe (BioChain Institute)

co = control = non-treated cells
A+T2 = cells treated with 5-aza-2`-deoxycytidine and trichostatin A

pGBIV = primary glioblastoma, WHO grade IV
sGBIV = secondary glioblastoma, WHO grade IV

1 weakly methylated
2 moderately methylated
3 strongly methylated

Supplementary Figure 16: (A) Methylation patterns associated with the 5´-CpG-rich genomic region 8 (CpG sites 642-656) of *miR-132/miR-212* in four glioblastoma cell lines and two non-neoplastic brain tissue samples (NB1, NB2). (B) Methylation patterns associated with the 5´-CpG genomic region 9 (CpG sites 790-815) of *miR-132/miR-212* in eight gliomas, four glioblastoma cell lines as well as three samples of non-neoplastic brain tissue samples (NB1 - NB3). Note: Methylation of these sequences in both non-neoplastic brain tissue and tumor samples.

controls/cell lines/ case no.	*miR-126* expression	CG methylation %	CpG sites 76	77	78	79	80	81	82	83	84	85	86	87	88	89	90	91
controls																		
hypermethylated DNA		100%	3	3	3	3	3	3	3	3	3	3	3	3	3	3	3	3
NB1		4%	0	0	0	0	0	0	0	0	1	0	0	0	0	1	0	0
NB3		4%	0	0	0	0	0	0	0	0	1	0	0	0	0	1	0	0
NB2		2%	0	0	0	0	0	0	0	0	1	0	0	0	0	0	0	0
cell lines																		
A172 co	0,47	83%	3	3	2	3	3	3	3	3	3	3	3	3	2	2	0	1
A172 A+T2	0,47	83%	3	2	2	3	3	3	3	3	3	3	3	3	2	2	1	1
U138 co	0,09	81%	1	1	2	3	3	3	3	3	3	3	3	3	3	1	2	2
U138 A+T2	0,20	79%	0	1	2	3	3	3	3	3	3	3	3	3	3	1	2	2
T98G co	0,19	48%	1	0	0	2	3	2	3	3	3	2	2	0	1	1	0	0
T98G A+T2	0,11	46%	0	0	0	2	3	3	3	3	3	1	2	0	0	2	0	0
TP365MG co	0,03	35%	1	1	0	1	1	2	2	3	3	1	1	0	0	1	0	0
TP365MG A+T2	0,10	29%	1	0	0	1	1	2	1	3	3	0	1	0	0	1	0	0
pGBIV																		
GB260	1,92	79%	2	2	0	2	3	3	3	3	3	3	3	2	2	3	2	2
GB973	7,17	71%	2	1	2	2	3	3	3	3	3	3	3	2	2	2	0	0
GB971	6,93	69%	2	1	0	2	3	3	3	3	3	3	3	3	3	1	0	0
GB1020	1,56	58%	1	1	1	2	3	3	3	3	3	2	2	2	0	2	0	0
GB970	0,27	56%	1	0	0	1	3	3	3	3	3	3	3	2	0	2	0	0
GB977	2,05	50%	0	0	1	2	3	3	3	3	3	2	2	1	0	1	0	0
GB666	14,95	49%	0	0	0	2	2	2	2	2	3	2	2	1	1	2	1	n.a.
GB825	1,87	43%	0	0	0	2	0	2	2	2	2	2	2	0	2	2	n.a.	n.a.
GB709	2,56	40%	0	0	0	1	2	2	2	2	2	2	2	2	0	2	0	0
GB637	0,63	40%	0	0	0	1	2	2	2	2	3	2	2	2	0	1	0	0
GB880	2,04	38%	0	0	0	2	2	2	3	2	2	2	1	0	0	2	0	0
GB803	1,25	35%	1	1	0	1	2	2	2	2	2	2	1	0	0	1	0	0
GB137	2,36	35%	1	0	0	1	2	2	3	2	3	1	1	0	0	1	0	0
GB866	0,90	31%	0	0	0	1	2	1	2	2	2	1	1	1	0	2	0	0
GB982	1,46	31%	2	0	0	1	0	2	2	2	2	1	1	0	0	2	0	0
GB113	0,68	21%	2	1	1	1	0	0	0	0	2	0	0	0	2	1	0	0
GB627	3,38	19%	0	0	0	1	1	1	2	1	2	0	0	0	0	1	0	0
GB969	3,51	15%	0	0	0	0	0	2	1	0	2	0	0	0	0	2	0	0
GB968	2,52	10%	0	1	0	0	0	0	0	1	1	0	0	0	0	2	0	0
GB718	6,63	10%	0	0	0	0	0	0	1	0	2	1	1	0	0	0	0	0
GB955	1,99	9%	0	0	0	1	0	n.a.	0	0	1	0	0	0	0	2	0	0
GB961	5,34	6%	0	0	0	0	0	0	0	0	1	1	0	0	0	1	0	0
GB714	1,45	4%	0	0	0	0	0	0	0	0	1	0	0	0	0	1	0	n.a.
GB607	7,57	0%	0	0	0	0	0	0	0	0	0	0	0	0	0	0	0	0
GB981	1,93	0%	0	0	0	0	0	0	0	0	0	0	0	0	0	0	0	0
GB81	1,61	0%	0	0	0	0	0	0	0	0	0	0	0	0	0	0	0	0
sGBIV																		
GB834	0,40	73%	2	2	2	3	3	3	3	3	3	3	3	2	2	1	0	0
GB988	0,57	46%	1	2	2	2	2	3	2	2	2	0	1	1	2	0	0	0
GB989	0,82	38%	1	1	0	1	2	2	2	2	2	2	2	0	0	1	0	0
GB987	1,04	36%	1	1	0	1	1	2	2	2	2	2	1	0	0	0	n.a.	n.a.
GB 4	1,39	31%	0	0	0	2	0	3	2	1	3	1	1	0	0	2	0	0
GB119	0,11	29%	1	1	0	1	0	2	1	2	2	1	2	0	0	1	0	0
GB239	3,80	27%	0	0	0	2	3	1	3	0	3	0	0	0	0	1	0	0
GB175	0,64	0%	0	0	0	0	0	0	0	0	0	0	0	0	0	0	0	0
AII																		
A 140	0,52	40%	2	1	0	2	1	3	3	2	3	1	1	0	0	0	0	0
A 208	1,36	25%	0	0	0	1	1	1	1	1	2	1	0	1	1	2	0	0
A 138	0,32	21%	0	0	0	0	2	2	2	2	2	0	0	0	0	0	0	0
A 157	0,18	13%	0	0	0	1	0	1	0	2	1	0	0	0	0	1	0	0
A 213	0,64	6%	0	0	0	0	0	0	0	0	2	0	1	0	0	0	0	0
A 211	0,64	4%	0	0	0	1	0	0	0	0	1	0	0	0	0	0	0	0
A 212	0,38	2%	0	0	0	0	0	0	0	0	1	0	0	0	0	0	0	0
A 151	0,80	0%	0	0	0	0	0	0	0	0	0	0	0	0	0	0	0	0
AAIII																		
AA 233	1,29	33%	0	0	0	0	2	2	2	2	2	2	2	0	0	1	0	1
AA 111	0,78	24%	0	0	0	1	2	2	2	0	2	0	0	0	0	1	1	n.a.
AA 236	0,65	15%	0	0	0	1	0	1	2	0	2	0	0	0	0	1	0	0
AA 134	0,95	13%	0	0	0	0	0	0	2	0	3	0	0	0	0	1	0	0
AA 189	0,41	12%	0	0	0	0	0	1	0	1	2	0	0	1	0	0	n.a.	n.a.
AA 101	1,13	10%	0	0	0	0	0	1	1	1	1	0	0	0	0	0	n.a.	n.a.
AA 1	2,47	5%	0	0	0	0	0	0	0	0	1	0	0	0	0	1	n.a.	n.a.
AA230	0,71	0%	0	0	0	0	0	0	0	0	0	0	0	0	0	0	0	0

NB1 = human normal brain (BioChain Institute)
NB2 = human fetal brain (BioChain Institute)
NB3 = human normal brain occipital lobe (BioChain Institute)

co = control = non-treated cells
A+T2 = cells treated with 5-aza-2`-deoxycytidine and trichostatin A

pGBIV = primary glioblastoma, WHO grade IV
sGBIV = secondary glioblastoma, WHO grade IV
AII = diffuse astrocytoma, WHO grade II;
AAIII = anaplastic astrocytoma, WHO grade III

0 not methylated
1 weakly methylated
2 moderately methylated
3 strongly methylated
n.a. not analyzed

Supplementary Figure 17: Methylation pattern and methylation scores of the 5´-CpG-rich genomic region 1 of *miR-126* in 50 gliomas and four glioblastoma cell lines as well as three non-neoplastic brain tissue samples (NB1 - NB3). Methylation patterns of 16 CpG sites (CpG sites 76 to 91) located in the 5´-CpG genomic region 1 of *miR-126* (nucleotides 139557805-139563005 on 9q34.3, UCSC Genome Browser, version February 2009) are shown. **Note:** pGBIV and sGBIV were hypermethylated relative to the normal brain tissue samples.

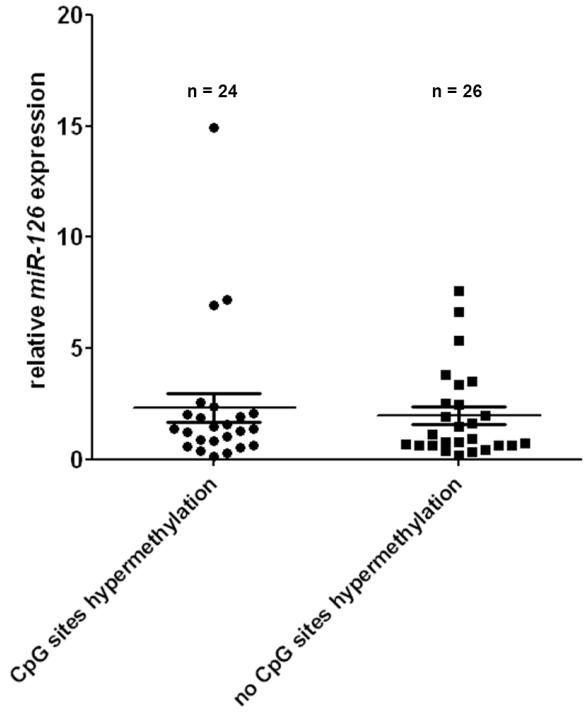

Supplementary Figure 18: *MiR-126* expression analysis in human gliomas in relation to the methylation status of CpG sites 76-91. Each tumour was assigned to one of two groups: low, no *miR-126* hypermethylation (methylation score 1, 2 or 3 in < 50% of the investigated CpG sites) or high, *miR-126* hypermethylation (methylation score 1, 2 or 3 in ≥ 50% of the investigated CpG sites). **Note:** There was no association between methylation and *miR-126* expression.

10 Danksagung

Beginnen möchte ich mit den Personen, denen meine Dissertation gewidmet ist, meinen Eltern. Ohne ihre grenzenlose und uneingeschränkte Unterstützung wäre ich nicht an diesem Punkt in meinem Leben, an dem ich jetzt glücklicherweise bin. Sie waren immer für mich da und haben meine innere Stärke aufgebaut und gefestigt, die ich während meiner Dissertationsarbeit und in manchen Lebenssituationen dringend gebraucht habe. Diese bedingungslose Liebe ist mein Fundament.

Mein weiterer und besonderer Dank gilt Herrn Prof. Dr. Guido Reifenberger für die Aufnahme in sein erstklassiges Team und die interessante Fragestellung meiner Promotionsarbeit. Mit Hilfe seiner fundierten wissenschaftlichen und persönlichen Unterstützung ist es mir gelungen, einen tieferen Einblick in die medizinischen Aspekte dieses spannenden Themas zu erhalten. Ich danke Ihnen für das Vertrauen, welches Sie mir entgegengebracht haben.

Ich bedanke mich sehr herzlich bei Frau Dr. Marietta Wolter für Ihre Betreuung über die gesamte Promotionsphase und für die ausgezeichnete Einarbeitung ins Laborleben. Durch Ihre intensiven und strukturierten Denkanstöße hat Sie mir gezeigt, was eine gute Wissenschaftlerin ausmacht. Dankbar anerkennen möchte ich die kritischen, äußerst konstruktiven und wertvollen inhaltlichen Anmerkungen bei der Erstellung dieses Manuskripts sowie Ihre geduldige Bereitschaft, jede offene Frage zu beantworten. Die gewährte wissenschaftliche Freiheit und die Weitergabe Ihrer Erfahrung kamen mir in zahlreichen Angelegenheiten sehr zugute.

Bedanken möchte ich mich zudem bei meinen externen bioinformatischen Kooperationspartnern, Herrn Prof. Dr. Benedikt Brors und Herrn Dr. Marc Zapatka, DKFZ Heidelberg, sowie Frau Dr. Edith Willscher, Universität Leipzig. Ohne ihre Hilfe wäre die biostatistische Auswertung der miRNA-Profiling-Daten nicht möglich gewesen. Des Weiteren danke ich Herrn Prof. Dr. Till Acker und Herrn Sascha Seidel, Institut für Neuropathologie, Universität Gießen, für die hervorragende Zusammenarbeit im Rahmen der Untersuchung von Hypoxie-regulierten miRNAs. Für die Unterstützung bei der Erstellung der Expressionsdaten für die ausgewählten miRNA-Zielgene gilt mein besonderer Dank Herrn Dr. Bernhard Radlwimmer, Abteilung Molekulare Genetik, DKFZ Heidelberg.

Herrn Prof. Dr. Dieter Willbold gilt ein besonderer Dank für die freundliche Übernahme der Betreuung meiner Promotion seitens der Mathematisch-Naturwissenschaftlichen Fakultät der Heinrich-Heine-Universität Düsseldorf und die Erstellung des Korreferats.

Was wäre eine Promotionszeit ohne Mitdoktoranden. Jene Mitstreiter, die alle Phasen des Promotionsprojekts mit Rat und Tat und dem ein oder anderen Scherzchen im Labor unterstützen. In diesem Zusammenhang möchte ich ein besonderes Wort des Dankes an „meine Mädels“, mit Namen Linda Stöckmann, Rebecca Ruland, Anneliese Forchmann, Nadine Lottmann und Carina Lindemann, richten. Durch Euer Fachwissen, die konstruktive Kritik und Euer großes Engagement habt ihr mich tatkräftig unterstützt. Eure Freundschaft sowie Hilfe in allen Lebenslagen haben für die erforderliche Abwechslung gesorgt. Hervorheben möchte ich Euer großes Verständnis und Euren Humor für meine Vorliebe, alle vorhandenen freien Plätzchen zu belagern. Ihr werdet mir fehlen!

Liebe Frau Dr. Natalie Schmidt, ich danke Dir besonders für die vielen schönen Stunden innerhalb unserer gemeinsamen turbulenten Doktorandenzeit. Wir sind miteinander durch so manches Tal gelaufen und haben am Ende zwei Berge bestiegen. Dein formatiertes Layout hat erheblich zum Gesamterfolg meiner Arbeit beigetragen.

Bei allen jetzigen und ehemaligen Mitgliedern des Instituts der Neuropathologie möchte ich mich für die freundliche und angenehme Arbeitsatmosphäre bedanken. In diesem Zusammenhang möchte ich Frau Dr. Kerstin Kaulich, Frau Petra Zipper, Frau Dr. Dr. Ana-Maria Florea, Frau Dr. Daniela Karra, Frau Vera Jansen und Herrn Dr. Bastian Malzkorn sowie Herrn Dr. Jörg Felsberg, Britta Friedensdorf und Heike Seul nennen, die mir mit ihren Erfahrungen immer tatkräftig zur Seite standen.

Nicht unerwähnt dürfen dabei auch Daniela Kittel und Christoph Fleisgarten bleiben, die nie abgeneigt waren, mir bei auftretenden Problemen zu helfen.

Die philosophischen Unterhaltungen mit Frau Erika Wolter und Frau Christa Mähler werden mir fehlen. Sie haben meine kreative Seite durch neue Ideen und Vorschläge wachgehalten und gefördert. Einen besonderen Dank richte ich an Frau Wolter, dass sie mir in schwierigen Situationen ein Stück von Ihrer Lebenserfahrung mit auf den Weg gegeben hat.

Ein ganz **besonderes Dankeschön** gilt,

meinem Freund Michael Kania. Er hat mich aufgerichtet und wieder angetrieben, mit mir den inneren Schweinehund bekämpft, mich immer wieder konstruktiv kritisiert und unterstützt wo er nur konnte. Hätte er mir nicht den Rücken freigehalten, wäre meine Arbeit in dieser Form nicht möglich gewesen. Dafür danke ich ihm von ganzem Herzen.

meinen besten Freunden, Friederike Schöll und Christ Violonchi, die mich seit einigen Jahren, sehr eng verbunden, begleiteten und mich jederzeit bedingungslos unterstützen.

Ich wünsche allen zuvor Genannten alles erdenklich Gute für die Zukunft!

11 Ehrenwörtliche Erklärung

Hiermit erkläre ich, dass ich die vorliegende Dissertation eigenständig und ohne unerlaubte Hilfe angefertigt und diese in der vorgelegten oder in ähnlicher Form noch bei keiner anderen Institution eingereicht habe.

Ort, Datum Unterschrift